

# Orogenic gold mineralization of the eastern Cordilleran gold belt, British Columbia: Structural ore controls in the Cariboo (093A/H), Cassiar (104P) and Sheep Creek (082F) mining districts

Geoscience BC Report 2017-15



**PANTERRA  
GEOSERVICES INC.**  
*Applied geological studies*

**Murray M. Allan  
David A. Rhys  
Craig J.R. Hart**



THE UNIVERSITY OF BRITISH COLUMBIA

# Orogenic gold mineralization of the eastern Cordilleran gold belt, British Columbia:

## Structural ore controls in the Cariboo (093A/H), Cassiar (104P) and Sheep Creek (082F) mining districts

---

**Geoscience BC<sup>1</sup> Report 2017-15**

**Prepared by MDRU<sup>2</sup>**

<sup>1</sup> Geoscience BC is an independent, non-profit organization that generates earth science in collaboration with First Nations, local communities, government, academia and the resource sector. Our independent earth science enables informed resource management decisions and attracts investment and jobs. Geoscience BC gratefully acknowledges the financial support of the Province of British Columbia.

<sup>2</sup> The Mineral Deposit Research Unit (MDRU) is an internationally-recognized collaborative venture between the mining industry and the Department of Earth, Ocean and Atmospheric Sciences at The University of British Columbia (UBC), established with assistance from the Natural Sciences and Engineering Research Council of Canada (NSERC), and devoted to solving mineral exploration-related problems. Contact: MDRU, 2020-2207 Main Mall, Vancouver, BC V6T 1Z4 Canada

---

### ***Suggested Citation:***

Allan, M.M., Rhys, D.A. and Hart, C.J.R., 2017, Orogenic gold mineralization of the eastern Cordilleran gold belt, British Columbia: Structural ore controls in the Cariboo (093A/H), Cassiar (104P) and Sheep Creek (082F) mining districts: Geoscience BC Report 2017-15, 108 p.

# Orogenic gold mineralization of the eastern Cordilleran gold belt, British Columbia: Structural ore controls in the Cariboo (093A/H), Cassiar (104P) and Sheep Creek (082F) mining districts

Murray M. Allan<sup>1</sup>, David A. Rhys<sup>2</sup> and Craig J.R. Hart<sup>1</sup>

<sup>1</sup> MDRU - Mineral Deposit Research Unit, Department of Earth, Ocean and Atmospheric Sciences, The University of British Columbia, Vancouver, BC, V6T 1Z4, Canada

<sup>2</sup> Panterra Geoservices Inc., Surrey, BC

## Suggested Citation:

Allan, M.M., Rhys, D.A. and Hart, C.J.R., 2017, Orogenic gold mineralization of the eastern Cordilleran gold belt, British Columbia: Structural ore controls in the Cariboo (093A/H), Cassiar (104P) and Sheep Creek (082F) mining districts: Geoscience BC Report 2017-15, 108 p.

**Keywords:** orogenic gold, veins, deformation, structural geology, ore controls, <sup>40</sup>Ar/<sup>39</sup>Ar geochronology, U-Pb geochronology, Cordilleran orogen, Cariboo, Wells-Barkerville, Cassiar, Salmo, Sheep Creek, gold deposit models

## INTRODUCTION

Orogenic gold accounted for 45% of British Columbia's historic lode gold production up to 2002 (Schroeter, 2003), and the vast majority of the province's >5 Moz historic placer production is ultimately linked to orogenic gold in bedrock sources. Reinvigorated greenfields and brownfields exploration activity in the Wells-Barkerville mining camp of the Cariboo gold district (Barkerville Gold Mines Ltd., 2017) emphasizes the ongoing and potential future economic importance of orogenic gold in British Columbia. However, successful exploration for orogenic gold deposits can be technically challenging, owing to structural complexities and inconsistent grade distributions typical of this deposit class.

Orogenic gold deposits in British Columbia preferentially occur in two main tectonic settings. The Bralorne-Pioneer mining camp (Hart and Goldfarb, 2017) is associated with Late Cretaceous to Paleocene movement on crustal-scale dextral strike-slip fault systems along the western margin of Stikine terrane near the eastern Coast Belt. These formed contemporaneously with oblique collision of the Pacific plate with the North American margin – a setting comparable to the Juneau mining camp on the western Coast Belt margin in southeast Alaska (Fig. 1). A second belt of orogenic gold deposits is crudely cospacial with the Jurassic to Cretaceous collisional suture between the accreted Intermontane Terranes and autochthonous strata of the ancient North American margin. This eastern belt includes the Cariboo gold district and Sheep Creek gold camp, which are hosted in autochthonous North American strata of the Kootenay terrane, and the Cassiar gold district, which is hosted in ophiolitic rocks of the Slide Mountain

terrane in the Sylvester Allochthon (Fig. 1). The structural architecture of each camp in this eastern belt is dominated by shallowly-dipping thrust faults, in the apparent absence of the steep, crustally significant shear zones that characterize Bralorne-Pioneer, Juneau, the Mother Lode belt of California, and examples of Archaean orogenic gold deposits, such as those in the Abitibi belt of Canada's Superior Province, and in the Eastern Goldfields of the Yilgarn craton of Western Australia (e.g., Groves et al., 2003).

This study determines the structural relationship of British Columbia's 'eastern Cordilleran gold belt' to Cordilleran deformation, and establishes new structural frameworks that differ from those documented in the economic geology literature. Three objectives are evaluated:

1. Camp-scale field studies focussing on geometric and kinematic relationships between ore zones, veins, and host rock structures;
2. New <sup>40</sup>Ar/<sup>39</sup>Ar geochronological data that constrain the timing of metamorphism, deformation, and hydrothermal alteration;
3. New U-Pb geochronological data on igneous intrusions spatially related to mineralization.

Models of deformation and ore formation build on several previous studies, and leverage information from previous Geoscience BC initiatives in the Cariboo (Rhys et al., 2009; Mortensen et al., 2011; Chapman and Mortensen, 2016) and southern Kootenay regions (Webster and Pattison, 2014; Webster, 2016).

For each of the Cariboo, Cassiar, and Sheep Creek study areas, the geology, structure, and geochronological framework is reported, followed by a comparative synthesis that emphasizes regional ore controls. Appendix materials include: analytical methodology for  $^{40}\text{Ar}/^{39}\text{Ar}$  analysis (Appendix 1),  $^{40}\text{Ar}/^{39}\text{Ar}$  results (Appendix 2), and U-Pb results (Appendix 3). Supplementary digital materials include: field station locations, descriptions and locations of rock samples, sample photographs, thin section scans, oriented field

photographs with locations, and attributed GIS shapefiles for the 1953 geological map of the Sheep Creek gold camp by W.H. Mathews.

Structural data, waypoints, oriented photographs, and field notes were recorded on an iPad with FieldMove™ software by Midland Valley Exploration Ltd. Digital structural data were compared routinely with analog compass measurements to ensure accuracy.

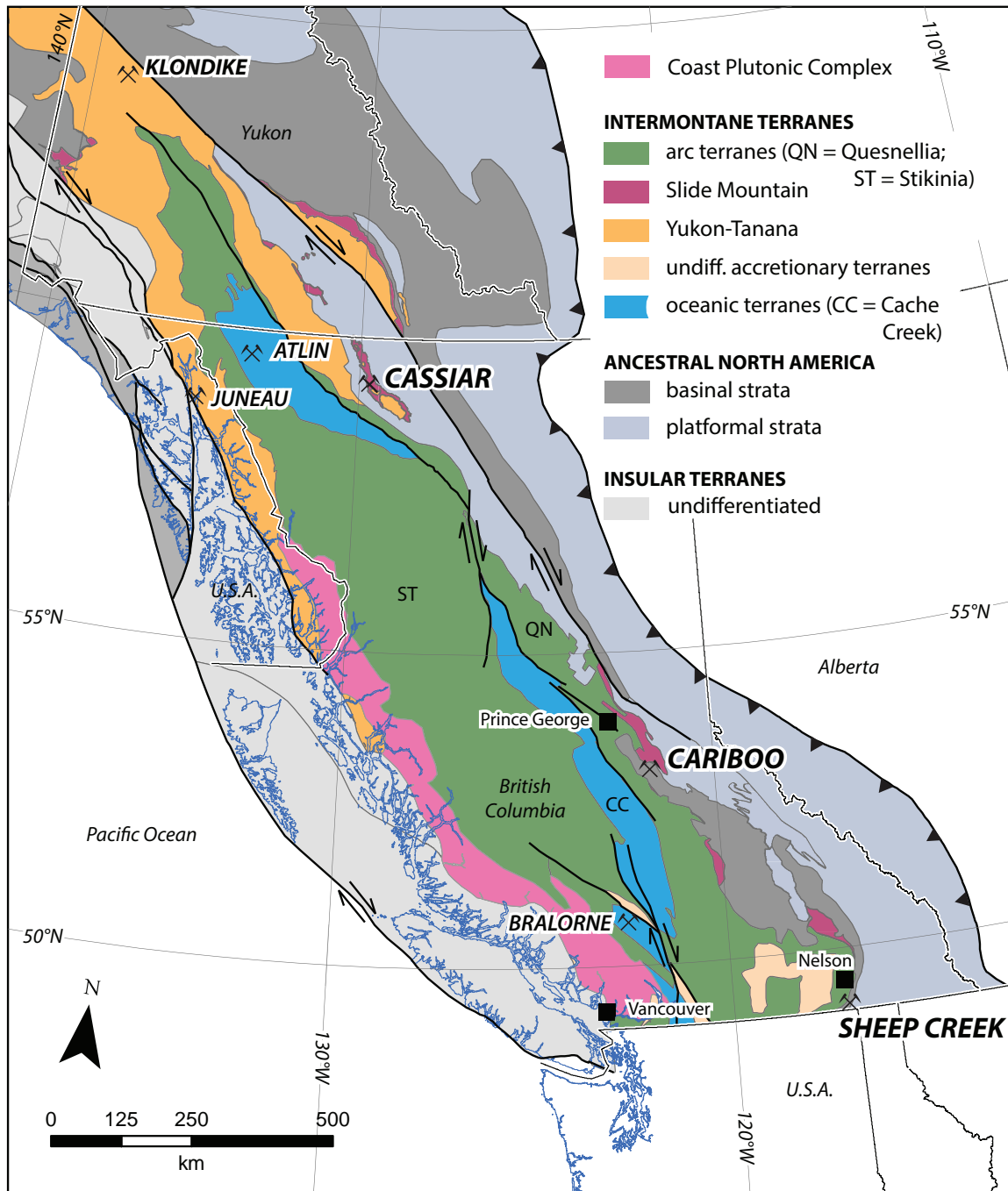


Figure 1. Terranes of the northeastern Cordillera, showing the location of significant orogenic gold districts.

---

# Cariboo Gold District

---

The Cariboo gold district in east-central B.C. is famous for its more than 150-year history of gold discovery and production, which includes up to 3.0 Moz of gold from alluvial sources (Levson and Giles, 1993), and 1.2 Moz ounces from lode deposits. The majority of gold production came from the Wells-Barkerville camp, but the district includes the numerous placer-producing creeks and bedrock gold occurrences of the surrounding region (Fig. 2).

## REGIONAL GEOLOGY

The Cariboo gold district is underlain by peri-cratonic Barkerville subterrane metasiliciclastic rocks and lesser carbonate and volcanic rocks of the Snowshoe Group, which represents the distal margin of ancestral North America (Fig. 2). The stratigraphic interpretation of the Barkerville subterrane, and its relationship to the adjacent Cariboo subterrane, has undergone numerous iterations since its original definition by Bowman (1889). The Barkerville subterrane is separated from the Cariboo subterrane to the east by the west-verging Pleasant Valley thrust, with the Snowshoe Group representing more distal, continental shelf and slope clastic facies, and marine sediments of the Cariboo subterrane representing more proximal shelf facies carbonates (Fig. 2). In the absence of well-constrained fossil or radiometric age control in the Snowshoe Group, stratigraphic relationships of the Barkerville subterrane to the better constrained Cariboo subterrane suggest it spans the late Proterozoic to Lower Paleozoic. It has also been long recognized that both the Barkerville subterrane shares direct tectono-stratigraphic tie to the Kootenay terrane in southeastern B.C. (Monger and Berg, 1984; Struik, 1986; Ferri and Schiarizza, 2006).

Regional mapping by Struik (1981, 1982a, 1982b, 1983a, 1983b) resulted in refinements to the internal stratigraphy of the Snowshoe Group. The stratigraphy was further re-interpreted and simplified by Ferri and co-workers (Ferri, 2001; Ferri and O'Brien, 2002, 2003; Ferri and Schiarizza, 2006), in recognition of a regional map patterns governed by a major second-phase nappe with an amplitude of ~25 km, giving rise to repetitions of the same sedimentary sequences across regional strike (Fig. 3).

The Barkerville subterrane is separated from Quesnel terrane by the east-vergent Eureka thrust (Struik, 1988; Fig. 2). In the hanging wall of the Eureka thrust, the Quesnel terrane is dominated by Mesozoic arc volcanic and sedimentary rocks of the Nicola Group, including the Middle to Upper Triassic "black phyllite" unit, which comprises dominantly fine-grained clastic and tuffaceous strata. Tectonic slices

of variably sheared mafic to ultramafic rock of the Crooked Amphibolite occur along the Kootenay-Quesnellia terrane boundary (Fig. 2). The unit is assigned to the Late Paleozoic Slide Mountain terrane.

Oceanic rocks of Slide Mountain terrane, including basalt, gabbro, chert, and argillite of the Antler Formation, were emplaced onto the Barkerville and Cariboo terranes along the Pundata thrust (Struik, 1988; Fig. 2). Metasedimentary rocks of the Snowshoe Group are also structurally overlain by the Island Mountain amphibolite, exposed as a series of klippen northwest of Wells (Fig. 2). The Island Mountain amphibolite has been variably correlated with rocks of the Snowshoe Group (Struik, 1988) and Slide Mountain terrane (Ash, 2001).

Historically, previous workers paid particular attention to the detailed stratigraphy and structure of the Snowshoe Group in the Wells-Barkerville mining camp. However, for the purpose of discussing regional deformation features, the broad stratigraphic definition summarized by Ferri and Schiarizza (2006) is used herein. This scheme subdivides the Snowshoe Group into three main packages, which from oldest to youngest are:

### ***Downey succession (Late Proterozoic to Early Cambrian):***

The Downey succession is dominated by green-grey micaceous quartzite to feldspathic quartzite, phyllite, and schist, with orthoquartzite ('Keithley quartzite') occurring near the top of the sequence. This succession includes the previously defined Keithley, Kee Khan, Ramos, and Tregillus successions defined by Struik (1988). The Downey succession includes alkaline mafic metavolcanic rocks, which range from thin horizons of chloritic phyllite in the Wells-Barkerville camp, to thick, regionally mappable exposures of chlorite ± actinolite phyllite and schist north of Cariboo Lake (Mount Barker volcanics; Fig. 2).

### ***Harvey's Ridge succession (Early Cambrian and younger):***

The Harvey's Ridge succession is defined mainly by dark grey to black carbonaceous and locally pyritic phyllite, siltstone, quartzite with light grey quartzite to feldspathic quartzite more abundant up-section. This succession includes carbonaceous phyllite of the previously defined 'Hardscrabble Mountain succession' of Struik (1988), as well as the 'Agnes conglomerate' in its upper part. The detailed stratigraphy of the Hardscrabble Mountain succession is particularly relevant in the Wells-Barkerville camp (Fig. 4), but is not described in detail here.

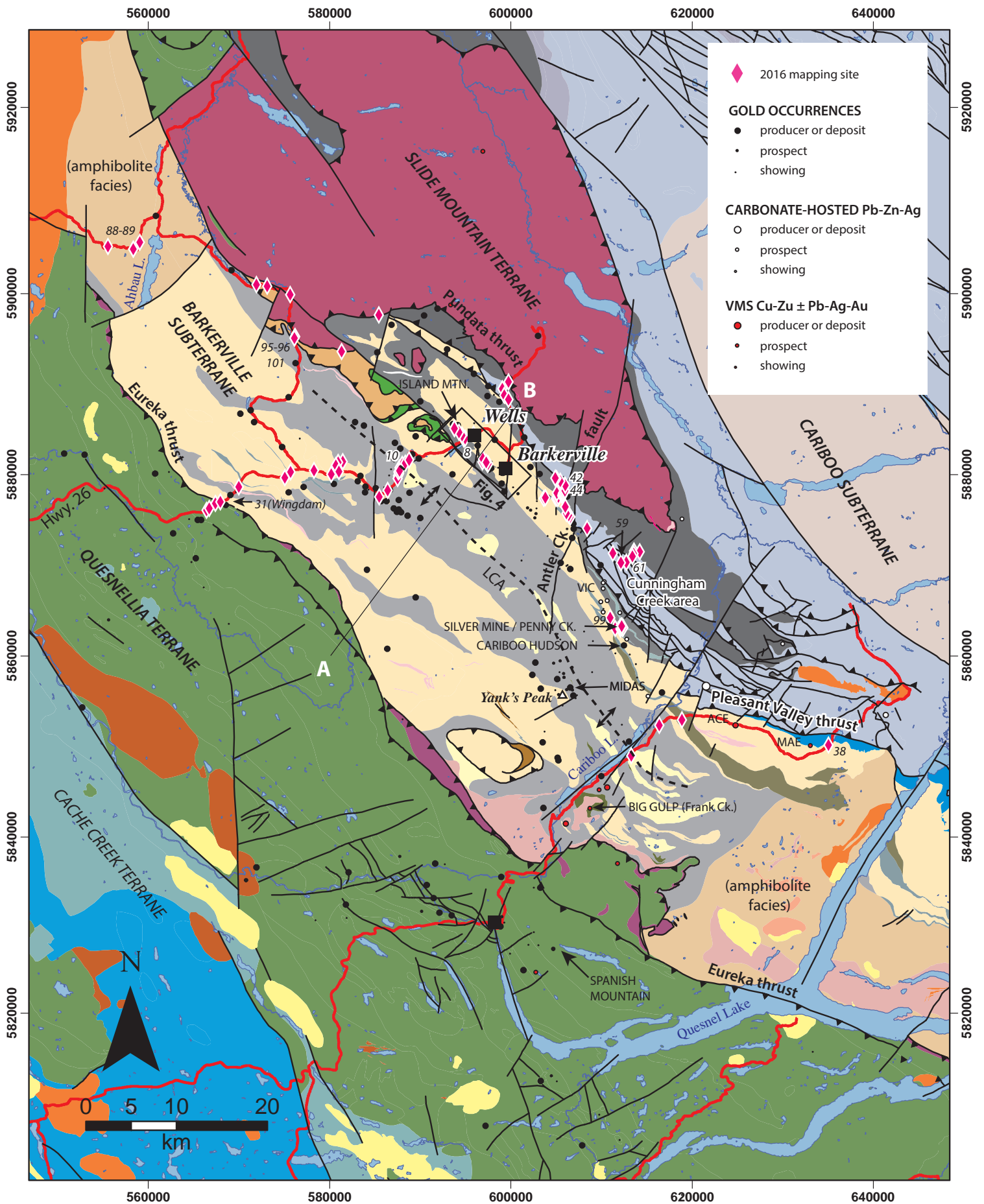


Figure 2. Geology of the Cariboo gold district and surrounding region (after digital compilation of Logan et al., 2010). Selected field stations mentioned in the text are labelled. LCA = Lightning Creek antiform.

## LEGEND

### Cenozoic layered rocks

 **undivided** – various volcanic and sedimentary rocks

### Post-accretionary plutonic rocks

 **undivided** (Permian to Tertiary) – quartz porphyry

 **undivided** (Cretaceous) – granite, alkali feldspar granite; includes rocks of the **Naver pluton** (KNa)

 **undivided** (Late Cretaceous to Paleogene) – undifferentiated pegmatitic rocks

 **Ste. Marie plutonic suite** (Middle Jurassic; 167-165 Ma) – K-feldspar megacrystic hornblende quartz monzonite, granodiorite and granite

### Overlap assemblages

 **undivided** (Lower to Middle Jurassic) – siltstone, shale, greywacke, polymictic conglomerate; minor limestone and andesite; locally includes Cretaceous conglomerate, sandstone and carbonaceous shale

### Quesnellia terrane

 **undivided** (Middle to Upper Triassic) – volcanic and sedimentary rocks of the **NICOLA GROUP** (muTrN/uTrN)

### Cache Creek terrane

 **undivided** (Permian to Triassic) – phyllite, siliceous phyllite, ribbon and massive chert, argillite, tuff, mafic volcanic rocks, serpentinite, limestone, sandstone, conglomerate

### Slide Mountain terrane

 **SLIDE MOUNTAIN GROUP, Antler Formation** (Mississippian to Permian) – pillowed basalt, basalt breccia, gabbro, diorite, argillite and chert; minor serpentinite and ultramafic rocks

 **Crooked amphibolite** (Carboniferous to Permian) – serpentinite, sheared ultramafic rock, amphibolite, talc schist

### Paleozoic plutonic rocks

 **undivided** (Mississippian) – diorite, diabase; minor pegmatite

 **Quesnel Lake gneiss** (Devonian to Mississippian) – megacrystic granodiorite to granite augen orthogneiss

## Northern Kootenay terrane (Barkerville subterrane)

### SNOWSHOE GROUP (Neoproterozoic to Paleozoic)

 **Goose Peak succession** (Paleozoic) – quartzite, phyllite, conglomerate

 **Bralco limestone** (Paleozoic) – marble, schist, gneiss

 **Harvey's Ridge succession** (Paleozoic) – dark grey to grey phyllite, schist, siltstone, quartzite; locally includes marble and schistose metavolcanic rocks

 **Hardscrabble facies** – black siltite, phyllite, micaceous quartzite, limestone

 **Hardscrabble facies (limestone)** – marble

 **Frank Peak / Badger Peak volcanic rocks** – mafic metavolcanic rocks: chlorite-actinolite schist and fragmental schist; locally includes phyllite, siltstone, quartzite

 **Downey succession** (Neoproterozoic to Paleozoic) – micaceous quartzite, quartzite, phyllite, schist, gneiss; locally includes marble and amphibolite; includes Ramos, Tregillus, Keithley, and Kee Khan successions

 **Downey succession (limestone)** – marble; locally includes calcareous phyllite, calcareous quartzite, amphibolite

 **Mount Barker volcanic rocks** – metavolcanic rocks: chlorite-actinolite schist, amphibolite, mafic metatuff; locally includes phyllite, quartzite, marble

 **Downey succession (undivided)** – schist, gneiss, schistose quartzite, phyllite, marble, amphibolite and siltite; minor quartzite and quartzite-clast conglomerate.

 **Tom succession** (Neoproterozoic to Paleozoic) – micaceous quartzite, phyllite, schist; possibly part of the Downey succession

 **Island Mountain succession** (Neoproterozoic to Paleozoic) – amphibolite; minor siliceous mylonite

### Cassiar terrane (Cariboo subterrane)

 **BLACK STUART GROUP** (Cambrian) – chert, limestone, dolostone and derived conglomerate and breccia; black shale, argillite, cherty argillite, quartzite, siltite and slate; some pillow basalt, schistose calcareous basaltic tuff and volcaniclastic

 **GOG GROUP** (Lower Cambrian) – includes interbedded quartz arenite, sandy dolomite, limestone and shale of the **Mural Formation** (ICmGMu)

 **CARIBOO GROUP, undivided** (Neoproterozoic to Lower Cambrian) – includes: limestone, slate, siltstone, argillite of the **Dome Creek Formation** (CmCD); mudstone, siltstone, shale fine clastic sedimentary rocks of the **Midas Formation** (uPrCmCM); quartzite, quartz arenite sedimentary rocks of the **Yanks Peak Formation** (uPrCmCY); mudstone, siltstone, shale fine clastic sedimentary rocks of the **Yankee Belle Formation** (uPrCYa); limestone, marble, calcareous sedimentary rocks of the **Cunningham Formation** (uPrCC); mudstone, siltstone, shale fine clastic sedimentary rocks of the **Isaac Formation** (uPrCI)

 **KAZA GROUP, undivided** (Neoproterozoic) – Lower Division comprising mudstone, siltstone, shale fine clastic sedimentary rocks (uPrKLsf); Middle and Upper Divisions comprising quartzite, quartz arenite sedimentary rocks (uPrKM, uPrKU)

Figure 2 (cont'd). Geologic legend corresponding to the regional map in Figure 2.

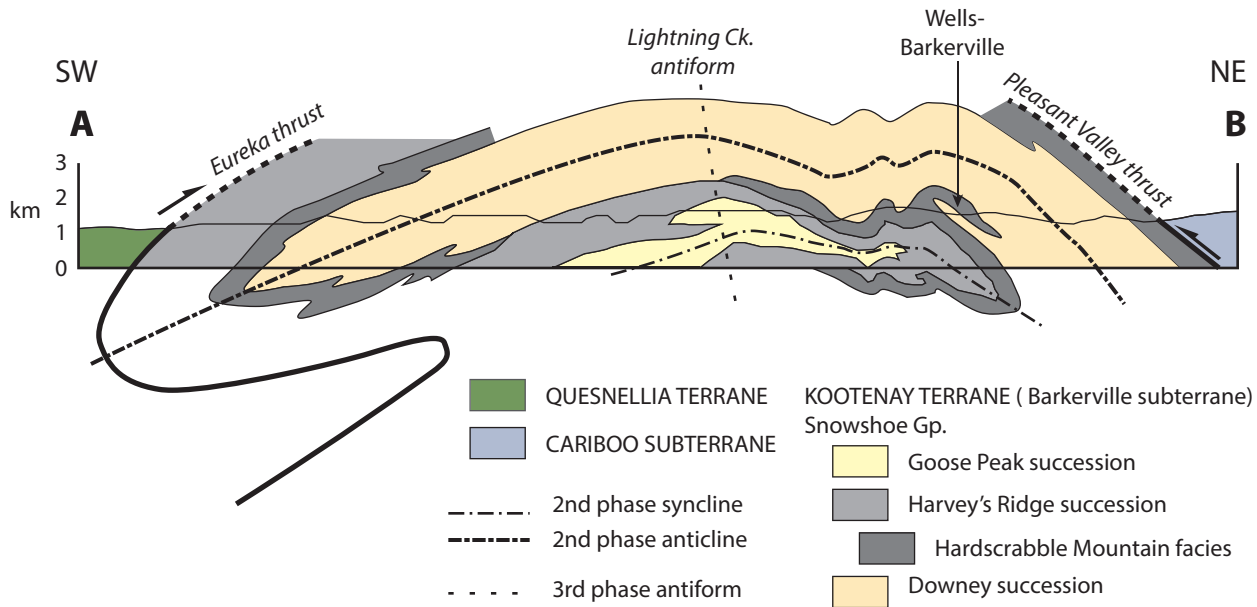


Figure 3. Simplified geologic cross-section through the Barkerville subterrane, showing the inferred nappe geometry (after Ferri and Schiarizza, 2006).

The Harvey's Ridge succession locally includes alkaline mafic metavolcanic rocks, including a large exposure south of Cariboo Lake (Frank Creek volcanics) associated with the Big Gulp VMS occurrence (Fig. 2). The Harvey's Ridge succession is in sharp contact with the underlying Downey succession (Ferri and Schiarizza, 2006).

**Goose Peak succession (Early Cambrian and younger):** The Goose Peak succession includes light grey to light green-grey quartzite to feldspathic quartzite with interbedded dark grey phyllite and siltstone. The Goose Peak succession is in apparent gradational contact with the underlying Harvey's Ridge succession.

The Snowshoe Group is intruded locally by felsic to mafic intrusive bodies, especially in the southern Cariboo Lake area (Ferri and O'Brien, 2003; Fig. 2). These include Early Mississippian granitic sills of the Quesnel Lake gneiss, which is particularly deformed near the Eureka thrust (Ferri and Schiarizza, 2006). Numerous bodies of Early Permian diorite to gabbro also occur, which may relate directly to formation of the Slide Mountain oceanic basin west of the ancestral North American margin (Ferri and Friedman, 2002; Ferri and O'Brien, 2002, 2003).

The deformation history of the Kootenay terrane (defined here as including Barkerville and Cariboo subterrane) is dominated by contractional deformation initiated by the eastward obduction of Quesnellia along the Eureka thrust, followed by southwest-vergent folding of this terrane

boundary and other early-formed structures. Peak metamorphic conditions associated with collision and tectonic thickening reached greenschist to amphibolite facies, and is dated in the Quesnel Lake area at  $174 \pm 4$  Ma on the basis of a U-Pb age for metamorphic titanite (Mortensen et al., 1987). The southwest-vergent folding event that coincided with peak metamorphism is overprinted by a late to post-metamorphic refolding event (Rees, 1987; Struik, 1988; Ferri and O'Brien, 2002).

Rocks of the Snowshoe Group in the Cariboo Gold District reached lower greenschist facies peak metamorphic conditions in the Jurassic, as indicated by muscovite, albite, chlorite, chloritoid, and carbonate bearing assemblages. Upper greenschist conditions were reached locally, as defined by biotite (Struik, 1988). Metamorphic grade increases along regional strike both to the northwest and southeast, as recognized in this study by quartz-muscovite-biotite-garnet-andalusite schist in the Ahbau Lake area, and quartz-feldspar-biotite-garnet-pyrite schist east of Cariboo Lake (Localities 88-89 and 38 respectively; Fig. 2).

Post-metamorphic lamprophyre dikes occur in the Cunningham Creek area at the Silver Mine and Penny Creek occurrences (Fig. 2). These dikes are massive and undeformed, and locally intrude pre-existing quartz-sulphide veins, as evidenced by xenoliths of vein and foliated wall rock clasts. The dikes in this area thus post-date all ductile strain, metamorphism, vein formation, and mineralization.

## Distribution of lode gold mineralization, Wells-Barkerville mining camp, Cariboo Gold District, B.C.

(after Rhys and Ross, 2001; Brown, 2009)

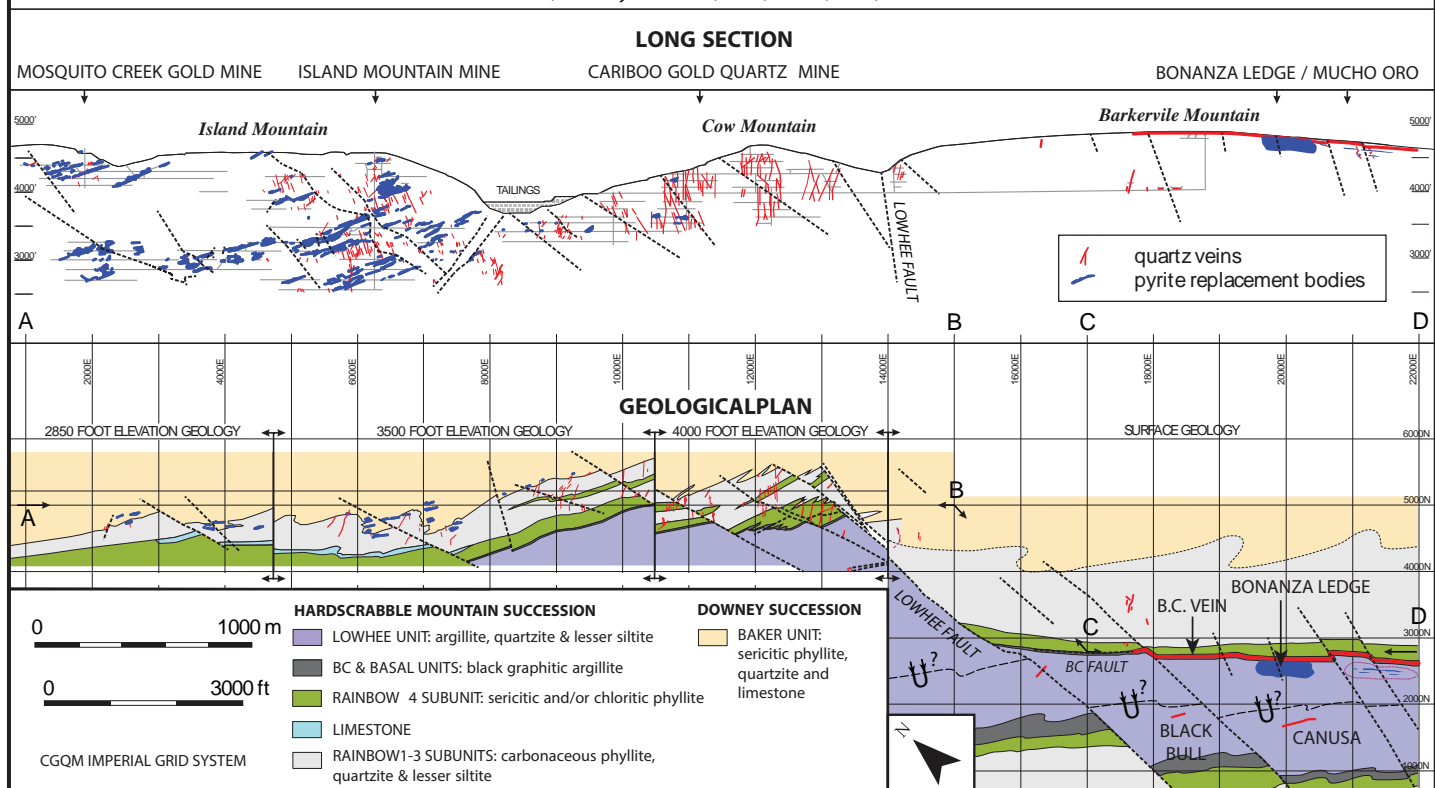


Figure 4. Geology and distribution of gold mineralization and mine workings in the Wells-Barkerville camp (after Rhys and Ross, 2001; Brown, 2009).

## ECONOMIC GEOLOGY

The majority of documented lode gold deposits in the Cariboo gold district occur in a northwest-trending belt hosted by Downey succession rocks along the eastern margin of the Barkerville subterrane (Figs. 2, 4). This belt extends from the Island Mountain area west of the town of Wells, to the Cunningham Creek area north of Cariboo Lake (Fig. 2). Clusters of gold mineralization also occur in the central part of the Barkerville subterrane, including veins of the past-producing Midas mine (BC MINFILE 093A 035) in the Yank's Peak area (Fig. 2). The most significant lode producers in the district are summarized in Table 1.

Gold mineralization in the Cariboo district is mostly in quartz-carbonate-pyrite veins that cross-cut ductile fabrics of the metasedimentary host rocks (Fig. 4). Approximately one-third of historic production was from pyritic replacement-style ore, occurring as elongate, manto-like bodies of generally massive, fine-grained pyrite with quartz-carbonate gangue (Ray et al., 2001). Replacement-style ore is typical of the Island Mountain area, and of the Bonanza Ledge zone, Barkerville Mountain (Fig. 4).

Auriferous veins in the Wells-Barkerville camp are dominated by quartz and ferroan carbonate as the main gangue minerals, and by pyrite as the predominant sulphide mineral,

along with minor galena, sphalerite, chalcopyrite, pyrrhotite, and scheelite. Cosalite ( $Pb_2Bi_2S_5$ ) and galenobismutite ( $Pb-Bi_2S_4$ ) are common and distinctive accessory minerals in the Wells-Barkerville camp (Warren, 1936; Skerl, 1948), and arsenopyrite has also been reported in textural association with gold in this area (Chapman and Mortensen, 2016). Vein-hosted mineralization dominated the 621 koz of underground gold production from the Cariboo Gold Quartz Mine at Cow Mountain, and is of economic interest at Island Mountain, where previous mining activities primarily targeted replacement-style ore (Barkerville Gold Mines Ltd., 2017; Fig. 4). Replacement-style ore is also pyrite-dominant, with accessory galena, sphalerite, and scheelite on the margins of ore bodies (Skerl, 1948). A detailed mineralogical investigation of lode and placer gold grains in the district by Chapman and Mortensen (2016) indicates a Ag content of gold alloy in the range of 3 – 30%.

Numerous examples of sediment-hosted Cu-Zn ± Pb-Ag-Au or Pb-Zn ± Ba mineralization occur in marine sedimentary rocks of the Barkerville and Cariboo subterrane, especially in a belt that is crudely defined by, and straddling, the trace of the Pleasant Valley thrust (Fig. 2). Examples of volcanogenic massive sulphide (VMS) style mineralization include the Big Gulp (BC MINFILE 093A 143), Ace (BC MINFILE 093A 142), and Mae (BC MINFILE 093A 083) Cu-Zn ± Pb-Au-Ag occurrences, all of which occur in phyllite or

Table 1: Lode gold production and resources, Cariboo gold district

Area / Deposit(s)	Mineralization style	Historic Lode Production	Resources
Cow Mountain (Cariboo Gold Quartz Mine)	vein	621 koz (1.68 Mt @ 11.5 g/t) (1933-1959) <sup>1</sup>	42 kt @ 9.3 g/t + 53 kt @ 12.7 g/t (Reserves) <sup>1</sup>
Barkerville Mountain (Bonanza Ledge, B.C. vein)	replacement and vein	13.0 koz (64.3 kt @ 6.3 g/t) (2014-2015) <sup>1</sup>	Meas: 64.4 koz @ 8.07 g/t Ind: 94.4 koz @ 6.72 g/t Inf: 18.6 koz @ 5.34 g/t <sup>1</sup>
Island Mountain (Aurum, Mosquito Creek)	replacement > vein	Aurum: 604 koz @ 14 g/t (1934-1967) <sup>2</sup> Mosquito Creek: 35 koz @ 11.7 g/t (1980-1987) <sup>1</sup>	
Cariboo Hudson (Hudson vein, Shasta vein,	vein > replacement	Hudson: 6.2 koz @ 14.9 g/t <sup>3</sup>	Shasta: 11.5 koz @ 11.2 g/t <sup>3</sup>

1. Brousseau et al., 2017

2. Barkerville Gold Mines Ltd., 2017 [<http://barkervillegold.com/projects>, accessed Oct 1, 2017]

3. BC MINFILE 093A

calc-silicate rocks of the Downey succession of the Barkerville subterrane (Fig. 2). Better known as host the numerous gold deposits of the Wells-Barkerville camp, the Downey succession was emphasized by Höy and Ferri (1998) for its potential to host Besschi-type VMS mineralization.

Sediment-hosted and potentially exhalative Pb-Zn mineralization includes the Vic Pb-Zn-barite occurrence (BC MINFILE 093A 070) and showings of the Cunningham Creek area (Fig. 2). The several conformable Pb-Zn and barite showings of the Cunningham Creek area (Fig. 2) are hosted in dark grey, carbonaceous pelite of the Hardscrabble facies of the Harvey's Ridge succession (Hoy and Ferri, 1998). This area also includes vein-hosted Ag-Pb-Zn-Cu-W-Sb ± Au mineralization of the past-producing 'Silver Mine' (BC MINFILE 093A 090), which was evaluated for structural comparison with Au-dominant veins of the Wells-Barkerville camp (Gavin, 2017; Fig. 2).

## STRUCTURAL GEOLOGY

Structural observations and measurements were made along Highway 26 connecting Quesnel and Barkerville, along networks of forestry service roads, and in mine workings and diamond drill core in the Wells-Barkerville camp (Fig. 2). In general, the strain history interpreted from field observations in this study are consistent with those detailed by previous workers in the region (e.g., Sutherland Brown, 1957; Struik, 1988; Rhys and Ross, 2001; Rhys et al., 2009). Furthermore, field observations and measurements are consistent with the interpretation that the Snowshoe Group is deformed into a major southwest-vergent recumbent nappe, with a second-order fold represented by the Lightning Creek antiform (Ferri and Schiarizza, 2006; Figs. 2-3). In this interpretation, the Downey succession forms the core of the early, first-order anticline. The axial trace of the first-phase recumbent fold is defined east of the Wells-Barkerville camp by structural repetition of the Hardscrabble Mountain facies of the Harvey's Ridge succession on either side of the Downey succession (Figs. 2-3). The east-

ern limb of this first-phase fold is stratigraphically right way up, whereas the western limb is overturned in the Wells-Barkerville mining camp (e.g., Benedict, 1945; Skerl, 1948).

In the interpretation of Ferri and Schiarizza (2006), a structural repetition of the Downey succession is observed on either limb of an open, regional-scale, second-order fold defined by the Lightning Creek antiform (Fig. 3). The outcome of the second phase of folding is to expose the stratigraphically youngest Goose Peak succession in the core of the Lightning Creek antiform.

### Ductile deformation

Snowshoe Group rocks in the Barkerville subterrane have undergone a protracted period of ductile deformation, recorded by early bedding-parallel foliation and shear fabrics, which are overprinted by folding, cleavage formation, and faulting (Struik, 1988). For clarity, the ductile structural history evolution of Snowshoe Group rocks is defined here by four main phases of ductile deformation. However, strain features are interpreted in the context of progressive strain, as opposed to a series of discrete, overprinting deformational events. This viewpoint is similar to that of Struik (1988), who emphasized the importance of the strain environment over the superposition of particular structural elements. Special emphasis was placed in this study on the kinematic and geometric relationships of semi-brittle to brittle features (veins, shears, joints, faults) with ductile features, such that mineralization and alteration could be interpreted in the context of a regional deformation model.

### Bedding

Bedding ( $S_0$ ) is recognized in Snowshoe Group rocks at outcrop scale by compositional layering in metasedimentary and metavolcanic rocks, which locally preserves excellent stratigraphic way-up indicators in the form of graded bed sets (Fig. 5a). Generally however, the younging direction of beds is difficult to define, as bedding is typically highly transposed and disrupted by shear, flow, folding, and boudinage.



Figure 5. (a) Graded bedding in weakly calcareous psammite to semipelite, showing an upward younging direction (Locality 42). (b) Rare recumbent  $F_1$  fold closures in semipelite, highlighted by ferroan carbonate laminae. In the general case where fold hinges are not observed, the  $S_1$  fabric is defined by a bedding-parallel transposition fabric (Locality 99). (c) Spaced  $S_2$  cleavage in impure marble (Locality 61). (d) Preferential formation of the  $S_2$  cleavage fabric in thin semipelitic layers (Locality 42). (e) Prominent rodding in outcrop of psammite and semipelite of the Downey succession (Locality 44). (f) Penetrative  $L_2$  lineation in gritstone defined by stretched quartz grains (Locality 8).

## D<sub>1</sub>

An early, penetrative, bedding-parallel fabric ( $S_1$ ) is expressed in most rocks of the Snowshoe Group, except locally within the Downey succession (specifically in the 'Ramos succession' of Struik, 1988). This  $D_1$  phase of deformation has been attributed by previous workers to relate to thrust emplacement of Mesozoic Nicola Group onto Barkerville subterrane along the Eureka thrust, with initiation of nappe-style folds (Struik, 1988). The  $S_1$  fabric is defined primarily by muscovite, and where original bedding features are observed (e.g., lithological contacts, graded bedding), the fabric is a composite  $S_0/S_1$  fabric. Elsewhere the  $S_1$  fabric is defined by rootless, recumbent isoclinal folds that likely formed as the result of bedding-parallel shear (Struik, 1988; Fig. 5b). In thicker, homogeneous rock sequences, where the earliest ductile fabric has an undefined relationship to bedding, the dominant fabric is generally assumed to be equivalent to  $S_1$ , although in some cases this  $S_1$  fabric is further transposed by overprinting fabrics. Transposed bedding generally dips northeast or southwest, consistent with the regional northwest strike of the Barkerville subterrane (Fig. 6).

The reasonable maximum age of  $D_1$  deformation is likely Late Triassic, as constrained by the age of Quesnellia rocks obducted onto Kootenay terrane. A reasonable minimum age of  $D_1$  deformation is given by the  $167 \pm 2$  Ma zircon age of Ste. Marie pluton located at the northern end of the Barkerville subterrane, which pierces the Eureka thrust (Struik et al., 1992).

Struik (1988) and Rees and Ferri (1983) observed mylonitic fabrics developed in Snowshoe Group rocks in close proximity to the Eureka thrust, and to exposures of Crooked amphibolite and Island Mountain amphibolite (Fig. 2). It was suggested that mylonite represents zones of highest ductile strain during thrust imbrication of these tectonic elements, and therefore, is coincident with  $D_1$  deformation. To date, the sense of shear has not been determined for these rocks, though Rees and Ferri (1983) suggested that Crooked amphibolite was thrust east over the Snowshoe Group, as determined from rotated feldspar megacrysts and shear fabrics in Quesnel Lake orthogneiss.

## D<sub>2</sub>

The bedding-parallel cleavage ( $S_1$ ) is folded by moderately to steeply dipping, northwest-trending, southwest-vergent  $F_2$  folds and overprinted, especially in pelitic rocks, by an axial planar crenulation cleavage fabric,  $S_2$  (Figs. 5c, 6).  $F_2$  folds are highly variable in geometry, ranging from open folds in more competent psammitic layers to tight to isoclinal folds in the less competent pelitic layers (Fig. 5d). In pelitic layers, the limbs of  $F_2$  folds are highly attenuated and exhibit a composite  $S_2/S_1$  transposition fabric. The  $S_2$  fabric is defined primarily by muscovite and locally by biotite, and coincides with peak metamorphic conditions in the district (Struik, 1988). The  $S_2$  cleavage fabric is locally dominant in pelitic layers, and is expressed as a weak, widely spaced cleavage in more competent psammitic to quartzitic units.

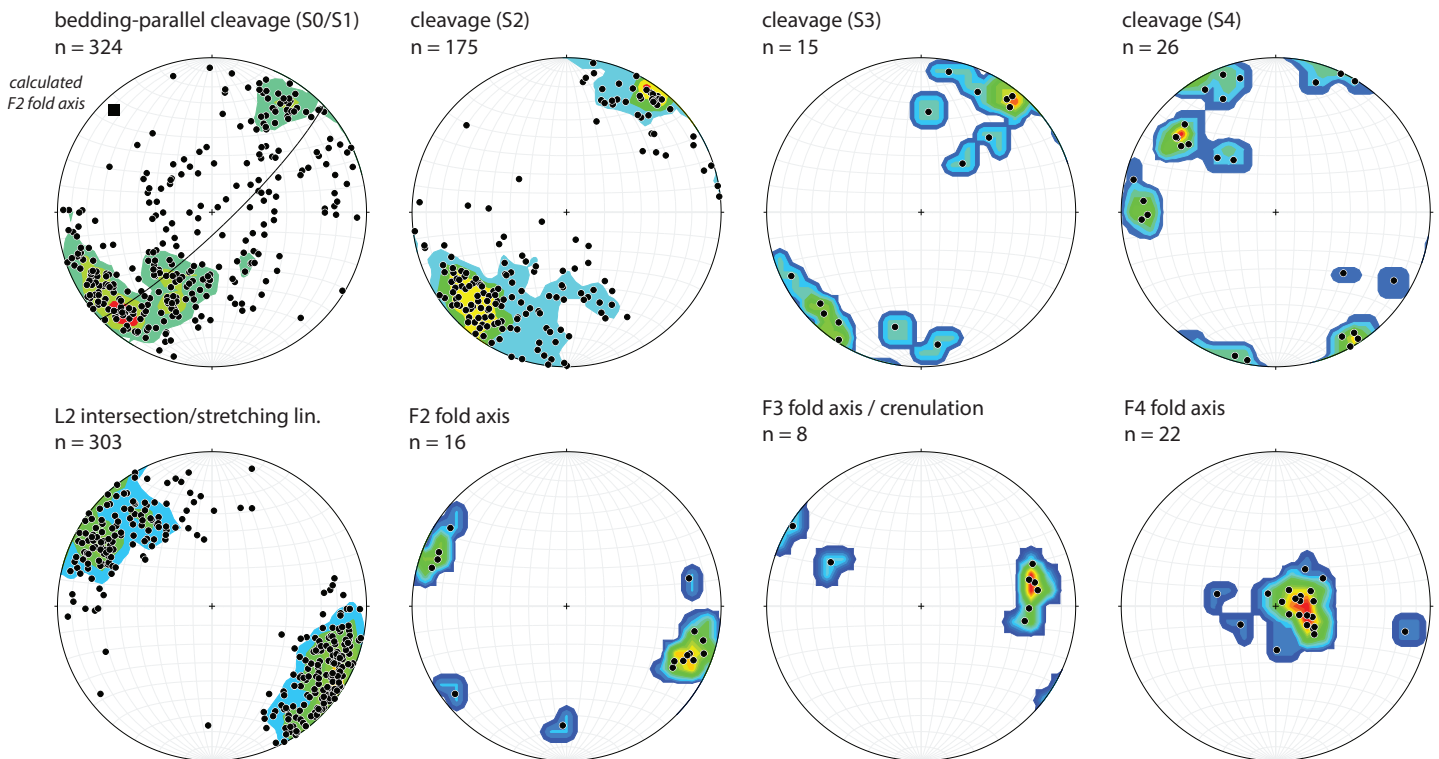


Figure 6. Ductile structural elements of the Cariboo gold district, plotted as equal area lower-hemisphere stereonet projections (poles to planar data).

A penetrative mineral stretching lineation coincides with the lineation defined by the intersection of  $S_2$  and  $S_1$  fabrics. This structural element is prominent throughout the district, and plunges gently to the northwest or southeast (Figs. 5e-f, 6). Most rocks of the Snowshoe Group are L-S tectonites, with the lineation typically defined by prolate aggregates of quartz, but also by elongated porphyroblastic phases such as pyrite and carbonate (Fig. 7a). L-tectonites are locally well developed, indicative of ductile attenuation in the direction of the stretching lineation under constrictional strain conditions.

Generally, the  $L_2$  direction is locally consistent, but varies significantly both along and across strike (Figs. 6, 8). The  $L_2$  lineation is consistently northwest-plunging in the Wells-Barkerville camp (domain C, Fig. 8) but along strike

to the southeast, plunges southeast in the Antler Creek area (domain D) and again to the northwest in the Cunningham Creek area (domain E). The regional structural plunge is therefore interpreted to porpoise with a wavelength of ~20 km in the eastern part of the Barkerville subterrane. Across strike variations are especially notable west of Jack of Clubs Lake, where the northwest structural plunge of the Wells-Barkerville district (domain C) flips to the southeast within rock dominantly of the Harvey's Ridge succession (domain B). Further west, the strike of the  $L_2$  lineation swings toward the west-northwest in accordance with the regional structural grain, and plunges west-northwest (domain A). This structural domain spans across the Eureka thrust and includes conglomerate and siltstone of Quesnellia terrane (Fig. 7b, 8).

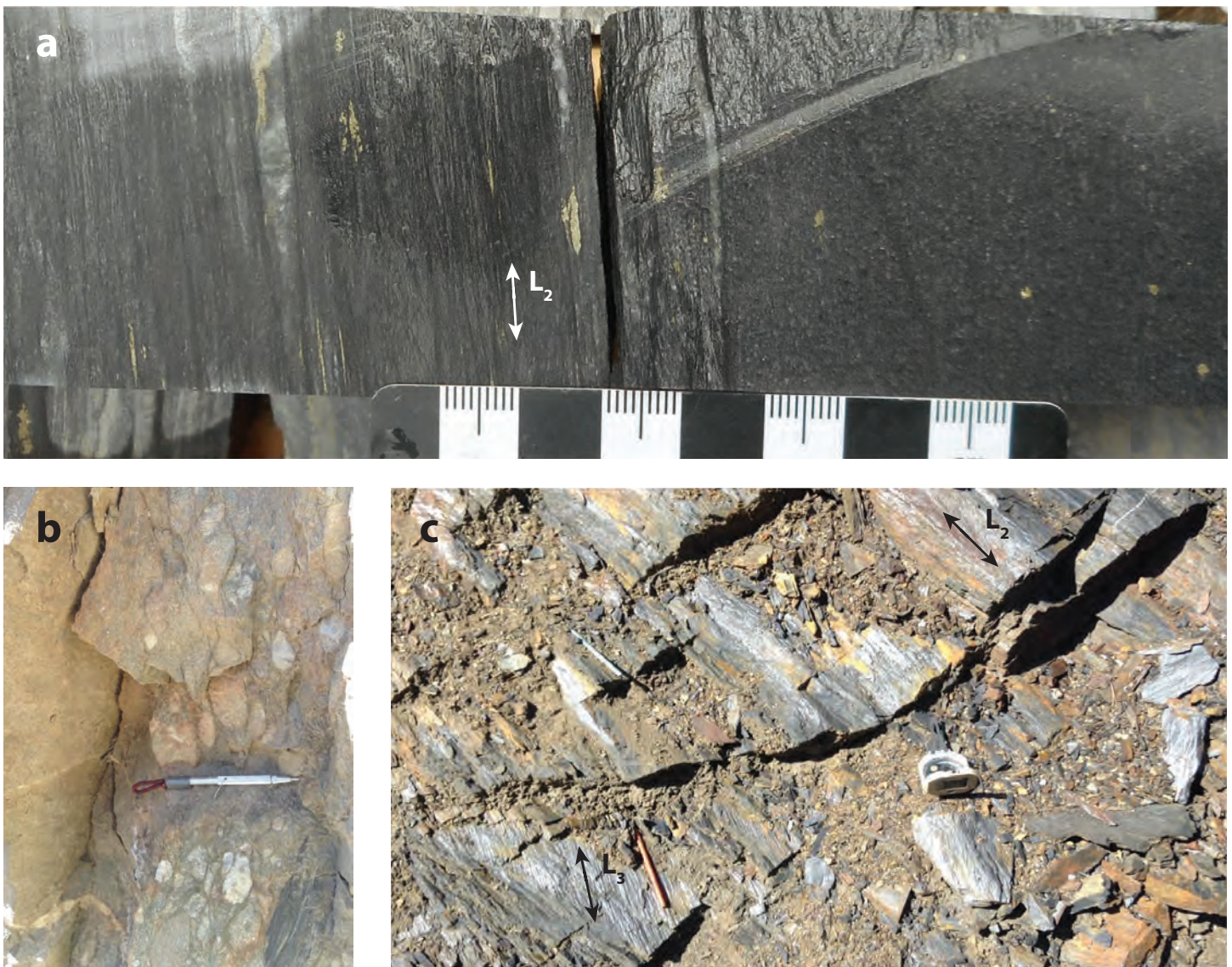


Figure 7. (a) Contact between carbonaceous psammite (right) and pelite (left), showing intense partitioning of ductile strain in the pelitic layer. The pelitic layer exhibits a penetrative  $L_2$  lineation nearly parallel with the cut surface, as defined by stretched quartz ribbons and pyrite aggregates. (b) Foliated and weakly lineated polymictic Wingdam conglomerate of the Quesnellia terrane (Locality 31). (c) Carbonaceous pelite showing both a prominent  $L_2$  lineation (defined by  $F_2$  fold hinges and parallel stretching / intersection lineation) and a weak, locally developed crenulation ( $L_3$ ) (Locality 10).

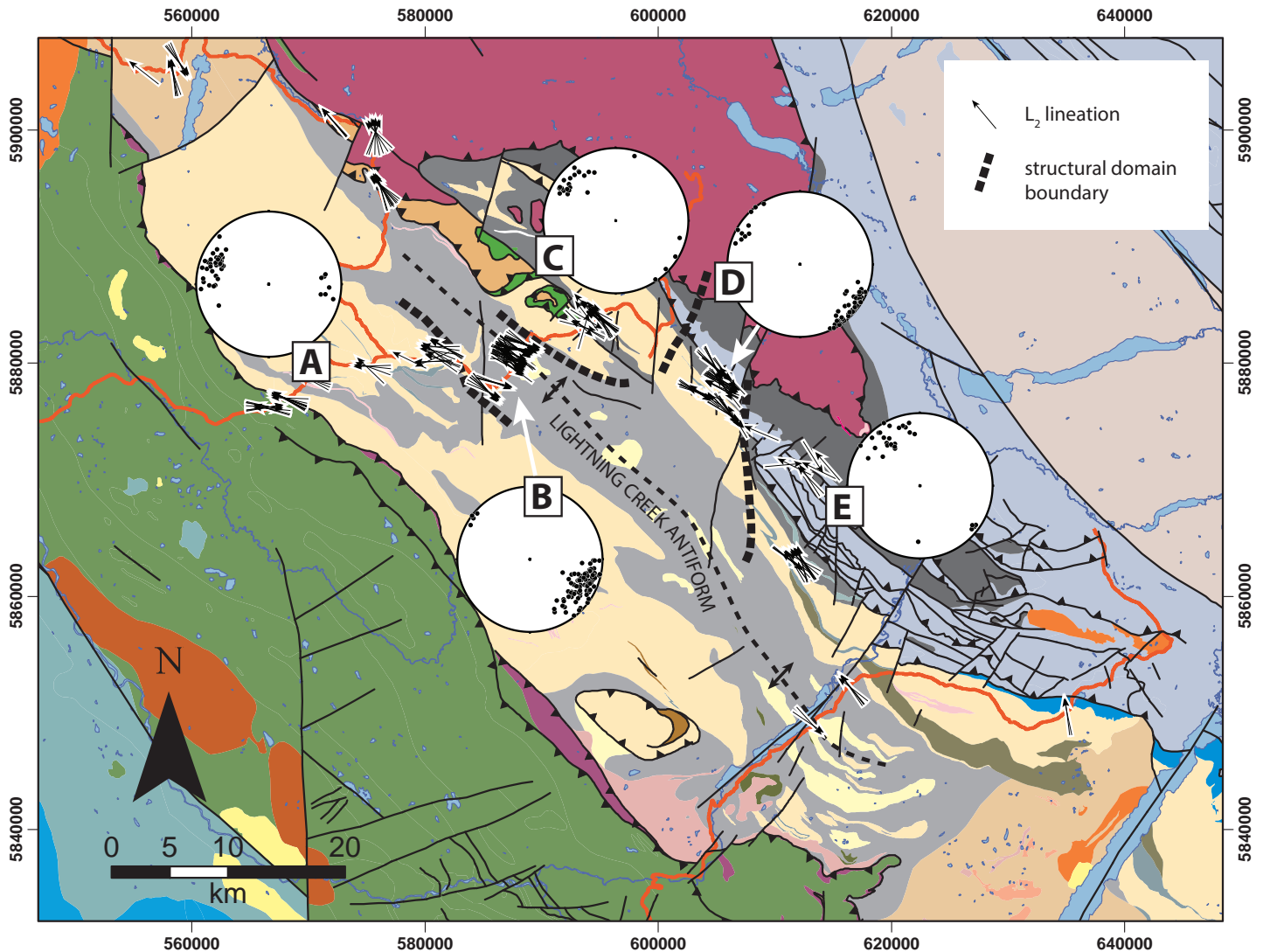


Figure 8. Regional variations in the  $L_2$  lineation, showing both along-strike and across-strike variations. Insets are lower-hemisphere equal area stereonets of  $L_2$  measurements. Geologic legend same as Figure 2.

**$D_3$**   
 An additional, steep and northwest-trending crenulation cleavage ( $S_3$ ) has been described locally in the Cariboo district (e.g., Struik, 1988; Rhys and Ross, 2001; Ferri and Schiarizza, 2006; Fig. 6). This crenulation cleavage is typically absent from more competent lithologies such as psammite and quartzite, but is expressed locally in pelitic rocks (Fig. 7c). Rhys and Ross (2001) noted that in the Wells-Barkerville area, the subhorizontal  $L_3$  crenulation lineation is typically rotated 5-40° anticlockwise of the more prominent  $L_2$  lineation. The  $S_3$  fabric has been interpreted to relate to broad-scale refolding of the regional nappe along the Lightning Creek antiform (Struik, 1988; Rhys and Ross, 2001; Fig. 2).

#### **Chevron folds**

A semi-brittle set of chevrons folds locally deform the pre-existing metamorphic fabric (either  $S_1$  or  $S_2$ ) of metasedimentary rocks of the Snowshoe Group. These folds have wavelengths of 10-20 cm and inter-limb angles of approximately 90°. Chevron folds generally have northeast-trending axial planes and subvertical fold axes (Fig. 6). These folds are particularly well expressed in the magnetite-bearing chlorite-muscovite schist unit exposed in the hanging wall of the B.C. vein in the Bonanza Ledge open pit at Barkerville Mountain (Rainbow 4 subunit of the Hardscrabble Mountain succession, Figs. 4, 9a). The relationship of these chevron folds relative to  $D_3$  features was not observed, so the timing of chevron folds is currently only constrained as post- $D_2$  (Fig. 9b). The timing of chevron fold development relative to veins, alteration, and mineralization is discussed further below.

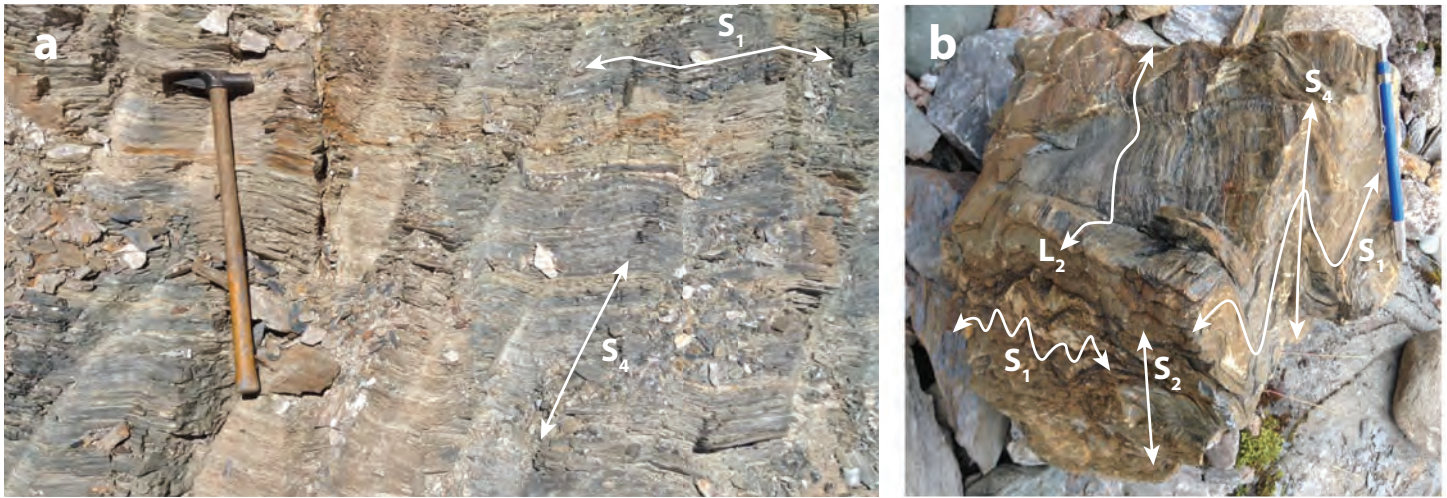


Figure 9. (a) Chlorite-muscovite phyllite affected by sericite-ferroan carbonate alteration (brown weathering zones) and chevron folding of the prominent  $S_1$  transposition fabric (Bonanza Ledge). (b) calcareous semipelite affected by at least three phases of ductile deformation, including formation of the main  $S_1$  fabric, formation of the  $S_2$  crenulation cleavage and  $L_2$  crenulation axis, and nearly orthogonal  $F_4$  refolding at a late stage (Locality 49).

### Mylonite

Mylonitic rocks are exposed in outcrop along the Ketcham Creek FSR approximately 22 km northwest of Wells (Localities 95-96 and 101; Fig. 2). These rocks are in the immediate footwall of the Pundata thrust, which emplaces mafic oceanic rock of the Antler Formation (Slide Mountain terrane) onto siliciclastic rocks of the Snowshoe Group. Mylonite is also observed in float elsewhere along the mapped trace of the Pundata thrust, in contrast to the characterization of Struik (1987) that the Pundata thrust was demarcated mainly of fault breccia. The mylonite at Locality 95-96 is dominated by quartz, feldspar, and muscovite, and is likely psammite of the Snowshoe Group. The mylonitic foliation is moderately north-northwest-dipping, and a penetrative mylonitic lineation plunges  $47^\circ$  toward  $347^\circ\text{N}$ . A consistent top-to-the-north-northwest shear sense is obtained from  $\sigma$ -type mantled quartz porphyroclasts and asymmetric boudinage of feldspar porphyroclasts (Fig. 10). This shear sense suggests that last ductile movement on the Pundata thrust at this locality was subparallel to the regional strike, such that Slide Mountain terrane was moving north-northwestward in an orogen-parallel fashion.

If mylonitization at this locality is correlative with formation of  $S_1$  bedding cleavage elsewhere in the Snowshoe Group as suggested by Struik (1988), then initial collision and imbrication of Slide Mountain terrane onto Barkerville subterrane would have been highly oblique to the margin of ancient North America. This interpretation, however, would require that mylonite at the base of the Pundata thrust escaped overprinting  $D_2$ -related penetrative bulk strain, and particular the formation of a northwest-trending  $S_2$  cleavage fabric. In the absence of dating studies on the formation of mylonitic fabric here, it remains possible that mylonitic fabrics associated with movement on the Pundata

thrust are later, potentially  $D_2$ -related features. The tectonic setting of these mylonites is explored further below.

### Faults

The Eureka thrust defines the western limit of the Barkerville subterrane, and accommodates obduction of the Quesnellia terrane onto the margin of ancestral North America (Fig. 2). An early origin of the Eureka thrust is emphasized by the occurrence of the same penetrative ductile strain features on either side of the fault. For example, the Wingdam conglomerate of the Quesnellia terrane occurs in the immediate footwall of the Eureka thrust, and is exposed in a roadcut along Highway 26 (Locality 31; Figs. 2, 7b). Polymictic conglomerate, gritstone, and sandstone at this location have a steeply north-northeast-dipping, penetrative  $S_1$  fabric parallel to bedding, which mimics the regional strike at that location. Rocks are overprinted by a weak and locally developed, subvertical, west to west-northwest-trending  $S_2$  fabric. A penetrative stretching lineation ( $L_2$ ) defined by elongate pebbles and quartz aggregates plunges shallowly to the west-northwest (Fig. 8). Widely spaced extensional quartz veins, typically less than 1 cm-wide, occur sub-perpendicular to the stretching lineation – a pervasive feature of Snowshoe Group in the Cariboo Gold District (see below). The structural elements present at Wingdam are identical to those developed throughout Snowshoe Group rocks in the Barkerville subterrane, so it is reasonable to assert that the Eureka thrust itself was involved in the same progressive deformation history (Fig. 3).

Several west-verging thrust faults, including the Pleasant Valley thrust, are mapped in the eastern part of the Barkerville subterrane and accommodate northeast-southwest shortening (Struik, 1988; Fig. 2). The timing of the Pleasant

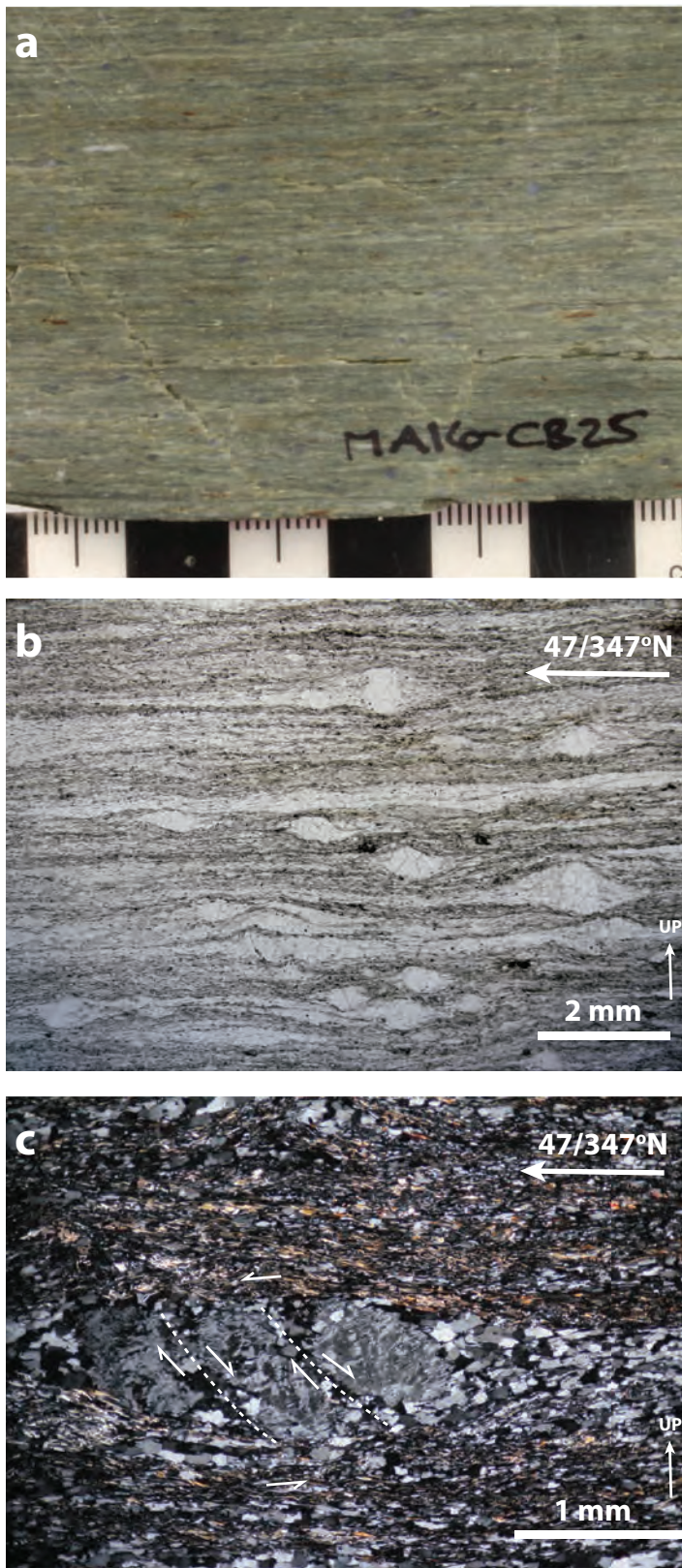


Figure 10. (a) Siliciclastic mylonite associated with the Pundata thrust (Sample MA16-CB25, Locality 95/96). (b) Plane-polarized microphotograph of same sample showing  $\sigma$ -type mantled quartz porphyroclasts. Stepping direction of porphyroclast mantles indicates top-to-the-left (top-to- $347^{\circ}\text{N}$ ) shear sense (Sample MA16-CB25). (c) Asymmetric boudinage of a feldspar porphyroclast in MA16-CB25, which indicates the same top-to- $347^{\circ}\text{N}$  shear sense (Sample MA16-CB25). Cross-polarized microphotograph.

Valley thrust is uncertain, but it was suggested by Ferri and Schiarizza (2006) that it could be closely related in timing and geometry to the post-nappe Pundata thrust and other thrusts northwest of Wells that emplace klippen of Slide Mountain terrane, Island Mountain amphibolite, and Tom Formation on top of the Snowshoe Group (Fig. 2).

The Cariboo district is transected by a set of steep, north to north-northeast-trending faults, including the Antler Creek fault (Fig. 2) and the Lowhee fault (Fig. 4). In map view, these faults have apparent dextral offsets of approximately 2-3 km and 700 m respectively, but some of the apparent horizontal offset on faults of this generation may be explained by a component of down-to-the-east normal movement. Carbonaceous clay gouge and strongly cleaved wall rock along the Lowhee fault reveal a steep easterly dip to the structure, and gouge fabrics indicate dextral strike-slip movement. Relict shear fabrics in gouge of the Lowhee fault indicate an earlier, semi-brittle to ductile character to the fault, suggesting that the structure may have initiated during the later stages of ductile deformation. The Antler Creek fault offsets both the Pleasant Valley thrust and Pundata thrust (Fig. 2), indicating that movement is primarily late and post-dates the collision-related thrust architecture of the region.

Steeply dipping, northeast-trending AC-joints are oriented sub-perpendicular to the penetrative  $L_2$  lineation, and these occur in all lithologies. Joint spacing is highly variable, but is generally denser in argillaceous units and more widely spaced in quartzite, psammite, or limestone units. These joints control the orientation of variably mineralized extensional veins (see below). Locally, AC-joint sets have been reactivated as steep, brittle fault features, presumably exploiting zones of pre-existing weakness (Fig. 11a).

## Veins

Three main groups of veins have been recognized through mining and mapping activities in the Cariboo district: 'transverse veins' (extensional veins), 'diagonal veins' (shear veins), and 'strike veins' (fault-fill veins). The orientations and kinematics of these veins are essential to understanding the structural evolution and metallogenesis of the Cariboo gold district, and are described in greater detail here:

### Extensional veins

Extensional veins are ubiquitously steeply dipping and northeast-trending, and are sub-perpendicular to the northwest-trending and shallowly plunging  $L_2$  lineation (Fig. 12). These veins are dominated by milky quartz and orange-brown-weathering ferroan carbonate gangue, with subordinate pyrite and muscovite (Figs. 11b-c). Locally, in calcareous host rocks, extensional veins may be dominated by carbonate (e.g., Locality 59; Fig. 2). Extensional veins are highly variable in thickness, from millimetre to decimetre scale, although centimetre-scale veins are the most typical.

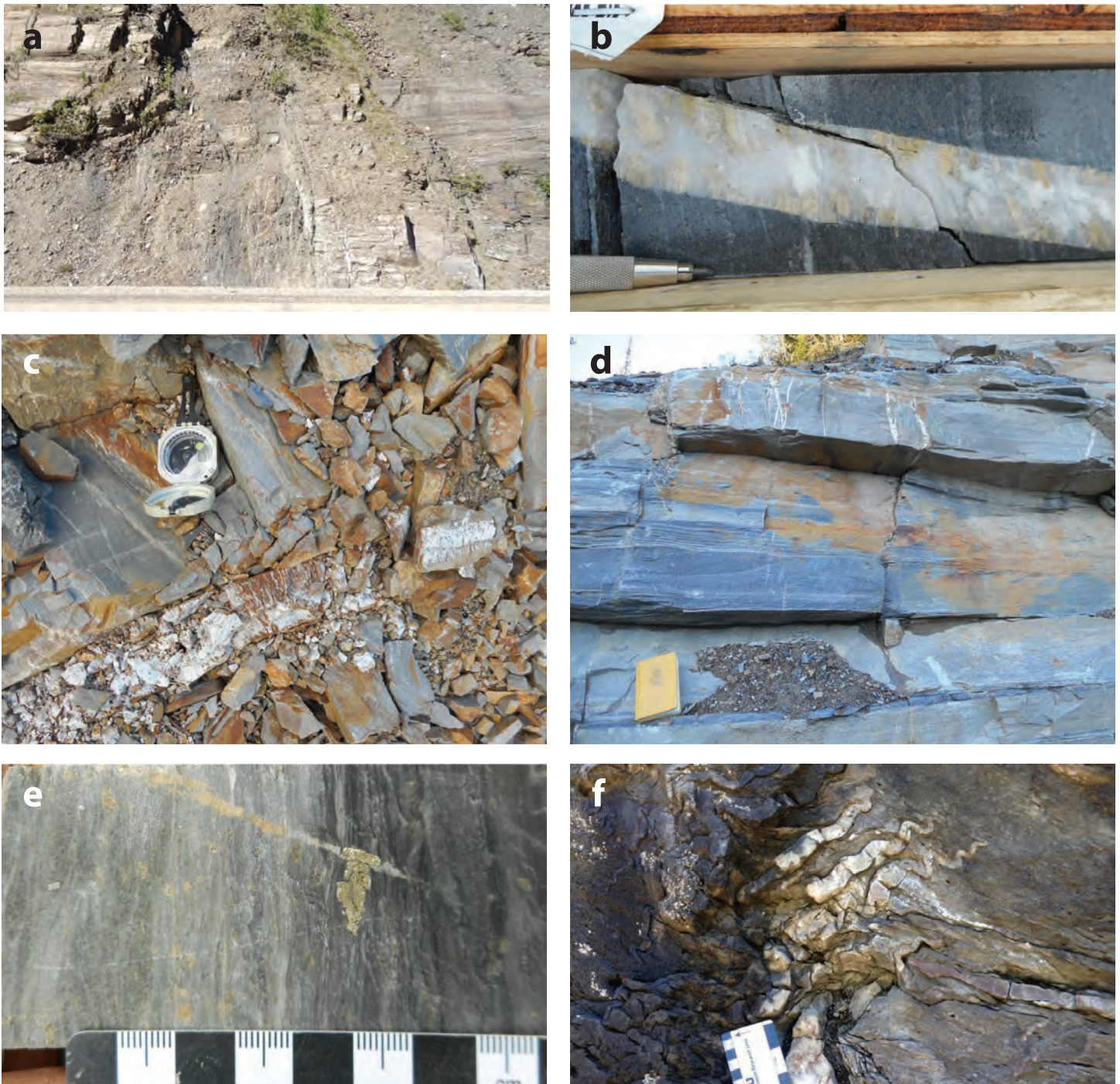


Figure 11. (a) Steep, north-trending fault zone with down-to-the-east movement. The fault zone coincides with a zone of high AC-joint and extensional vein density, at a high angle to the prominent  $L_2$  lineation (Locality 10). (b) Barren quartz-ferroan carbonate extensional vein cutting psammite at a high angle to the penetrative  $L_2$  lineation (approximately in the plane of the cut drill core surface). Note the fibrous habit of the vein margins. (c) Steep, northeast-trending extensional quartz-ferroan carbonate vein, typical of the Cariboo gold district (Locality 42). (d) Lithological control on the width and density of extensional veins (view to the northeast. Note a component of down-to-the-east movement indicated by the veinlet array in the centre of the photograph (Locality 42). (e) Extensional quartz-carbonate-pyrite veinlet in which vein mineralogy coincides with heterogeneities in the wall rock composition. Note the restriction of vein carbonate to the pale grey-green horizon on the left containing pale orange carbonate porphyroblasts, and the restriction of pyrite to the vein section immediate adjacent to a lens of pyrite in the wall rock. (f) Ptygmatic folding of early extensional quartz veins by overprinting  $D_2$  deformation (Locality 10).

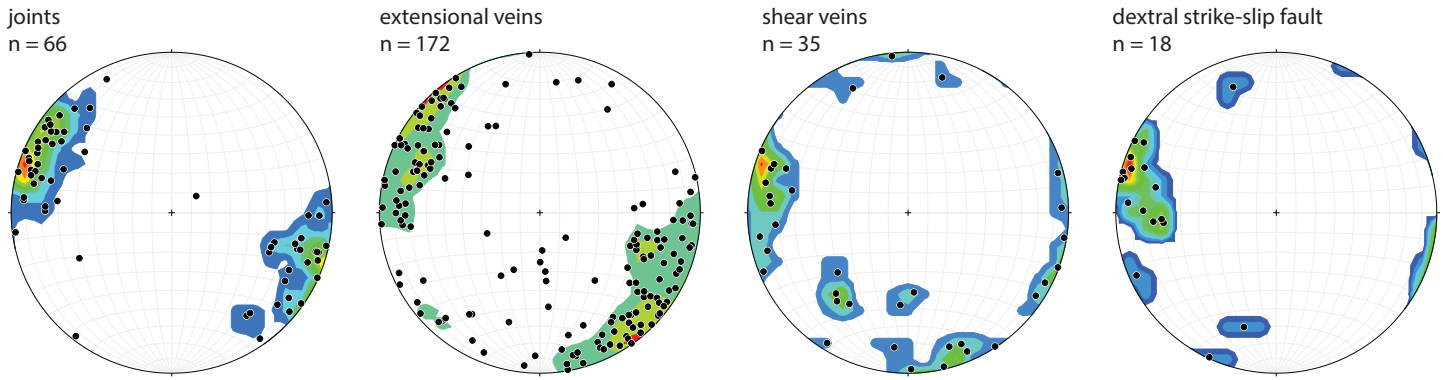


Figure 12. Brittle structural elements of the Cariboo gold district, plotted as equal area lower-hemisphere stereonet projections (poles to planar data).

Extensional veins typically have limited strike and dip extent. Where hosted in heterogeneous psammite-semipelite-pelite packages, veins are typically restricted to psammite, or they diminish in thickness according to increasing mica content (Fig. 11d). This observation suggests that in the late, low-strain contraction deformation history of the Snowshoe Group, bedding-parallel stretching of competent units was accommodated primarily by brittle failure and formation of fracture-filling veins, whereas micaceous units underwent ductile thinning even at the latest stages of deformation.

Fibrous to columnar growth habits are common in extensional veins, with grains oriented sub-perpendicular to vein walls (Figs. 11b-c). Veins with this growth habit grew incrementally by epitaxial growth of new vein material onto the wall rock substrate, as recognized by optical continuity of adjacent vein and wall rock grains when observed petrographically. The mineralogy of the veins is most commonly inherited from the immediate wall rock, such that variations in the quartz, carbonate, muscovite, and pyrite content of fibrous veins may directly reflect grain-scale compositional heterogeneities in the host rock (Fig. 11e). Larger extensional veins may have fibrous or columnar margins, but are typically dominated by massive quartz. These veins may have vuggy interiors defined by inward growth of prismatic quartz crystals, indicative of vein growth into open space as dictated by high rates of dilation relative to fluid and/or silica supply.

Though many extensional veins in the Snowshoe Group are undeformed and represent the latest stage of brittle deformation, others are overprinted by deformation. Ptygmatically folded extensional veins are common, and indicate progressive ductile tightening of mesoscopic folds that locally underwent brittle failure and veining at an early stage of deformation (Fig. 11f). More typically, sigmoidal vein arrays represent *en echelon* arrays of extensional veins that were deformed by ductile, semi-brittle, or brittle shear in the plane of the array (Fig. 13a). Mutually cross-cutting or

joining shear and extensional features indicate that overall, however, they are kinematically linked (Figs. 13-14).

Extensional veins are commonly pyrite-bearing and may contain gold mineralization. In the underground workings of the Wells-Barkerville camp, extensional veins were historically overlooked in most cases in favour of higher-grade shear veins or replacement-style ore. However, these represent an attractive additional target for future underground development (Barkerville Gold Mines Ltd., 2017).

### Shear veins

Veins and vein arrays dominated by strike-slip or oblique-slip movement (shear veins) occur in two main orientations in the Cariboo district: (1) a north-northwest to north-northeast striking set dominated by dextral shear sense and a component of down-to-the-east normal displacement; (2) an approximately east-southeast striking set dominated by sinistral shear sense (Figs. 12, 14). Shear veins of either orientation are commonly flanked by, or terminate as, *en echelon* vein arrays with extensional vein tips oriented approximately northeast. Shear sense is typically given by the sense of rotation of  $S_1$ ,  $S_2$ , or  $L_2$  fabrics, or of previously formed extensional veins (Fig. 13a).

Shear veins typically have complex internal textures that indicate multiple phases of vein mineral growth and deformation (Fig. 13c). However, they are typically dominated by massive, bull quartz (Fig. 13b, d) and may contain sheared wall rock or vein fragments. Shear veins are commonly mineralized, are typically higher grade than extensional veins, and comprise an important part of historic underground gold production in the Wells-Barkerville camp. Field observations of north-strike dextral faults containing quartz vein fragments in gouge, and with adjacent zones of sericite-carbonate alteration, indicates that some shear veins evolved into larger displacement strike-slip or oblique-slip faults (Fig. 14).

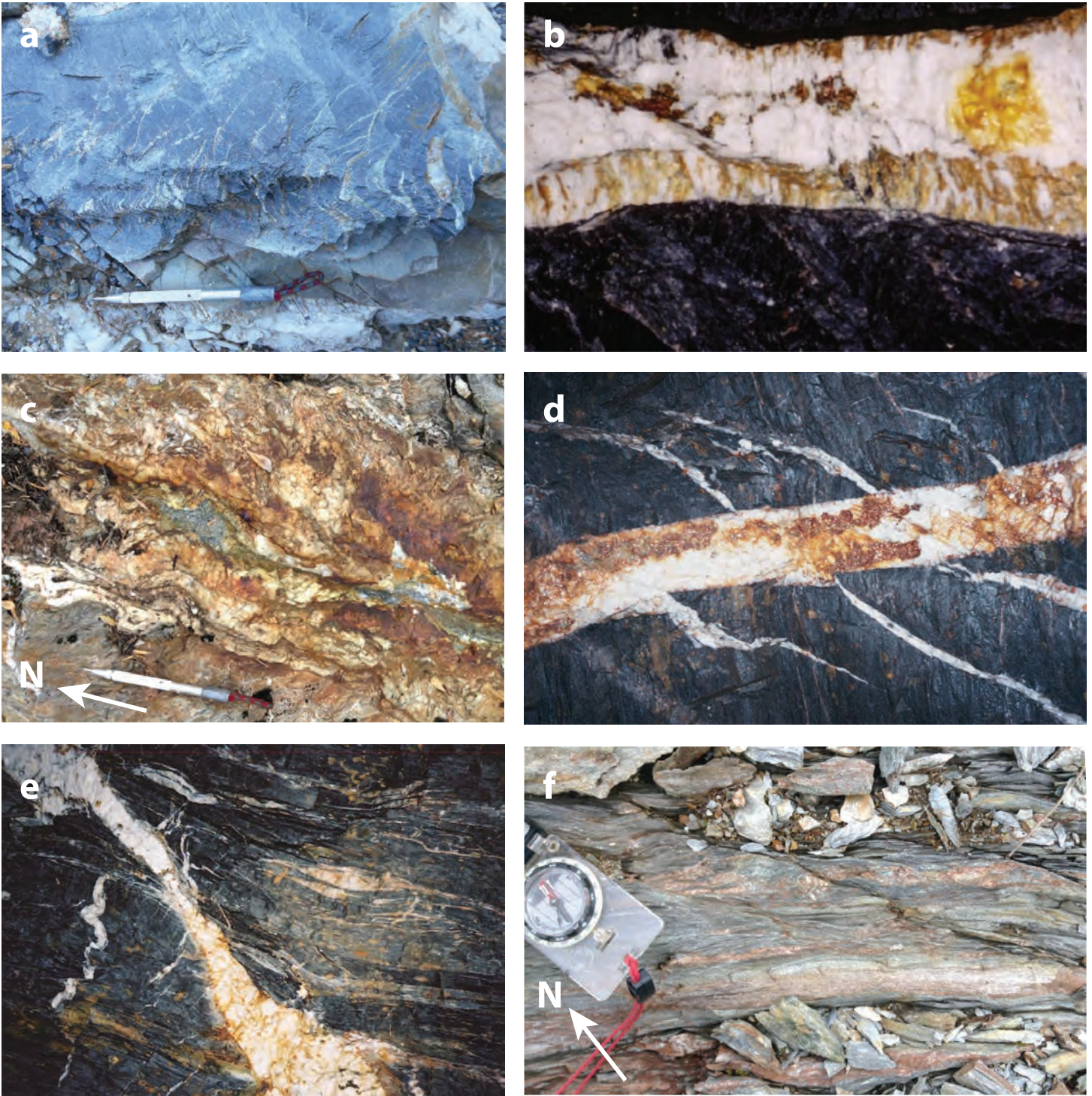


Figure 13. Semi-brittle to brittle shear features of the Cariboo gold district. (a) Sigmoidal vein array in which an *en echelon* array of extensional quartz veinlets has been overprinted by an inner zone of mainly ductile sinistral shear (Locality 42). (b) Shear band cutting a previously formed, extensional quartz-ferroan carbonate vein, Cariboo Gold Quartz mine (from Rhys et al., 2009). (c) North-trending pyritic shear vein with well-developed internal shear fabrics and external rotation of host rock foliation (Locality 80). Dextral shear sense. (d) Pyritic shear vein flanked by an extensional vein array, Cariboo Gold Quartz mine, 1200 level, view up at the back (from Rhys and Ross, 2001). (e) Multiple vein generations, including early barren veins transposed into the  $S_2$  foliation (top right), intermediate-aged veins that are ptlygmatically folded (left), and a late, pyritic shear vein with flanking extensional veins (middle). View to south, Cariboo Gold Quartz mine, 1200 level (from Rhys and Ross, 2011). (f) Calcareous pelite cut by north-northwest-trending,  $C'$  type shear bands with dextral shear sense. These shear bands mimic the orientation and shear sense of shear veins and faults of more significant strike length (Locality 99).

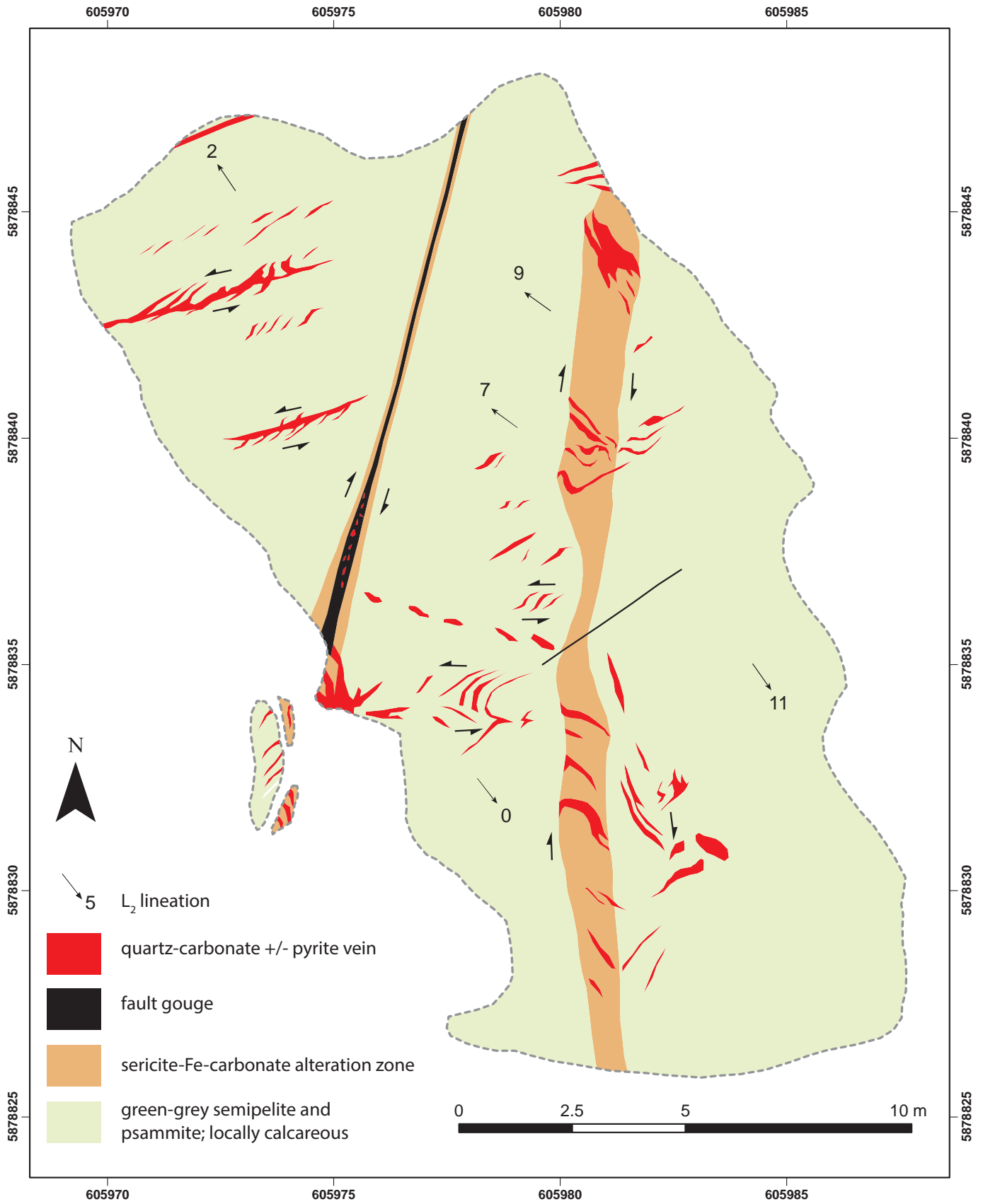


Figure 14. Detailed geologic map of a metaturbidite exposure showing the kinematic relationships between north-east trending extensional veins, east-northeast trending sinistral shear veins, and north to north-northeast trending dextral shear zones (Locality 42). The western shear zone is a fault with brittle gouge, flanked by extensional veins (southwest corner of map), indicating that the fault likely originated as a dextral shear vein. Note the coincidence of sericite-ferroan carbonate alteration with the dextral shear zones.

### 'Strike veins'

A small number of economically significant 'strike veins' in the Cariboo district share the same map trend as the regional stratigraphic fabric. A corridor of strike veins is present in the Barkerville and Cow Mountain area, and includes the B.C., Canusa, and Black Bull veins (Fig. 4). The largest and most significant is the B.C. vein, which occupies the steeply northeast-dipping B.C. fault in the Barkerville Mountain area (Fig. 4). The fault system associated with the B.C. vein is semi-conformable with a carbonaceous phyllite member of the Hardscrabble Mountain succession (Fig. 4). The vein is overlain in the hanging wall by a distinctive magnetite-bearing muscovite-chlorite phyllite unit (Rainbow 4 sub-unit), and underlain in the footwall by variably calcareous metasilstone that hosts replacement-style mineralization in the Bonanza Ledge zone (Lowhee unit; Fig. 15a).

The B.C. vein is typically several metres thick but is boudinaged into several bodies along strike. The vein is internally deformed and faulted, as indicated by stylolites, shear fabrics, cross-cutting seams of carbonaceous gouge, and slickensided surfaces (Fig. 15b). Latest movement on the

B.C. vein structure was oblique reverse-dextral, as indicated by striated quartz surfaces, oblique cleavage and gouge fabrics in drill core and outcrop (Rhys and Ross, 2001). The B.C. vein is well mineralized in the Bonanza Ledge zone of Barkerville Mountain, with grades commonly exceeding 10 g/t Au (Rhys and Ross, 2001). Mineralized portions of the vein are characterized by breccia containing fragments of early, barren vein material in relatively undeformed cement of quartz and pyrite. Although the B.C. vein is spatially coincident with replacement-style mineralization at Bonanza Ledge, Rhys and Ross (2001) argued that the B.C. vein is a distinctly later structure that obliquely cuts pre to syn- $D_2$  mineralization in the footwall.

The argentiferous quartz-sulphide vein exposed at Silver Mine (Fig. 2) occupies a steep, north-northwest-trending fault that separates black, carbonaceous phyllite to the west from non-carbonaceous phyllite to the east. The vein is also internally deformed and was interpreted on the basis of its orientation and its relationship to extension and shear veins in the area to be a fault-fill vein similar in structural setting to the B.C. vein (Gavin, 2017).

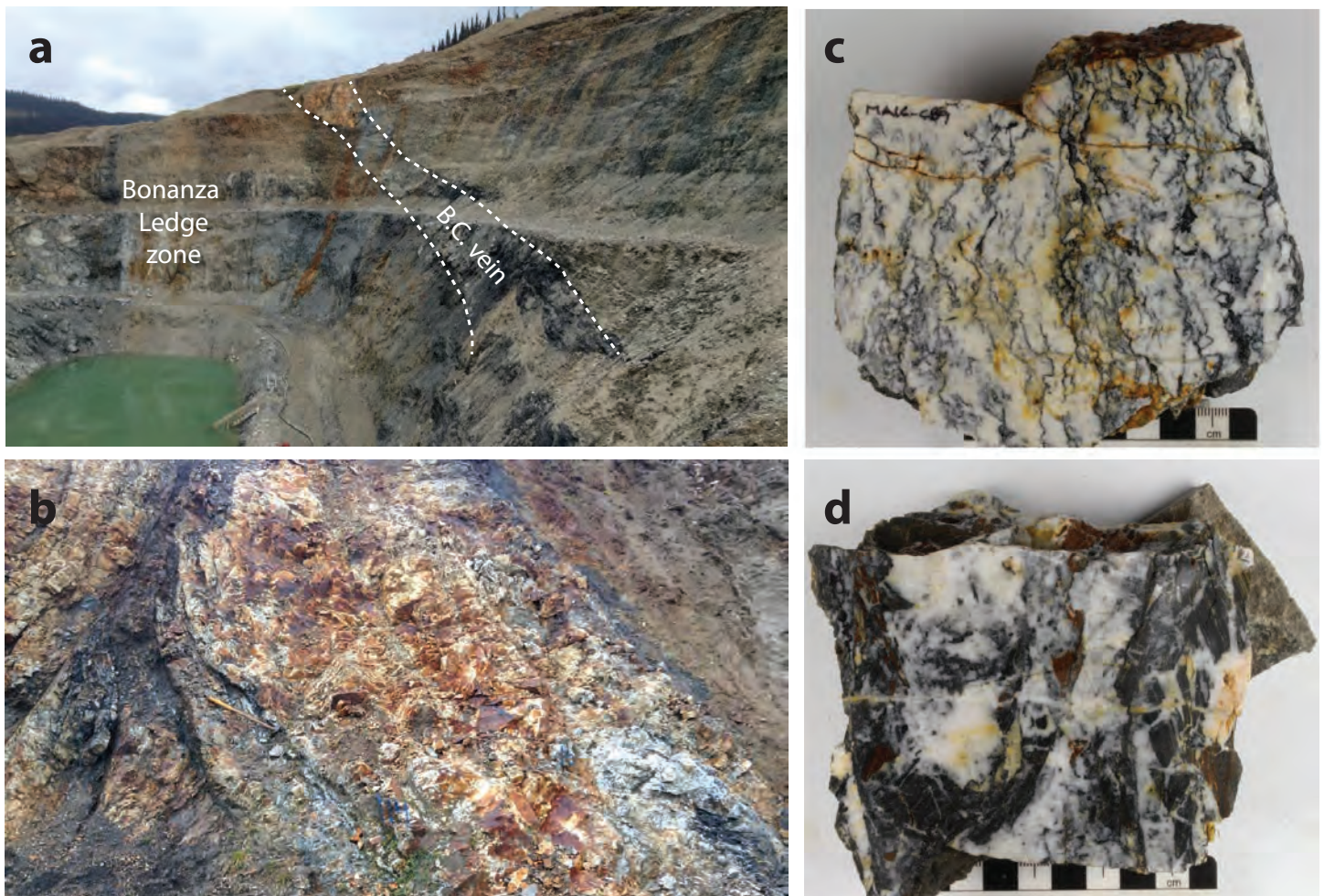


Figure 15. (a) Trace of the B.C. vein through the Bonanza Ledge open pit (view to the northwest). (b) Brecciated portion of the B.C. vein, intersected by sheared seams of carbonaceous pelite. (c) Sample of the B.C. vein cut by numerous carbonaceous stylolites (Sample MA16-CB9). (d) Sample of the B.C. vein showing carbonaceous wallrock fragments in quartz cement (Sample MA16-CB6).

### Chevron fold-related veins

Extensional veins are locally coincident with the northeast-trending axial planes of late, angular kinks and chevron folds. In a few cases, veins occupy the outer hinge of chevron folds as tensile accommodation features (Fig. 16a). However, in the general case, through-going extensional veins that parallel the axial planes of chevron folds are kinematically compatible with earlier, southwest directed (orogen-normal) progressive  $D_2$  deformation, rather than having any temporal or kinematic relationship with the chevron folds that formed by northwest-southeast (orogen-parallel) shortening (Fig. 16b). An appropriate interpretation is that pre-existing veins or vein margins represent mechanical discontinuities on which the overprinting semi-brittle chevron folds nucleate.



Figure 16. (a) Rare example of a  $D_4$  fold-related vein. This fibrous quartz-carbonate vein formed as an extensional accommodation feature during  $F_4$  folding perpendicular to the  $L_2$  lineation. (b)  $F_4$  kink fold superimposed on a pre-existing extensional vein.

### Timing of mineralization and alteration

Most of the visible alteration in the Cariboo gold district occurs as bleached zones of fracture-controlled or stratigraphically controlled sericite-carbonate-pyrite  $\pm$  quartz alteration that are chlorite and/or carbon-destructive (Fig. 17a). Alteration is typically associated with quartz  $\pm$  carbonate  $\pm$  sulphide veins, and extends symmetrically as vein haloes into the wall rock a few centimetres away from narrow veins, and up to a few metres away from the largest veins. Alteration is more pronounced adjacent to veins with massive to prismatic quartz textures, suggesting that host rocks are out of equilibrium with acidic,  $CO_2$ -charged fluids. In contrast, fibrous veins typically have little or no associated visible alteration, indicating their formation under rock-buffered conditions with limited introduction of external fluid components. Alteration is locally conformable to stratigraphy, as dictated by the relative reactivity and permeability of individual horizons in the Snowshoe Group (Fig. 9a).

Vein formation in the Cariboo Gold District occurred throughout the Snowshoe Group's progressive strain history, as indicated by the overprinting of ductile deformation on early veins (Fig. 11f), and the formation of undeformed veins and alteration haloes that overprint all ductile features. Similarly, hydrothermal alteration and mineralization was introduced at several stages during progressive deformation. Early hydrothermal features include syn- to late- $D_1$  pyrite and carbonate porphyroblasts (Fig. 17a), which are locally overprinted by  $S_2$  fabrics (Fig. 17b), or stretched into parallelism with the  $L_2$  stretching lineation (Fig. 7a). An example of ductily deformed mineralization is the replacement-style ore at Bonanza Ledge, in which pyrite veinlets are overprinted by  $D_2$ -related folding and boudinage, pyrite grains have developed pressure shadows, and alteration minerals have been transposed into  $S_2$  surfaces (Rhys and Ross, 2001; Mortensen et al., 2011).

In general, early veins are only weakly mineralized in the Cariboo gold district, with typical gold grades  $< 2$  g/t (Mortensen et al., 2011). In contrast, the majority of ore-grade gold-bearing veins are weakly strained to unstrained, and therefore formed at the latest stages of progressive deformation (i.e., syn-late  $D_2$ ). Recent observations by Barkerville Gold Mines Ltd. (2017) suggest that much of the gold was introduced and/or remobilized during the latest brittle deformation of vein features themselves, such that veins may represent favourable host rocks to mineralization.

## GEOCHRONOLOGY

Samples of metamorphic and hydrothermal mica were analyzed by  $^{40}\text{Ar}/^{39}\text{Ar}$  methods to constrain the age of deformation and mineralizing events in the Cariboo district, building on previous geochronological studies (Alldrick, 1983; Andrew et al., 1983; Rhys et al., 2009; Mortensen et al., 2011). Biotite from lamprophyre dikes cutting argentiferous veins in the Silver Mine area (Fig. 2) was also analyzed to constrain the age of mafic alkaline magmatism.

All  $^{40}\text{Ar}/^{39}\text{Ar}$  analyses were performed by Alfredo Camacho at the University of Manitoba using the methods described in Appendix 1. Data and step-heating age spectra are provided in Appendix 2.

### $^{40}\text{Ar}/^{39}\text{Ar}$ Results

Sample MA16-CB05 is a muscovite-bearing extensional calcite vein from a cliff-forming roadcut of massive, grey to buff-coloured dolomitic marble of the Neoproterozoic Cunningham Formation of the Cariboo Group, Cariboo subterrane (Locality 59; Fig. 2). An initial analysis of muscovite yielded a poor  $^{40}\text{Ar}/^{39}\text{Ar}$  age spectrum, complicated by high Ca/K ratios arising from calcite intergrowths. A subsequent analysis of muscovite grains treated with dilute hydrochloric yielded a plateau age of  $155.4 \pm 0.3$  Ma, which is interpreted as the age of extensional vein formation.

Sample MA16-CB23 is a fibrous quartz-carbonate-muscovite-pyrite vein that cuts weakly calcareous psammite and semipelite from a package of graded metaturbidite, most likely of the Midas Formation of the Neoproterozoic Cariboo Group, Cariboo subterrane (Locality 42/100; Fig. 2). Muscovite in this vein is immediately adjacent to a thin micaceous layer in the host rock, whereas quartz and minor carbonate occur immediately adjacent to calcareous psammite. Two aliquots of vein muscovite both yielded slightly rising  $^{40}\text{Ar}/^{39}\text{Ar}$  age spectra, with the age of muscovite growth estimated at 155 – 153 Ma (Table 2).

Sample MA16-CB15 is a quartz-sericite-pyrite vein that cuts phyllite in historic workings of the Silver Mine occurrence (BC MINFILE 093A 090; Fig. 2). Coarse, randomly oriented sericite in the vein most likely represents hydrothermally altered wall rock. Sericite yielded a rising  $^{40}\text{Ar}/^{39}\text{Ar}$  age spectrum, with a reasonable plateau age of  $136.7 \pm 0.2$  Ma defined by intermediate argon release steps (Table 2). MA16-CB21 is a similar sericite-bearing vein sample from the Penny Creek occurrence, which yielded an asymptotically rising  $^{40}\text{Ar}/^{39}\text{Ar}$  age spectrum indicating  $\sim 140$  Ma sericite that is partially reset by a thermal overprint. The results of this study are in close agreement with previous  $^{40}\text{Ar}/^{39}\text{Ar}$  age determinations for muscovite in the nearby Jewelry Box ( $141.0 \pm 1.6$  Ma) and Hibernian ( $137.4 \pm 1.6$  Ma) veins (BC MINFILE 093A 051; Mortensen et al., 2011).

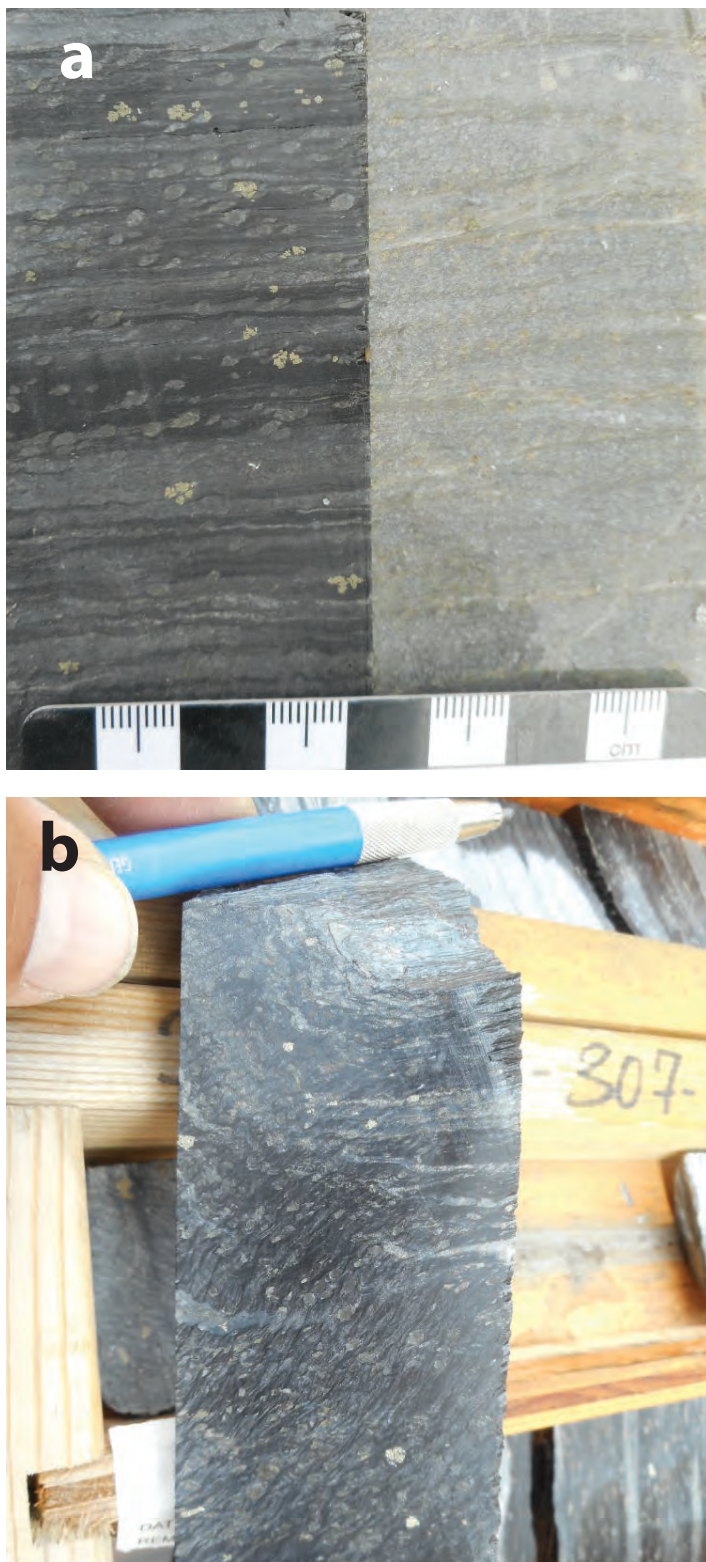


Figure 17. (a) Left: carbonaceous pelite with porphyroblasts of pale grey carbonate and brassy pyrite, potentially linked to an early, syn-deformational phase of hydrothermal alteration. Right: Same lithology on the left, affected by late-stage, carbon-destructive, sericite-carbonate alteration. (b) Same carbonaceous pelite lithology as in Figure 17a, overprinted by an  $S_2$  crenulation cleavage that post-dates carbonate and pyrite porphyroblasts. The drill core specimen is cut obliquely to the  $L_2$  crenulation axis ( $L_2$  visible at the top of the specimen, parallel to the pencil),

Table 2:  $^{40}\text{Ar}/^{39}\text{Ar}$  results, Cariboo gold district

Sample (Mineral)	Terrane	Location / Unit	Description	Age (Ma) $\pm 2\sigma$	Analytical Notes
MA16-CB05 (muscovite)	Cariboo	Locality 59 / Cunningham Fm. (Cariboo Gp.)	Coarse muscovite in calcite vein; vein cuts pale grey dolomitic marble	155.4 $\pm$ 0.6	Sample treated with dilute HCl; plateau age; steps 2-4 of 4; MSWD = 2.2; prob = 0.11; includes 74.7% of the $^{39}\text{Ar}$
MA16-CB23 (sericite)	Cariboo	Locality 100/42 / Midas Fm.? (Cariboo Gp.)	fibrous quartz-carbonate-muscovite-pyrite vein	154.6 $\pm$ 0.8 (aliquot 1) 153.6 $\pm$ 1.5 (aliquot 2)	Aliquot 1: rising age spectrum; steps 5-11 of 12; MSWD = 17; prob = 0.0; includes 81.6% of the $^{39}\text{Ar}$ Aliquot 2: rising age spectrum; steps 4-7 of 13; MSWD = 8.2; prob = 0.0; includes 57.5% of the $^{39}\text{Ar}$
MA16-CB15 (sericite)	Barkerville	Silver Mine / Harvey's Ridge succession (Hardscrabble Mountain succession)	Quartz-pyrite vein, including sericitized phyllite seams	136.7 $\pm$ 0.2 (aliquot 2)	Rising spectrum; steps 4 – 7 of 12; MSWD = 1.7; prob. = 0.17; includes 59.9% of the $^{39}\text{Ar}$
MA16-CB21 (sericite)	Barkerville	Penny Creek	quartz-pyrite-sericite vein	~140 Ma	Rising spectrum, no plateau
RG16-CB03 (biotite)	N/A	Silver Mine / lamprophyre	Biotite-clinopyroxene-olivine lamprophyre; talc-serpentine-carbonate altered	114.2 $\pm$ 1.2	Grain 1: weighted average of steps 3-4 of 4; includes 89.0% of the $^{39}\text{Ar}$
RG16-CB06 (biotite)	N/A	Silver Mine / lamprophyre	Biotite-clinopyroxene-olivine lamprophyre; talc-serpentine-carbonate altered; pyritic	112.2 $\pm$ 1.7	Grain 4: weighted average of steps 2-3 of 4; includes 96.7% of the $^{39}\text{Ar}$
WB15 (biotite)	N/A	Penny Creek / lamprophyre	Altered lamprophyre with fresh biotite	113.4 $\pm$ 0.8	excellent plateau; steps 4-7 of 7; MSWD = 0.50; prob. = 0.68; includes 86% of the $^{39}\text{Ar}$

Lamprophyre dikes are abundant in the Cunningham Creek area, and cut mineralized quartz veins at the Silver Mine and Penny Creek occurrences (Fig. 2; Gavin, 2017). Sample RG16-CB03 from Silver Mine is a brown weathering, dark grey fresh, biotite-clinopyroxene-olivine lamprophyre that contains xenoliths of recrystallized vein quartz and wall rock fragments. The rock contains 1-3 mm phenocrysts of talc-serpentine-carbonate altered clinopyroxene and olivine in a groundmass of plagioclase and weakly chlorite-altered biotite. Three single grain analyses of hand-picked biotite from this sample yielded ages of 116 to 112 Ma, with Grain 1 yielding the most precise result of 114.2  $\pm$  1.2 Ma (Table 2). This result is interpreted as the age of lamprophyre dike emplacement. Sample RG16-CB06 is a similar xenolithic biotite-clinopyroxene-olivine lamprophyre dike from Silver Mine. This sample contains minor disseminated pyrite and is cut locally by quartz-pyrite veinlets. Single biotite grains yield  $^{40}\text{Ar}/^{39}\text{Ar}$  age results in the range of 115 – 110 Ma, with Grain 3 yielding the most precise result of 112.2  $\pm$  1.7 Ma (Table 2). These results are in close agreement with a 113.4  $\pm$  0.8 Ma  $^{40}\text{Ar}/^{39}\text{Ar}$  biotite age reported from a lamprophyre dike at Penny Creek (Sample WB15, Table 2; Mortensen, unpublished data).

## DISCUSSION – CARIBOO GOLD DISTRICT

### Structural setting of mineralization

The orientations, deformation features, and shear sense of veins in the Cariboo gold district indicate they are kinematically compatible with  $D_2$ -related ductile deformation features (Figs. 6, 12). Veins are therefore interpreted as the semi-brittle to brittle expression of progressive  $D_2$ -related northeast-southwest shortening (Fig. 18). Some  $D_2$ -related veins are overprinted by ductile deformation and thus formed during the early or intermediate stages of bulk deformation. These early veins are typically barren or have low gold grades, whereas the majority of well-mineralized veins formed later in the compressional deformation sequence.

Extensional veins formed parallel to the maximum stress direction ( $\sigma_1$ ) and perpendicular to the minimum stress direction ( $\sigma_3$ ). The orientations of mineral fibres in these veins are independent indicators of the northwest-southeast dilation vector of these veins. Brittle failure of the rock mass also led to the formation of conjugate shear veins oblique to  $\sigma_1$ , with northerly trending shear veins accommodating dextral-normal shear, and east-northeast-trending veins accommodating sinistral movement. Shear veins experienced repeated episodes of vein growth and shear failure, consistent with the interplay of deformation under low-permeability, over-pressured fluid conditions, and the precipitation of new vein material associated with transient

seismic rupture and high-permeability, high fluid flux conditions. Similarly, the high degree of strain evident in strike veins is consistent with their orientation at a high angle to  $\sigma_1$ . The non-ideal geometry of strike veins relative to  $\sigma_1$  is consistent with the abundance of dissolution features (stylolites), incremental growth features (crack-seal textures), and strain markers (boudinage, carbonaceous or argillaceous shear bands).

Vein thickness and density throughout the Cariboo gold district is typically high in competent layers such as psammite or quartzite, as compared with less competent, intervening layers with high mica content. Ongoing ductile deformation of micaceous rocks – even during the late stages of  $D_2$  deformation – ensured that permeability was generally only maintained in the most competent units. The permeability structure of the metamorphic package was therefore dynamically linked to the mechanical response of heterogeneous lithostratigraphy during progressive deformation.

Whereas the argument for lithological controls on gold mineralization in the Cariboo gold district is mainly a structural one, rock composition is an important consideration for the localization of replacement-style pyritic ores. The massive pyritic ores of the Island Mountain area preferentially replace northwest-plunging,  $L_2$ -parallel mullions of marble of the Downey succession, especially in the antiformal hinges of  $F_2$  folds (Fig. 4). Replacement-style ore in the Bonanza Ledge zone replaces calcareous semipelite, indicating that a variety of calcareous units in the Snowshoe Group strata

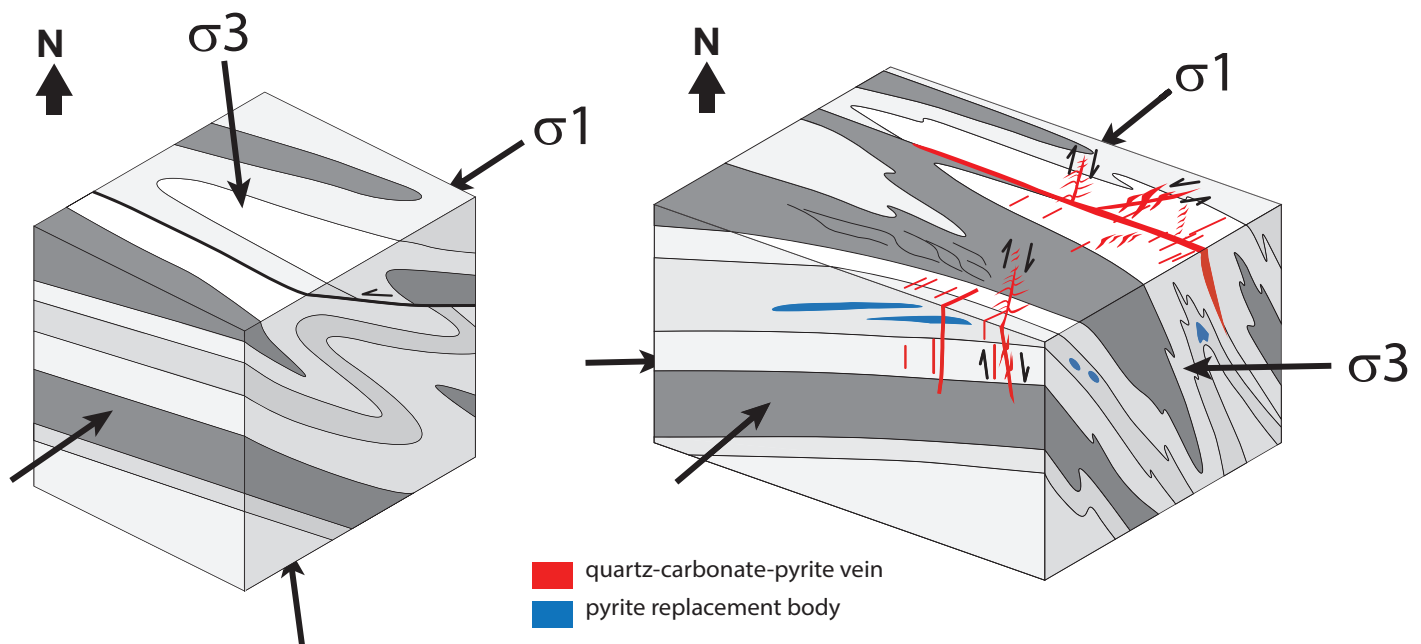


Figure 18. Block models illustrating initial formation of the Cariboo gold district's fold and thrust architecture (left), followed by vein formation and mineralization as the consequence of brittle failure during progressive, coaxial, northwest-southeast directed shortening. The precise timing of brittle failure is a complex function of host rock tensile strength, temperature, and strain rate, such that vein formation is envisaged as diachronous throughout the district.

tigraphy may be favourable for this style of mineralization. Furthermore, the local plunge of  $L_2$  is an important exploration consideration in targeting replacement-style ore elsewhere in the Cariboo (Fig. 8).

Angular kink and chevron folds that cross-cut veins, alteration, and  $D_2$ -related ductile features in the Wells-Barkerville camp are abundant, but are not recognized as a penetrative strain feature in rocks of the Snowshoe Group. For example, the narrow belt of chevron folds developed in chloritic phyllite in the hanging wall of the B.C. vein in the Bonanza Ledge zone (Fig. 9a) is not developed in rocks of similar competency elsewhere, suggesting a highly localized strain environment.

A 'train wreck' model is proposed for chevron fold formation that explains the paradox of orogen-normal axial planes in the apparent absence of bulk orogen-parallel shortening throughout the stratigraphy (Fig. 19). This model envisages segments of the orogen undergoing active northeast-southwest shortening in a transpressional environment, accompanied by ductile thinning and lateral extrusion of less competent rock material. Where extruding material enters a segment of the orogen in a neutral stress state, or potentially experiencing orogen-normal extension, it buckles into semi-brittle folds with axial planes perpendicular to the direction of extrusion. This 'train wreck' effect could potentially concentrate where lateral extrusion is impeded by a physical barrier such as a fault that cuts stratigraphy, or perhaps within a zone of high vein density. This model envisages that chevron folds formed as post- $D_2$  features, post-dating veins and alteration, but that they are indirectly linked to  $D_2$ -related shortening in an adjacent segment of the orogenic belt.

An alternative model relates the formation of angular folds to a reorganization of fold geometries during post- $D_2$  orogenic collapse. Semi-brittle open chevron and kink folds of the dominant  $L_2$  shape fabric occurs mesoscopically (Figs. 9b, 16). At a broader scale, orogenic collapse-related warping of the regional lineation could lead to zones of inner arc compression that manifests as semi-brittle folds oriented at a high angle to pre-existing fabrics. Detailed structural maps at the scale of 10s to 100s of metres could contribute to resolving this hypothesis.

### Age of mineralization and deformation

Argon-argon dating results indicate that rocks of the Cariboo subterrane, in thrust contact with the Barkerville subterrane, experienced brittle deformation as early as 155 to 153 Ma, as evidenced by the formation of fibrous extensional veins. These ages are similar to those obtained for deformed, pre-mineralization veins in the Cariboo Gold Quartz mine (BC MINFILE 093H 019) and Myrtle prospect (BC MINFILE 093H 025) in the Wells-Barkerville camp (Rhys et al., 2009). The contemporaneity of deformed veins in the Barkerville subterrane with undeformed veins in the Cariboo subterrane is consistent with the relative structural positions, and the relative competency of the host rocks. Ductile strain locally outlasted the formation of ca. 155-153 Ma brittle features in Snowshoe Group rocks of the Barkerville subterrane, whereas extensional veins in competent carbonate and siliciclastic rocks of the Cariboo subterrane formed during the latest stages of  $D_2$  deformation at a higher structural level.

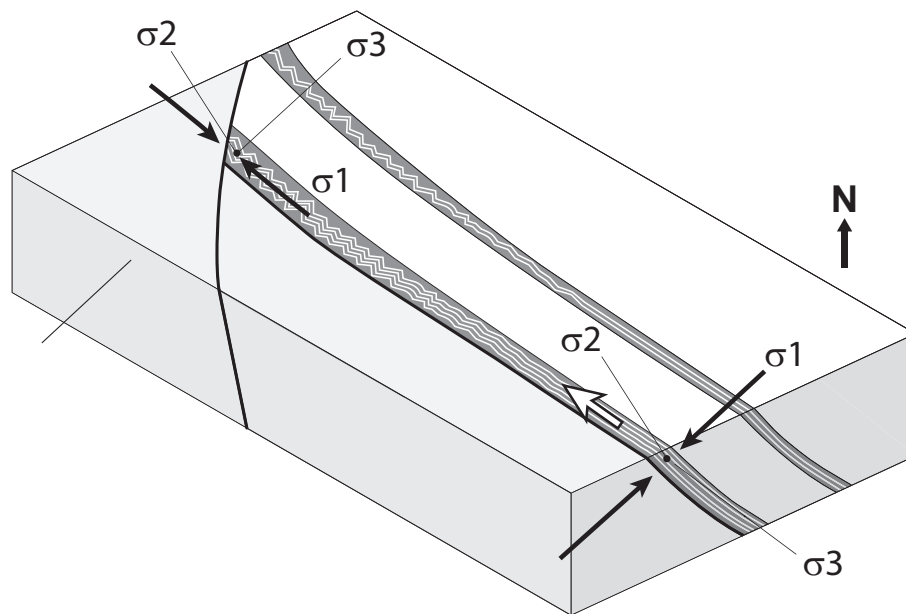


Figure 19. "Train wreck" block model for formation of late, locally developed chevron cross-folds. From right to left, the model envisages lateral extrusion of ductile material from a zone of orogen-normal shortening. Extruded material undergoes layer-parallel shortening as it encounters a zone undergoing orogen-normal extension.

Vein-related mineralization in the Mosquito Creek, Cariboo Gold Mine, and Bonanza Ledge areas formed between ca. 148 and 141 Ma (Rhys et al., 2009). Replacement-style pyritic ore from the Mosquito Creek mine also yielded a  $148.5 \pm 1.0$  Ma age (Rhys et al., 2009), suggesting that replacement-style ores and vein ores at this locality were essentially contemporaneous and likely derived from a common ore fluid. Replacement-style ore at Bonanza Ledge yielded a younger age of  $\sim 138$  Ma, in spite of petrographic evidence for pre-D<sub>2</sub> mineralization (Rhys and Ross, 2001; Rhys et al., 2009). Vein-related mineralization in the Cunningham Creek area (Silver Mine, Penny Creek, Jewelry Box, and Hibernian occurrences) yielded ages ranging from ca. 142 to 134 Ma (Mortensen et al., 2011; this study). It thus appears that mineralization in the Cariboo gold district potentially formed over a  $\sim 15$  m.y. timeframe from ca. 149 to 134 Ma, whereas rocks in Barkerville subterrane started to undergo brittle deformation as early as 155 Ma as indicated by deformed veins. The common structural setting of veins throughout this period thus requires that the same progressive D<sub>2</sub> deformational regime was active from Late Jurassic to Early Cretaceous.

The Late Jurassic (ca. 155-151 Ma) onset of brittle deformation in the Barkerville and Cariboo subterrane overlaps with 161-150 Ma vein formation and mineralization in the Spanish Mountain gold deposit, which is located approximately 65 km south of Wells near the community of Likely, and hosted in black phyllite of the Quesnellia terrane (BC MINFILE 093A 043; Mortensen et al., 2011; Fig. 2). However, mineralization in the Barkerville subterrane is notably younger (148-135 Ma), in spite of the similar late- to post-D<sub>2</sub> structural timing of mineralization in both areas. The diachronous nature of mineralization in the Cariboo gold district may partly relate to the deeper structural position of the Barkerville subterrane relative to Quesnellia terrane in the Late Jurassic. Whereas rocks of the Barkerville subterrane were experiencing incipient brittle behaviour in the early Late Jurassic, rocks at Spanish Mountain had already been exhumed to higher crustal levels and were thus more amenable to incursion of mineralizing fluids through interconnected fault-fracture networks.

Lamprophyre dikes intruded the Cariboo gold district ca. 115-112 Ma, and approximately 20 m.y. after the youngest mineralization in the district. By nature of intruding along the same structures as mineralized veins in the Cunningham Creek area, these mantle-derived, mafic alkaline melts likely exploited crustally significant structural networks that were already present, and perhaps established during gold mineralization.



---

# Cassiar Gold District

---

The Cassiar gold district is located in the Cassiar Mountains of north-central British Columbia, near the settlement of Jade City and a few kilometres southeast of the former asbestos-mining town of Cassiar (Fig. 20). The district has produced over 100 koz of alluvial gold in over 140 years of placer gold mining, and at least 350 koz from bedrock sources that have been exploited sporadically since the 1930s.

## REGIONAL GEOLOGY

Gold in the district occurs in the Sylvester Allochthon, a thrust-imbricated composite klippe of terranes that has been deformed into a major synformal basin (McDame synlinorium of Gabrielse, 1963). The structurally lowermost terrane of the Sylvester Allochthon includes greenschist metamorphosed argillite, massive to pillowed basalt, and serpentinite representing ultramafic intrusions, which collectively correlate with the Late Paleozoic Slide Mountain terrane (Nelson and Bradford, 1989; Gabrielse et al., 1993; Nelson, 1993).

The Mississippian to Triassic assemblages of the Slide Mountain terrane structurally overlie Neoproterozoic (Hadrynian) to Early Mississippian, shelf to platformal North American strata of the Cassiar terrane. These form a west-dipping, thrust-imbricated belt in the Liard Plain to the east (Gabrielse et al., 1993; Nelson and Bradford, 1993), and are also exposed in a narrow 1 to 5-kilometre belt west of the Cassiar gold district (Fig. 20).

The Slide Mountain portion of the Sylvester Allochthon is subdivided into two main thrust-stacked packages (Nelson and Bradford, 1993). The lower package (Division I) consists of lower Mississippian to mid-Permian pelagic and hemipelagic sedimentary sequences including chert, carbonaceous argillite, sandstone, and siltstone, as well as gabbro, diorite, and diabase sills (Nelson and Bradford, 1989; Nelson and Friedman, 2004). This package occurs in thrust contact with the underlying autochthonous Earn Group, whose thickness is structurally modified from > 500 m in the east, to < 50 m in the west (Nelson and Bradford, 1989; 1993).

The upper package of the Slide Mountain terrane (Division II) is composed mainly of lower Mississippian to mid-Permian massive to pillowed MORB (mid-ocean ridge basalt), diabase, chert, and argillite, with intervening structural slivers of ultramafite and gabbro (Nelson and Bradford, 1989; Nelson, 1993). The volcanic-sedimentary sequences that comprise the thick, lower part of Division II

are structurally overlain by the Table Mountain sediments, which define the structurally highest unit of Division II. The dominantly argillaceous sequence includes conodonts and *Halobia*-bearing limestone, defining it as Late Triassic and thus the youngest unit of the Slide Mountain terrane in the Sylvester Allochthon (Harms et al., 1989; Nelson and Bradford, 1989). Gold-bearing veins in the Cassiar gold district are hosted exclusively in Division II of the Sylvester Allochthon, and particularly in basalt below the Table Mountain thrust, which defines the structural base of the Table Mountain sediments.

The structurally highest package of the Sylvester Allochthon (Division III) is exposed as klippen southeast of the Table Mountain area (Harms et al., 1989), and consists of Pennsylvanian to Upper Permian limestones and mafic to felsic volcanic rocks of the Huntergroup volcanics, an island arc assemblage correlated elsewhere with the oldest portions of the Quesnellia terrane (equivalent with Harper Ranch terrane; Nelson, 1993).

The narrow belt of autochthonous strata exposed west of the Sylvester Allochthon is intruded to the west by the mid-Cretaceous Cassiar batholith (Fig. 20), an approximately 400 km-long body averaging 15-20 km wide. The Cassiar batholith and adjacent autochthonous rocks are intruded by felsic stocks and plutons of Late Cretaceous and Eocene age (not depicted at the scale of the regional geology in Figure 20). Diabase and lamprophyre dikes cross-cut Slide Mountain terrane rocks and mineralized quartz veins in the Cassiar gold district.

## ECONOMIC GEOLOGY

Gold in the Cassiar region was discovered in 1874 as alluvial deposits in McDame Creek (Fig. 20). This led to the production of approximately 65 – 70 koz of gold from McDame, Snowy, Troutline, and Quartzrock creeks by 1895 (Diakow and Panteleyev, 1981; Cowley, 2017; Fig. 20). An additional 30-40 koz of placer gold have been mined since, for a total estimated placer production of 108 koz (Cowley, 2017).

Hard rock exploration in the 1930s led to the discovery of several significant gold-bearing veins, and exploration and small-scale mining have continued sporadically since (Diakow and Panteleyev, 1981; Cowley, 2017). At least 2400 diamond and percussion holes were drilled in the district, and over 350 koz have been recovered from various underground and open pit mines (Cowley, 2017). The two main exploration foci are the Taurus area, which includes 35 koz of historic gold production from the Taurus, Sable, and

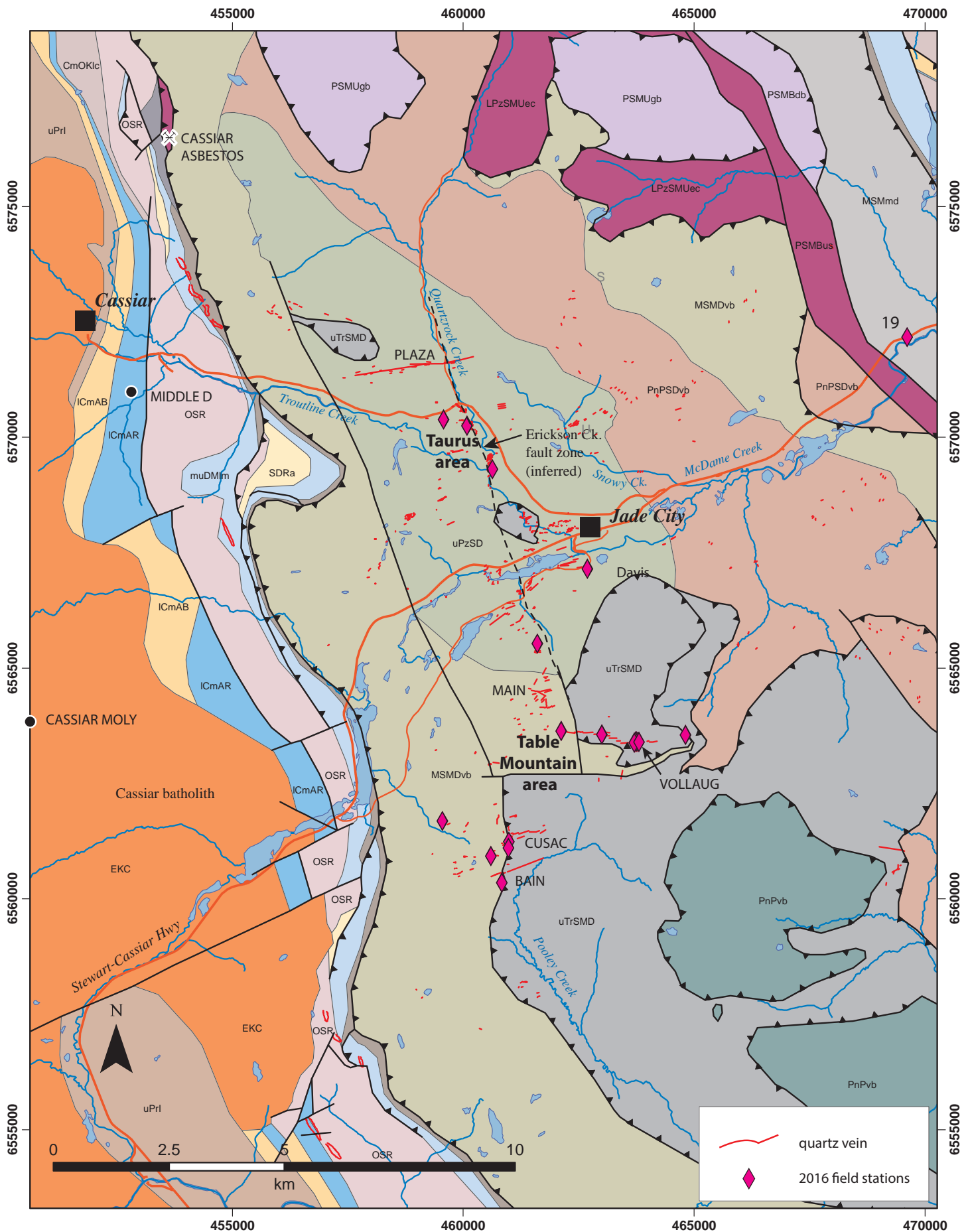


Figure 20. Geology of the Cassiar gold district and surrounding region (after Nelson and Bradford, 1993).

## LEGEND

### Intrusive rocks

**EKC** **Cassiar batholith (Early Cretaceous)** – biotite-hornblende and biotite-muscovite granite, locally megacrystic; quartz monzonite, granodiorite

### Quesnellia terrane

**DIVISION III, SYLVESTER ALLOCHTHON** - Pennsylvanian to Permian

**PnPvb** **Huntergroup volcanics** – Augite (-hornblende-plagioclase) porphyry, lapilli tuff, tuffaceous sandstone, limestone, minor chert and argillite.

### Slide Mountain terrane

**DIVISION II, SYLVESTER ALLOCHTHON** - Mississippian to Triassic

**uTrSMD** **Table Mountain Sediments** – Slate, calcareous siltstone, *Halobia*-bearing platy grey limestone.

**PSMUgb** **Zus Mountain gabbro** – gabbro, in part layered, foliated.

**LPzSMUed** **Cassiar-Quartzrock Creek Ultramafite** – serpentinite, harzburgite tectonite, pyroxenite, gabbro; includes serpentinite of the Blue Dome fault zone.

**PnPSDvb** Basalt flows and tuffs (including maroon, red and green), volcanoclastics, variegated chert, polymictic breccia, phyllite, argillite, quartz-chert sandstone, rhodonite, diabase.

**uPzSD** Massive and pillowed basalt flows (olivine-phyric near Mt. Sylvester), lesser tuff.

**MSMDvb** Basalt, diabase, grey and green chert, black, grey and green argillite, calcarenite, quartz-chert sandstone, chert-pebble conglomerate.

**DIVISION I, SYLVESTER ALLOCHTHON** - Mississippian to Permian

**MSMmd** Black, grey and green argillite, quartz-chert sandstone, grey, green and black chert, calcarenite, minor tuff, siliceous exhalite; includes up to 10% diabase, basalt sills

### Cassiar terrane (autochthonous North American strata)

**DMEmb** **EARN GROUP** (Upper Devonian to Lower Mississippian) – Slate (variably graphitic, calcareous, pyritic), siltstone, sandstone, conglomerate, porcellanite, light green tuffaceous shale, dark grey limestone, siliceous and baritic exhalite.

**muDMlm** **McDAME GROUP** (Devonian) – Limestone, dolostone, limestone-dolostone breccia; in part subdividable into upper member: light grey, platy, limestone, with local karst breccia; lower member: dolostone, dark grey fetid, limestone, carbonate breccia.

**OSR** **ROAD RIVER GROUP** (Ordovician to Silurian) – Black, commonly limy slate, locally graptolitic; argillaceous limestone.

**CmOKlc** **KECHIKA GROUP** (Cambrian to Ordovician) – Limestone, argillaceous limestone, pale calcareous slate, phyllitic limestone, calcareous phyllite, pyritic and carbonaceous slate and shale; conglomerate and greenstone; may include dark slates of Road River Group.

**ICmAR** **ATAN GROUP, Rosella Formation** (Lower Cambrian) – limestone, dolostone, calcareous shale, brown, grey and green-grey slate.

**ICmAB** **ATAN GROUP, Boya Formation** (Lower Cambrian) – quartzitic sandstone, siltstone, slate and phyllite.

**uPrI** **INGENIKA GROUP, undivided** (Neoproterozoic) – quartzite, micaceous quartzite, phyllite, schist, gneiss, limestone, shale, sandstone, sandy limestone, dolomite, chlorite-muscovite schist, slate, argillite, micaceous crystalline limestone, pebble conglomerate.

Figure 20 (cont'd). Geologic legend corresponding to Figure 20.

Plaza mines, and the Table Mountain area, from which 316 koz of gold were extracted from the Main (Erickson), Bain, Cusac, and Vollaug mines (Fig. 20).

The Cassiar region is perhaps best known for its asbestos deposits, which exploited altered ultramafic rocks exposed in the basal sole thrust along the western margin of the Sylvester Allochthon (Fig. 20). Asbestos mining at Cassiar ceased in 1992, however nephrite jade continues to be produced from the same ultramafic rocks.

In addition, numerous Late Cretaceous intrusion-related mineral occurrences occur west of the Sylvester Allochthon. These include examples of porphyry Mo ± Cu and skarn-style Mo ± Cu-W mineralization within or proximal to Late Cretaceous intrusions, such as the Cassiar Moly occurrence (BC MINFILE 104P 035), which is associated with the  $73.0 \pm 0.5$  Ma Troutline stock (Panteleyev and Friedman, unpublished data in Ash, 2001; Fig. 20). Silver-lead-zinc enriched veins and mantos hosted in autochthonous North American strata represent the distal expressions of Late Cretaceous magmatic-hydrothermal activity. Examples include the Middle D occurrence (BC MINFILE 104P 080) near the town of Cassiar (Fig. 20), and the active Silvertip Ag-Pb-Zn mine located near the northern end of the Sylvester Allochthon, 12 km south of the B.C.-Yukon border (BC MINFILE 104O 038; Bradford and Godwin, 1988).

## STRUCTURAL GEOLOGY

Detailed studies documenting the structural environment of gold in the Cassiar gold district have been carried out by several workers (e.g., Anderson and Hodgson, 1989; Ball, 1997; Rhys, 2009). The structural evolution of the district broadly includes thrust imbrication of the host rock sequences, ductile deformation of the host rocks, formation of brittle deformation features and mineralized veins, and post-mineralization faulting. Although  $D_1$ ,  $D_2$ ,  $D_3$ , etc... terminology is employed here to describe overprinting structural elements, deformation is interpreted in the context of progressive deformation.

### Thrust faulting

The thrust-imbricated architecture of Slide Mountain terrane rocks in the Cassiar gold district has been noted by several workers as an important controlling factor in the localization of gold-bearing veins (e.g., Diakow and Panteleyev, 1982; Sketchley et al., 1986; Anderson and Hodgson, 1989; Nelson and Bradford, 1989; Ball, 1997; Rhys, 2009). Thrust imbrication of the volcanic-sedimentary sequence in the Table Mountain and Taurus areas is defined as  $D_1$ . This event resulted in interleaved panels of mafic volcanic rocks separated by seams highly deformed ultramafic rocks and argillaceous sediments in the Table Mountain area. Minor recumbent folds are associated with this phase

of deformation.

A maximum age for obduction and thrust imbrication of the Slide Mountain terrane is constrained by the Late Triassic depositional age of the Table Mountain sediments, and a reasonable minimum age is provided by the Early Cretaceous age of hydrothermal sericite within thrust structures (Harms, 1985; Struik et al., 1992; Nelson and Bradford, 1993; Ash, 2001; this study). Although a Jurassic age for initial thrust imbrication is most likely, a Late Permian post-tectonic diorite intrusion in the northern Sylvester Allochthon requires that at least some pre-Late Permian deformation also took place (Harms, 1985).

### Ductile deformation features

Superimposed on the thrust faults are several phases of ductile fabrics that are interpreted to reflect ongoing progressive deformation related to crustal thickening during and after initial accretion and imbricate thrusting of Sylvester Allochthon lithologies.

#### $D_2$

Thrust-related shear zones exhibit a penetrative, shallowly to moderately dipping planar fabric ( $S_2$ ) that is preferentially developed in ultramafic and sedimentary rocks, and in mafic rocks immediately adjacent to thrust faults (Fig 21a). The  $S_2$  fabric is subparallel to bedding and to layering in listwaenite-altered ultramafic units, and defines probable shear zones up to several tens of metres thick (Rhys, 2009). This fabric was interpreted by Anderson and Hodgson (1989) as a shear-related C-fabric.

A prominent lineation that is shallowly to moderately plunging and northwest-trending occurs throughout the district, and is defined by mullions, mineral aggregates, elongate basalt pillows, and stretched clasts in fragmental rocks (Anderson and Hodgson, 1989; Rhys, 2009; Fig. 21b-e). Linear fabrics are especially well-developed in zones of high strain in and near thrust faults, and are here defined as  $L_2$ .

#### $D_3$

A third deformation event ( $D_3$ ) resulted in formation of a locally developed fabric ( $S_3$ ) that is steeply dipping and northwest-striking, and associated with open folding of lithologic contacts and thrust surfaces. The  $S_3$  fabric is preferentially developed in ultramafic and argillaceous units. A district-wide, northwest-striking intersection lineation is developed at the intersection of  $S_3$  and  $S_2$  fabrics and is parallel to the  $L_2$  stretching lineation in high strain zones (Fig. 21e). This deformation event is presumed to relate to the formation of the McDame synlinorium, which has a northwest-trending axial plane and shallow plunge, consistent with northeast-southwest directed shortening.

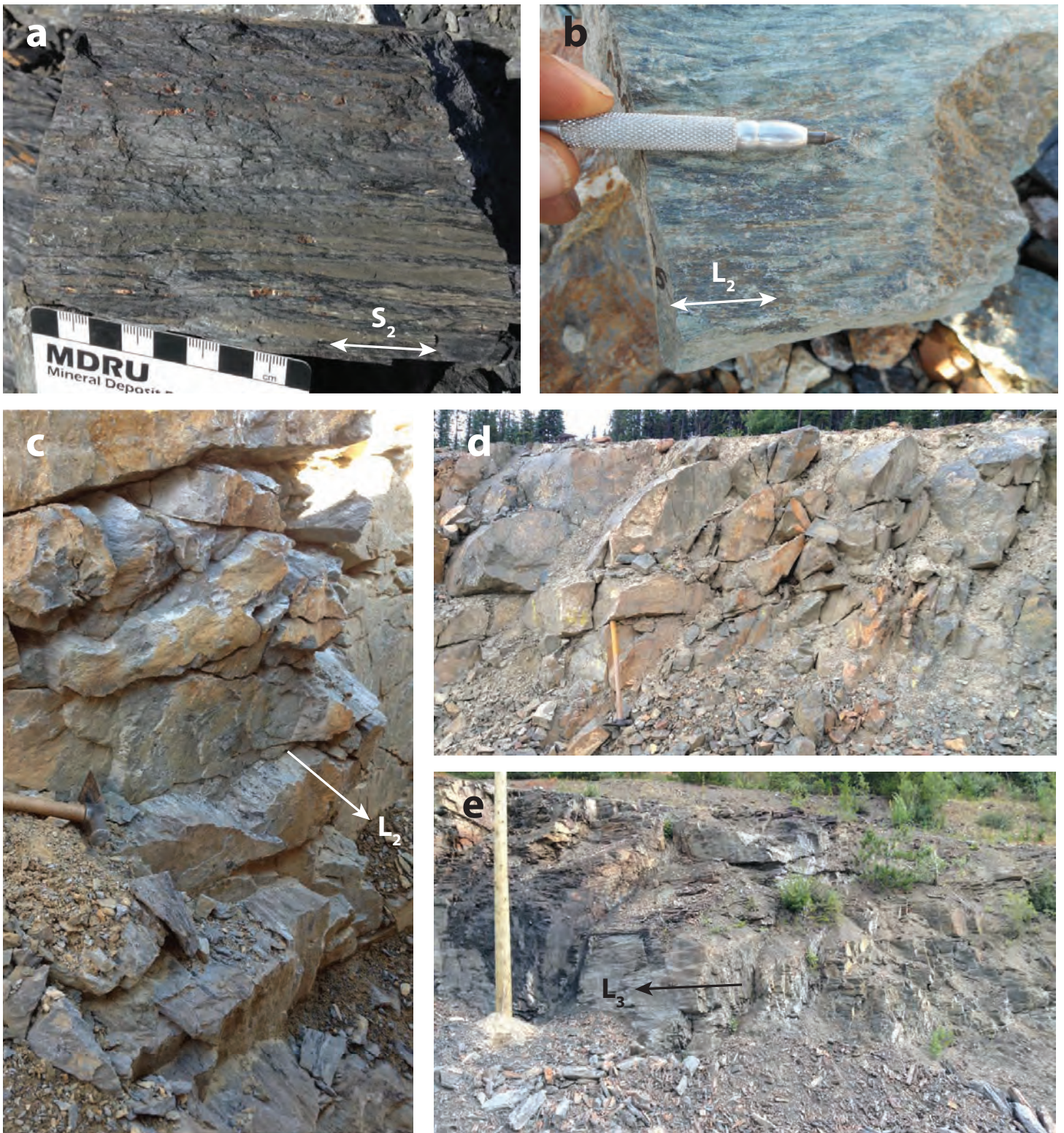


Figure 21. (a)  $S_2$ -foliated carbonaceous argillite containing pyrite porphyroblasts with quartz-filled pressure shadows (Sample MA16-CB5, Bain mine). (b) Metabasalt showing a penetrative lineation defined by aligned actinolite aggregates (Sample MA16-CB6, Bain mine). (c) Strongly lineated talc-altered ultramafite at the Bain decline. The southeast-plunging lineation is interpreted to relate to northwest-vergent shear. (d) Pillow basalt in the Sable pit, Taurus area, showing a crude shallowly south-southeast-plunging lineation defined by elongation of pillows and mineral aggregates (view toward 202°N). (e) Rodding and pencil cleavage development in a sequence of argillaceous metasediments, defined by intersection of steep ( $S_3$ ) and shallow ( $S_2$ ) planar fabrics (Locality 19 - Division I, Sylvester Allochthon).

## D<sub>4</sub>

A late phase of ductile deformation is recorded locally in argillaceous rocks, and is expressed as a northeast-trending and steeply dipping crenulation cleavage (S<sub>4</sub>) (Rhys, 2009).

## Dikes

Ductile deformation and mineralization features of the Cassiar gold district are cut by sets of diabase and lamprophyre dikes (Ball, 1997). These dikes intrude vein systems locally and are cut by late faults (below). Lamprophyre dikes in the district contain abundant granitic xenoliths (Fig. 22) in which sodic metasomatism of K-feldspar has generated riebeckite-carbonate-albite alteration assemblage (Ball, 1997). Xenolithic lamprophyre dike samples from the Bain mine area were collected for <sup>40</sup>Ar/<sup>39</sup>Ar dating of biotite to determine the dike emplacement age, and for U-Pb dating of zircons to identify the provenance of granitic clasts (see below).



Figure 22. Granitic xenolith in biotite lamprophyre from the Bain mine, affected by a concentric zone of carbonate alteration.

## Late faults

All metamorphic rocks of the Cassiar gold district are cut by late, brittle faults that are typically north-northwest or northeast-trending (Fig. 21). The northeast-trending set are steeply southeast-dipping and exhibit normal-oblique movement, as indicated by slickenline data (Ball, 1997; Rhys, 2009). The steep, northwest-trending Alison Drift fault cuts the Alison vein into several segments with dextral-normal (down-to-the-east) movement (Anderson and Hodgson, 1989). Ball (1997) attributes late brittle faults to northwest-directed extension with a subvertically oriented maximum compressive stress. Late faults of this generation also controlled a late stage of hydrothermal activity, as indicated by silica-cemented epithermal vein breccias, clay

alteration of metavolcanic rocks, and tufa deposits (Ball, 1997).

## Fractures

A consistently steep and northeast-trending set of joints is developed through the Cassiar region, both in rocks of the Sylvester Allochthon and in structurally underlying autochthonous strata (Ball, 1997). These joints are sub-perpendicular to northwest-trending cleavages and lineations, which Ball (1997) links to regional-scale northeast-southwest shortening after obduction of the Sylvester Allochthon (Fig. 21e). From the orientations of joints and lineations, Ball (1997) suggested a subhorizontal maximum compressive stress ( $\sigma_1$ ) trending 046°N, and a minimum stress ( $\sigma_3$ ) plunging 08° toward 136°N.

## Veins

Gold mineralization in the Cassiar gold district occurs predominantly in metabasalt-hosted quartz veins surrounded by pale tan-coloured zones of visible alteration characterized by quartz-sericite-ferroan carbonate  $\pm$  pyrite and destruction of chlorite and actinolite (Fig. 23). In some cases, an inner grey alteration zone is present, defined by more intense quartz-sericite-pyrite alteration (Anderson and Hodgson, 1989). Alteration zones are typically symmetrical about veins (e.g., Fig. 23a), but Anderson and Hodgson (1989) noted that alteration is more extensive in the hanging wall of larger shear veins. Three main categories of veins are recognized on the basis of their structural setting: shear veins, extensional veins, and veins that occupy thrust faults.

### Shear veins

Shear veins are by far the most economically significant in the Table Mountain area, and comprise high-grade zones within large-tonnage, low-grade targets in the Taurus area. Shear veins may be tens to hundreds of metres in strike length and range from a few centimetres to several metres in width. In the Table Mountain area, shear veins typically strike east to east-northeast with steep northerly dips, although north-northeast-trending shear veins also occur. In the Taurus area, west-northwest-trending shear veins are the most abundant. East to east-northeast-trending shear veins in the Table Mountain area accommodated top-to-the-northwest, sinistral oblique-normal movement, as indicated by offset lithologic markers, shear fabrics, and by geometric and deformational relationships between extensional and shear veins (Anderson and Hodgson, 1989; Ball, 1997; Rhys, 2009; Fig. 24a-d).

Shear veins are variably massive to banded, with bands typically defined by seams of grey deformed quartz, carbonaceous material, sulphides (pyrite, tetrahedrite, sphalerite, and chalcopyrite), or tourmaline (Sketchley, 1984; Rhys, 2009; Fig. 24c,f). Ferroan carbonate is a common gangue

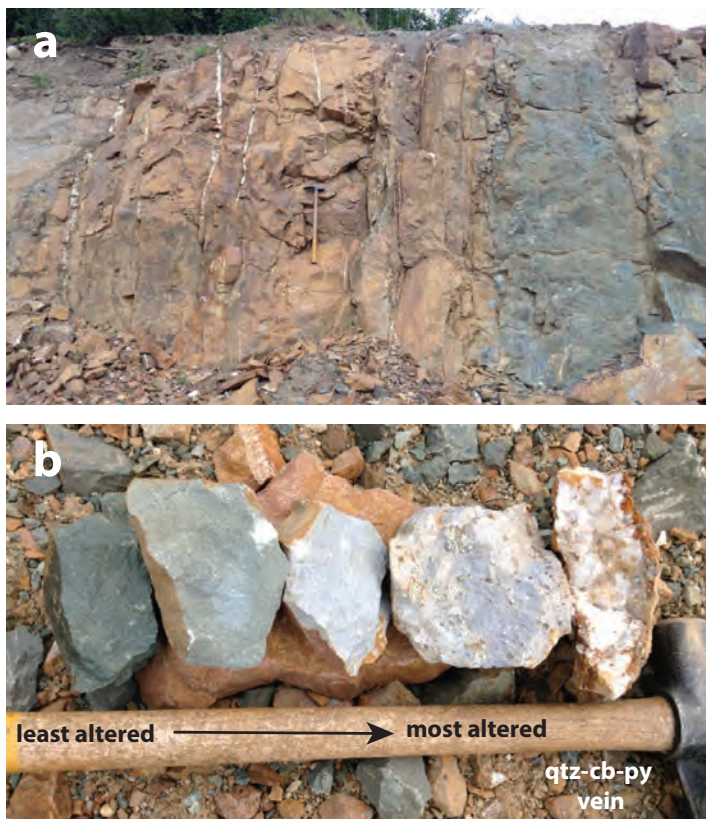


Figure 23. (a) Swarm of extensional quartz-ferroan carbonate-pyrite-chalcopyrite-tourmaline veins cutting metabasalt in the Sable pit, Taurus area. The veins coincide with a zone of characteristically brown-orange weathering quartz-sericite-carbonate-pyrite alteration. (b) Spectrum of alteration intensity in metabasalt, ranging from weak, distal sericite-carbonate alteration to a texturally and mineralogically destructive inner alteration zone of quartz-ferroan carbonate-sericite-pyrite alteration (unweathered samples, Sable pit).

phase, and typically occurs near vein margins or as paragenetically late vein fill. Pyrite occurs as disseminations and seams, and is particularly abundant in carbonaceous partings and as hydrothermal replacement of included wall rock fragments (Anderson and Hodgson, 1989).

Cataclastic reworking of shear veins is especially prominent along vein margins, where brecciated fragments of vein quartz, carbonate, and wall rock are cemented by combinations of white to clear grey quartz, pyrite, carbonate, or carbonaceous material (Anderson and Hodgson, 1989; Fig. 24e). Veins are commonly cut by late fractures that have in-fill of grey quartz, tetrahedrite, chalcopyrite, and sphalerite (Anderson and Hodgson, 1989).

### Extensional veins

Steeply dipping sets of extensional veins occur throughout the Cassiar gold district, and are oriented sub-perpendicular to the local lineation. These typically strike north-northeast to northeast in the Table Mountain area, and east-northeast in the Taurus area (e.g., Sable pit, Fig. 25). Extensional veins range from millimetre-scale veinlets to larger veins several tens of centimetres wide, and have limited strike and

dip extents of tens of centimetres to metres at most (Rhys, 2009). Extensional veins provide reliable shear sense indicators where they occur as sigmoidal arrays, typically on the fringes of shear veins (Fig. 25b-c) or as arrays accommodating displacement at the termination of shear veins (Fig. 25d). Mutually joining or cross-cutting shear and extensional veins suggest that they are temporally and kinematically linked.

Extensional veins may have paragenetically early, fibrous to columnar quartz - ferroan carbonate  $\pm$  tourmaline margins. The orientation of these grains is sub-perpendicular to vein margins and sub-parallel to penetrative lineations in the host rock, thus providing an unambiguous northwest-southeast orientated dilation vector. Otherwise, veins are filled mainly by massive quartz with rare vuggy interiors. Extensional veins are locally sulphide bearing and typically have lower and less continuous grades than shear veins (Rhys, 2009). However, mineralized zones dominated by extensional veins may represent near-surface bulk-tonnage targets such as the Taurus area (Cowley, 2017).

### Thrust-filling veins

In addition to the steeply dipping extensional and shear veins described above, shallowly to moderately dipping quartz veins occupy thrust faults at the margins of listwanitized ultramafic units or at volcanic-sedimentary contacts. The most notable example is the Vollaug vein, which occupies the Table Mountain thrust between hanging wall argillites and footwall mafic and ultramafic rocks (Fig. 26a). The vein is up to several metres thick and can be traced discontinuously for 2700 m along strike (Fig. 20). The vein is dominated by massive, milky quartz dissected by shears bands defined by seams of argillaceous material and sulphides (Fig. 26b). Ductile shear fabrics in the vein signify that vein formation accompanied, and was outlasted by, long-lived movement along the Table Mountain thrust. Black stylolitic seams defined by carbonaceous material and sulphides occur subparallel to the orientation of the Vollaug vein, indicating that pressure solution of quartz was driven by subvertical compaction perpendicular to the vein (Fig. 26c). The Vollaug vein is locally dismembered by boudinage.

Thrust-filling veins locally refract downward into mafic metavolcanic rocks, where they express as shear veins in the Table Mountain area (Rhys, 2009). Zones where shear veins transition into flat-lying thrust-filling faults have historically hosted high gold grades (Anderson and Hodgson, 1989; Fig. 24a,d).

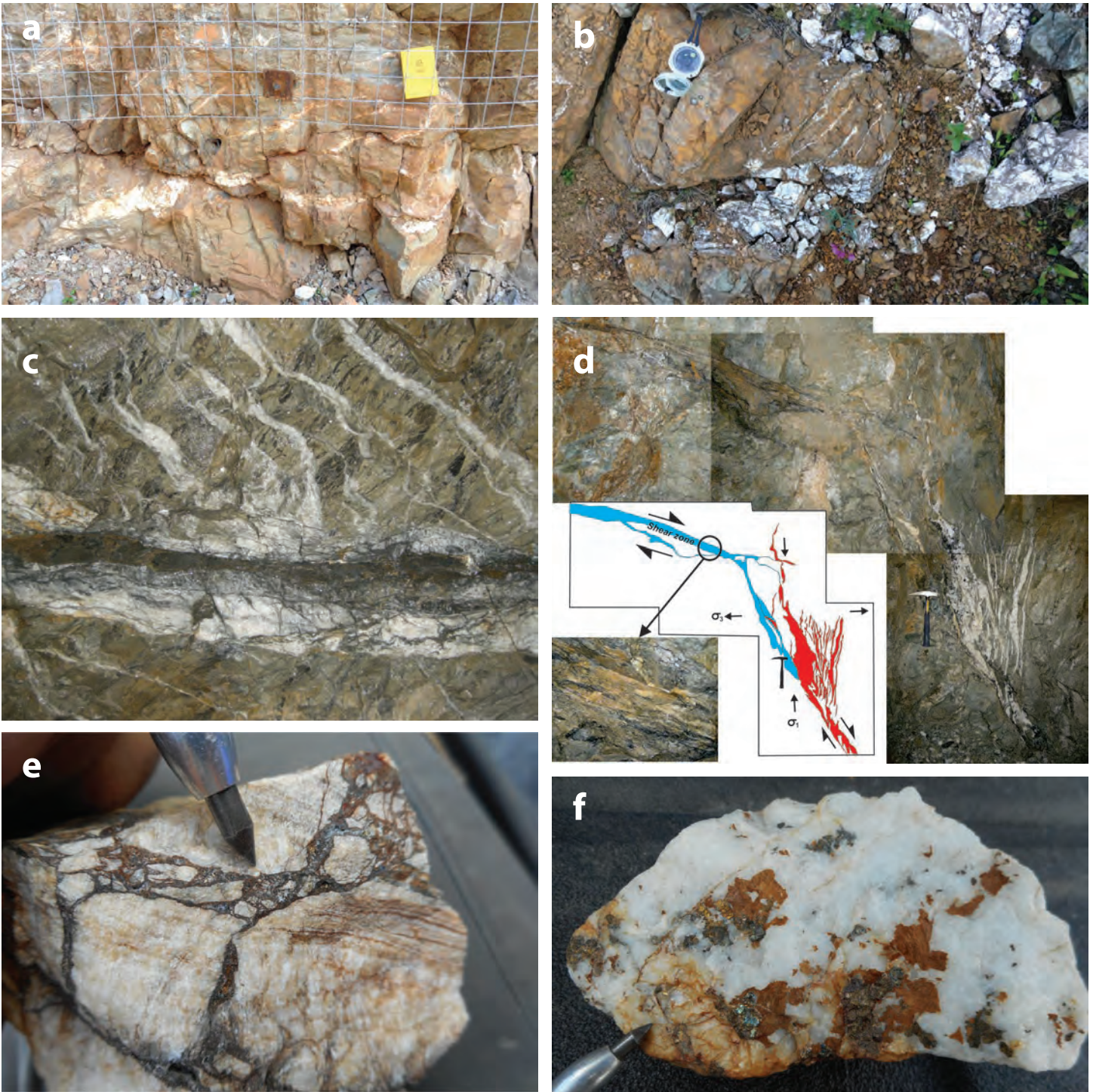


Figure 24. (a) Shallowly dipping quartz-carbonate shear vein refracting downwards to the left, with a top to the north (left) shear sense provided by an *en echelon* array of extensional veins in the top part of the photograph (view to the west; Cusac mine portal). (b) Steeply dipping, east-northeast trending quartz-carbonate-pyrite shear vein in the Table Mountain area. A flanking extensional vein array indicates a component of sinistral shear on the vein. (c) West-northwest-trending banded shear vein fringed by northeast trending quartz extensional veinlets (Bain workings). Note the high angle of extensional veins to the northwest-trending foliation (runs from lower left to upper right). The shear sense as viewed is dextral, but the view is up at the back, so the shear sense in plan view is sinistral. From Rhys, 2009. (d) Vein exposure in carbonate-sericite altered mafic sediments, illustrating possible larger scale structural controls on vein development (Bain workings). The shallowly dipping carbonate-rich shear zone in the top left (blue) refracts downward into a steeply dipping shear vein (red). Shear sense in this example is top to the right (south), as indicated by internal shear markers in the shallow shear zone (inset), and by a horsetailing array of extensional quartz veins in the hanging wall of the shear vein. From Rhys, 2009. (e) Vein sample characterized by clasts of banded carbonate cemented by grey quartz, ankerite, and fine-grained sulphides. (f) Sample of ore grade quartz-ferroan carbonate-pyrite-sphalerite-chalcopyrite vein material, Main mine.

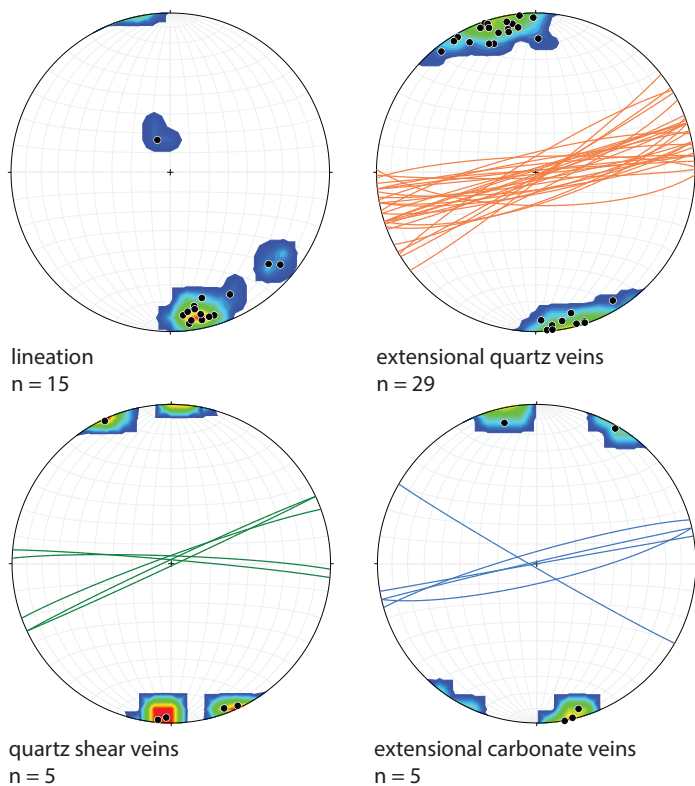


Figure 25. Equal area lower hemisphere stereonet plots of structural elements at the Sable pit, Taurus area, emphasizing the prevalence of steep extensional veins at a high angle to the penetrative lineation of the host metabasalts.



Figure 26 (right). (a) View of Vollaug vein mine workings, looking east. The vein occupies a thrust fault separating Table Mountain sediments in the hanging wall from a mainly metabasalt sequence in the footwall. (b) Table Mountain sediments in the hanging wall of the Vollaug vein, comprising dismembered lozenges of more resistant psammitic layers separated by zones of intensely sheared carbonaceous pelite. (c) Internally sheared block of the Vollaug vein, with shear bands defined by seams of carbonaceous material and sulphides. (d) Stylolites within the Vollaug vein, indicating compaction-related dissolution of quartz.

## GEOCHRONOLOGY

Samples were selected to constrain the timing of alteration and mineralization in the Cassiar gold district, and to provide new insights into the timing of lamprophyre emplacement and the provenance of granitic xenoliths therein. Argon-argon and U-Pb results are in Appendices 2 and 3, respectively.

### <sup>40</sup>Ar/<sup>39</sup>Ar Results

Sample 04MM-36\_100.1m is massive, quartz-ferroan carbonate vein from the Main Mine in the Table Mountain area, from which coarse, pale green sericite was hand-picked. An initial analysis yielded a slightly rising age spectrum, with a single step that released 65% of the <sup>39</sup>Ar giving an age of 129.9 ± 0.2 Ma. A second aliquot yielded a rising age spectrum, with the final two heating steps releasing 56% of the <sup>39</sup>Ar and giving an age of ~129 Ma. The results indicate a probable 130-129 Ma age of vein formation, with a subsequent thermal event that resulted in partial Ar loss.

Sample T-95-35\_129.5m is coarse, randomly oriented, pale green sericite that was collected from clots within a massive quartz-ferroan carbonate vein from the Taurus area. The first aliquot this sample released 96.3% of the <sup>39</sup>Ar in the first 5 of 12 heating steps, which produced a rising age spectrum flattening at 143 Ma. A second aliquot yielded a convex-upward age spectrum characterized by a gradually rising spectrum peaking at 142 Ma after 69.6% of the <sup>39</sup>Ar was released. The results suggest that hydrothermal sericite growth was in the earliest Cretaceous (143-142 Ma) or earlier, followed by partial argon loss during a subsequent thermal event.

Sample TA12-02\_23.3m is biotite collected from phenocrysts in a steeply dipping biotite lamprophyre dike that cuts sericite-ankerite altered and mineralized basalt in the 88 Hill zone of the Taurus area (McKeown et al., 2013). Two of three single grain analyses yield 113.1 ± 0.4 Ma (Aliquot 1, final 2 of 4 steps releasing 95.2% of the <sup>39</sup>Ar) and 113.0 ± 1.3 Ma (Aliquot 3, final 2 of 5 steps releasing 76.7% of the <sup>39</sup>Ar). A third aliquot yielded an age of 110.7 ± 1.0 Ma (Aliquot 2, final 1 of 4 steps releasing 79.8% of the <sup>39</sup>Ar). Together these results support an intrusive age of lamprophyre dikes at Taurus at ~113 Ma. This result is within error of a 110 ± 8 Ma K-Ar biotite age reported for a lamprophyre dike from the Table Mountain area (A. Panteleyev, unpublished data cited in Nelson, 1990 and Ash, 2001).

Sample MA16-CS04 is biotite hand-picked from 2-4 mm phenocrysts in biotite-pyroxene lamprophyre with a fine-grained plagioclase-dominant groundmass, and which contains approximately 0.5 – 5 cm rounded to sub-rounded xenoliths of medium-grained to pegmatitic felsic granitoid (Fig. 22). The sample was collected from mine waste near the Bain mine portal, so field relationships are not apparent.

However, based on analogy with the xenolithic lamprophyre described by Ball (1997), the sample most likely originated from a post-mineralization dike that is in close proximity to mineralization. A single grain analysis yielded an excellent plateau age of 77.1 ± 0.1 Ma, representing 96.6% of the <sup>39</sup>Ar released. This is interpreted as the crystallization age of the lamprophyre.

### U-Pb Results

Zircons were extracted from the lamprophyre dike sample collected from the Bain mine (MA16-CS04) to test the age of granitic xenoliths and/or xenocrysts. Nineteen grains were extracted and imaged by SEM-CL and analyzed by laser ablation ICP-MS, using methods similar to those in Beranek and Mortensen (2011). Grains range in size from 50 to 200 μm, with external morphologies that range from rounded to faceted. Most grains exhibit complex internal CL textures including oscillatory and sector zoning indicative of magmatic growth, embayments, and metamorphic and/or magmatic overgrowths. Fourteen of 19 zircon grains yielded Pre-Cambrian ages, of which three yielded nearly concordant low-precision single zircon ages of ~2920 Ma, ~1750 Ma, and ~1290 Ma. These grains are interpreted as derived from cratonic basement or zircon-bearing autochthonous strata, either entrained in the melt as xenocrysts, or as grains encapsulated within xenoliths of crystalline basement. An additional concordant analysis yielded an age of 201 ± 5 Ma, which is problematic given the known restriction of intrusions of this age to Quesnellia terrane rocks (Takla Group) west of the Cassiar batholith. Three concordant U-Pb results have a mean <sup>206</sup>Pb/<sup>238</sup>U age of 109.5 ± 5.4 Ma, and are the youngest known grains in the sample. These grains are tentatively interpreted to be derived from the granitic clasts, and are consistent in age with early phases of the Cassiar batholith (Driver et al., 2000; Rasmussen, 2013).

## DISCUSSION – CASSIAR GOLD DISTRICT

### Structural setting of mineralization

Structural observations made by several workers in the Table Mountain area suggest that steeply dipping shear veins were dominated by normal movement, implying formation under conditions of subvertical maximum compressive stress,  $\sigma_1$  (e.g., Anderson and Hodgson, 1989; Rhys, 2009; Fig. 27). Furthermore, the northwest-trending slip vectors determined for most shear veins are parallel to the prominent stretching lineation, such that veins and shallowly dipping shear fabrics are kinematically related features arising from subvertical shortening and northwest-southeast extension of the host rocks. This interpretation of the prevailing stress conditions is further corroborated by the subvertical orientation of extensional veins (Anderson and Hodgson, 1987), and by subhorizontal stylolitic seams in thrust-filling veins.

The above model envisages mineralized shear and extensional veins as generally late, brittle, low-strain features arising from progressive deformation focused along earlier formed thrust faults and shear zones. The intensity of subhorizontal ductile shear fabrics in thrust-filling veins (e.g., Vollaug vein, Fig. 25c) suggests that these veins were initially formed at an early stage, but accommodated high degrees of ductile shear strain thereafter.

The relationship of steep veins in the Cassiar district to movement along shallow-dipping thrust and surfaces is well established, thus requiring a subvertical orientation for the maximum principal stress direction,  $\sigma_1$  (Rhys, 2009; Figs. 24d, 27). Locally however, shear and extensional veins appear to be kinematically compatible with a steep, northwest-trending ductile fabric ( $S_3$ ), but with a penetrative northwest-trending lineation that is indistinguishable from the  $L_2$  fabric (e.g., west end of 88 Hill, Taurus area; Appendix 6). This scenario implies that at least locally, some veins may have formed under progressive, subhorizontal, northeast-southwest directed shortening. Because the timing of these  $D_3$ -related fabric and vein features may be ambiguous, it is permissible that the direction of maximum stress ( $\sigma_1$ ) and intermediate stress ( $\sigma_2$ ) periodically alternated such that both orogen-normal shortening and subvertical flattening were part of the same overall tectonic regime under which northwest-southeast extension occurred.

Anderson and Hodgson (1989) considered a tectonic model whereby the shear zones that host gold-bearing veins in the Cassiar gold district formed in response to horizontal extension linked to the concurrent foundering of the McDame synclinorium and exhumation of the Omineca geanticline to the west. In this model, the basal thrust of the Sylvester Allochthon is essentially reactivated as a low-angle detachment fault, and the steep faults and veins of the Cassiar gold district represent brittle accommodation structures.

The great thickness of mechanically resistant metavolcanic rock in the Sylvester Allochthon likely restricted the degree to which orogen-normal lateral shortening could be accommodated by ductile structures. This condition likely favoured the gravitational unloading of the tectonically thickened Sylvester Allochthon by means of lateral escape along low-angle zones of weakness defined by pre-existing thrust faults and/or readily deformable layers of ultramafic and argillaceous rocks. Progressive top-to-the-northwest movement along these surfaces, as indicated by a penetrative linear shape fabric, ultimately led to brittle failure and formation of steep veins and faults.

### Age of mineralization and deformation

Geochronological results in the Cassiar district support an Early Cretaceous age for alteration related to gold mineralization. An initial K-Ar sericite age of  $131 \pm 5$  Ma (Diakow and Panteleyev, 1982) was corroborated by the K-Ar results of Sketchley and co-workers (1986), which range from 137 – 112 Ma but with four of five results providing a mean age of  $129 \pm 4$  Ma. Subsequent  $^{40}\text{Ar}/^{39}\text{Ar}$  analyses of sericite yielded slightly older plateau ages of 135 – 133 Ma (Layer and Drake, 1997) and a sample of vein sericite from Quartzrock Creek reported by Ash (2001) yields a rising age spectrum suggestive of a similar  $\sim 134$  Ma age of vein formation. Argon-argon results presented above support a similar 130–129 Ma age for hydrothermal sericite in the Table Mountain area (Sample 04MM-36\_100.1m), but with evidence for partial thermal resetting, potentially related to emplacement of the Cassiar batholith. Hydrothermal sericite from Taurus (Sample T-95-35\_129.5m) also shows evidence for a thermal overprint, but heating steps yielded ages up to 143 Ma, which indicates that at least locally, veining and alteration may have formed at least 8 m.y. earlier than previously documented. The apparent 143–129 Ma age range of vein formation also indicates that at least locally, penetrative ductile features in the host rock sequence were older and potentially Jurassic features.

Lamprophyre dikes were emplaced at 113 Ma, consistent with a previous determination by A. Panteleyev (unpublished data in Nelson, 1990 and Ash, 2001). However, the 77 Ma age for the xenolith-bearing lamprophyre dike at the Bain mine requires at least two separate dike events: a mid-Cretaceous event that was broadly contemporaneous with early phases of the Cassiar batholith, and a Late Cretaceous event that predates ca. 73 Ma emplacement of quartz monzonite of the Troutline stock and formation of associated porphyry molybdenite mineralization (BC MIN-FILE 104P 035).

The shallow-dipping thrust architecture of the Cassiar gold camp has been identified by previous workers (e.g., Nelson, 1990; Ball, 1997) as conducive to formation of a vertical plumbing system along which mineralizing fluids could ascend. Nelson (1990) and Ball (1997) each considered a

magmatic component to mineralization, an assertion supported by the common occurrence of granitic xenoliths in lamprophyre dikes and spatial coincidence of these dikes with zones of mineralization. Ball (1997) speculated that sodic metasomatism of granitic clasts in lamprophyre dikes was produced by a subjacent alkaline igneous complex that was also responsible for the production of alkali-carbonate wall rock alteration and gold-silver mineralization in the district.

The geochronological results of this study suggests that at least some lamprophyre dikes were Late Cretaceous and post-dated Early Cretaceous gold mineralization by 50-60 m.y. Metasomatism of granitic xenoliths was likely generated by the hydrous, alkaline lamprophyric melt itself, in which K-feldspar bearing granitic clasts would be out of equilibrium with the surrounding melt. There is no

evidence to support the suggestion that this metasomatism was caused by an alkaline intrusion of appropriate age to generate gold mineralization in the district. Moreover, zircons extracted from the same ca. 77 Ma lamprophyre sample yielded ca. 110 Ma zircon xenocrysts, indicating that lamprophyre dikes intruded through igneous rocks that are equivalent in age to early phases of the Cassiar batholith, and may support the interpretation that the batholith is a sheet-like body intruding semi-conformably with, and dipping eastwardly beneath autochthonous strata below the Sylvester Allochthon (as implied by map patterns and cross-section in Nelson and Bradford, 1993). Furthermore, the age data suggest that any buried intrusion post-dates gold mineralization by approximately 20 m.y. and is genetically unrelated.

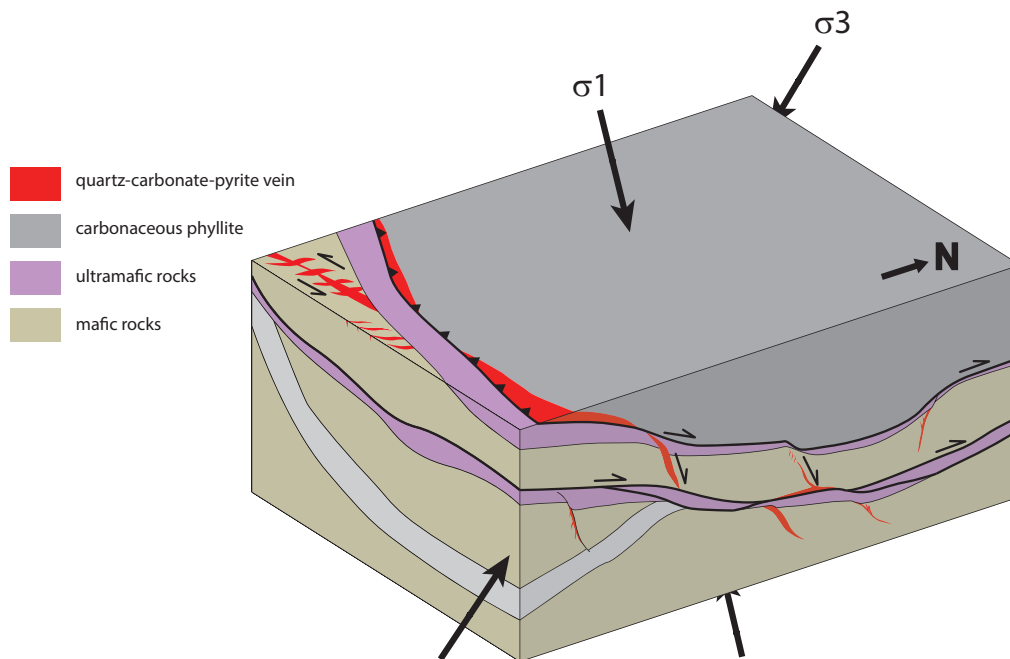


Figure 27. Summary block diagram of the main structural elements of the Cassiar gold district. The model indicates top-to-the-northwest movement along low-angle shear surfaces, with concomitant formation of thrust-filling veins, moderately dipping shear veins with a sinistral-normal shear sense, and subvertical extensional veins. The model implies subvertical shortening in the  $\sigma_1$  direction and subhorizontal extension ( $\sigma_2$ ) in the direction of the penetrative regional lineation. The sinistral strike-slip component of movement on east-northeast trending shear veins implies that the maximum principal stress direction is steeply inclined toward the northeast.

---

# Sheep Creek Gold Camp

---

The Sheep Creek gold camp is 12 km southeast of the town of Salmo in the Kootenay region of southern British Columbia (Fig. 28). The camp is part of the broader Salmo mining district, in which mineral occurrences represent a variety of commodities, deposit styles, and mineralization ages (see below).

The Sheep Creek gold camp comprises numerous underground mine workings within an approximately 10 km-long, north-trending belt of mineralized quartz veins. Total historic production from 1899 to 1951 was 736,000 oz Au, 365,000 oz Ag, 377,000 lbs Pb, and 312,000 lbs Zn from 1.72 Mt of ore (average grade of 13 g/t Au) (Mathews, 1953). An estimated 127 koz of gold reserves remain, although there are no current NI 43-101 compliant resources (Schroeter and Lane, 1991; Höy and Dunne, 2001). Surprisingly, there has been little effort to determine ore controls in the Sheep Creek gold camp, considering its rich mining history and outstanding questions regarding its metallogenesis.

## REGIONAL GEOLOGY

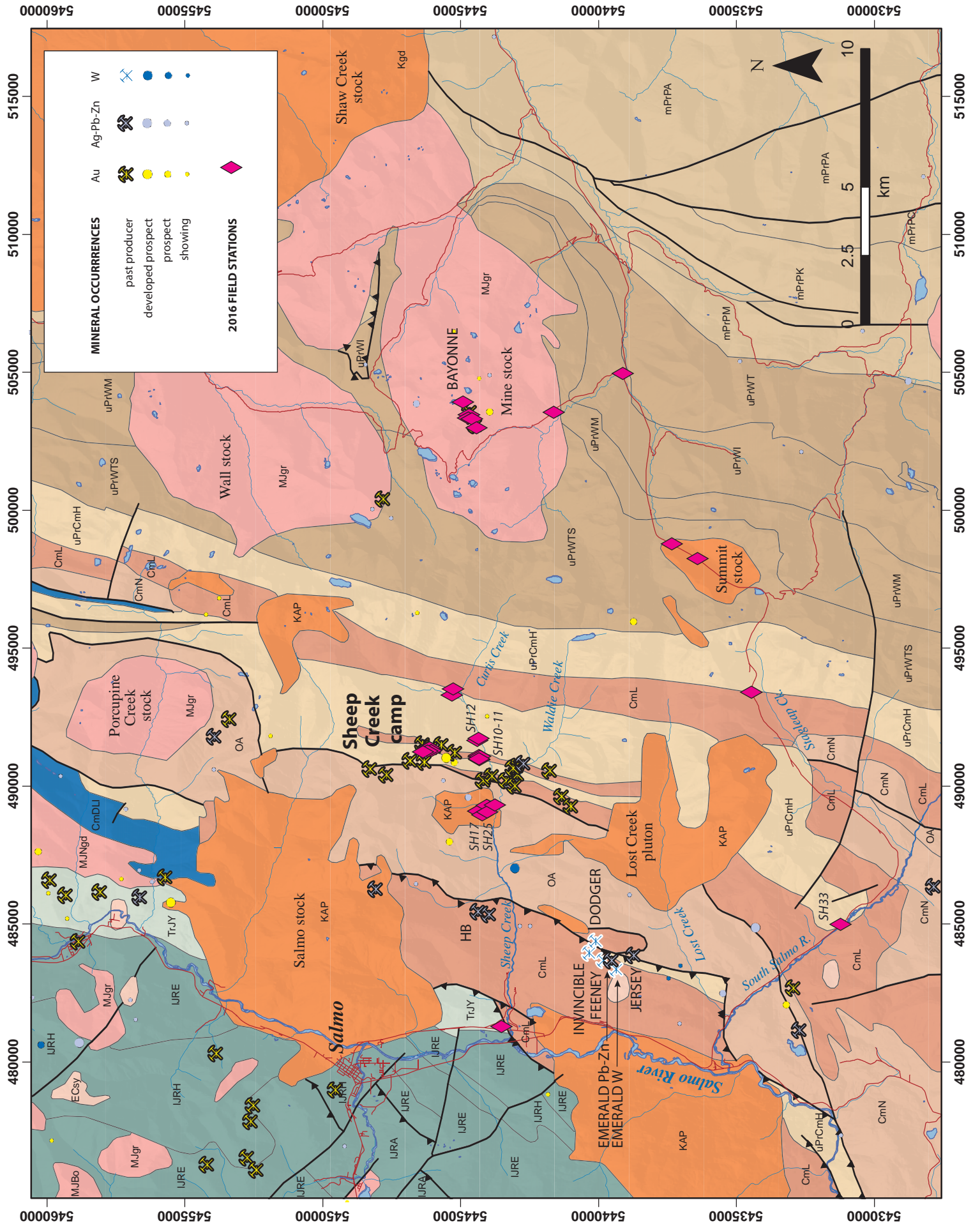
The Sheep Creek gold camp is underlain by a north-northeast-trending package of Neoproterozoic to early Paleozoic autochthonous North American strata in the southern Kootenay arc, and is 9 km east of the west-dipping boundary with Quesnellia terrane (Figs. 1, 28). From oldest to youngest, the Sheep Creek camp stratigraphy includes the Three Sisters Formation of the uppermost Windermere Supergroup, the Quartzite Range Formation and Reno Formation of the Hammill Group, and the Laib Formation (Fig. 28). These rocks reached chlorite-grade peak regional metamorphic conditions, and were subsequently overprinted by contact metamorphism associated with syn- to post-collisional plutons of Jurassic to Cretaceous age (Webster, 2016). A regionally significant north-northeast-trending anticline (Sheep Creek anticline) is flanked to the west by a parallel syncline-anticline pair, and these represent the dominant structures of the Sheep Creek camp (Figs. 28, 29).

The Three Sisters Formation is exposed in the core of the Sheep Creek anticline (Fig. 29), and includes interlayered quartzite (Fig. 30a), micaceous gritstone, and green chlorite-muscovite phyllite. The top of the Three Sisters Formation includes several feet of a distinctive chloritic marker horizon that contains dolomite rhombs (Mathews, 1953). The narrow, approximately 250 to 300 m-wide map exposure of Three Sisters Formation as defined on Matthews' 1953 geologic map of the Sheep Creek camp (Fig. 29) is not represented at the scale of the current digital geology of the Kootenay region (Höy et al., 1994; Fig. 28).

The Quartzite Range Formation stratigraphically and structurally overlies the Three Sisters Formation, and from oldest to youngest, comprises: quartzite, minor argillite, gritstone and greenschist of the Motherlode member; argillite and argillaceous quartzite of the Lower Nugget member; quartzite and argillaceous quartzite of the Middle Nugget member; quartzite and argillaceous quartzite of the Upper Nugget member (Fig. 30b-c); and quartzite and argillaceous quartzite of the Navada member (Fig. 30d). The Quartzite Range Formation is overlain by argillite, argillaceous quartzite, quartzite, and gritstone of the Reno Formation. The Reno Formation in turn is overlain by the Laib Group, comprising a lower member of limestone and argillite, and an upper member of argillite and minor argillaceous quartzite. Field observations and structural measurements in this study are from units of the Quartzite Range Formation (Upper Nugget and Navada members), Reno Formation, and Laib Group on the western, overturned limb of the Sheep Creek antiform.

Magmatic units are well-represented in the Salmo region, where they occur as large plutons, stocks, and dikes (Fig. 28). Approximately 10 km east of the Sheep Creek camp, Middle Jurassic plutons of the Nelson plutonic suite are represented by massive to foliated biotite-hornblende quartz monzonite and granodiorite of the Mine and Wall stocks (Fig. 28). Uranium-lead zircon ages on the Mine and Wall stocks are 171 Ma and 167 Ma, respectively (Archibald et al., 1983; Logan, 2002b). The Mine and Wall stocks generated staurolite-bearing contact metamorphic assemblages in pelitic host rocks, which provide pressure constraints of 3.5 – 4.2 kbar, equivalent to 13 – 15 km for the paleodepth of pluton emplacement (Logan, 2002b; Webster, 2016). The slightly younger (162 Ma) Porcupine Creek stock is located 9 km north of the Sheep Creek camp (Fig. 28) and has a cordierite-andalusite-bearing contact metamorphic assemblage that indicates a lower pressure of 2.5 – 3.3 kbar, equivalent to 9 – 12 km (Webster, 2016).

The Sheep Creek gold camp is also surrounded by numerous mid-Cretaceous (115 – 90 Ma) plutons of the Bayonne plutonic suite, which include the Salmo stock to the west and the Lost Creek pluton to the south (Fig. 28). This suite includes the 300 to 500 m-diameter Sheep Creek stock, which is only 1.5 to 2 km to the west of the Sheep Creek camp (Figs. 28-29). The Sheep Creek stock is characterized by massive, coarse-grained biotite granite that weathers recessively into grus (Fig. 31a). Locally, this coarse phase is in gradational contact with a more resistant quartz-feldspar porphyritic phase with a grey, fine-grained matrix (Fig. 31b). These phases of the Sheep Creek stock are cut by a similar but more densely porphyritic dike phase containing



## LEGEND

ECsy	<b>Corywell plutonic suite</b> (Eocene) – syenite to monzonite
Kgd, KAP	<b>undivided plutonic rocks</b> (mid-Cretaceous) – granodiorite; includes granitoids of the <b>Bayonne magmatic suite</b> (KAP of Höy et al., 1994)
MJgr	<b>undivided plutonic rocks</b> (Middle Jurassic) – granite, alkali-feldspar granite, and related granitoids
IJR	<b>ROSSLAND GROUP</b> (Lower Jurassic) –includes: basaltic volcanic rocks of the <b>Elise Formation</b> (IJRE); mudstone, siltstone, shale of the <b>Archibald Formation</b> (IJRA); mudstone siltstone, shale of the <b>Hall Formation</b> (IJRH)
TrJY	<b>Ymir Group</b> (Triassic to Jurassic) – limestone, slate, siltstone, argillite
OA	<b>Active Formation</b> (Ordovician) – mudstone, siltstone, shale, fine clastic sedimentary rocks
CmDLI	<b>LARDEAU GROUP, Index Formation</b> (Cambrian to Devonian) – mudstone, siltstone, shale, fine clastic sedimentary rocks
CmL	<b>Laib Formation</b> (Cambrian) – undivided sedimentary rocks
uPrCmH	<b>HAMMILL GROUP</b> (Neoproterozoic to Cambrian) – quartzite, quartz arenite sedimentary rocks (includes <b>Reno</b> and <b>Quartzite Range Formations</b> )
uPrW	<b>WINDERMERE SUPERGROUP</b> (Neoproterozoic) – includes: quartz and quartz arenite of the <b>Three Sisters Formation</b> (uPrWTS); argillite, greywacke, wacke, conglomerate of the <b>Monk Formation</b> (uPrWM); greenstone, greenschist metamorphic rocks of the <b>Irene Formation</b> (uPrWI); conglomerate, coarse clastic rocks of the <b>Toby Formation</b> (uPrWT)
mPrP	<b>PURCELL SUPERGROUP</b> (Mesoproterozoic) – includes: quartz and quartz arenite of the <b>Mount Nelson Formation</b> (mPrPM); undivided sedimentary rocks of the <b>Dutch Formation</b> (mPrPD); dolomitic carbonate rocks of the <b>Kitchener Formation</b> (mPrPK); siltstone, argillite, and quartzite of the <b>Creston Formation</b> (mPrPC); argillite, greywacke, wacke, conglomerate of the <b>Aldridge Formation</b> (mPrPA);

Figure 28 (left). Regional geologic map of the Sheep Creek gold camp (BC Digital Bedrock Geology from Höy et al., 1994)

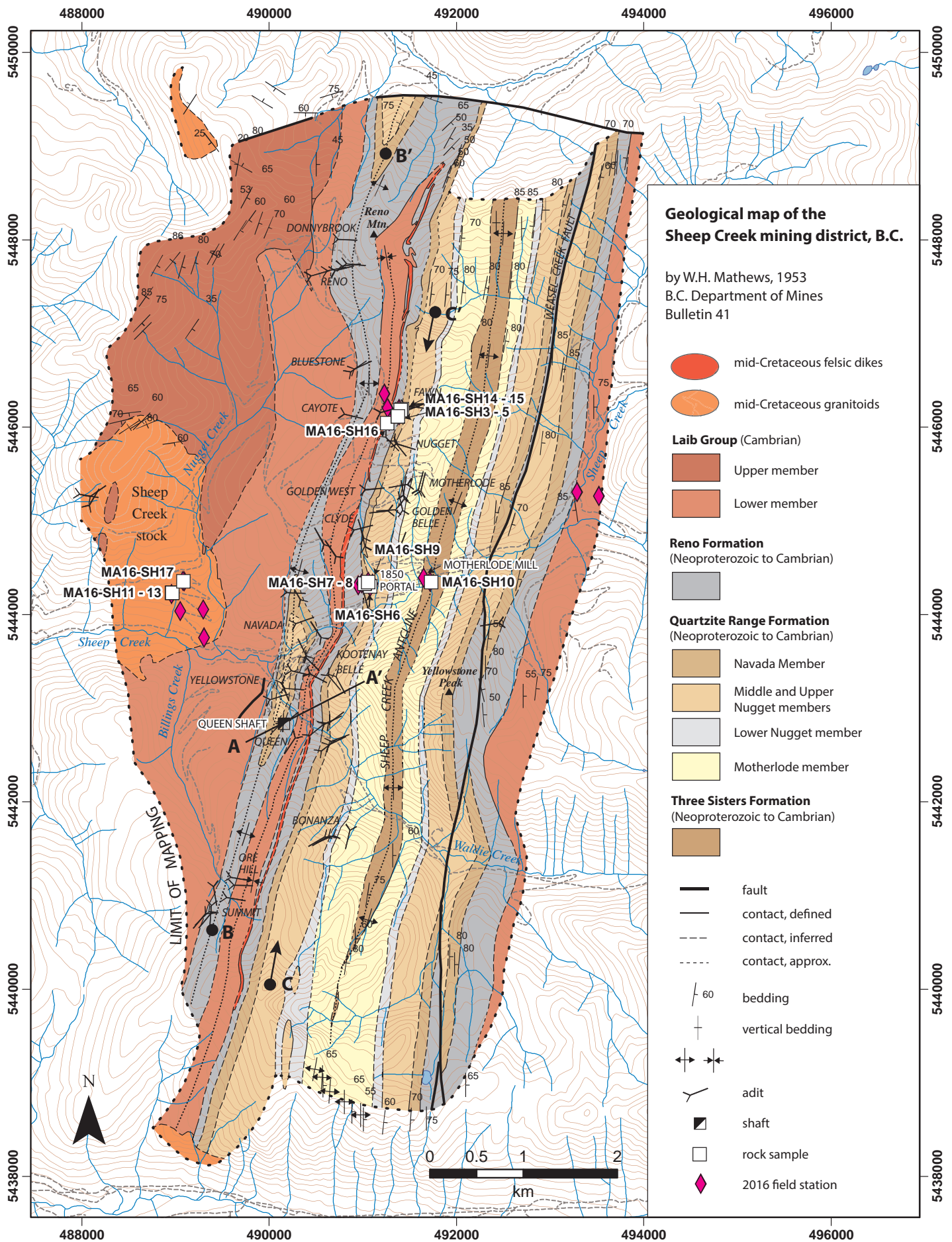


Figure 29. Geologic map of the Sheep Creek gold camp, after Mathews (1953). End points only of sections B-B', C-C' are indicated.



Figure 30. (a) Graded bedding in quartzite of the Three Sisters Formation (Locality SH12). (b) Gritstone of the Upper Nugget member of the Quartzite Range Formation, showing elongation of grains parallel to the regional north-northeasterly strike (Locality SH10); (c) View to the north of cross-bedded quartzite of the Upper Nugget member of the Quartzite Range Formation; way up is to the left (west), indicating bedding is overturned (Locality SH10). (d) View to the north of moderately east-dipping argillaceous quartzite of the Navada member, Quartzite Range Formation, showing slightly shallower  $S_2$  axial planar cleavage fabric relative to transposed bedding ( $S_0/S_1$ ) (Locality SH11).



Figure 31. (a) Coarse-grained biotite granite of the Sheep Creek stock (Locality SH17). (b) Gradational contact between coarse and fine-grained porphyritic variants of the Sheep Creek stock (Locality SH17). (c) Quartz-feldspar porphyry dike intruding granite of the Sheep Creek stock (Locality SH25). (e-f) Olivine-biotite lamprophyre cutting the Sheep Creek stock (Locality SH17).

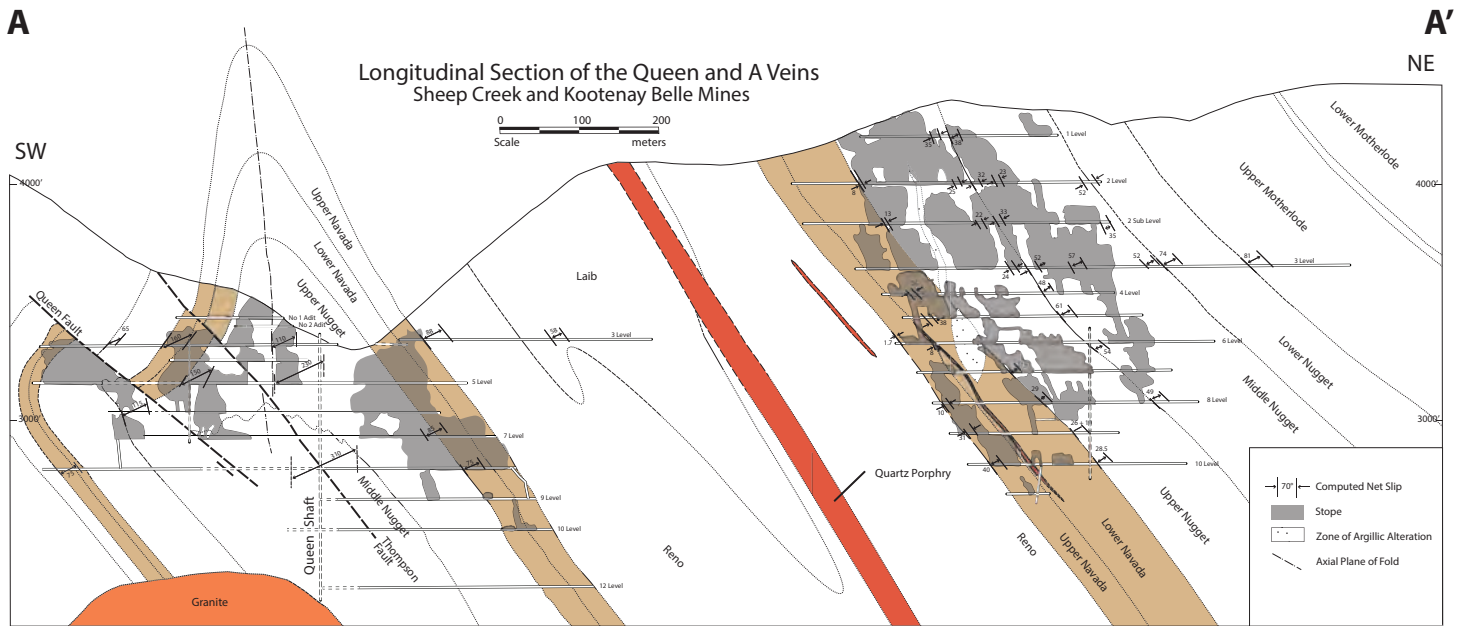


Figure 32. Longitudinal cross-section through underground workings of the Queen and A veins, showing the western anticline (left) and the east-dipping, overturned limb of the Sheep Creek anticline (right). Note the restriction of mine workings to the Nevada and Nugget members of the Quartzite Range Formation, and stratigraphically below the argillite-dominated Reno Formation. After Figure 7 in Mathews, 1953.

15% feldspar phenocrysts (4-10 mm) and 5% quartz phenocrysts (3-6 mm) in a fine-grained equigranular matrix (Fig. 31c). The Sheep Creek stock yielded a K-Ar biotite age of  $98.3 \pm 1.1$  Ma (Archibald et al., 1983), which is interpreted as the minimum emplacement age.

Granitic rocks resembling those of the mid-Cretaceous suite have also been documented below zones of gold mineralization in parts of the Sheep Creek gold camp (Mathews, 1953). The Queen Shaft penetrated coarse granite below productive mine levels, and Mathews (1953) noted "marked metamorphism in the impure quartzites" in parts of the Queen vein system (Figs. 29, 32).

Argillaceous rocks in the contact aureole of the Sheep Creek stock are variably hornfelsed, although phyllitic units observed in the vicinity of the Nugget mine some 2 km east have no visible evidence of a mineralogical or textural overprint. However, in the northern part of the Sheep Creek camp (Reno mine) and in the vicinity of the Sheep Creek stock, Mathews (1953) reported andalusite and another porphyroblastic phase appearing as "dark-grey spots...of lens-shaped segregations of quartz and mica", which fits the description of pinitized cordierite. Mathews also noted tremolite in calcareous sediments at the same locations. These metamorphic assemblages are consistent with emplacement of the Sheep Creek stock at  $\sim 2.5$  kbar or approximately 9 km paleodepth (Logan, 2002a).

A north-northeast-trending swarm of quartz porphyry dikes intrudes sediments and mineralized vein features of the Sheep Creek camp (Mathews, 1953; Figs. 29, 32), although the age was unknown prior to this study. The dikes are characterized by sparse ( $\sim 1\%$ ) euhedral quartz phenocrysts in a fine, equigranular (aplitic) groundmass (Fig. 31d). It was noted by Mathews (1953) that these dikes post-date dextral movement on the northeast-trending vein fractures that host mineralization. However, Mathews doubted that the porphyry "is also later than the sulphide mineralization" due to rare pyrite veinlets that cut the porphyry, and minor sphalerite along the vein-porphyry contact.

All units of the Sheep Creek camp are cut by biotite-olivine  $\pm$  augite bearing lamprophyre dikes (Fig. 31e-f), and these occur in underground workings where they locally cut zones of mineralization (Mathews, 1953). Lamprophyre dikes are typically steep and north-trending, except where they intrude along vein and fracture systems at a high angle to the attitude of the host sedimentary rocks (Mathews, 1953). Lamprophyre dikes contain abundant quartzite and rare granitic xenoliths (Mathews, 1953), the latter potentially derived from a concealed plutonic body beneath the Sheep Creek camp.

## ECONOMIC GEOLOGY

In addition to gold production from quartz veins in the Sheep Creek camp, past mining activity in the Salmo region exploited a wide variety of other mineralization styles and ages, including carbonate-hosted Pb-Zn ± Ag, intrusion-related W-Mo ± Cu-Au, and polymetallic veins (Höy and Dunne, 2003; Fig. 28).

The Kootenay Pb-Zn-Ag belt tracks the entire trace of the Kootenay arc, and is mainly hosted by Lower Cambrian carbonates of the Badshot Formation, the equivalent of which is the Reeves Member of the Laib Formation in the Salmo Pb-Zn camp. Southern Kootenay carbonate-hosted lead-zinc deposits have been described or summarized by several previous workers, and have been variably interpreted as Mississippi Valley Type (MVT), sedimentary exhalative (SEDEX), or Irish-type Pb-Zn deposits (Fyles and Hewlett, 1959; Sangster 1970, Höy, 1982; Nelson 1991, Paradis, 2007; Paradis et al., 2015).

The past-producing, carbonate-hosted HB Pb-Zn-Ag-Cd mine is located 5 km west of the Sheep Creek gold camp, and is hosted in dolomitized limestone of the Reeves Member of the Laib Formation (BC MINFILE 082FSW004; Fig. 28). Mining operations at HB between 1912 and 1978 yielded 6.6 Mt of ore from which 950 koz of Ag, 260 kt of Zn, and 49.5 kt of Pb, 2 kt of Cd and minor Cu and Au were recovered (BC MINFILE 082FSW0004). The past-producing Jersey and Emerald Pb-Zn mines are located in the same stratigraphy 6 km to the south of HB (Fig. 28), where between 1919 and 1970 they produced 8.0 Mt of ore grading 1.95% Pb and 3.83% Zn (Giroux and Grunenberg, 2010). Jersey contains an indicated resource of 5.3 Mt grading 1.04 % Pb and 2.60 % Zn, and an inferred resource of 16.9 Mt grading 1.00% Pb and 2.18% Zn at a 1.5% combined Pb-Zn cut-off grade (Giroux and Grunenberg, 2010).

Lead-zinc mineralization at Jersey and Emerald are spatially associated with a cluster of undeformed, equigranular biotite granite stocks and associated W ± Mo skarn mineralization of the Emerald Tungsten, Dodger, Feeney, and Invincible mines (BC MINFILE 082FSW010, 08FSW011, 08FSW247, 082FSW2188 respectively; Fig. 28). These systems are notable for elevated Au, Bi, As, Te, and Sn. These deposits collectively produced 1.60 Mt of ore grading 0.76% WO<sub>3</sub> (Giroux and Grunenberg, 2010). As of 2014, the Emerald Tungsten mine has a current indicated resource of 256 kt ore grading 0.19 % WO<sub>3</sub> and an inferred resource of 1122 kt ore grading 0.28 % WO<sub>3</sub> (Park and Grunenberg, 2015). Tungsten mineralization is associated with biotite granite of the Emerald stock, which yielded a <sup>206</sup>Pb/<sup>238</sup>U zircon age of 102.2 ± 2.3 Ma (Webster, 2016).

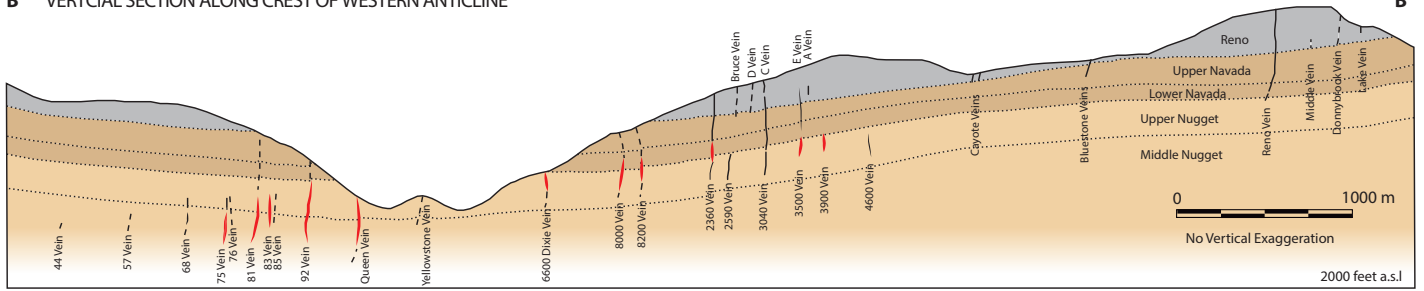
Near Salmo, polymetallic Ag-Pb-Zn ± Au veins occur in fine-grained siliciclastic rocks of the Quesnellia terrane (Rosslund Group), and these are spatially associated with a cluster of plutons related to the Middle Jurassic Bonning-

ton pluton (Fig. 28). A similar suite of polymetallic veins occurs 12 km east of the Sheep Creek camp at the Bayonne mine, which produced 42,174 oz gold and 120,665 oz silver from 81,782 t of ore (16.0 g/t Au; 45.9 g/t Ag; BC MINFILE 082FSE030; Fig. 28). Veins cut biotite-hornblende granodiorite of the Middle Jurassic Mine stock, and are continuous along strike for nearly 1 km toward ~070°N. The age of Bayonne mineralization is approximately 145 Ma, as determined by Ar-Ar dating of vein sericite (Logan, unpublished data in Webster, 2016), and thus is genetically unrelated to hydrothermal fluids related to crystallization of the Middle Jurassic host rocks.

Underground gold mining in the Sheep Creek gold camp targeted numerous high-grade veins hosted in Neoproterozoic to Cambrian siliciclastic rocks of the Hammill Group. The geology of the Sheep Creek gold camp is described in superb detail by Mathews (1953), and barring future underground rehabilitation and mining, is the best current source of descriptive information on mineralization. Mathews (1953) summarized the gold mineralization as follows:

The gold deposits of the Sheep Creek camp consist essentially of quartz veins containing as a rule minor amounts of sulphides. Pyrite is the only abundant sulphide; galena and sphalerite are present, but as a rule it is only where the veins cut limestone that these two minerals occur in commercial quantities. Nearly all the production of gold has been from those parts of the veins where one or both walls consist of quartzite of either the Nugget or the Nevada members of the Quartzite Range formation. Vein fractures cutting argillite are generally devoid of quartz or are occupied by only a thin band of barren vein matter. The extent of the productive part of any vein along the vein is, therefore, limited by the distribution of favourable quartzite in its walls. Within the favourable quartzites, oreshoots make up varying proportions of the veins. The upper limit of orebodies is most commonly the ground surface, or in the Western anticline the crest of the quartzite beds, but in places in the southern part of the camp, even within a single type of rock, veins become narrower upward to the point that they cannot be mined economically. In general, vein widths do not diminish downward; on the contrary, vein widths are average or greater than average on the lowest levels of most mines. However, high-grade ore occurs less abundantly in the lower levels, and the proportion of the vein that could be mined profitably diminishes. On the lowest levels on which several veins have been explored no ore was found, or the proportion of ore to submarginal parts of the vein was such that no net profit resulted from exploring and mining the veins on those levels. In the veins that have been explored, oreshoots have been found within a vertical range that is not more than 1,600 feet for any vein. This productive range is found at elevations that from north to south are progressively lower.

**B** VERTICAL SECTION ALONG CREST OF WESTERN ANTICLINE



**C** VERTICAL SECTION ALONG TOP OF NUGGET MEMBER ON WESTERN LIMB OF EASTERN ANTICLINE

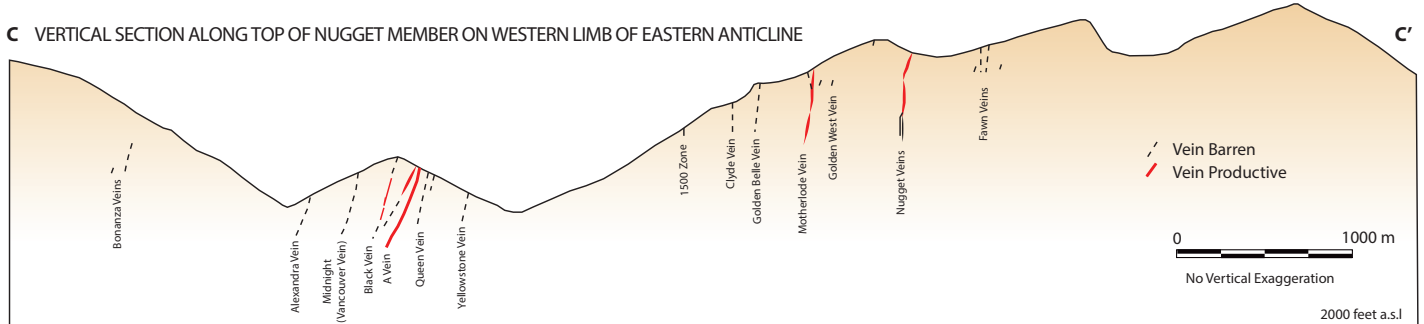


Figure 33. Vertical sections B-B' and C-C' indicated on Figure 29, oriented along the regional strike and at a high angle to quartz veins (After Figure 9 in Mathews, 1953).

The restriction of gold-bearing veins to favourable quartzite stratigraphy is illustrated by the distribution of underground workings in the Queen and Kootenay Belle mine areas south of Sheep Creek (Figs. 28, 32). Here mineralization is confined to the Upper and Middle Nugget and Nevada members of the Quartzite Range Formation, which structurally underlie argillaceous sediments of the Reno Formation in the western anticline, but which structurally underlie argillite and argillaceous quartzite of the Lower Nugget member in the overturned western limb of the Sheep Creek anticline (Fig. 32). The link between gold distribution and favourable quartzite stratigraphy of the Nugget and Nevada members is maintained along the north-south strike length of the western anticline and the western limb of the Sheep Creek anticline (Sections B-B' and C-C', Fig. 33).

The most productive veins of the Sheep Creek camp occupy northeast-trending fault-fracture zones with dextral strike-slip displacement (see below). A less abundant conjugate set of northwest-trending faults have sinistral strike-slip movement, although these do not host mineralization (Mathews, 1953). Vein quartz is typically massive; comb or vuggy textures are rare (Mathews, 1953; Fig. 34). Alteration of the quartz-dominant wall rock is lacking except locally for bleaching of quartzite close to vein margins. Sericite is the most common alteration mineral associated with mineralization, and occurs as randomly oriented flakes intergrown with quartz and pyrite, or as septa of altered wall rock.

Vein quartz is isotopically heavy with  $\delta^{18}\text{O}$  values averaging  $14.4 \pm 3\%$  (VSMOW), and contains low to moderate salinity  $\text{H}_2\text{O}-\text{CO}_2 + \text{CH}_4$  fluid inclusions that indicate trapping conditions of  $300 \pm 50^\circ\text{C}$  and fluctuating pressures of 1-2 kbar (Hardy, 1992). Vein calcite yields average  $\delta^{13}\text{C}$  values of  $-2.5 \pm 1.3\%$  (PDB) and limestone and calcareous argillites in the area have similar values of  $-1.9 \pm 2.3\%$ , which led Hardy (1992) to suggest a carbon source dominated by the local sedimentary sequence.



Figure 34. (a) Barren extensional quartz veins cutting white quartzite near the 1850 portal; (b) Pyritic fractures cutting massive quartz ore from the Nugget mine. It is unclear whether quartz is space-filling vein material or recrystallized quartzitic host rock; (c) Quartz-pyrite vein material from the 1850 portal.

## STRUCTURAL GEOLOGY

Consistent structural features were observed in all three outcrop areas of the Sheep Creek gold camp visited in this study, which include the 1850 Portal, Motherlode mill area, and the Nugget portal (Fig. 29). All three areas are located on the western limb of the Sheep Creek anticline, and consistent relationships between bedding, cleavage, and brittle deformation features were observed. Examples of the structural elements observed in the field are shown in the Figure 35, along with equal area stereonet plots of the compiled structural features in Figure 36.

Host rocks in the Sheep Creek camp consistently strike north-northeast (Figs. 29, 36). Where quartzite and argillaceous quartzite of the upper Quartzite Range Formation (Upper Nugget and Nevada members) and Reno Formation outcrop near the Nugget mine portal and 1850 portal, bedding ( $S_0$ ) is overturned and dips steeply to moderately to the east-southeast. Cross-bedding in quartzite, defined locally by heavy mineral layers, defines stratigraphic younging to the west, which is consistent with outcrops' mapped position on the western, overturned limb of the Sheep Creek

anticline. In argillaceous layers, bedding is modified by a ductile transposition fabric ( $S_1$ ) oriented parallel to the compositional layering ( $S_0$ ). Near the Motherlode mill, rocks of the stratigraphically underlying Three Sisters Formation are represented by strongly deformed muscovite-chlorite phyllite interlayered with argillaceous gritstone. Here the  $S_1$  transposition fabric is especially strongly developed.

A penetrative cleavage fabric ( $S_2$ ) is locally developed in argillaceous layers of the Quartzite Range Formation and Reno Formation. The  $S_2$  fabric is north-northeast striking, moderately east-southeast dipping, and in most cases, is shallower than transposed bedding ( $S_0/S_1$ ) (Figs. 30d, 36). This geometry is consistent with the  $S_2$  fabric being related to formation of the Sheep Creek anticline and related north-northeast-trending  $F_2$  folds. This fabric is effectively absent in pure quartzite units, except in the thin, millimetre to centimetre-scale argillaceous tops of metre-scale beds. The dip of the  $S_2$  cleavage is highly variable (Fig. 36), due in part to refraction of cleavage across layers of different mica content.



Figure 35. (a) View to the west of outcrop near the 1850 Portal. The steep, E-dipping fracture sets correspond to the transposed bedding surface ( $S_0/S_1$ ). Note the strong subhorizontal stretching lineation defined by deformation-related grooves on the bedding surface ( $L_2$ ). Widely spaced  $S_3$  kink bands and parallel joints are developed nearly perpendicular to the  $L_2$  lineation. (b) View to northwest of a bedding surface ( $S_0/S_1$ ), overprinted by a subhorizontal  $L_2$  lineation and a set of broad, moderately southeast-plunging  $F_3$  crenulations. (c) Argillaceous quartzite float showing a well-developed set of  $F_3$  crenulations (top-to-bottom) overprinting the main  $L_2$  fabric. (d) Spaced fibrous (extensional) quartz veinlets and associated  $F_3$  kinks cutting argillaceous quartzite perpendicular to both transposed bedding ( $S_0/S_1$ ) and the  $L_2$  lineation.

The intersection of the  $S_2$  cleavage fabric and transposed bedding ( $S_0/S_1$ ) results in a locally well-defined intersection lineation ( $L_2$ ), which is consistently subhorizontal and north-northeast-trending (Figs. 35-36). A penetrative,  $L_2$ -parallel shape fabric is also apparent on bedding surfaces, which is defined by combinations of: (1) deformation-related, centimetre to decimetre-scale grooves on the bedding surface (Fig. 35a); (2) aggregate lineation or rodding of quartz in argillaceous quartzite; and (3) elongate detrital grains in gritty units (Fig. 30b). Rare examples of mesoscopic  $F_2$  folds are also observed, and fold axes of these are consistently parallel to  $L_2$  fabrics.

The host rock sequence is commonly intersected at a high angle by east-trending sets of crenulations and kink bands ( $S_3$ ; Figs. 35-36). Crenulations are commonly low-amplitude and are best developed in argillaceous units or argillaceous tops of quartzite beds. The attitude of the  $S_3$  crenulation cleavage fabric is normally difficult to assess in argillaceous quartzite, although the trace of these crenulations ( $L_3$ ) is normally obvious on the  $S_0/S_1$  surface (Fig. 35). Where kink bands are developed in the argillaceous tops of quartzite beds, they are typically widely spaced (on the or-

der of 50 cm or more). In pure quartzite beds the  $S_3$  fabric is generally absent, although barren quartz veins of the same orientation are common. Where these quartz veins intersect argillaceous tops of quartzite beds, a deflection of the host rock  $S_0/S_1$  fabric at the margin of the vein is common. The orientation of  $S_3$  fabrics is variable, ranging from a strike of  $070^\circ\text{N}$  to  $126^\circ\text{N}$ . However, this variability is consistent with the range of vein orientations (below), and is appropriately interpreted in the context of conjugate deformation bands.

All sedimentary rocks of the Sheep Creek camp have well-defined, steeply dipping joints oriented nearly perpendicular to the penetrative  $L_2$  elongation fabric (Figs. 35a, 36). Extensional quartz veins from a few millimetres to several centimetres also share this orientation (Fig. 34a). A second set of quartz veins is orientated  $070^\circ\text{N}$  to  $080^\circ\text{N}$ , and show strong field evidence for a component of dextral shear along the vein surface. Shear sense indicators include rotation of wall-rock fabrics and sigmoidal vein arrays (Fig. 37). The shear veins observed and measured in the field are consistent in orientation and dextral shear sense with the gold-mineralized veins described by Matthews (1953). Pyrite or other sulphides are rare to absent in the bedrock

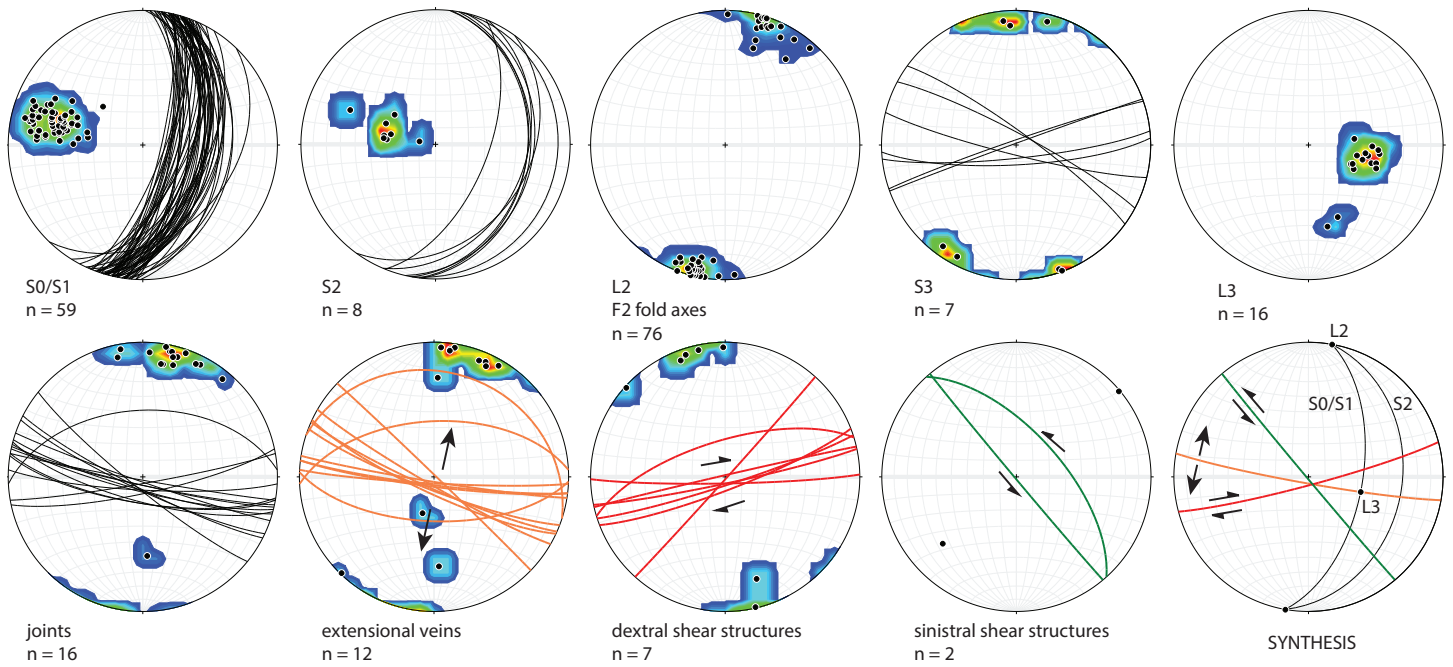


Figure 36. Equal-area lower hemisphere stereonet projections of all planar and lineation measurements collected at the Sheep Creek camp. See text for discussion.

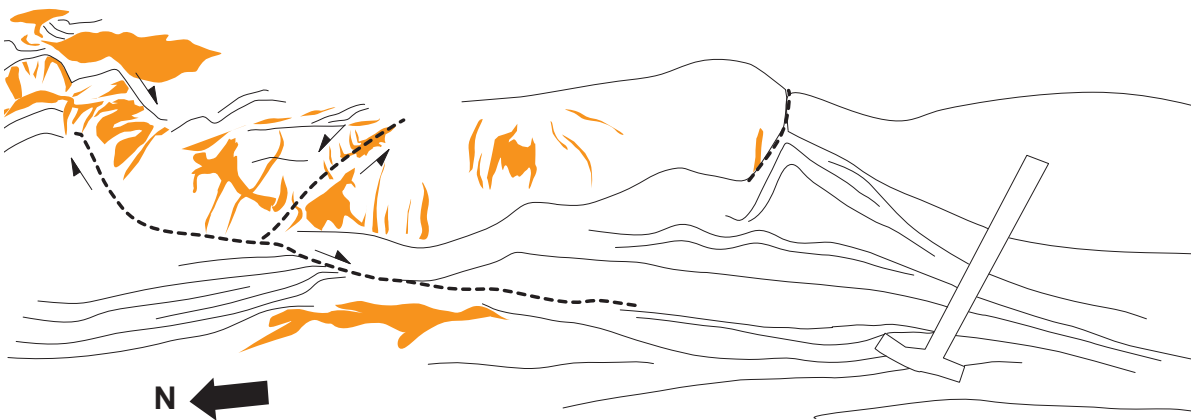


Figure 37. Deformed sequence of quartzite (top) and phyllite (bottom) in the creek below the Motherlode mill (Three Sisters Fm., Locality SH12). The main structural feature is a northeast-trending dextral shear that deflects into parallelism with the main planar fabric of the phyllite unit. Northwest-trending antithetic accommodation structures with sinistral movement are developed in the more competent quartzite unit, as indicated by a right-stepping *en echelon* array of quartz veins (centre-left).

localities visited in this study, although mineralized vein material from the Nugget mine was observed and sampled from an ore stockpile near Salmo (Fig. 34b-c).

Mathews (1953) describes two sets of post-mineralization faults. A north-trending set dips steeply to the east and accommodates normal movement up to 300m (e.g., Weasel Creek fault, Fig. 29). Minor shallowly-dipping faults with displacements of a few metres have also been reported in underground workings (Mathews, 1953).

## Regional comparisons

### **Along-strike projection of the Sheep Creek camp**

The same stratigraphy present in the Sheep Creek camp is exposed along the Salmo-Creston segment of Highway 3, and provides an opportunity to compare and contrast the style and intensity of deformation both proximal and distal to mineralization (Fig. 28). Figures 38 and 39 summarize structural observations and measurements made along a cliff-forming roadcut in argillaceous quartzite of the Hamill Group (most likely Upper Nugget or Nevada member equivalent; Locality SH33 in Fig. 28). Metre-scale folding of quartzite beds at this locality gives rise to significant variability in bedding orientation ( $S_0/S_1$ ), but a consistent fold axis and elongation fabric ( $L_2$ ) was measured plunging moderately to the southwest (average orientation of  $36^\circ/219^\circ\text{N}$ ). The plunge of fold axes at this location is consistent with the mapped fold closure of a major anticline cored by Hammill Group rocks in this area (Fig. 28).

A prominent set of quartz  $\pm$  muscovite  $\pm$  pyrite veins dips steeply to the northeast, nearly perpendicular to the  $L_2$  fabric. A second set of quartz veins oriented  $\sim 20^\circ$  clockwise from the first set accommodate sinistral shear, as indicated by flanking right-stepping en echelon arrays of extensional veins (Figs. 38-39). The same structural elements described above in the Sheep Creek camp are represented in this roadcut, and with the same relative orientations. The main difference is that the penetrative  $L_2$  lineation and fold axes plunge to the southwest (Fig. 39), in contrast with the subhorizontal geometries of the Sheep Creek camp (Fig. 33). In addition, sinistral shear zones are well represented along this Hwy 3 outcrop, whereas dextral shear structures are better developed in the Sheep Creek camp. A shear vein containing quartz and muscovite from this locality was sampled to date the onset of brittle deformation (see  $^{40}\text{Ar}/^{39}\text{Ar}$  results below; Fig. 38d).

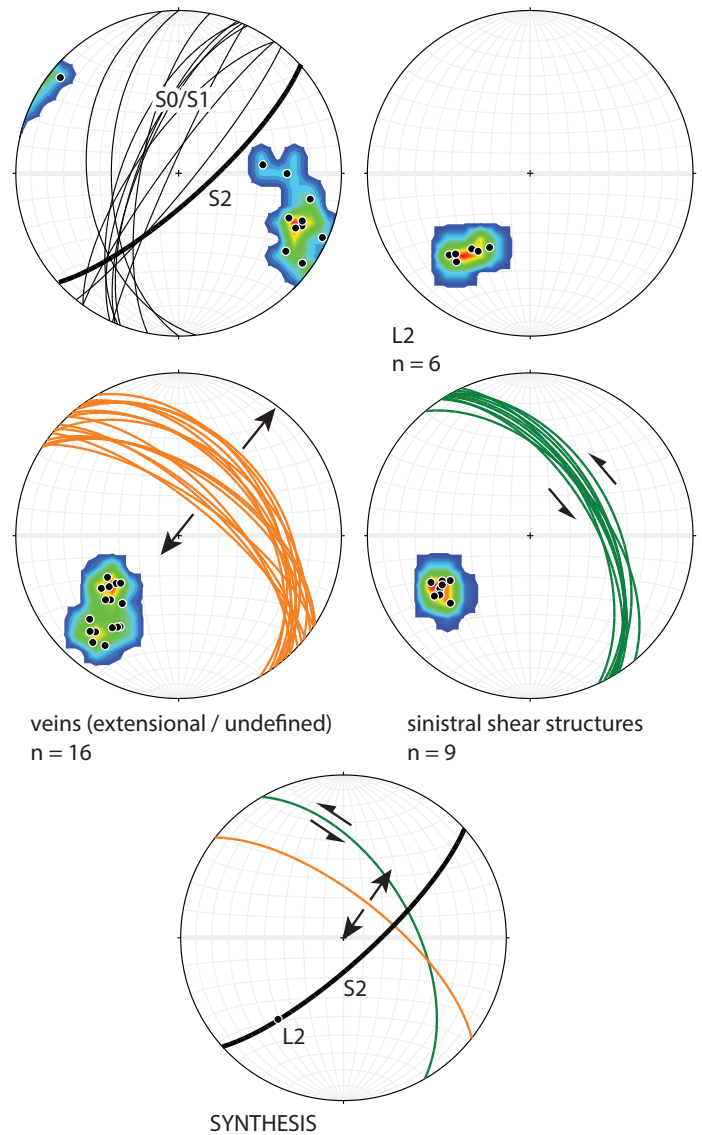


Figure 38. Equal-area stereonet projections of planar and linear structural data collected at Locality SH33 along Highway 3.



Figure 39 (right). (a) View toward 100°N of quartzite roadcut, located 15 km south of the Sheep Creek camp along Highway 3. Note the prominent southeast-plunging lineation developed on the northwest-dipping bedding surface. Spaced quartz veins in the foreground are purely extensional, whereas those in the background accommodate sinistral shear. (b-c). *En echelon* quartz vein arrays overprinted by a sinistral shear vein. (d) quartz-muscovite vein sampled for  $^{40}\text{Ar}/^{39}\text{Ar}$  analysis (Sample MA16-SH24).

### **Bayonne mine**

The Bayonne vein system comprises massive to vuggy, auriferous quartz-ankerite-galena-sphalerite-chalcopyrite-pyrite-tetrahedrite veins hosted in massive, medium-grained hornblende-biotite granodiorite of the Mine stock (Figs. 28, 40). Veins are flanked by brown-weathering haloes of ankerite-sericite  $\pm$  pyrite alteration (Fig. 40a-c). Individual veins strike from north to northeast, but the most prominent set is subvertical and strikes 065°N to 070°N, parallel to the mapped trace of the Bayonne vein. Striated vein and joint surfaces indicate late fault movement

on the Bayonne vein system, and a single in situ example of stepped slickensides on a steeply southeast-dipping, northeast-trending fault surface indicates dextral strike-slip movement (Fig. 40d). A much greater number of observations and measurements are required to assemble a meaningful structural and kinematic model for Bayonne, to test whether it may have formed under a similar stress regime to Sheep Creek.



Figure 40. (a) Gossanous fractures developed in granodiorite parallel to the Bayonne vein. (b) progression from fresh biotite-hornblende granodiorite of the Mine stock (left) to increasing degrees of mafic-destructive chlorite and sericite alteration, and sericite-ankerite alteration of feldspar. (c) quartz-pyrite-chalcopyrite-sphalerite vein with intensely carbonate-sericite altered granodiorite host rock. (d) subhorizontal stepped slickensides on a northeast-striking fault surface near the eastern limit of the Bayonne vein.

## GEOCHRONOLOGY

New  $^{40}\text{Ar}/^{39}\text{Ar}$  and U-Pb geochronology results help to constrain the age of deformation, mineralization, and magmatic events in the Sheep Creek camp. Argon-argon and U-Pb data are presented in Appendices 2 and 3, respectively, and the results of individual samples are presented below.

### $^{40}\text{Ar}/^{39}\text{Ar}$ analysis

#### **Metamorphic rocks**

Sample MA16-SH10 is quartz-muscovite phyllite from the Three Sisters Formation that is exposed in the creek bed below the Motherlode mill (Fig. 35). A pressed pellet of hand-scraped muscovite yielded a monotonically rising age spectrum from 86 to 132 Ma, with a set of intermediate steps increasing gradually from 102 to 107 Ma. Similar results were obtained from finely divided sericite from the same sample, although a maximum age of 115 Ma was reached. Analyses from this sample are consistent with partial to near-total argon loss in the mid-Cretaceous, overprinting an apparent minimum metamorphic age of 132 Ma.

Sample MA16-SH14 is a specimen of thinly interbedded quartzite and muscovite phyllite cut by fibrous quartz veinlets at a high angle to transposed bedding. A pressed pellet of muscovite scraped from the sample yielded a rising age spectrum with a plateau age of  $101.0 \pm 0.1$  Ma at intermediate heating steps (steps 2-5 of 11, representing 70.4% of the  $^{39}\text{Ar}$ ; MSWD = 2.7; probability = 0.043). An analysis of finely divided muscovite from the same sample yielded a similar age spectrum with a plateau of 102-101 Ma at intermediate heating steps. Results are compatible with near-total resetting of argon in muscovite in the mid-Cretaceous, with more radiogenic components likely reflecting an earlier metamorphic origin of the muscovite.

Sample MA16-SH24 is a quartz-muscovite shear vein cutting quartzite of the Hammill Group, in a roadcut along the Salmo-Creston Highway that represents similar stratigraphy and structural elements as those described above for the Sheep Creek camp (Locality SH33, Fig. 28; Figs. 36-37). Coarse, pale green sericite from this vein yielded a  $^{40}\text{Ar}/^{39}\text{Ar}$  plateau age of  $133.0 \pm 0.2$  Ma (steps 6-11 of 12, representing 71.2% of the  $^{39}\text{Ar}$ ; MSWD = 2.5; probability = 0.029). This age is interpreted to date vein formation, so is thus the minimum age of  $D_2$ -related ductile fabrics in the host rock.

#### **Ore material**

Sample MA16-SH03 is a specimen of quartz-pyrite vein material that contains narrow seams of pale sericite, from an ore stockpile from the Nugget mine (Fig. 34b-c). Sericite yielded a rising  $^{40}\text{Ar}/^{39}\text{Ar}$  age spectrum reaching 104 Ma in the final heating step (associated with only 28% of the  $^{39}\text{Ar}$  released). A second aliquot of the same sample yielded a similar rising age spectrum from 91 to 115 Ma, with an inflection point  $\sim 102$  Ma. A similar sample of vein ore

material from the Nugget mine (Sample MA16-SH05) gave a similar  $^{40}\text{Ar}/^{39}\text{Ar}$  age spectrum rising from 94 to 116 Ma. The analyses of these two samples are consistent with a 116-115 Ma minimum age of sericite formation, with subsequent thermal resetting in the mid-Cretaceous.

#### **Intrusive Rocks**

Sample MA16-SH13 is a biotite-olivine lamprophyre dike cutting the Sheep Creek stock (Fig. 31e-f). Biotite yielded a plateau age of  $53.0 \pm 0.1$  Ma (steps 10-12 of 12, representing 62.6% of the  $^{39}\text{Ar}$ ; MSWD = 0.42; probability = 0.66). This Eocene age is the emplacement and crystallization age of the dike.

### U-Pb analysis

#### **Sheep Creek stock**

Three phases of the Sheep Creek stock were sampled and analyzed for U-Pb zircon ages by laser ablation ICP-MS: massive, coarse-grained biotite granite of the main phase of the stock (MA16-SH12; Fig. 31a); quartz-feldspar granite porphyry with a fine-grained equigranular groundmass, in gradational contact with the coarse-grained phase (MA16-SH11; Fig. 31b); and a cross-cutting quartz-feldspar porphyry unit (MA16-SH17; Fig. 31c).

The coarse-grained granite (MA16-SH12) yielded clear, colourless zircon grains that were typically 125-200  $\mu\text{m}$  long with idiomorphic external morphology. Internal zoning revealed by SEM-CL imaging is dominantly oscillatory, with some grains showing clear core-rim relationships. Seventeen of 20 single-grain analyses yielded concordant or nearly concordant U-Pb isotopic ratios. Sixteen of these 17 analysis give a mean  $^{206}\text{Pb}/^{238}\text{U}$  age of  $104.3 \pm 1.2$  Ma, but with wide scatter likely reflecting a protracted magmatic history (MSWD = 3.6; probability = 0.0).

The porphyritic phase of the Sheep Creek stock (MA16-SH11) yielded zircons ranging in size from 50 to 250  $\mu\text{m}$ , ranging in external shape from rounded to idiomorphic, and with a variety of internal morphologies including simple oscillatory zoning patterns and complex core-rim relationships. Of the 14 grains analyzed, seven were xenocrysts ranging in age from late Paleoproterozoic to Triassic. The remaining seven zircon grains gave nearly concordant Early Cretaceous ages ranging from 130 to 101 Ma. A cluster of five nearly concordant ages give a mean  $^{206}\text{Pb}/^{238}\text{U}$  age of  $102.0 \pm 1.6$  Ma (MSWD = 1.8; probability = 0.13). The texturally transitional nature of this porphyritic phase with coarse-grained biotite granite requires that the phases are coeval, and moreover that the true crystallization age of the coarse phase is likely closer to 102 Ma, as suggested by the  $101.6 \pm 1.1$  Ma mean  $^{206}\text{Pb}/^{238}\text{U}$  age of the four youngest zircons in sample MA16-SH12.

The late quartz-feldspar porphyry unit (MA16-SH17) is more densely porphyritic than the earlier phase that is

coeval with the coarse granite, and it has a finer-grained, dark grey matrix. Zircon grains isolated from this sample are stubby to elongate, doubly terminating prisms ranging from 100 to 300  $\mu\text{m}$  long, and with a few exceptions exhibit simple oscillatory growth zoning. A single equant grain with complex internal zoning yielded a late Mesoproterozoic age. The remaining 17 of 18 analyses yielded mainly concordant results with an error-weighted mean  $^{206}\text{Pb}/^{238}\text{U}$  age of  $102.3 \pm 0.7$  Ma (MSWD = 2.0; probability = 0.01), which is interpreted as the unit's crystallization age. This age agrees within  $2\sigma$  error of the older porphyritic rock, suggesting they are broadly coeval and intimately related to emplacement of the Sheep Creek stock.

An aplitic dike containing sparse, euhedral quartz and feldspar phenocrysts (MA16-SH16; Fig. 31d) was collected near the Nugget mine to date this unit, which is described by Matthews (1953) as cutting the northeast-trending, mineralized shear veins, but which itself locally hosts sulphide minerals. The altered groundmass of this sample is overprinted by 0.5-1 mm radiating aggregates that were identified as K-feldspar on the basis of energy-dispersive X-ray spectroscopy. The majority of zircons from this sample are small (50 to 100  $\mu\text{m}$ ), equant to stubby grains with rounded to prismatic external habit. Internal zoning is highly variable and indicating a range of complex growth histories. Of the 16 grains analyzed, 13 are Proterozoic xenocrysts. Three of the remaining zircons yielded concordant to weakly discordant mid-Cretaceous ages that give an error-weighted mean  $^{206}\text{Pb}/^{238}\text{U}$  age of  $102.3 \pm 4.2$  Ma (MSWD = 1.4; probability = 0.25). This is interpreted as the emplacement age of the dike, which agrees within error with the age of the Sheep Creek stock and related porphyritic phases.

## DISCUSSION – SHEEP CREEK GOLD CAMP

### Structural setting of mineralization

Ductile and brittle structural elements of the Sheep Creek camp are best explained by progressive shortening in the direction of  $100^\circ\text{N}/280^\circ\text{N}$  (Fig. 41). Shortening in this direction accounts for the formation of north-northeast-trending folds, and the overall strain is essentially coaxial, although a component of strike-slip simple shear is likely required to explain the penetrative subhorizontal stretching lineation ( $L_2$ ) oriented parallel to  $F_2$  fold axes. Progressive shortening at a high angle to the strike of the orogen led to the formation of conjugate kink bands ( $S_3$ ), Mode I cracks ( $L_2$ -perpendicular joints, extensional quartz veins), and conjugate structures accommodating strike-slip movement.

Lack of safe underground access precluded *in situ* observations of mineralized features in the Sheep Creek camp in this study. However, Matthews (1953) associates mineralization with sets of northeast-trending vein-fracture zones with dextral strike-slip movement, matching the orientation and shear sense of those observed in outcrop. Therefore, mineralization is most reasonably interpreted to have formed at the latest brittle stage of progressive shortening associated with Mesozoic collision of the Intermontane terranes with Proterozoic to Paleozoic strata of the ancient North American margin. Deformation associated with this collision was clearly complete before mid-Cretaceous time, as evidenced by plutons of the Bayonne suite that cross-cut folds and thrust faults of the Cordilleran orogen in the Salmo region (Fig. 28).

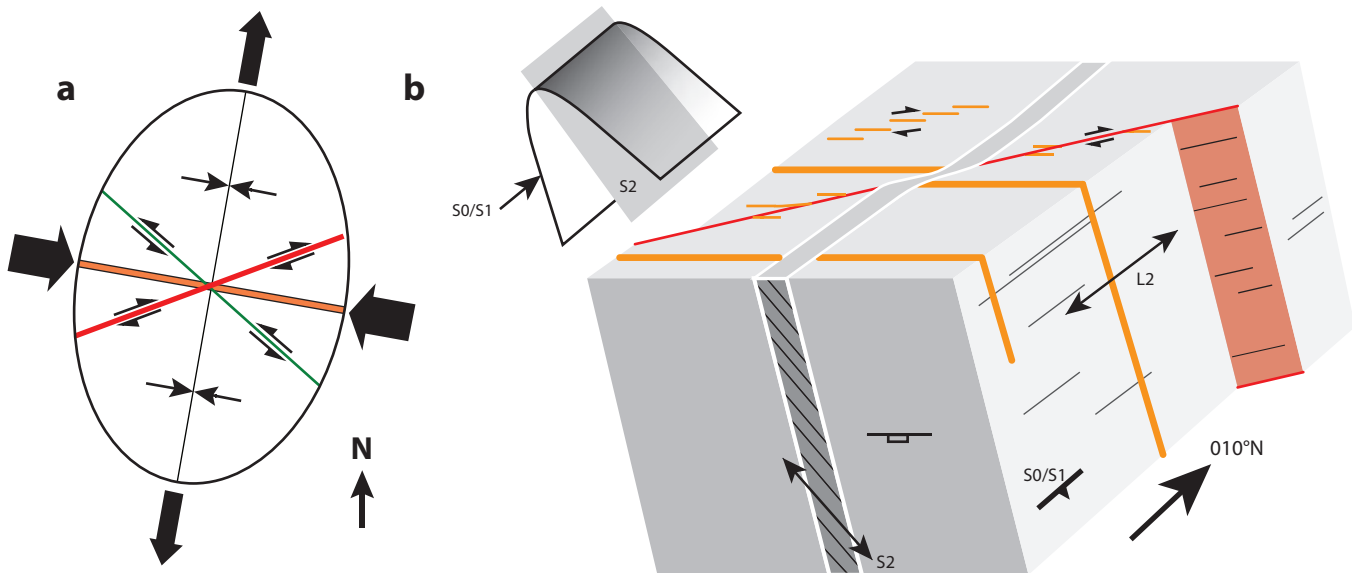


Figure 41. (a) Summary strain ellipse (plan view) and (b) block diagram illustrating the main structural elements of the Sheep Creek camp. The dark grey horizon in the middle of the block model signifies a more easily deformed argillaceous lithology.

## Age of mineralization and deformation

Interpreting the age of deformation and hydrothermal activity in the Sheep Creek gold camp is complicated by post-collisional, ca. 102 Ma mid-Cretaceous granitoids, which include the Sheep Creek stock (this study), the Emerald stock (Webster and Pattison, 2014), and aplite dikes cutting zones of mineralization in the Sheep Creek gold camp (Mathews, 1953; this study). Direct observations of granitoids and associated contact metamorphism in underground workings of the Queen vein (Mathews, 1953) require that at least parts of the Sheep Creek area are underlain by, and affected by the thermal and/or hydrothermal effects of buried intrusions. This inference is supported by the intrusion of a mid-Cretaceous dike swarm along the entire strike length of the camp, and by post-mineralization lamprophyre dikes with granitic xenoliths, potentially suggesting that the district is underlain by a large, single magma chamber from which the Sheep Creek and Emerald stocks also emanate.

Contact metamorphic effects of this magmatic episode not only include formation of hornfels and andalusite-cordierite assemblages proximal to the Sheep Creek stock, but also resulted in cryptic recrystallization of the sedimentary sequences hosting gold ore, and potentially, of auriferous veins themselves. This thermal overprint is illustrated by micaceous quartzite of the Reno Formation near the Nugget mine, in which the majority of the quartz groundmass has annealed to produce unstrained, polygonal grain boundaries, and in which relict domains of strained metamorphic quartz define the metamorphic fabric (Fig. 42a-b). The same effect is observed in pyritic ore of the Nugget mine, which is characterized by annealed quartz intergrown with idiomorphic pyrite and seams of randomly oriented sericite (Fig. 42c-d). The fine grain size and weak relict fabric of this specimen likely indicates that the sample is pyritized quartzite wall rock as opposed to fracture-filling vein material.

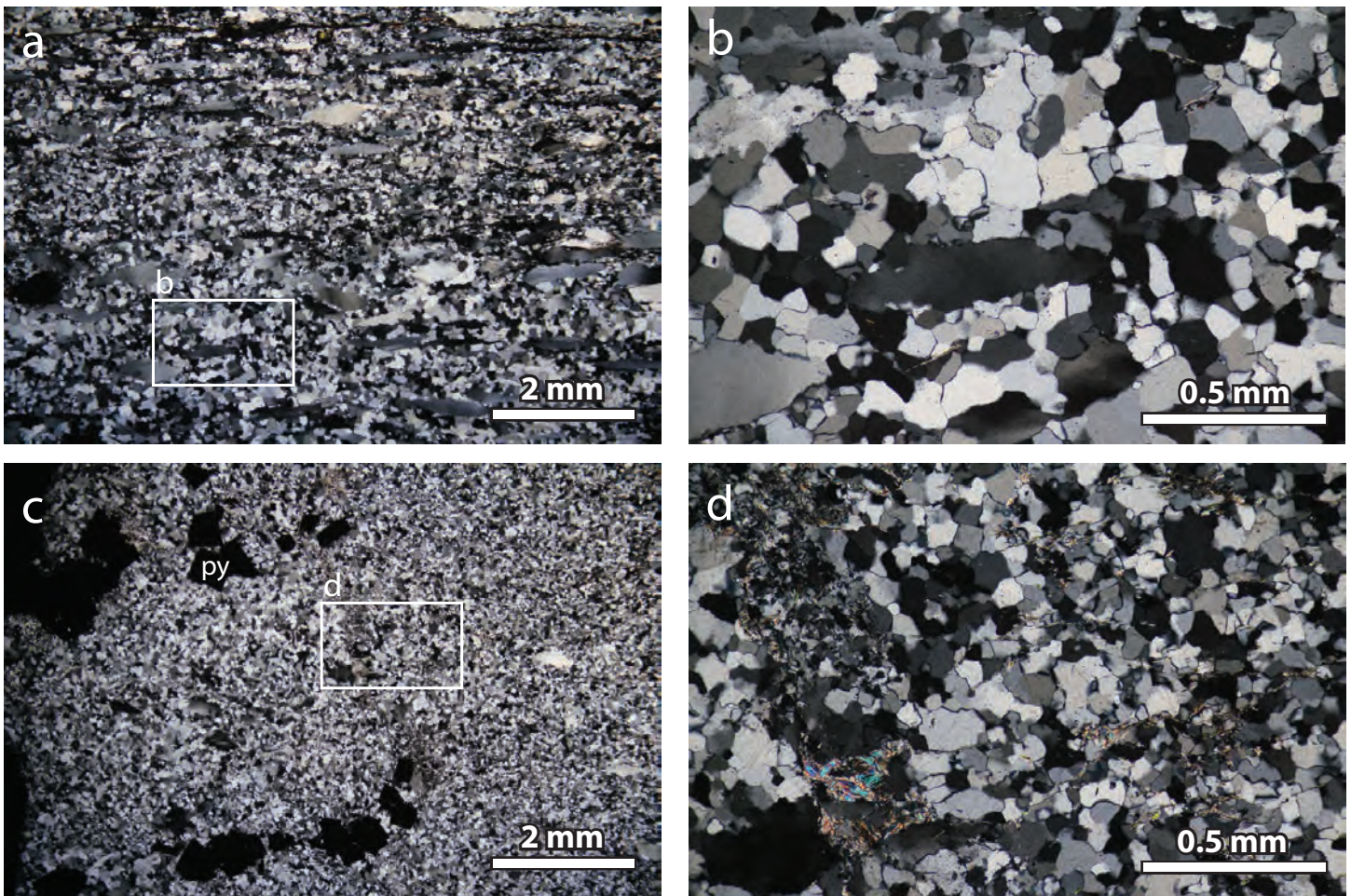


Figure 42. Cross-polarized photomicrographs of barren (a-b) and mineralized (c-d) quartzite from the Nugget mine. A contact metamorphic overprint has resulted in near-total annealing of the quartz groundmass. Domains of strained quartz in (a) and (b) define the relict metamorphic fabric.

Argon-argon results from the Sheep Creek camp are consistent with widespread mid-Cretaceous resetting of metamorphic muscovite and vein-hosted sericite. Unfortunately, the degree of argon loss precludes a conclusive determination of the original alteration and mineralization age by  $^{40}\text{Ar}/^{39}\text{Ar}$  methods. However, Hammill Group quartzite exposed along the Salmo-Creston highway represents the along-strike projection of the Sheep Creek camp. A robust  $^{40}\text{Ar}/^{39}\text{Ar}$  plateau age of  $133.0 \pm 0.2$  Ma for mica in barren shear veins at this locality represents the age of low-strain brittle deformation, and thus the minimum age of penetrative ductile deformation in the host rocks. This age is also a reasonable estimate for gold mineralization at the Sheep Creek camp, although mineralization may be somewhat younger because the time period over which shear veins accommodated strike-slip movement and focused ore fluids is unknown.

The Early Cretaceous age of deformation implied by the  $^{40}\text{Ar}/^{39}\text{Ar}$  results of this study is consistent with the conclusions of Webster (2016), who estimated that autochthonous strata in the southern Kootenay region were deformed and metamorphosed between 144 and 134 Ma. Webster's (2016) age estimate was based on analogy with deformation and metamorphism in the northern Kootenay arc, outside the influence of overprinting contact metamorphic effects. The inferred ~133 Ma age of gold mineralization in the Sheep Creek camp is bracketed by Middle Jurassic and mid-Cretaceous magmatism with well-defined contact metamorphic assemblages and bathozones, such that the crustal depth of vein formation and mineralization is well-constrained to 9-12 km.

---

# Synthesis and Discussion

---

## Models for gold mineralization

Several features of gold mineralization in each of the Cariboo, Cassiar, and Sheep Creek study areas are consistent with the orogenic gold deposit model (e.g., Groves et al., 1998; Bierlein and Crowe, 2000; Goldfarb et al., 2001). Firstly, mineralization is associated with greenschist facies metamorphic belts, much like the vast majority of global orogenic gold deposits. This association is most clearly highlighted in the Cariboo gold district, in which lode and placer gold occurrences are spatially confined to greenschist facies rocks and notably absent from lithostratigraphically equivalent amphibolite facies rocks to the northwest and southeast (Fig. 2).

Mineralization is most closely associated with fluid inclusion-rich (milky) quartz  $\pm$  ferroan carbonate veins with low modal quantities of pyrite and other sulphides. Texturally, ore-bearing veins in each study area are characterized by a range of features such as laminated textures, stylolites, shear fabrics, and vein breccia, collectively indicating poly-phase growth and deformation of veins within active deformation zones along which fluid cycling was linked to seismic activity (e.g. Sibson et al., 1988; Cox et al., 1991).

Mineralization in each camp is characterized by high typical ore grades (several grams per tonne), as well as typically high Au/Ag ratios. As is typical in orogenic districts, secondary ore minerals and metal signature correlate with differences in local host rock composition, such that gold ore hosted in metabasalt has a Ag-Cu-Pb-Zn  $\pm$  Sb signature (Cassiar district; Sketchley, 1984; Rhys, 2009), ore hosted in siliciclastic rocks has a mainly Ag-Pb-Bi signature (Wells-Barkerville camp; Rhys and Ross, 2001), ore hosted by carbonaceous pelite and variably calcareous siliciclastic rocks has a Ag-rich, Pb-Zn  $\pm$  Cu-W signature (Cunningham Creek areas of the Cariboo gold district; Gavin, 2017), and ore hosted in calcareous host rocks have a Pb-Zn signature (minor component of the ore in the Sheep Creek camp; Mathews, 1953). The dependence of metal signatures on host rock lithology suggests a high degree of rock-buffering on the fluid composition, a feature proposed for orogenic gold deposits on the basis of stable isotopic and thermodynamic arguments (e.g., Evans et al., 2006).

Ore fluid compositions in each study area are also typical of orogenic gold deposits globally. Fluid inclusion studies in each district have identified low-salinity, H<sub>2</sub>O-CO<sub>2</sub>-NaCl  $\pm$  CH<sub>4</sub> fluid compositions, with moderate fluid inclusion homogenization temperatures of  $\sim$ 200-300°C (Nelson, 1990; Hardy, 1992; Dunne and Ray, 2001). Furthermore, a weakly acidic, carbonic fluid composition is consistent with seric-

ite-carbonate dominant alteration assemblages of metabasalt and metasiliciclastic rocks of the Cassiar and Cariboo gold districts, respectively. As expected, alteration is cryptic to absent in non-reactive quartzite host rocks of the Sheep Creek camp.

Notably, there is no current geological or geochronological evidence that connects the formation of gold mineralization with magmatism in the Cariboo, Cassiar, or Sheep Creek study areas. Hypotheses by Nelson (1990) and Ball (1997) that mineralization of the Cassiar gold district was genetically linked to a buried intrusion are not supported by the ages of zircon xenocrysts in lamprophyre dikes, which indicate that granitoids underlying the district are significantly younger than Early Cretaceous mineralization. Similarly, geological and geochronological evidence in the Sheep Creek camp do not support the suggestions of Mathews (1953) and Logan (2002a) that gold mineralization is genetically linked to mid-Cretaceous magmatism of the Bayonne suite. Rather, the relationship of gold mineralization to ca. 102 Ma intrusions appears to be only spatial, as indicated by contact metamorphic effects affecting the <sup>40</sup>Ar/<sup>39</sup>Ar systematics and textures of both host rocks and mineralized features. Moreover, gold mineralization in the Sheep Creek camp is structurally linked the late brittle expression of collisional deformation, the age of which is constrained to  $\sim$ 133 Ma through <sup>40</sup>Ar/<sup>39</sup>Ar analysis of late-tectonic veins outside the influence of overprinting thermal effects in the Sheep Creek camp.

## Tectonic setting

The orogenic gold deposit model highlights the relationship of mineralization to zones of collisional deformation in convergent continental margin settings (e.g., Groves et al., 1998; Bierlein and Crowe, 2000), and examples of orogenic gold in British Columbia are no different in this regard. Examples of orogenic gold in B.C. span nearly the entire breadth of the province and underscore a range of collisional tectonic environments permissible for this gold deposit style. Whereas the Juneau gold belt in southeast Alaska occurs in a forearc environment (Goldfarb et al., 1998), the B.C. examples occur either within accreted pericratonic terranes (e.g., Bralorne-Pioneer, Atlin, Cassiar), or within shelf to basinal marine strata fringing the ancient continental margin (e.g., Cariboo, Sheep Creek) (Fig. 1).

The Cariboo gold district and Sheep Creek camp emphasize the prospectivity of parautochthonous sedimentary strata of the eastern Northern American Cordillera for orogenic gold. Whereas these districts occur in metamorphic belts in close proximity to the eastern margin of Quesnellia

terrane, orogenic gold may also occur in North American strata well inboard of the limit of accreted peri-cratonic terranes. This possibility is indicated by examples of orogenic gold in Selwyn Basin, Yukon Territory, such as the 3 Aces gold prospect (Golden Predator, 2017). Together, examples of orogenic gold deposits in B.C. and elsewhere in the North American Cordillera emphasize that other factors, such as regional and local structures, are more important ore controls than the specific tectonic position within the accretionary orogen.

## Structural setting

In each of the Cariboo, Cassiar, and Sheep Creek areas, veins and related brittle structures are geometrically and kinematically compatible with the inferred stress conditions that formed ductile structural elements in the host rocks, and therefore, formed under the same progressive deformational regime (Figs. 18, 27, 41). The horizontal component of shortening in each district is perpendicular to the orogenic strike, such that subvertical extensional veins formed nearly perpendicular to fold axes, lineations, and planar fabrics in the host rocks, and conjugate shear veins further accommodated orogen-normal shortening in the brittle regime (Fig. 43). In detail, veins in each district formed diachronously, such that early veins were overprinted by ductile deformation and late veins record the latest, low-strain expression of orogen-normal shortening in the brittle regime. Early veins include ptlygmatically folded extensional veins, as well as fault-filling veins, which were overprinted by shear fabrics prior to late brittle reactivation and mineralization (e.g., Vollaug vein, Cassiar district; B.C. vein, Wells-Barkerville camp).

The relative geometry of extensional, shear, and fault-filling veins in the Cariboo, Cassiar, and Sheep Creek camps is entirely consistent with well-studied examples of orogenic gold globally, such as the Val d'Or camp of Canada's Superior province (Poulsen and Robert, 1989; Fig. 44). However, the absolute geometry differs in that extensional veins are subvertical in the B.C. examples, indicating that the minimum principal stress direction ( $\sigma_3$ ) is subhorizontal. In contrast, the Val d'Or model emphasizes subhorizontal extensional veins, steep shear zones with a reverse sense of movement, and a subvertical  $\sigma_3$  direction (Fig. 44). The structural regime in Cassiar deviates even more significantly from the Val d'Or model, whereby major shear zones are subhorizontal and the maximum compression stress ( $\sigma_1$ ) is subvertical, features more consistent with detachment faulting.

Pre-mineralization ductile deformation was manifested in the Cariboo and Sheep Creek camps as the formation and tightening of upright folds, formation of penetrative axial planar fabrics, and development of a prominent mineral stretching and intersection lineation parallel to fold axes and the regional strike. The penetrative subhorizontal stretching lineation most likely formed in response to a

component of strike-slip simple shear strain within a strain environment dominated by orogen-normal shortening, *i.e.*, transpression. Similar structural elements exist in the Cassiar district, except that the inferred regional shortening direction was primarily subvertical, such that shear was partitioned into low-angle zones defined by ultramafic and argillaceous horizons within the pre-existing thrust architecture. The sense of movement in these zones was top-to-the-northwest (orogen-parallel), as indicated by mineral lineations in shear zones and by kinematic indicators in veins associated with late movement on the same structures (Rhys, 2009).

In each district, field observations indicate that the most competent lithologies underwent essentially homogeneous pure shear (coaxial) strain, whereas simple shear strain was highly compartmentalized, for example within certain specific pelitic horizons in the Cariboo gold district (Fig. 13d) or within fault-filling veins (e.g., B.C. vein, Fig. 13b; Vollaug vein, Fig. 26c). The shallow plunge of mineral lineations in each study area indicate that shortening perpendicular to the orogen (with a component of subvertical flattening in Cassiar district) was partly accommodated by ductile attenuation (extrusion) parallel to the orogen, *i.e.*, lateral escape. Whereas extrusion of material away from zones of active deformation is an expected feature of transpression, lateral extrusion of material is less common than vertical extrusion (Massey and Moecher, 2013), as exemplified by the predominantly subvertical lineations in well-studied examples of orogenic gold (Fig. 44). One possible explanation that applies to the Cassiar and Cariboo areas is that gravitational loading by shallow-dipping thrust sheets of ophiolitic assemblages inhibits vertical escape of material from zones of deformation at structural lower levels, such that material is vertically constricted and escapes laterally to accommodate shortening.

The top-to-the-north-northwest movement of thrust-bound elements of the Slide Mountain terrane, documented in the Sylvester Allochthon in the Cassiar gold district, also occurs in the Cariboo gold district of east-central British Columbia. In the Cariboo district, microstructural kinematic indicators in mylonite in the immediate footwall of the Pundata thrust indicate north-northwest movement of the thrust sheet of Antler Formation (Slide Mountain terrane) relative to the structurally underlying Snowshoe Group (Fig. 10). The age of mylonitization is unknown relative to Late Jurassic to Early Cretaceous mineralization in the Barkerville subterrane. However, the similar orientation of cleavages and fold axes in metasediments of the Antler Formation to those in the Snowshoe Group indicates a common deformation history (Struik, 1987), and also that the Pundata thrust was established as early as the Early Jurassic as a syn- $D_1$  structure. The thrust is also locally folded (Struik, 1987), so it was likely overprinted and reactivated by  $D_2$ -related deformation in the Middle to Late Jurassic. Regardless of the precise timing of mylonitization, the top-to-the-north-northwest shear sense is highly oblique to

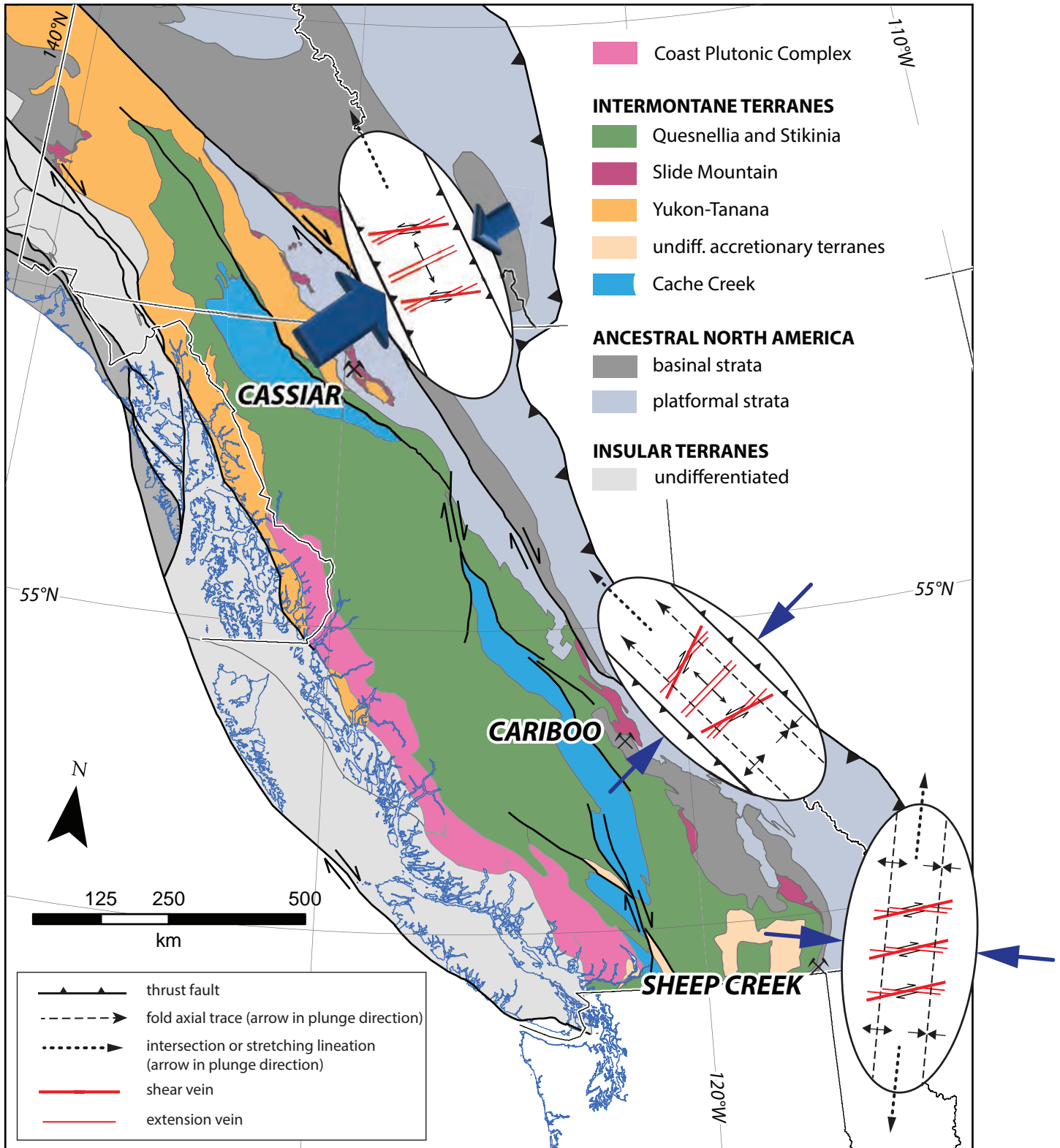


Figure 43. Summary strain ellipses for the structural setting of the Cassiar, Cariboo, and Sheep Creek areas. In each case, the horizontal component of shortening (blue arrows) is perpendicular to the orogenic strike, and consistent geometric and kinematic relationships are maintained between folds, lineations, and brittle features. The vertical component of shortening in the Cassiar district is indicated by block arrows inclined out of the figure.

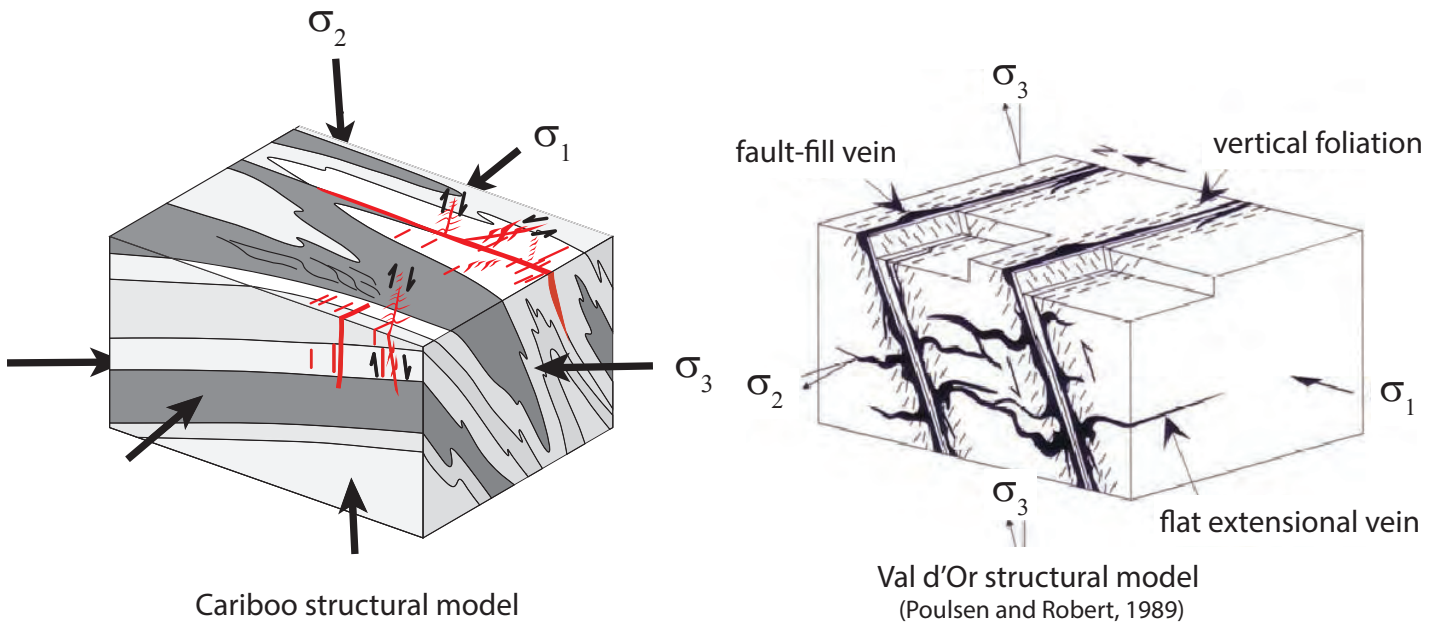


Figure 44. Comparison of structural models between the Cariboo district (this study) and Val d'Or camp, Abitibi district (Poulsen and Robert, 1989). The Cariboo model represents a 90° rotation of the Val d'Or model, such that lineations are subhorizontal and extensional veins are subvertical. Steep fault-filling veins oriented at a high angle to  $\sigma_1$  in the Val d'Or model are analogous to 'strike veins' in the Cariboo.

the regional northeast-southwest shortening direction, and thus it is reasonable to consider a syn-D<sub>2</sub> tectonic model in which thrust-bound sheets of Slide Mountain terrane escaped laterally in response to the same transpressional strain conditions responsible for lateral extrusion within the Barkerville subterrane.

Whereas many global examples of orogenic gold feature a major transcurrent fault zone as the first-order structural control (e.g., Groves et al., 1998), such features are notably absent in each of the Cariboo, Cassiar, and Sheep Creek districts. Particularly in the Cassiar district, low-angle thrust faults are the most obvious first-order structural control on mineralization. Whereas steep faults are commonly invoked as crustally-significant fluid conduits, maximum fluid flow occurs along transiently interconnected, soft-linked fracture-fault networks that are outboard of the main shear zone (Micklethwaite and Cox, 2006). The vertical distribution of ore fluids in each of the B.C. camps appears to have been achieved in a similar manner, but in the absence of a steep principal structure. In the Cassiar district, the self-sealing of low-angle thrust surfaces by ductile deformation, listwaenite alteration of ultramafic rocks, and/or formation of fault-filling veins may indeed have enhanced fluid-rock interactions and ore-forming potential within brittle fracture networks within the more resistant, intervening metabasalt layers. In this sense, this study highlights shallow-dipping fold-and-thrust architecture as a viable structural environment for orogenic gold mineralization.

### Lithospheric controls

The distribution of mineral occurrences in the North American Cordillera is at least partly controlled by structures in cratonic basement, which underlies accreted terranes of the B.C. Cordilleran orogen and extends at least as far west as the current position of the Cache Creek terrane (Cook et al., 1992; Nelson et al., 2013 and references therein). Major cratonic basement structures oriented at a high angle to the Cordilleran orogen thus project westward beneath the accreted terranes, and coincide with significant along-strike variations in Proterozoic to Paleozoic sedimentation, which in turn have affected subsequent patterns of deformation, magmatism, and mineralization (Nelson et al., 2013 and references therein).

The role, if any, of cratonic basement structure in orogenic mineralization in the Cariboo and Cassiar districts is unknown. However, basement structure may partly explain why orogenic gold mineralization is localized in the Sheep Creek relative to adjacent segments of the Cordilleran orogen. A structural corridor of northeast-trending faults in southeastern B.C. is inferred to be the supracrustal expression of the Red Deer zone and Vulcan low to the east (McMechan, 2012), major sutures or shear zones within the Archean Hearne Province (Hoffman, 1988; Ross et al., 1991). McMechan (2012) recognized the long-lived influence of these orogen-transverse basement structures on the metallogeny of the Kootenay region, which includes Paleozoic carbonate-hosted Pb-Zn deposits such as the world-class Sullivan mine, Cretaceous magmatic-hydrothermal systems, and Nb-rich carbonatites. It is speculated that the

gold endowment of the Sheep Creek camp, which coincides with the western projection of the Vulcan low, may have arisen due to anomalous heat flow and hydrothermal fluid activity in the Early Cretaceous due to reactivation of this underlying basement structure. Moreover, the main east-northeast orientation of mineralized veins in the Sheep Creek camp and adjacent Bayonne mine is sub-parallel to the trace of the Vulcan low, suggesting that structures of this orientation may be predisposed to higher degrees of strain and enhanced ore potential.

Post-collisional lamprophyre dikes are common to all gold districts studied, and in the case of Cassiar and Cariboo, have been observed to intrude along mineralized quartz veins. It is therefore reasonable to suggest that the crust-penetrating structural pathways exploited by mantle-derived alkaline melts were also present during orogenic gold mineralization. The correlation of Eocene lamprophyre dikes and mineralization in parts of the Kootenay region has been suggested to relate to extensional reactivation of orogen-transverse basement structures (McMechan, 2012), and a similar deep structural control may also explain the coincidence of orogenic gold deposit and post-mineralization mafic alkaline magmatism in the Cassiar, Cariboo and Sheep Creek camps.

## CONCLUSIONS

The 'eastern Cordilleran gold belt' of B.C. contains deposits of significant mining and exploration interest, which are most readily explained by the orogenic gold model. Deposits in this belt are typical of Phanerozoic orogenic gold deposits globally, in that they formed during collisional deformation in an accretionary tectonic environment (Bierlein and Crowe, 2000). The main ore controls in each of the gold districts are summarized below:

### ***Cariboo gold district***

Gold mineralization in the Cariboo district occurs in vein arrays with predictable geometries relative to the attitudes of cleavages and lineations in the host rocks (Fig. 18). Much of the high-grade gold in the Wells-Barkerville camp occurs in north-trending, dextral to dextral-normal shear veins. Steep, northeast-trending extensional veins oriented perpendicular to mineral lineations in the host rock also represent an important component of ore. Fault-filling 'strike' veins also occur parallel to the northwest-trending stratigraphy, and represent attractive gold targets. Replacement-style ore in the Cariboo district is preferentially hosted in calcareous horizons, and may form high-grade ore zones with plunges that parallel fold axes and lineations. Vein-hosted mineralization in the Cariboo district preferentially forms in competent lithologies, and in particular psammite of the Hardscrabble Mountain succession in the Wells-Barkerville mining camp. Heterogeneous lithostratigraphy is inferred to be an important ore control in the district,

whereby micaceous units deformed in a predominantly ductile manner and served as permeability barriers, thus focussing ore fluids into zones of enhanced structural permeability in the intervening competent layers. Veining and mineralization in the Cariboo gold district appears to have formed diachronously from 149 to 134 Ma, which is consistent with observations of multiple phases of overprinting deformation on vein features.

### ***Cassiar gold district***

Gold-bearing veins in the Cassiar district occur within a broad, north-trending corridor linking the Table Mountain and Taurus areas (Fig. 20). Mineralization occurs almost exclusively in metabasalt that structurally underlies the Table Mountain sediments, so the Table Mountain thrust is an important delimiter of ore potential. Mineralized veins in the Cassiar district have predictable geometries. These include: steep to moderately dipping, east-trending shear veins with both a normal and sinistral shear sense; and steep, northeast-trending extensional veins. Veins are kinematically related to northwest-directed movement on low-angle shear zones that are largely focused within thin ultramafic or argillaceous horizons (Fig. 27). Veins such as the Vollaug may also occupy low-angle thrust faults. Ore potential appears to be greatest in the immediate footwall of low-angle shear zones, perhaps explained by the ponding of ore fluids below low-permeability shear zones. In this sense, listwaenite-altered ultramafic rocks defining hydrothermally altered shear zones are an important guide to exploration in the district (Ash, 2001). Veins in the Cassiar gold district formed diachronously between 143 and 129 Ma, consistent with their formation during progressive deformation.

### ***Sheep Creek gold camp***

Gold-bearing veins in the Sheep Creek camp are mainly constrained to competent quartzite horizons of the Nugget and Nevada members of the Quartzite Range Formation, and below argillaceous rocks of the Reno Formation (Figs. 32-33). This stratigraphic control is mechanical, as argillaceous rocks represent an aquiclude to mineralizing fluids, whereas structural permeability was generated favourably in more competent horizons. Gold-bearing veins formed preferentially within northeast-trending dextral shear veins, and in response to approximately east-west oriented collisional deformation. It is speculated that gold mineralization of the Sheep Creek camp, along with numerous other mineral occurrences in the southern Kootenay region, may have been related to anomalous heat and/or fluid flow controlled by orogen-transverse structures in Archean basement (McMechan, 2012). Gold mineralization in the Sheep Creek camp is estimated at ~133 Ma, and is genetically unrelated to ca. 102 Ma intrusions and associated  $W \pm Mo$  skarn systems in the Salmo region.

Field observations, structural mapping, and geochronological data in each district unequivocally tie the formation of mineralized veins to progressive collisional deformation associated with the Cordilleran orogeny in the Late Jurassic

to Early Cretaceous. Late, brittle veins are the final structural record of collision-related deformation, and thus signal the transition to orogenic collapse.

From an exploration standpoint, structural mapping of ductile deformation features provides an excellent predictive framework for mineralized features:

- Shear veins, which typically represent the highest-grade features, form obliquely to fold axes, planar fabrics, and mineral lineations, with a shear sense that can be predicted from the orientation of ductile features and the inferred  $\sigma_1$  direction;
- Extensional veins may provide a vector toward higher grade shear veins, or may themselves represent ore-grade material. Structural targeting predicts their formation nearly perpendicular to fold axes and linear shape fabrics;
- Stratabound replacement-style gold mineralization that is genetically related to vein-hosted mineralization (e.g., Island Mountain, Cariboo gold district) may occur in high-grade ore shoots parallel to linear structural elements (e.g., fold hinges and mullions);
- Zones of higher vein density and mineralization potential may occur in antiformal hinge zones (e.g., western anticline, Sheep Creek gold camp), or below shallowly dipping thrust faults (Cassiar district).

The host rock geology is another important general exploration consideration. Heterogeneous lithostratigraphy allows for contrasts in deformation style and permeability, such that the more competent units are more likely to be mineralized than weaker, more readily deformed units. Host rock composition is another important consideration, whereby calcareous units may provide opportunities for replacement-style mineralization (e.g., Island Mountain, Cariboo gold district), or where iron-rich lithologies such as basalt have the potential to host disseminated gold adjacent to discrete brittle structures (e.g., Cassiar district). However, the quartzite-dominated stratigraphy of the Sheep Creek camp suggests that non-reactive rocks may also be viable hosts for orogenic gold mineralization.

Regional targeting for orogenic gold in other parts of the B.C. Cordillera might consider that regional greenschist grade metamorphic rocks are structurally favourable compared with amphibolite grade or higher. The intensity of regional compressional to transpressional deformation is another important consideration, especially given the correlation of known orogenic gold camps with highly strained host rocks. Other factors include the proximity to major, potentially terrane-bounding faults, the distribution of known mineral occurrences, regardless of age or deposit style, and the presence of orogen-transverse basement structures.

## ACKNOWLEDGEMENTS

This project has benefited from the technical input of numerous individuals, including but not limited to Jim Mortensen (UBC), Paul Schiarizza (BCGS), JoAnne Nelson (BCGS), Ewan Webster (Yukon College), Terence Harbort (Barkerville Gold Mines Ltd.), Lesley Hunt (China Minerals Mining Corp.), and Ed Laurence (Yellowstone Resources Ltd.). We are indebted to Barkerville Gold Mines Ltd. and in particular Terence Harbort, Paul Geddes, Chris Lodder, Ruben Padilla, Wanda Carter, Maggie Layman, Alex Whithlowsky, Jason Kosec, and Natalie Cook for excellent technical interactions and for providing lodging and logistical support during the Cariboo portion of the fieldwork. Access to the Cassiar district was facilitated by Bernard Kahlert, and Lesley Hunt provided lodging and invaluable logistical support. Ed Laurence of Yellowstone Resources Ltd. was a wealth of local knowledge in the Salmo area, and provided land access to the Sheep Creek camp.

The project benefited from three excellent field assistants: Rachel Gavin (UBC) and Carl Spence-Jones (University of Leeds) in the Cariboo, and Rachel Kim (MDRU-UBC) in the Sheep Creek camp. Alfredo Camacho (University of Manitoba) performed all  $^{40}\text{Ar}/^{39}\text{Ar}$  analyses, and is thanked for providing excellent advice on mineral separations and data interpretation. Bahram Najafian (MDRU) carried out mineral processing for U-Pb geochronology. Johanna McWhirter (MDRU) provided project management support, and Luana Yeung (MDRU) carried out digitization and drafting of historic Sheep Creek maps and sections under the guidance of Sara Jenkins (MDRU).

Funding for this project was generously provided by Geoscience BC.

## REFERENCES

- Alldrick, D.J., 1983, The Mosquito Creek mine, Cariboo gold belt (93H/4); in *Geological Fieldwork 1982*; B.C. Ministry of Energy, Mines and Petroleum Resources, Paper 1983-1, p. 99-112.
- Anderson, P.G. and Hodgson, C.J., 1989, The structure and geological development of the Erickson gold mine, Cassiar District, British Columbia, with implications for the origin of mother-lode-type gold deposits: *Canadian Journal of Earth Sciences*, v. 26, p. 2645-2660.
- Andrew, A., Godwin, C.I. and Sinclair, A.J., 1983, Age and genesis of Cariboo gold mineralization determined by isotopic methods; in *Geological Fieldwork 1982*, B.C. Ministry of Energy, Mines and Petroleum Resources, Paper 1983-1, p. 305-313.
- Archibald, D.A., Glover, J.K., Price, R.A., Farrar, E. and Carmichael, D.M., 1983, Geochronology and tectonic implications of magmatism and metamorphism, southern Kootenay Arc and neighbouring regions, southeastern British Columbia. Part I: Jurassic to mid-Cretaceous, *Canadian Journal of Earth Sciences*, v. 20, p. 1891-1913.
- Ball, M.C.N., 1997, Geology of the McDame gold camp, Cassiar, British Columbia: implications for lode-gold metallogenesis: Unpublished PhD thesis, Queens University, 350 p.
- Barkerville Gold Ltd., 2017, [<http://barkervillegold.com/projects/>, accessed September 1, 2017]
- Benedict, P.C., 1945, Structure at Island Mountain Mine, Wells, B.C.: *Canadian Institute of Mining and Metallurgy, Transactions*, v. 48, p. 755-770.
- Beranek, L.P., and Mortensen, J.K., 2011, The timing and provenance record of the Late Permian Klondike orogeny in north-western Canada and arc-continent collision along western North America: *Tectonics*, v. 30, p. TC5017.
- Bierlein, F.P. and Crowe, D.E., 2000, Phanerozoic orogenic lode gold deposits: *Society of Economic Geologists, SEG Reviews*, v. 13, p. 103-139.
- Bowman, A., 1889, Report on the geology of the mining district of Cariboo, British Columbia: Geological Survey of Canada, Annual Report for 1887-1888, v. III, part 1, p. 1-49.
- Bradford, J.A. and Godwin, C.I., 1988, Midway silver-lead-zinc manto deposit, northern British Columbia (104O/16): B.C. Ministry of Energy, Mines and Petroleum Resources, *Geological Fieldwork*, 1987, Paper 1988-1, p. 353-360.
- Brousseau, K., Faure, S. and Pelletier, C., 2017, Technical report for the Cariboo gold project and mineral resource estimate on the Barkerville Mountain Project: NI 43-101 Technical Report for Barkerville Gold Mines Ltd., 250 p.
- Brown, J.A., 2009, 2009 Technical report for the Cariboo Gold Project: Volume I – Report and Appendix I: Internal report for International Wayside Gold Mines Ltd. and Barkerville Gold Mines Ltd., 277 p.
- Chapman, R.J. and Mortensen, J.K., 2016, Characterization of gold mineralization in the Northern Cariboo Gold District, British Columbia, Canada, through integration of compositional studies of lode and detrital gold with historical placer production: a template for evaluation of orogenic gold districts: *Economic Geology*, v. 111, p. 1321-1346.
- Cook, F.A., Varsek, J.L., Clowes, R.M., Kanasewich, E.R., Spencer, C.S., Parrish, R.R., Brown, R.L., Carr, S.D., Johnson, B.J., and Price, R.A., 1992, Lithoprobe crustal reflection cross section of the southern Canadian Cordillera, 1, Foreland thrust and fold belt to Fraser River fault: *Tectonics*, v.11, p. 12–35.
- Cowley, P., 2017, Technical report on the Cassiar gold property, British Columbia, Canada: China Minerals Mining Corp., NI-43-101 & 43-101F1 technical report, 103 p. [<http://www.chinamineralsmining.com>, accessed September 26, 2017]
- Cox, S.F., Wall, V.J., Etheridge, M.A., and Potter, T.F., 1991, Deformational and metamorphic processes in the formation of mesothermal vein hosted gold deposits—examples from the Lachlan fold belt in central Victoria, Australia: *Ore Geology Reviews*, v. 6, p. 391–423.
- Diakow, L.J. and Panteleyev, A., 1982, Cassiar gold deposits, McDame Lake area. In: *British Columbia Ministry of Energy, M.a.P.R., Geological Branch, Paper 1982-1 (Ed.), Geological fieldwork 1980*, p. 156-161.
- Driver, L.A., Creaser, R.A., Chacko, T. and Erdmer, P., 2000, Petrogenesis of the Cretaceous Cassiar batholith, Yukon-British Columbia, Canada: Implications for magmatism in the North American Cordilleran Interior: *GSA Bulletin*, v. 112(7), p. 1119-1133.
- Dunne, K.P.E. and Ray, G.E., 2001, Preliminary fluid inclusion study of quartz vein and massive-banded-stringer pyrite mineralization in the Wells-Barkerville gold belt, east-central British Columbia: *British Columbia Ministry of Energy and Mines, Geological Fieldwork 2000*, Paper 2001-1, p. 169-190.
- Evans, K.A., Phillips, G.N. and Powell, R., 2006, Rock-buffering of auriferous fluids in altered rocks associated with the Golden Mile-style mineralization, Kalgoorlie Gold Field, Western Australia: *Economic Geology*, v. 101, p. 805-817.
- Ferri, F., 2001, Geology of the Frank Creek - Cariboo Lake area, central British Columbia, (NTS 93A/11,14): B.C. Ministry of Energy and Mines, Open File 2001-11, 1:50,000.
- Ferri, F. and Friedman, R. 2002, New U-Pb and geochemical data from the Barkerville Subterranean, in Cook, F., and P. Erdmer (compilers), *Slave-Northern Cordillera Lithospheric Evolution (SNORCLE) Transect and Cordilleran Tectonics Workshop Meeting (February 21-24)*, Pacific Geoscience Centre, Lithoprobe Report No. 82, 165 pp.
- Ferri, F. and O'Brien, B.H., 2002, Preliminary geology of the Cariboo Lake area, central British Columbia (093A/11, 12, 13 and 14), in *Geological Fieldwork 2001*: B.C. Ministry of Energy and Mines, Paper 2002-1, p. 59-81.
- Ferri, F. and O'Brien, B.H., 2003, Geology of the Cariboo Lake area, central British Columbia: B.C. Ministry of Energy and Mines, Open File 2003-1, 1:50,000.
- Ferri, F. and Schiarizza, P., 2006, Re-interpretation of Snowshoe group stratigraphy across a southwest-verging nappe structure and its implications for regional correlations within the Kootenay terrane. *Geological Association of Canada Special Paper*, 45: 415-432.
- Fyles, J.T. and Hewlett, C.G., 1959, Stratigraphy and structure of the Salmo lead-zinc area: *British Columbia Department of Mines, Bulletin No. 41*, 174 p.

- Gabrielse, H., 1963, McDame map-area, Cassiar district, British Columbia: Geological Survey of Canada, Memoir 319, 138 p.
- Gabrielse, H., Mortensen, J.K., Parrish, R.R., Harms, T.A., Nelson, J.L., van der Heyden, P., 1993, Late Paleozoic plutons in the Sylvester Allochthon, northern British Columbia: In Radiogenic ages and isotopic studies, Report 7, Geological Survey of Canada, Paper 93-2, p. 107-118.
- Gavin, R., 2017, Structural setting of argeniferous veins, Cariboo gold district, east-central British Columbia: Unpublished B.Sc. (Honours) thesis, University of British Columbia, 66 p. <DOI: 10.14288/1.0347675>
- Goldfarb, R.J., Groves, D.I., Gardoll, S., 2001, Orogenic gold and geologic time: a global synthesis: *Ore Geology Reviews*, v. 18, p. 1-75.
- Groves, D.I., Goldfarb, R.J., Robert, F., Hart, C.J.R., 2003, Gold deposits in metamorphic belts: overview of current understanding, outstanding problems, future research, and exploration significance: *Economic Geology*, v. 98, p. 1-29.
- Golden Predator, Ltd., 2017, 3 Aces Project [<http://www.goldenpredator.com/project/3-Aces/>, accessed October 12, 2017]
- Goldfarb, R.J., Phillips, G.N. and Nokleberg, W.J., 1998, Tectonic setting of synorogenic gold deposits of the Pacific Rim: *Ore Geology Reviews*, v. 13, p. 185-218.
- Hardy, R., 1990, Preliminary report of research in the Sheep Creek camp, Salmo, British Columbia: British Columbia Geological Survey, Geological Fieldwork 1989, Paper 1990-1, p. 247-249.
- Harms, T.A., 1985, Cross-section through the Sylvester allochthon and underlying Cassiar platform, northern British Columbia: Current Research, Part B, Geological Survey of Canada, Paper 85-1B, p. 341-346.
- Harms, T.A., Ball, M., Fischer, P. and Nelson, J., 1989: Geology of the Needlepoint Mountain map area, NTS 104/P4 (NE1/4): B.C. Ministry of Energy, Mines and Petroleum Resources, Open File 1989-19.
- Hoffman, P.F., 1988, United plates of America: The birth of a craton: *Annual Review of Earth and Planetary Sciences*, vol. 16(1), p. 543-603.
- Hope, J. and Eaton, D., 2002, Crustal structure beneath the western Canada Sedimentary Basin: constraints from gravity and magnetic modelling: *Canadian Journal of Earth Sciences*, v. 39, p. 291-312.
- Höy, T., 1982, Stratigraphic and structural setting of stratabound lead-zinc deposits in southeastern British Columbia: *CIM Bulletin* 75, p. 114-134
- Höy, T., Church, N., Legun, A., Glover, K., Gibson, G., Grant, B., Wheeler, J.O., Dunn, K.P.E., 1994. BC Ministry of Energy and Mines Open File 1994-8 [<http://www.em.gov.bc.ca/Mining/Geoscience/PublicationsCatalogue/OpenFiles/1994/Pages/1994-8.aspx>, accessed April 1, 2016]
- Höy, T. and Dunne, K., 2001, Metallogeny and mineral deposits of the Nelson-Rossland map area: Part II: The Early Jurassic Rossland Group, southeastern British Columbia: B.C. Ministry of Energy and Mines, Bulletin 109, 196 p.
- Höy, T. and Ferri, F., 1998, Stratabound base metal deposits of the Barkerville subterranean, central British Columbia (093A/NW), in *Geological Fieldwork 1997*: B.C. Ministry of Employment and Investment, Geological Survey Branch, Paper 1998-1, p. 13-1 - 13-12.
- Layer, P.W. and Drake, J., 1997, A <sup>40</sup>Ar/<sup>39</sup>Ar dating study from the Cassiar area, British Columbia; internal report prepared for the Geological Survey Branch, Ministry of Energy and Mines, unpublished report, 32 p.
- Levson, V.M., and Giles, T.R., 1993, Geology of Tertiary and Quaternary gold-bearing placers in the Cariboo region, British Columbia (93A, B, G, H): British Columbia Ministry of Energy, Mines and Petroleum Resources, Bulletin 89, 202 p.
- Logan, J.M., 2002a. Intrusion-related gold mineral occurrences of the Bayonne magmatic suite, BC Geological Survey, Geological Fieldwork 2001, Paper 2002-1, p. 237-246.
- Logan, J.M., 2002b. Intrusion-related mineral occurrences of the Cretaceous Bayonne magmatic belt, Southeast British Columbia, BC Ministry of Energy and Mines, Geological Survey Branch, Geoscience Map 2002-1, scale 1:500 000, 1 sheet [<http://www.empr.gov.bc.ca/Mining/Geoscience/Publication-sCatalogue/Maps/GeoscienceMaps/Documents/GM2002-01.pdf>, accessed October 21, 2016]
- Logan, J.M., Schiarizza, P., Struik, L.C., Barnett, C., Nelson, J.L., Kowalczyk, P., Ferri, F., Mihalynuk, M.G., Thomas, M.D., Gammon, P., Litt, R., Jackaman, W. and Ferbey, T. (compilers), 2010, Geoscience Map 2010-1: Bedrock geology of the QUEST map area, central British Columbia: Geological Survey of Canada Open File 6476 (Geoscience BC Report 2010-5).
- Massey, M.A. and Moecher, D.P., 2013, Transpression, extrusion, partitioning, and lateral escape in the middle crust: Significance of structures, fabrics, and kinematics in the Bronson Hill zone, southern New England, U.S.A.: *Journal of Structural Geology*, v. 55, p. 62-78.
- Matthews, W.H., 1953, Geology of the Sheep Creek camp, British Columbia Department of Mines, Bulletin No. 31, 94 p.
- McKeown, M., Baker, D., and Voordouw, R., 2013, 2012 Taurus property drilling project, Cassiar gold project: B.C. Ministry of Energy, Mines and Petroleum Resources, Assessment Report 33501A, 105 p.
- McMechan, M.E., 2012, Deep transverse basement structural control of mineral systems in the southeastern Canadian Cordillera: *Canadian Journal of Earth Science*, vol. 49, p. 693-708.
- Micklethwaite, S. and Cox, S.F., 2006, Progressive fault triggering and fluid flow in aftershock domains: Examples from mineralized Archaean fault systems: *Earth and Planetary Science Letters*, v. 250, p. 318-330.
- Monger, J.W.H. and Berg, H.C., 1984, Lithotectonic terrane map of western Canada and southeastern Alaska, in Silberling, N.J. and Jones, D.L., eds., *Lithotectonic terrane maps of the North American Cordillera*, part B: U.S. Geological Survey, Open-File Report 84-523, p. B1-B31.
- Mortensen, J.K., Montgomery, J.M. and Phillipone, J., 1987, U-Pb zircon, monazite, and sphene ages for granitic orthogneiss of the Barkerville terrane, east-central British Columbia: *Canadian Journal of Earth Sciences*, v. 24, p. 1261-1266.

- Nelson, J.A., 1990, Evidence for a cryptic intrusion beneath the Erickson-Taurus gold-quartz vein system, near Cassiar, B.C. (104P/4, 5): B.C. Ministry of Energy, Mines and Petroleum Resources, Geological Fieldwork 1989, Paper 1990-1, p. 229-233.
- Nelson J.L., 1991, Carbonate-hosted lead-zinc ( $\pm$  silver, gold) deposits of southeastern British Columbia: In *Ore Deposits, Tectonics and Metallogeny*. British Columbia Ministry of Energy and Mines, Paper 1991-4, p. 71-88.
- Nelson, J.L., 1993, The Sylvester Allochthon: upper Paleozoic marginal basin and island arc terranes in northern British Columbia: *Canadian Journal of Earth Sciences*, v. 30, p. 631-643.
- Nelson, J.A. and Bradford, J.A., 1989, Geology and mineral deposits of the Cassiar and McDame map areas, British Columbia (104P/3, 5), B.C. Ministry of Energy, Mines and Petroleum Resources, Geological Fieldwork 1988, Paper 1989-1, p. 323-338.
- Nelson, J., and Bradford, J.A., 1993, Geology of the Midway-Cassiar area, northern British Columbia: B.C. Geological Survey Branch, Bulletin 83, 94 p. and map, 1:100 000, 1 sheet.
- Nelson J.A., Bradford, J., MacLean, M., and Maddison, L., 1989, Geology and metallogeny of the Cassiar and McDame map areas (NTS 104P/3; 104P/5), B.C., Ministry of Energy, Mines and Petroleum Resources, Open File 1989-09, 1:25 000, 8 sheets.
- Panteleyev, A., 1985, Cassiar map area (104 P/4, 5): In *Geology in British Columbia 1977-1981*, B.C. Ministry of Energy, Mines and Petroleum Resources, p. 188-190.
- Paradis, S., 2007, Carbonate-hosted Zn-Pb deposits in southern British Columbia – potential for Irish-type deposit; *Geological Survey of Canada, Current Research 2007-A10*, 7 p.
- Paradis, S., Keevil, H., Simandl, G.J. and Raudsepp, M., 2011, Carbonate-hosted nonsulphide Zn-Pb mineralization of southern British Columbia, Canada: *Mineralium Deposita*, v. 50, p. 923-951.
- Park, V. and Grunenberg, P., 2015, Drilling report for the Jersey-Emerald Property: B.C. Ministry of Energy and Mines, Assessment Report #35243, 783p.
- Poulsen, K. H., and Robert, F., 1989, Shear zones and gold: Practical examples from the southern Canadian Shield: In Burnsall, J. T., ed., *Mineralization and shear zones*, Geological Association of Canada, Short Course Notes 6, p. 239-266.
- Rasmussen, K., 2013, The timing, composition, and petrogenesis of syn- to post-accretionary magmatism in the northern Cordilleran miogeocline, eastern Yukon and southwestern Northwest Territories: Unpublished PhD thesis, University of British Columbia, 788 p.
- Ray, G.E., Webster, I.C.L., Ross, K. and Hall, R. (2001): Geochemistry of auriferous pyrite mineralization at the Bonanza Ledge, Mosquito Creek mine and other properties in the Wells-Barkerville area, British Columbia; in *Geological Fieldwork 2000*, BC Ministry of Forests, Mines and Lands, Paper 2001-1, p. 135-167.
- Rees, C.J., 1987, The Intermontane - Omineca Belt boundary in the Quesnel Lake area, east-central British Columbia: Tectonic implications based on geology, structure and paleomagnetism: Ph.D. thesis, Carleton University, Ottawa, Ontario, 421 p.
- Rees, C. J. and Ferri, F., 1983, A kinematic study of mylonitic rocks in the Omineca Intermontane belt tectonic boundary in east-central British Columbia: *Current Research, Part B, Geological Survey of Canada, Paper 83-IB*, p. 121-125.
- Rhys, D., 2009, Cassiar Camp – summary of setting, style and exploration potential of gold vein systems: preliminary report for discussion purposes: unpublished report to Hawthorne Gold Corp., 24 p.
- Rhys, D.A., and Ross, K.V., 2001, Evaluation of the geology and exploration potential of the Bonanza Ledge zone, and adjacent areas between Wells and Barkerville, east central British Columbia: Surrey, BC, Panterra Geoservices Inc., Unpublished report, 113 p.
- Rhys, D.A., Mortensen, J.K., and Ross, K., 2009, Investigations of orogenic gold deposits in the Cariboo gold district, east-central British Columbia (parts of NTS 093A, H): *Progress report: Geoscience BC, Report 2009-1*, p. 49-74.
- Ross, G.M., Parrish, R.R., Villeneuve, M.E., and Bowring, S.A., 1991, Geophysics and geochronology of the crystalline basement of the Alberta Basin, western Canada: *Canadian Journal of Earth Sciences*, vol. 28(4), p. 512-522.
- Sangster D.F., 1970, Metallogensis for some Canadian lead-zinc deposits in carbonate rocks. *GAC Proceedings*, v. 22, p. 27-36.
- Schroeter, T.G., 2003, Gold production and resources in British Columbia (1858-2002): B.C. Ministry of Energy, Mines and Petroleum Resources, Open File 2003-05.
- Schroeter, T.G. and Lane, R.A., 1991, A century of gold production in British Columbia (1890-1990): B.C. Ministry of Energy, Mines and Petroleum Resources, Open File 1991-19, 42 p.
- Sibson, R.H., Robert, F., Poulsen, K.H., 1988, High-angle reverse faults, fluid pressure cycling, and mesothermal gold-quartz deposits: *Geology*, v. 16, p. 551-555.
- Skерl, A.C. 1948. Geology of the Cariboo Gold Quartz Mine; *Economic Geology*, v. 43, pp. 571-597.
- Sketchley, D.A., Sinclair, A.J., and Godwin, C.I., 1986, Early Cretaceous gold- silver mineralization in the Sylvester allochthon, near Cassiar, north central British Columbia: *Canadian Journal of Earth Sciences*, v. 23(1455),p. 1458.
- Struik, L.C., 1981, Snowshoe Formation, central British Columbia: Geological Survey of Canada, Paper 81-1A, p. 213-216.
- Struik, L.C., 1982a, Bedrock geology of Cariboo Lake (93A/14), Spectacle Lakes (93H/3), Swift River (93A/13), and Wells (93H/4) map areas, central British Columbia: Geological Survey of Canada, Open File 858, 1:50,000.
- Struik, L.C., 1982b, Snowshoe Formation, central British Columbia: Geological Survey of Canada, Paper 82-1B, p. 117-124.
- Struik, L.C., 1983a, Bedrock geology of Spanish Lake (93A/11) and parts of adjoining map areas, central British Columbia: Geological Survey of Canada, Open File 920, 1:50,000.
- Struik, L.C., 1983b, Bedrock geology of Quesnel Lake (93A/10) and part of Mitchell Lake (93A/15) map areas, central British Columbia: Geological Survey of Canada, Open File 962, 1:50,000.

- Struik, L.C., 1988, Structural geology of the Cariboo gold mining district, east-central British Columbia: Geological Survey of Canada, Memoir 421, 100 p.
- Struik, L.C., Parrish, R.R. and Gerasimoff, M.D., 1992, Geology and age of the Naver and Ste. Marie plutons, central British Columbia; in Radiogenic Age and Isotopic Studies, Report 5, Geological Survey of Canada, Paper 91-2, p. 155-162.
- Sutherland Brown, A., 1957, Geology of the Antler Creek area, Cariboo District, British Columbia: B.C. Department of Mines and Petroleum Resources, Bulletin 38, 101 p.
- Warren, H.V., 1936, A gold-bismuth occurrence in British Columbia: Economic Geology, v. 31, p. 205–211.
- Webster, E.R., 2016, Tectonothermal evolution of the Southern Omineca Belt, Southern British Columbia: Unpublished PhD thesis, University of Calgary, 313 p.
- Webster, E.R. and Pattison, D.R.M., 2014, U-Pb dates for the Nelson and Bayonne magmatic suites in the Salmo-Creston area, southeastern British Columbia: tectonic implications for the southern Kootenay Arc (parts of NTS 082F/02, /03, /06, /07): In Geoscience BC Summary of Activities 2013, Geoscience BC, Report 2014-1, p. 99–114.

## APPENDIX 1 - $^{40}\text{Ar}/^{39}\text{Ar}$ Methodology

(A. Camacho, University of Manitoba)

All  $^{40}\text{Ar}/^{39}\text{Ar}$  analytical work was performed at the University of Manitoba using a multi-collector Thermo Fisher Scientific ARGUSVI mass spectrometer, linked to a stainless steel Thermo Fisher Scientific extraction/purification line and Photon Machines (55 W) Fusions 10.6 CO<sub>2</sub> laser. Argon isotopes (from mass 40 to 37) were measured using Faraday detectors with low noise  $1 \times 10^{12} \Omega$  resistors and mass 36 was measured using a compact discrete dynode (CDD) detector. The sensitivity for argon measurements is  $\sim 6.312 \times 10^{17}$  moles/fA as determined from measured aliquots of Fish Canyon Sanidine (Dazé et al., 2003; Kuiper et al., 2008).

Standards and unknowns were placed in 2 mm deep wells in 18 mm diameter aluminium disks, with standards placed strategically so that the lateral neutron flux gradients across the disk could be evaluated. Planar regressions were fit to the standard data, and the  $^{40}\text{Ar}/^{39}\text{Ar}$  neutron fluence parameter,  $J$ , interpolated for the unknowns. Uncertainties in  $J$  are estimated at 0.1 - 0.2% ( $1\sigma$ ), based on Monte Carlo error analysis of the planar regressions (Best et al., 1995). All specimens were irradiated in the Cadmium-lined, in-core CLICIT facility of the Oregon State University TRIGA reactor. The duration of irradiation was 10 hours and using the Fish Canyon sanidine (28.2 Ma; Kuiper et al., 2008) and GA1550 biotite (98.5 Ma; Spell & McDougall, 2003) standards.

Irradiated samples were placed in a Cu sample tray, with a KBr cover slip, in a stainless steel high vacuum extraction line and baked with an infrared lamp for 24 hours. Single crystals were either fused or step-heated using the laser, and reactive gases were removed, after  $\sim 3$  minutes, by three NP-10 SAES getters (two at room temperature and one at 450 °C) prior to being admitted to an ARGUSVI mass spectrometer by expansion. Five argon isotopes were measured simultaneously over a period of 6 minutes. Measured isotope abundances were corrected for extraction-line blanks, which were determined before every sample analysis. Line blanks averaged  $\sim 3.05$  fA for mass 40 and  $\sim 0.01$  fA for mass 36.

Mass discrimination was monitored by online analysis of air pipettes and gave a mean of  $D = 1.0035 \pm 0.0014$  per amu, based on 39 aliquots interspersed with the unknowns. A value of 295.5 was used for the atmospheric  $^{40}\text{Ar}/^{36}\text{Ar}$  ratio (Steiger and Jäger, 1977) for the purposes of routine measurement of mass spectrometer discrimination using air aliquots, and correction for atmospheric argon in the  $^{40}\text{Ar}/^{39}\text{Ar}$  age calculation. Corrections are made for neutron-induced  $^{40}\text{Ar}$  from potassium,  $^{39}\text{Ar}$  and  $^{36}\text{Ar}$  from calcium, and  $^{36}\text{Ar}$  from chlorine (Roddick, 1983; Renne et al., 1998; Renne and Norman, 2001). Data collection was performed using Pychron (Ross, 2017) and data reduction, error propagation, age calculation and plotting were performed using

MassSpec software (version 8.091; Deino, 2013). The decay constants used were those recommended by Steiger and Jäger (1977).

## References

- Best, M.G., Christiansen, E.H., Deino, A.L., Grommé, C.S., Tingey, D.G., 1995. Correlation and emplacement of a large, zoned, discontinuously exposed ash flow sheet; the  $^{40}\text{Ar}/^{39}\text{Ar}$  chronology, paleomagnetism, and petrology of the Pahrnagat Formation, Nevada. *J. Geophys. Res.* 100, 24593-24609.
- Dazé, A., Lee, J.K.W., Villeneuve, M., 2003. An intercalibration study of the Fish Canyon sanidine and biotite  $^{40}\text{Ar}/^{39}\text{Ar}$  standards and some comments on the age of the Fish Canyon Tuff. *Chem. Geol.* 199, 111-127.
- Kuiper, K.F., Deino, A., Hilgen, F.J., Krijgsman, W., Renne, R., Wijbrans, J.R., 2008. Synchronizing Rock Clocks of Earth History. *Science* 320, 500-504.
- Renne, P.R., Cassata, W.S., Morgan, L.E., 2009. The isotopic composition of atmospheric argon and  $^{40}\text{Ar}/^{39}\text{Ar}$  geochronology: time for a change? *Quatern. Geochronol.* 4, 288-298.
- Renne, P.R., Norman, E.B., 2001. Determination of the half-life of  $^{40}\text{Ar}$  by mass spectrometry. *Phys. Rev. C* 63 (047302), 3.
- Renne P.R., Swisher C.C., Deino A.L., Karner D.B., Owens T.L. and DePaolo D.J., 1998. Intercalibration of standards, absolute ages and uncertainties in  $^{40}\text{Ar}/^{39}\text{Ar}$  dating. *Chem. Geol.* 145, 117-152.
- Ross, J. 2017. <https://github.com/NMGRL/pychron>. DOI 10.5281/zenodo.9884.
- Roddick, J.C., 1983. High precision intercalibration of  $^{40}\text{Ar}$ - $^{39}\text{Ar}$  standards. *Geochim. Cosmochim. Acta* 47, 887-898.
- Steiger R.H. and Jäger E., 1977. Subcommittee on geochronology: convention on the use of decay constants in geo- and cosmochronology. *Earth Planet. Sci. Lett.* 36, 359-362.
- Spell T.L. and McDougall I., 2003. Characterization and calibration of  $^{40}\text{Ar}/^{39}\text{Ar}$  dating standards. *Chem. Geol.* 198, 189-211.

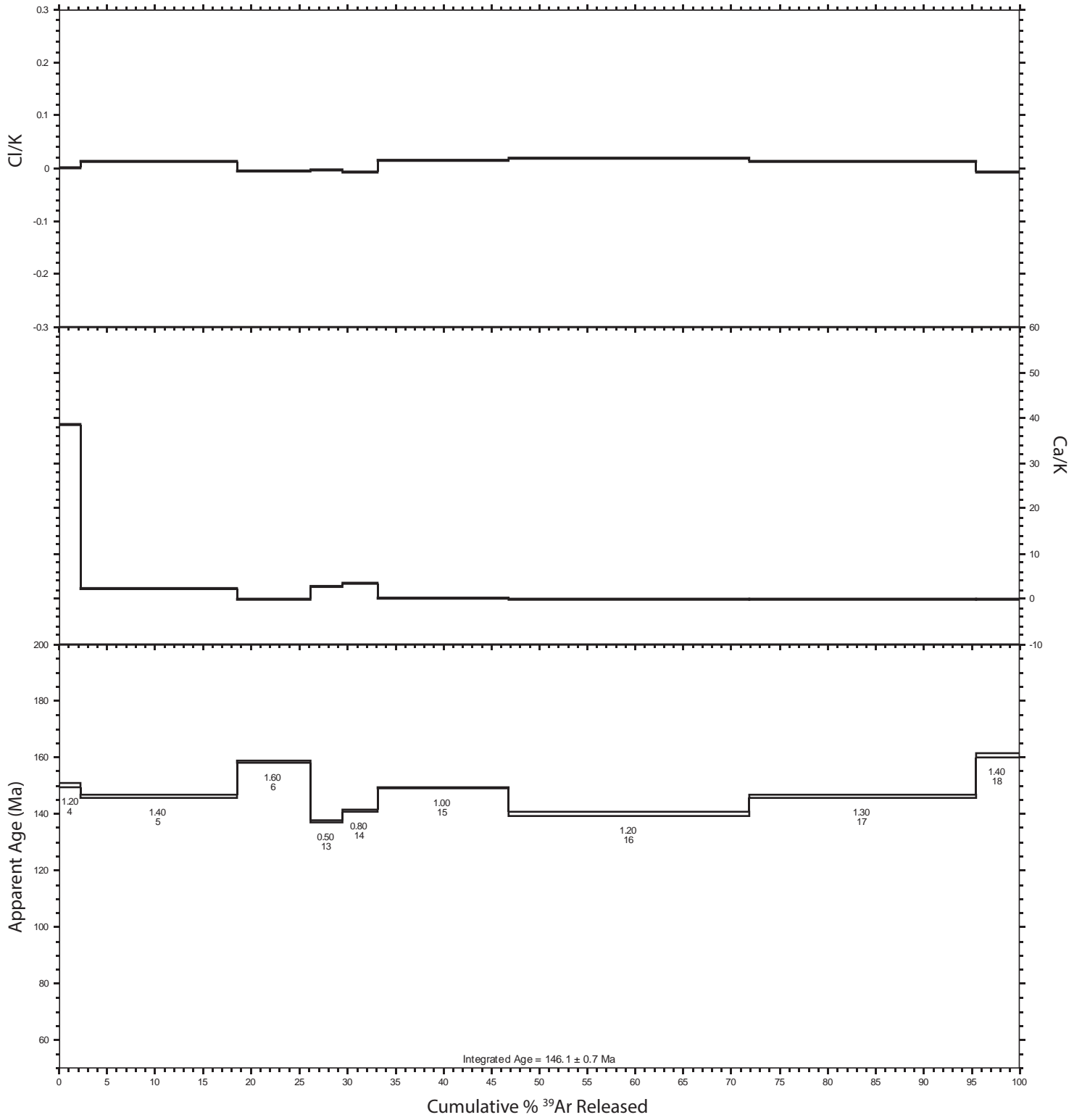
# APPENDIX 2 - $^{40}\text{Ar}/^{39}\text{Ar}$ Results

CARIBOO - calcite-muscovite vein cutting dolomitic marble  
 MA16-CB05 (muscovite)

Sample	Mineral	J	$\pm$ (1 $\sigma$ )	Relative Isotopic abundances (fAmps)*										Ca/K	$\pm$	Cl/K	$\pm$	$^{40}\text{Ar}^*/^{39}\text{Ar}_{(K)}$	$\pm$	$^{40}\text{Ar}^*$	Age	$\pm$																	
MA16-CB05	muscovite	0.0018696	2.89E-06	Ar40	$\pm$	Ar39	$\pm$	Ar38	$\pm$	Ar37	$\pm$	Ar36	$\pm$	(1 $\sigma$ )	(1 $\sigma$ )	(1 $\sigma$ )	(1 $\sigma$ )	(1 $\sigma$ )	(1 $\sigma$ )	(1 $\sigma$ )	(1 $\sigma$ )	(1 $\sigma$ )	(1 $\sigma$ )	(1 $\sigma$ )	(1 $\sigma$ )	(1 $\sigma$ )	(1 $\sigma$ )	(1 $\sigma$ )	(1 $\sigma$ )	(1 $\sigma$ )	(1 $\sigma$ )	(1 $\sigma$ )							
calcite vein with coarse white mica; cutting pale grey coarsely recrystallized dolomitic marble																																							
ALIQUOT 1																																							
Power (%)																																							
0.50	341.9913	0.0918	9.6616	0.0636	0.1771	0.0305	13.4487	0.0277	0.1305	0.0018	12.656	0.105	0.011	0.009	32.033	0.233	90.14	105.3	0.7																				
0.80	367.5716	0.1044	8.3080	0.0667	0.1499	0.0298	34.7828	0.0303	0.1770	0.0024	38.434	0.363	0.008	0.011	39.978	0.355	89.19	130.5	1.1																				
1.00	412.5267	0.1001	8.5399	0.0644	0.1260	0.0292	48.1847	0.0311	0.2325	0.0027	52.075	0.469	-0.005	0.010	43.062	0.365	87.58	140.2	1.1																				
1.20	856.7023	0.1321	17.3249	0.0680	0.2599	0.0290	72.3416	0.0317	0.3138	0.0032	38.402	0.227	0.000	0.005	46.207	0.214	92.24	150.0	0.7																				
1.40	5569.6670	0.3958	121.8009	0.4530	2.0976	0.0697	32.1008	0.0444	0.3454	0.0135	2.394	0.014	0.013	0.002	44.998	0.186	98.38	146.2	0.6																				
1.60	2794.0230	0.2117	57.0544	0.1130	0.5844	0.0332	0.5726	0.0319	0.0110	0.0023	0.091	0.005	-0.006	0.002	48.892	0.119	99.89	158.4	0.4																				
1.80	17.1106	0.0633	0.3675	0.0706	0.0198	0.0302	-0.0364	0.0268	0.0045	0.0012	-0.901	0.693	0.114	0.244	42.908	8.558	92.24	139.7	26.8																				
2.00	12.2905	0.0638	0.2530	0.0630	0.0056	0.0316	-0.0181	0.0282	0.0213	0.0012	-0.651	1.037	-0.017	0.370	23.631	6.229	48.68	78.3	20.2																				
2.50	21.6302	0.0648	0.5918	0.0607	-0.0455	0.0321	-0.0206	0.0267	0.0217	0.0012	-0.317	0.416	-0.278	0.163	25.669	2.782	70.28	84.9	9.0																				
3.00	30.6479	0.0691	0.6507	0.0587	-0.0008	0.0290	0.0214	0.0267	0.0414	0.0014	0.300	0.380	-0.074	0.132	28.293	2.722	60.10	93.3	8.7																				
3.50	26.8354	0.0636	0.5960	0.0616	0.0698	0.0302	-0.0007	0.0296	0.0418	0.0011	-0.011	0.458	0.266	0.153	24.287	2.654	53.97	80.4	8.6																				
4.00	30.5697	0.0614	0.8539	0.0603	-0.0007	0.0298	0.0254	0.0297	0.0411	0.0013	0.271	0.322	-0.064	0.104	21.573	1.638	60.29	71.6	5.3																				
Sample MA16-CB05 Mineral muscovite† J 0.0018741 $\pm$ (1 $\sigma$ ) 1.26E-06																																							
calcite vein with coarse white mica; cutting pale grey coarsely recrystallized dolomitic marble																																							
ALIQUOT 2																																							
Power (%)																																							
0.50	1011.5840	0.1514	21.9833	0.0673	0.2378	0.0307	-0.0130	0.0283	0.0287	0.0010	-0.014	0.029	-0.005	0.004	45.589	0.150	99.16	147.9	0.5																				
0.70	743.5085	0.1336	15.5615	0.0637	0.2230	0.0313	0.0321	0.0286	0.0026	0.0009	0.046	0.042	0.006	0.006	47.689	0.206	99.90	154.4	0.6																				
0.90	1417.9950	0.1611	29.3785	0.0705	0.3205	0.0306	0.0640	0.0255	0.0057	0.0011	0.048	0.020	-0.004	0.003	48.169	0.126	99.88	155.9	0.4																				
1.10	951.6137	0.1434	19.8122	0.0698	0.1970	0.0293	0.0630	0.0272	0.0024	0.0008	0.071	0.031	-0.007	0.004	47.957	0.179	99.93	155.3	0.6																				
† treated with HCl																																							
* Corrected for blank, mass discrimination, and radioactive decay																																							
Sensitivity 6.312E-17 $\pm$ 1.047E-18 (mol/fAmp)																																							



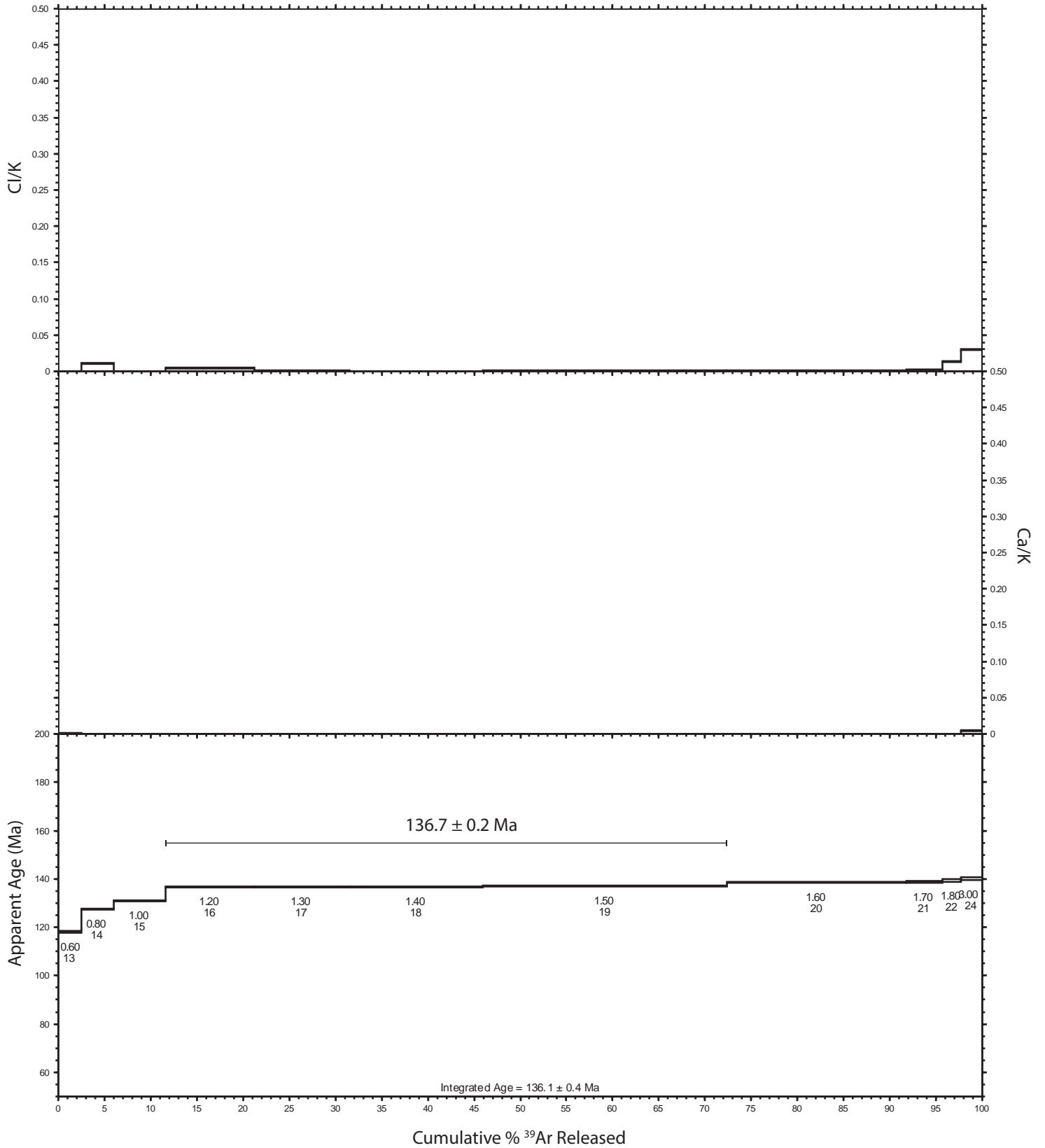
CARIBOO - calcite-muscovite vein cutting dolomitic marble  
 MA16-CB05 (muscovite) - ALIQUOT 1 (prior to HCl treatment)



CARIBOO - quartz-sericite vein hosted in phyllite, Silver Mine  
 MA16-CB15 (sericite)

Sample	Mineral	J	± (1σ)	Relative Isotopic abundances (fAmps)*															
MA16-CB15	sericite	0.0018682	2.81E-06																
quartz-sericite vein hosted by phyllite, Silver Mine																			
ALIQUOT 1				Relative Isotopic abundances (fAmps)*															
Power (%)	Ar40 ± (1σ)	Ar39 ± (1σ)	Ar38 ± (1σ)	Ar37 ± (1σ)	Ar36 ± (1σ)	Ca/K ± (1σ)	Cl/K ± (1σ)	<sup>40</sup> Ar*/ <sup>39</sup> Ar(K) ± (1σ)	<sup>40</sup> Ar* (%)	Age (Ma)	± (1σ)								
0.60	624.0143	0.1216	16.4920	0.0635	0.1870	0.0307	-0.0432	0.0273	0.0300	0.0011	-0.022	0.014	-0.004	0.006	37.278	0.151	98.58	121.5	0.5
0.80	1127.2590	0.1275	28.7491	0.0671	0.3200	0.0303	-0.0018	0.0270	0.0207	0.0009	-0.001	0.008	-0.004	0.003	38.976	0.098	99.46	126.8	0.3
1.00	1815.7030	0.1764	45.1025	0.0692	0.5957	0.0301	-0.0009	0.0269	0.0357	0.0012	-0.001	0.005	0.002	0.002	40.002	0.069	99.42	130.0	0.2
1.20	2920.2570	0.2122	70.8310	0.0713	0.7707	0.0285	-0.0572	0.0274	0.0352	0.0013	-0.007	0.003	-0.004	0.001	41.059	0.051	99.64	133.3	0.2
1.40	4259.7120	0.2808	102.0787	0.0742	1.1738	0.0268	0.0214	0.0292	0.0367	0.0014	0.001	0.002	-0.002	0.001	41.601	0.042	99.75	135.0	0.1
1.60	6017.5080	0.3489	141.5419	0.0754	1.6710	0.0306	-0.0599	0.0263	0.0583	0.0015	-0.004	0.002	-0.001	0.001	42.369	0.037	99.71	137.4	0.1
1.80	5725.4420	0.3630	133.2887	0.0760	1.5540	0.0294	-0.0058	0.0263	0.0356	0.0011	-0.001	0.002	-0.002	0.001	42.853	0.038	99.82	138.9	0.1
2.00	820.2759	0.1468	18.4292	0.0654	0.2972	0.0299	0.0306	0.0291	0.0038	0.0008	0.013	0.013	0.011	0.005	44.427	0.166	99.87	143.8	0.5
2.50	565.6137	0.1069	12.2355	0.0611	0.1722	0.0305	-0.0155	0.0277	0.0056	0.0008	-0.011	0.019	0.005	0.007	46.068	0.240	99.71	148.9	0.7
3.00	211.1870	0.0780	4.0185	0.0601	0.1116	0.0322	-0.0390	0.0243	0.0043	0.0007	-0.082	0.051	0.045	0.024	52.206	0.806	99.39	167.9	2.5
4.00	135.3280	0.0706	2.9874	0.0671	0.0444	0.0285	0.0168	0.0287	0.0021	0.0007	0.047	0.082	0.007	0.028	45.075	1.045	99.55	145.9	3.2
ALIQUOT 2																			
0.60	692.6884	0.1284	17.2228	0.0645	0.2598	0.0302	-0.0020	0.0292	0.2348	0.0024	-0.001	0.014	0.001	0.005	36.171	0.147	89.98	118.0	0.5
0.80	944.2154	0.1423	23.6368	0.0660	0.2990	0.0309	0.0304	0.0259	0.0633	0.0014	0.010	0.009	0.000	0.004	39.136	0.115	98.02	127.3	0.4
1.00	1529.7860	0.1614	37.4688	0.0670	0.4290	0.0311	-0.0065	0.0269	0.0694	0.0015	-0.002	0.006	-0.003	0.002	40.259	0.078	98.66	130.8	0.2
1.20	2756.9490	0.2345	64.9937	0.0671	0.7693	0.0310	0.0334	0.0282	0.0724	0.0016	0.004	0.004	-0.002	0.001	42.067	0.050	99.22	136.5	0.2
1.30	2917.8760	0.2072	68.9578	0.0731	0.8245	0.0324	0.0039	0.0278	0.0416	0.0013	0.000	0.003	-0.001	0.001	42.113	0.050	99.58	136.6	0.2
1.40	4095.8700	0.2738	96.9031	0.0712	1.1110	0.0306	-0.0016	0.0276	0.0409	0.0014	-0.001	0.002	-0.002	0.001	42.120	0.037	99.70	136.7	0.1
1.50	7516.9280	0.3460	177.7849	0.0817	2.1628	0.0307	0.0273	0.0291	0.0462	0.0018	0.001	0.001	0.000	0.001	42.181	0.027	99.82	136.8	0.1
1.60	5600.9820	0.3044	130.8172	0.0779	1.5279	0.0300	0.0099	0.0269	0.0326	0.0014	0.000	0.002	-0.002	0.001	42.718	0.032	99.83	138.5	0.1
1.70	1103.4610	0.1359	25.8767	0.0653	0.2491	0.0294	0.0060	0.0296	-0.0066	0.0011	0.002	0.010	-0.007	0.003	42.695	0.113	100.18	138.5	0.4
1.80	600.0206	0.1190	14.1093	0.0638	0.1384	0.0331	0.0214	0.0270	-0.0201	0.0012	0.013	0.017	-0.006	0.007	42.925	0.202	100.99	139.2	0.6
2.00	395.0962	0.0930	9.2407	0.0640	-0.0057	0.0316	0.0175	0.0264	-0.0078	0.0010	0.016	0.025	-0.037	0.010	42.982	0.309	100.58	139.3	1.0
3.00	641.2839	0.1167	14.8298	0.0642	0.2051	0.0309	0.0508	0.0267	0.0018	0.0011	0.029	0.016	0.005	0.006	43.185	0.195	99.92	140.0	0.6
* Corrected for blank, mass discrimination, and radioactive decay																			
Sensitivity 6.312E-17 ± 1.047E-18 (mol/fAmp)																			

CARIBOO - quartz-sericite vein hosted in phyllite, Silver Vein mine  
 MA16-CB15 (sericite) - ALIQUOT 2



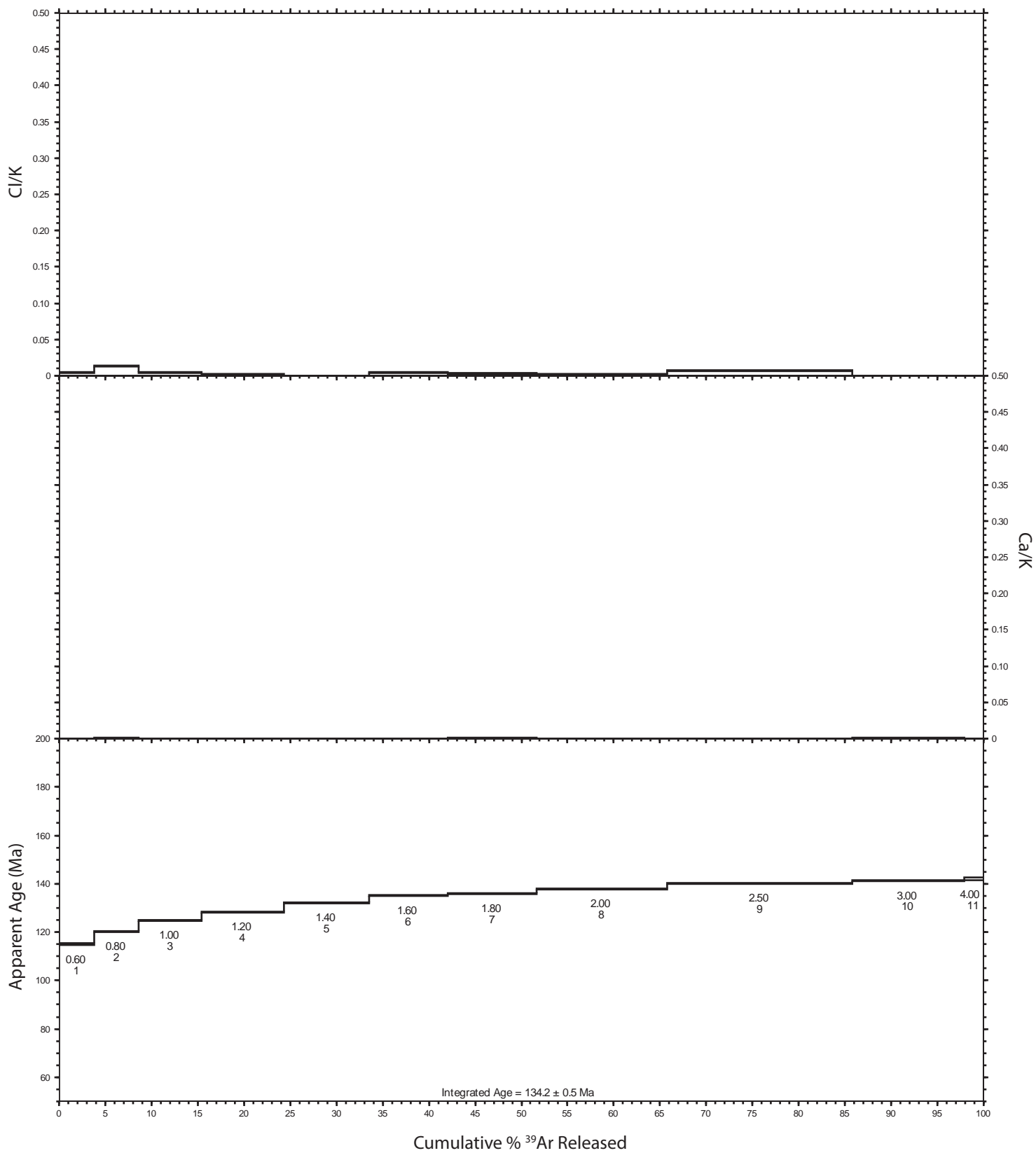
CARIBOO - quartz-pyrite-sericite vein, Penny Creek vein  
 MA16-CB21a (sericite)

Sample	Mineral	J	± (1σ)	Relative Isotopic abundances (fAmps)*																			
MA16-CB21a	sericite	0.0018696	2.89E-06	Ar40	± (1σ)	Ar39	± (1σ)	Ar38	± (1σ)	Ar37	± (1σ)	Ar36	± (1σ)	Ca/K	± (1σ)	Cl/K	± (1σ)	<sup>40</sup> Ar* / <sup>39</sup> Ar <sub>(K)</sub>	± (1σ)	<sup>40</sup> Ar* (%)	Age (Ma)	± (1σ)	
ALIQUOT 1																							
Power (%)																							
0.60	1019.7060	0.1331	28.6609	0.0628	0.2890	0.0279	0.0175	0.0272	0.0380	0.0011	0.005	0.008	-0.007	0.003	35.168	0.095	98.90	114.9	0.3				
0.80	1344.0960	0.1325	36.4138	0.0695	0.4536	0.0307	0.0621	0.0266	0.0151	0.0009	0.014	0.006	0.000	0.002	36.770	0.089	99.67	119.9	0.3				
1.00	1949.5300	0.1923	50.7843	0.0658	0.5775	0.0323	0.0279	0.0246	0.0136	0.0009	0.004	0.004	-0.003	0.002	38.289	0.073	99.79	124.7	0.2				
1.20	2620.5610	0.2150	66.5312	0.0704	0.7363	0.0292	0.0150	0.0284	0.0110	0.0010	0.001	0.004	-0.003	0.001	39.319	0.069	99.88	128.0	0.2				
1.40	2810.1640	0.2051	69.2039	0.0648	0.8197	0.0316	-0.0078	0.0278	0.0113	0.0011	-0.001	0.003	-0.001	0.001	40.537	0.068	99.88	131.8	0.2				
1.60	2640.7630	0.1964	63.4495	0.0763	0.7763	0.0296	0.0426	0.0268	0.0116	0.0011	0.005	0.004	0.000	0.001	41.544	0.077	99.87	134.9	0.2				
1.80	3026.9280	0.2451	72.2413	0.0664	0.8894	0.0298	0.0338	0.0293	0.0114	0.0011	0.003	0.003	0.000	0.001	41.832	0.070	99.89	135.8	0.2				
2.00	4493.3170	0.2664	105.8490	0.0751	1.2867	0.0312	0.0273	0.0273	0.0142	0.0011	0.002	0.002	0.000	0.001	42.388	0.066	99.91	137.6	0.2				
2.50	6468.9710	0.3256	149.7316	0.0804	1.7336	0.0279	0.1259	0.0267	0.0208	0.0014	0.006	0.001	-0.002	0.001	43.140	0.063	99.91	139.9	0.2				
3.00	3936.3470	0.2875	90.3751	0.0740	1.1426	0.0317	-0.0799	0.0271	0.0108	0.0009	-0.008	0.003	0.001	0.001	43.497	0.070	99.92	141.0	0.2				
4.00	686.4806	0.1239	15.6509	0.0663	0.1875	0.0302	-0.0026	0.0301	0.0034	0.0009	-0.002	0.016	-0.001	0.006	43.774	0.201	99.85	141.9	0.6				

\* Corrected for blank, mass discrimination, and radioactive decay  
 Sensitivity 6.312E-17 ± 1.047E-18 (mol/fAmp)



CARIBOO - quartz-pyrite-sericite vein, Penny Creek vein  
 MA16-CB21a (sericite)

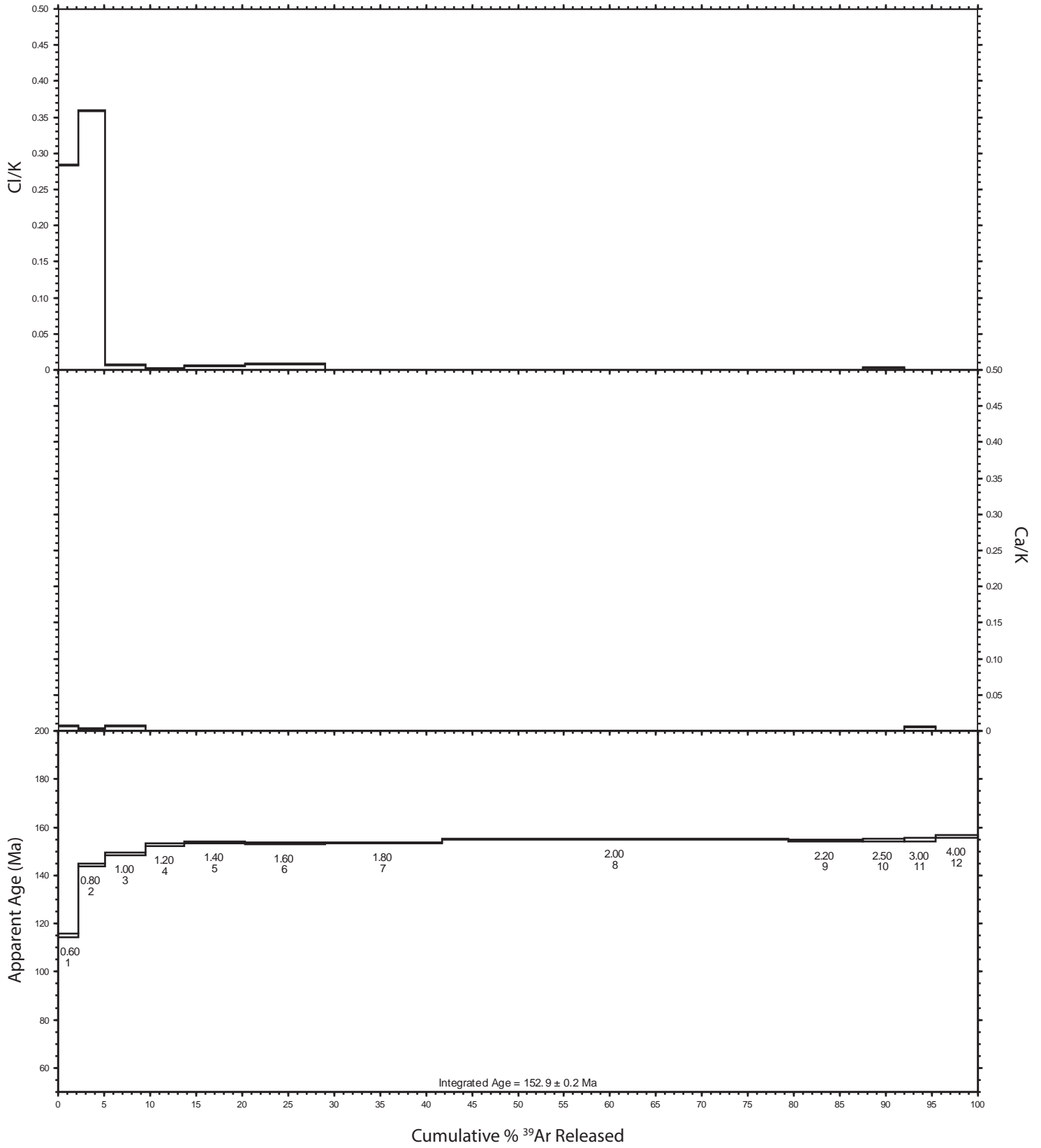


CARIBOO - fibrous muscovite vein cutting metaturbidite  
 MA16-CB23 (sericite)

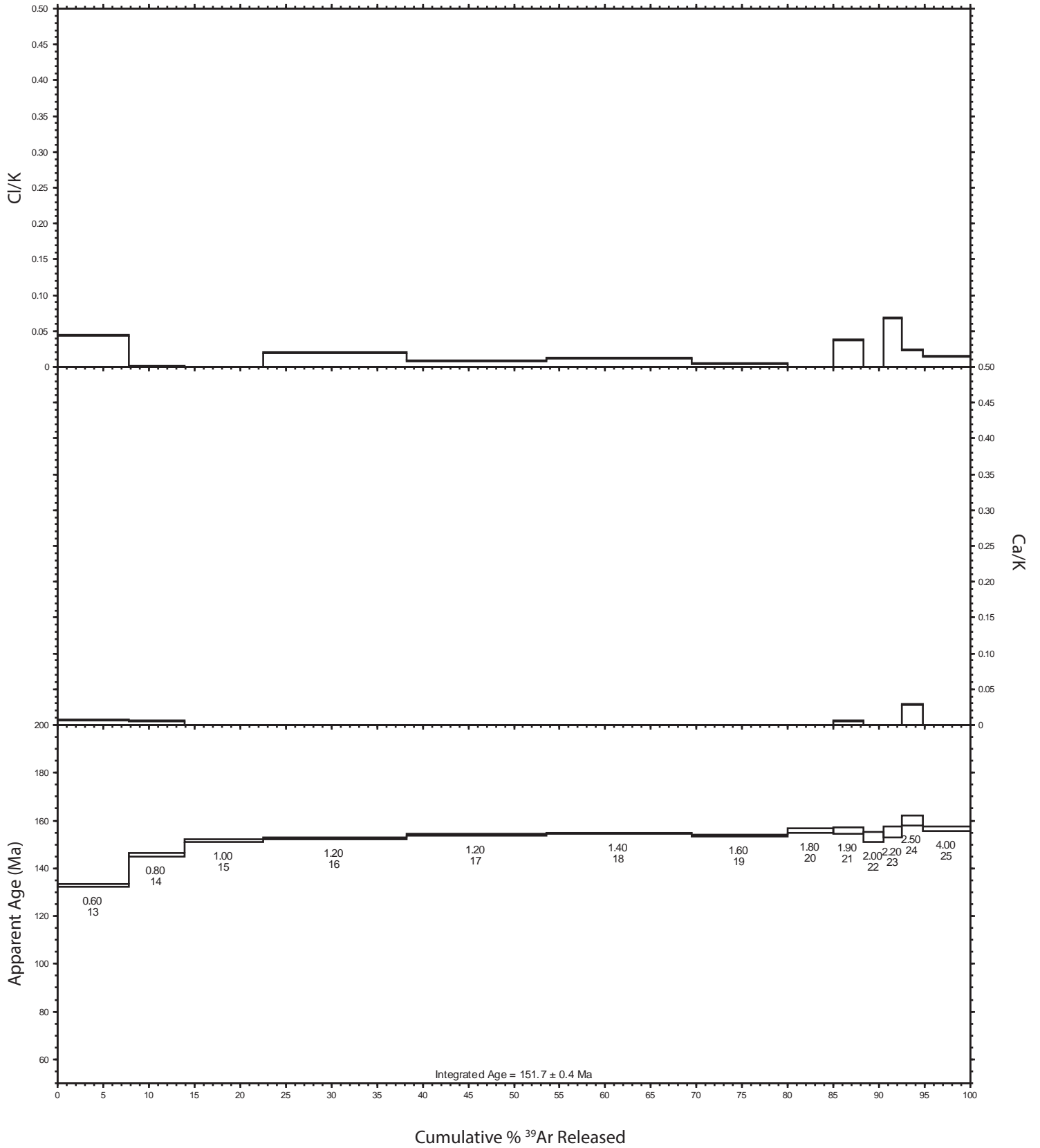
Sample	Mineral	J	± (1σ)	Relative Isotopic abundances (fAmps)*																			
MA16-CB23	sericite	0.0018497	1.09E-06	muscovite vein cutting psammite-pelite metaturbidite																			
ALIQUOT 1				Ar40	± (1σ)	Ar39	± (1σ)	Ar38	± (1σ)	Ar37	± (1σ)	Ar36	± (1σ)	Ca/K	± (1σ)	Cl/K	± (1σ)	<sup>40</sup> Ar*/ <sup>39</sup> Ar(K)	± (1σ)	<sup>40</sup> Ar*	Age (Ma)	± (1σ)	
Power (%)																							
0.60	378.8825	0.0942	9.7455	0.0602	0.1619	0.0296	0.3538	0.0304	0.1088	0.0018	0.284	0.025	0.007	0.009	35.575	0.233	91.54	115.0	0.7				
0.80	574.5316	0.1065	12.2084	0.0604	0.1772	0.0318	0.5596	0.0263	0.0867	0.0015	0.359	0.017	0.003	0.008	44.958	0.233	95.57	144.1	0.7				
1.00	871.3702	0.1284	18.3565	0.0638	0.2794	0.0298	0.0167	0.0290	0.0613	0.0015	0.007	0.013	0.007	0.005	46.459	0.169	97.92	148.7	0.5				
1.20	879.1748	0.1279	18.1768	0.0615	0.2252	0.0339	0.0043	0.0269	0.0372	0.0013	0.001	0.012	-0.001	0.006	47.738	0.168	98.75	152.7	0.5				
1.40	1347.4560	0.1559	27.7681	0.0655	0.3004	0.0270	0.0217	0.0268	0.0488	0.0013	0.006	0.008	-0.005	0.003	47.981	0.118	98.93	153.4	0.4				
1.60	1787.9250	0.1838	37.0508	0.0733	0.4423	0.0321	0.0409	0.0257	0.0403	0.0014	0.008	0.006	-0.001	0.003	47.910	0.098	99.33	153.2	0.3				
1.80	2583.5120	0.2105	53.6186	0.0739	0.6448	0.0326	-0.0495	0.0267	0.0401	0.0013	-0.008	0.004	-0.001	0.002	47.937	0.068	99.54	153.3	0.2				
2.00	7759.7500	0.3462	159.4749	0.0807	1.8885	0.0293	-0.0054	0.0294	0.0672	0.0016	-0.001	0.001	-0.001	0.001	48.509	0.026	99.74	155.0	0.1				
2.20	1652.8140	0.1819	34.1741	0.0653	0.4074	0.0299	-0.0205	0.0292	0.0116	0.0010	-0.005	0.007	-0.001	0.003	48.240	0.095	99.79	154.2	0.3				
2.50	922.0682	0.1390	19.0455	0.0643	0.1988	0.0297	0.0093	0.0281	0.0065	0.0009	0.003	0.012	-0.005	0.005	48.289	0.168	99.79	154.3	0.5				
3.00	708.5212	0.1105	14.5984	0.0625	0.2090	0.0299	-0.0523	0.0278	0.0065	0.0009	-0.029	0.015	0.006	0.006	48.376	0.214	99.73	154.6	0.7				
4.00	943.6529	0.1344	19.2371	0.0591	0.2106	0.0302	-0.0580	0.0265	0.0137	0.0009	-0.024	0.011	-0.004	0.005	48.817	0.155	99.57	156.0	0.5				
ALIQUOT 2																							
0.60	714.4180	0.1280	16.4500	0.0625	0.2626	0.0345	0.0934	0.0271	0.1198	0.0018	0.045	0.013	0.007	0.006	41.258	0.165	95.05	132.7	0.5				
0.80	589.1580	0.1132	12.7819	0.0646	0.1890	0.0306	0.0015	0.0260	0.0279	0.0011	0.000	0.016	0.006	0.007	45.425	0.239	98.60	145.5	0.7				
1.00	855.9930	0.1292	17.9128	0.0620	0.1884	0.0304	-0.0603	0.0285	0.0286	0.0011	-0.027	0.013	-0.006	0.005	47.288	0.169	99.01	151.3	0.5				
1.20	1584.1110	0.1619	32.9714	0.0676	0.3871	0.0320	0.0843	0.0315	0.0399	0.0012	0.020	0.008	-0.002	0.003	47.664	0.101	99.26	152.4	0.3				
1.20	1515.4610	0.1575	31.9483	0.0646	0.3482	0.0311	0.0324	0.0280	-0.0810	0.0020	0.008	0.007	-0.002	0.003	48.159	0.102	101.58	153.9	0.3				
1.40	1617.8990	0.1931	33.2059	0.0636	0.3914	0.0310	0.0532	0.0275	0.0410	0.0013	0.012	0.007	-0.002	0.003	48.334	0.096	99.25	154.5	0.3				
1.60	1065.9580	0.1651	22.1129	0.0642	0.2039	0.0285	0.0135	0.0296	0.0126	0.0009	0.004	0.011	-0.009	0.004	48.012	0.144	99.65	153.5	0.4				
1.80	510.1008	0.1115	10.4069	0.0664	0.1044	0.0317	-0.0188	0.0261	0.0088	0.0008	-0.015	0.020	-0.007	0.009	48.740	0.320	99.49	155.7	1.0				
1.90	342.2573	0.0884	7.0056	0.0563	0.0995	0.0316	0.0327	0.0267	0.0029	0.0007	0.037	0.031	0.006	0.013	48.710	0.403	99.75	155.6	1.2				
2.00	216.3763	0.0819	4.5341	0.0639	0.0489	0.0323	-0.0295	0.0263	-0.0013	0.0009	-0.053	0.047	-0.004	0.021	47.776	0.693	100.17	152.8	2.1				
2.20	205.7547	0.0741	4.2289	0.0624	-0.0258	0.0275	0.0358	0.0281	0.0015	0.0008	0.068	0.054	-0.053	0.019	48.528	0.736	99.79	155.1	2.3				
2.50	237.8823	0.0827	4.7300	0.0600	0.1057	0.0269	0.0137	0.0260	0.0030	0.0007	0.023	0.045	0.029	0.017	50.078	0.652	99.63	159.8	2.0				
4.00	531.1138	0.1038	10.7867	0.0680	0.1215	0.0317	0.0197	0.0279	0.0099	0.0009	0.014	0.021	-0.003	0.009	48.943	0.317	99.45	156.3	1.0				
* Corrected for blank, mass discrimination, and radioactive decay																							
Sensitivity				6.312E-17 ± 1.047E-18 (mol/fAmp)																			



CARIBOO - fibrous muscovite vein cutting metaturbidite  
 MA16-CB23 (sericite) - ALIQUOT 1



CARIBOO - fibrous muscovite vein cutting metaturbidite  
 MA16-CB23 (sericite) - ALIQUOT 2



CARIBOO (Silver Mine) - lamprophyre dike  
 RG16-CB03 (biotite)

Sample	Mineral	J	± (1σ)	Relative Isotopic abundances (fAmps)*																		
RG16-CB03	biotite	1.896E-03	2.210E-06	Ar40	± (1σ)	Ar39	± (1σ)	Ar38	± (1σ)	Ar37	± (1σ)	Ar36	± (1σ)	Ca/K	± (1σ)	Cl/K	± (1σ)	<sup>40</sup> Ar*/ <sup>39</sup> Ar(K)	± (1σ)	<sup>40</sup> Ar*	Age (Ma)	± (1σ)
lamprophyre dike, Silver Mine																						
<b>GRAIN 1</b>																						
0.50		7.6423	0.0638	0.1868	0.0624	0.0517	0.0294	-0.0206	0.0259	0.0177	0.0012			-1.080	1.421	0.714	0.528	12.841	4.833	31.41	43.4	16.1
1.00		120.8270	0.0770	2.0679	0.0643	0.0185	0.0275	0.0441	0.0281	0.1966	0.0023			0.208	0.135	-0.061	0.039	30.323	1.031	51.92	100.8	3.3
2.00		313.1214	0.0988	8.3080	0.0646	0.1241	0.0319	0.0696	0.0286	0.0922	0.0018			0.082	0.034	0.002	0.011	34.394	0.286	91.31	114.0	0.9
4.00		345.6150	0.1211	9.8728	0.0626	0.0899	0.0318	0.0828	0.0252	0.0147	0.0011			0.082	0.025	-0.010	0.010	34.549	0.230	98.75	114.5	0.7
<b>GRAIN 2</b>																						
0.50		6.5280	0.0691	0.1942	0.0624	0.0619	0.0307	0.0790	0.0267	0.0143	0.0010			3.993	1.901	0.850	0.547	12.047	4.297	35.81	40.7	14.4
1.00		8.6537	0.0673	0.2365	0.0629	-0.0376	0.0298	0.0053	0.0265	0.0004	0.0011			0.218	1.112	-0.497	0.397	36.024	9.993	98.50	119.2	32.0
2.00		116.4061	0.0767	3.2330	0.0591	0.0703	0.0300	0.0378	0.0258	0.0118	0.0011			0.114	0.079	0.026	0.027	34.916	0.667	97.03	115.6	2.1
4.00		145.6646	0.0761	4.2184	0.0566	-0.0013	0.0319	-0.0107	0.0279	0.0022	0.0008			-0.025	0.066	-0.037	0.022	34.353	0.480	99.55	113.8	1.5
<b>GRAIN 3</b>																						
0.50		8.3481	0.0626	0.1608	0.0622	0.0559	0.0298	0.0539	0.0269	0.0229	0.0010			3.298	2.126	0.897	0.656	10.007	4.447	19.27	33.9	14.9
1.00		30.6838	0.0656	0.8036	0.0641	0.0887	0.0334	0.3755	0.0289	0.0255	0.0011			4.607	0.522	0.268	0.125	29.033	2.433	75.96	96.7	7.9
2.00		148.3816	0.0716	4.2480	0.0555	0.0847	0.0301	0.1230	0.0256	0.0111	0.0009			0.285	0.060	0.021	0.021	34.155	0.466	97.83	113.2	1.5
4.00		140.2751	0.0776	4.0719	0.0639	0.0112	0.0325	0.2493	0.0265	0.0071	0.0010			0.604	0.066	-0.028	0.024	33.947	0.556	98.58	112.5	1.8

\* Corrected for blank, mass discrimination, and radioactive decay  
 Sensitivity 6.312E-17 ± 1.047E-18 (mol/fAmp)



CARIBOO (Silver Mine) - lamprophyre dike  
 RG16-CB06 (biotite)

Sample	Mineral	J	± (1σ)	Relative Isotopic abundances (fAmps)*																		
RG16-CB06a	biotite	1.873E-03	1.474E-06	Ar40	± (1σ)	Ar39	± (1σ)	Ar38	± (1σ)	Ar37	± (1σ)	Ar36	± (1σ)	Ca/K	± (1σ)	Cl/K	± (1σ)	<sup>40</sup> Ar*/ <sup>39</sup> Ar(K)	± (1σ)	<sup>40</sup> Ar*	Age (Ma)	± (1σ)
lamprophyre dike, Silver Vein Mine																						
<b>GRAIN 1</b>																						
0.50		0.9290	0.0657	0.0962	0.0647	-0.0144	0.0319	-0.0256	0.0244	0.0018	0.0007	-2.860	3.397	-0.479	1.033	3.979	3.505	41.27	13.4	11.8		
2.00		286.2063	0.0966	8.9389	0.0600	0.1659	0.0302	0.0673	0.0285	0.1226	0.0019	0.081	0.035	0.011	0.010	27.951	0.214	87.35	92.1	0.7		
4.00		829.2939	0.1328	27.3711	0.0659	0.3588	0.0308	-0.0472	0.0282	0.1216	0.0017	-0.019	0.011	0.000	0.003	28.966	0.090	95.66	95.3	0.3		
5.00		1133.9860	0.1335	33.2143	0.0711	0.3097	0.0298	0.0126	0.0242	0.0616	0.0015	0.004	0.008	-0.009	0.003	33.571	0.093	98.39	110.0	0.3		
<b>GRAIN 2</b>																						
0.50		0.0362	0.0592	-0.1952	0.0670	0.0585	0.0309	-0.0363	0.0267	-0.0006	0.0007	2.008	1.652	-0.906	0.567	-1.006	1.170	540.47	-3.4	4.0		
2.00		15.5323	0.0687	0.6516	0.0611	0.0226	0.0295	0.0195	0.0278	-0.0019	0.0010	0.323	0.467	0.067	0.134	24.710	2.430	103.72	81.6	7.8		
4.00		467.2814	0.1028	14.5612	0.0604	0.1416	0.0325	-0.0389	0.0292	0.0345	0.0012	-0.029	0.022	-0.008	0.007	31.369	0.146	97.81	103.0	0.5		
5.00		176.6974	0.0920	4.9596	0.0640	-0.0140	0.0306	-0.0125	0.0261	0.0075	0.0008	-0.029	0.060	-0.044	0.018	35.154	0.473	98.73	115.1	1.5		
<b>GRAIN 3</b>																						
0.50		6.1172	0.0633	0.2068	0.0706	0.0013	0.0296	0.0316	0.0265	0.0080	0.0008	1.660	1.520	-0.039	0.423	18.203	6.522	61.55	60.5	21.3		
2.00		233.9247	0.0778	6.4750	0.0646	0.0625	0.0299	0.1414	0.0256	0.0338	0.0012	0.237	0.043	-0.010	0.014	34.576	0.365	95.76	113.2	1.2		
4.00		185.6448	0.0791	5.3014	0.0581	0.0646	0.0273	0.2008	0.0265	0.0200	0.0011	0.411	0.055	-0.002	0.015	33.901	0.392	96.86	111.1	1.2		
5.00		7.7635	0.0599	0.1983	0.0612	0.0039	0.0270	0.0317	0.0287	-0.0002	0.0007	1.798	1.739	0.022	0.402	39.463	12.570	100.82	128.7	39.6		
* Corrected for blank, mass discrimination, and radioactive decay																						
Sensitivity 6.312E-17 ± 1.047E-18 (mol/fAmp)																						

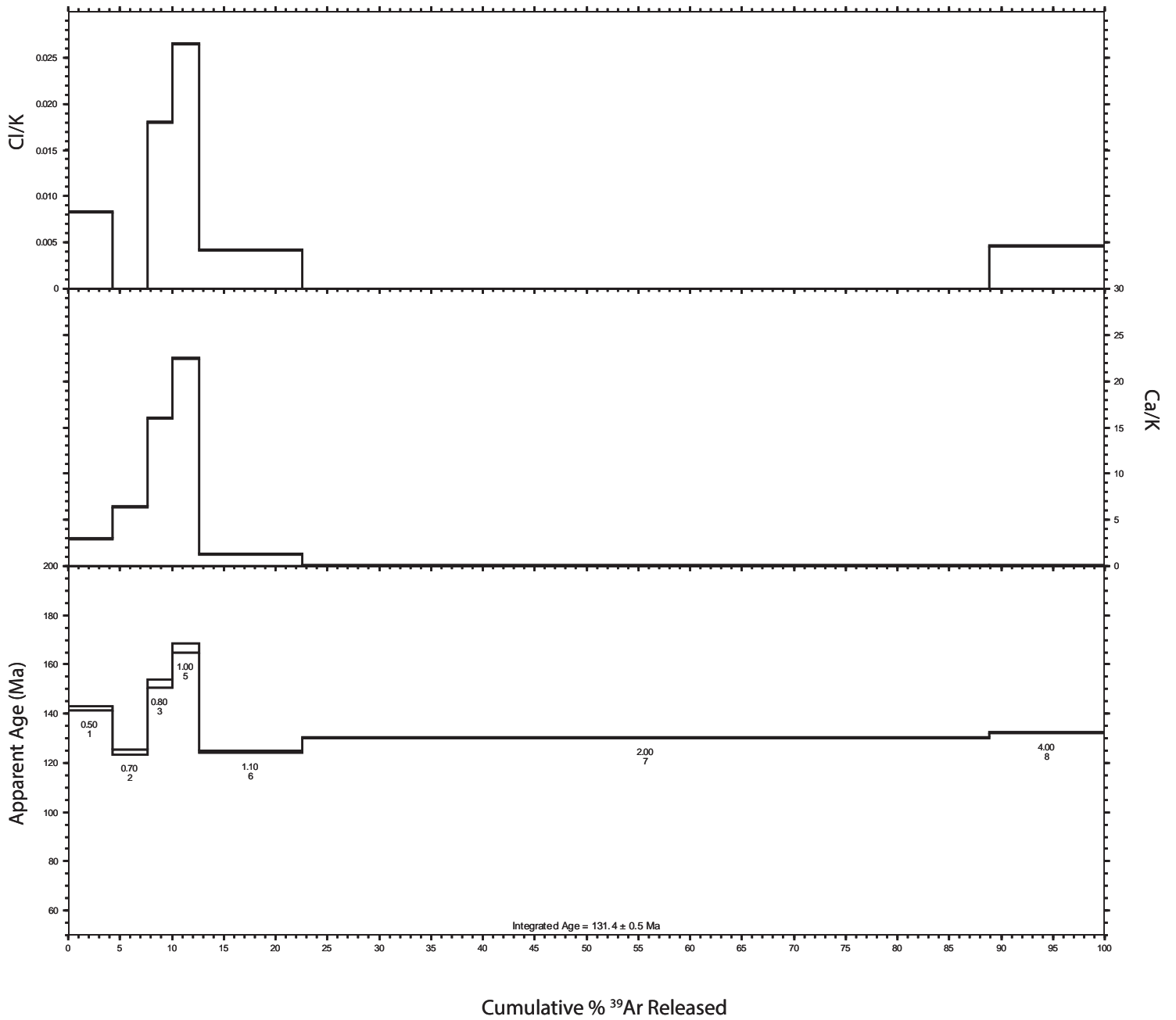


# CASSIAR - quartz-sericite vein, Main Mine 04MM-36\_100.1m (sericite)

Sample	Mineral	J	± (1σ)	Relative Isotopic abundances (fAmps)*																			
04MM-36_10 sericite		0.0018772	1.43E-06																				
quartz-carbonate-sericite vein, Main Mine																							
ALIQUOT 1				Relative Isotopic abundances (fAmps)*										Ca/K		Cl/K		<sup>40</sup> Ar* / <sup>39</sup> Ar <sub>(K)</sub>		<sup>40</sup> Ar*		Age	
Power (%)	Ar40 ± (1σ)	Ar39 ± (1σ)	Ar38 ± (1σ)	Ar37 ± (1σ)	Ar36 ± (1σ)	Ca/K ± (1σ)	Cl/K ± (1σ)	<sup>40</sup> Ar* / <sup>39</sup> Ar <sub>(K)</sub> ± (1σ)	<sup>40</sup> Ar* (%) ± (1σ)	Age (Ma) ± (1σ)													
0.50	500.7079	0.1051	10.4441	0.0624	0.1867	0.0311	2.7702	0.0263	0.1589	0.0019	2.982	0.036	0.008	0.009	43.583	0.284	90.87	141.9	0.9				
0.70	327.3768	0.0923	8.2189	0.0641	0.0493	0.0298	4.6562	0.0267	0.0620	0.0014	6.381	0.069	-0.022	0.011	37.918	0.315	95.04	124.0	1.0				
0.80	294.5414	0.0831	5.8344	0.0629	0.1222	0.0331	8.2405	0.0274	0.0894	0.0016	15.983	0.198	0.018	0.017	46.824	0.535	92.29	152.0	1.7				
0.90	317.9839	0.0931	4.9806	0.0641	0.0351	0.0312	12.4729	0.0278	0.1399	0.0019	28.482	0.404	-0.029	0.019	57.209	0.781	88.77	184.0	2.4				
1.00	345.9065	0.1000	6.2806	0.0635	0.1503	0.0295	12.4564	0.0271	0.1032	0.0017	22.522	0.259	0.027	0.014	51.491	0.552	92.81	166.5	1.7				
1.10	952.0348	0.1285	24.2611	0.0711	0.3510	0.0313	2.6892	0.0287	0.1081	0.0020	1.250	0.015	0.004	0.004	37.967	0.130	96.77	124.2	0.4				
2.00	6446.6170	0.3230	160.3287	0.1009	1.9557	0.0368	0.4175	0.0293	0.2181	0.0037	0.029	0.002	-0.001	0.001	39.783	0.060	99.00	129.9	0.2				
4.00	1095.3210	0.1558	26.9024	0.0697	0.3747	0.0293	0.1223	0.0259	0.0184	0.0012	0.051	0.011	0.005	0.003	40.489	0.121	99.51	132.2	0.4				
ALIQUOT 2																							
0.50	150.3404	0.0809	4.2006	0.0625	0.0444	0.0298	0.0132	0.0276	0.0081	0.0009	0.035	0.075	-0.006	0.021	35.198	0.546	98.41	115.4	1.7				
0.80	690.7434	0.1192	18.6671	0.0644	0.2304	0.0300	0.0664	0.0241	0.0854	0.0016	0.040	0.015	-0.002	0.005	35.631	0.134	96.35	116.8	0.4				
1.00	982.6776	0.1373	25.8221	0.0718	0.3481	0.0285	0.0579	0.0428	0.1522	0.0020	0.025	0.019	0.000	0.003	36.291	0.113	95.42	118.9	0.4				
1.20	1621.1110	0.1936	41.6776	0.0895	0.4856	0.0350	0.0562	0.0288	0.1508	0.0028	0.015	0.008	-0.004	0.002	37.803	0.093	97.25	123.7	0.3				
1.40	2072.4690	0.1920	52.3448	0.1038	0.6833	0.0364	0.0727	0.0294	0.1177	0.0034	0.015	0.006	0.001	0.002	38.904	0.089	98.32	127.2	0.3				
1.60	2507.1760	0.2361	62.9218	0.1365	0.8218	0.0358	0.1085	0.0329	0.1068	0.0039	0.019	0.006	0.002	0.002	39.320	0.096	98.74	128.5	0.3				
* Corrected for blank, mass discrimination, and radioactive decay																							
Sensitivity 6.312E-17 ± 1.047E-18 (mol/fAmp)																							

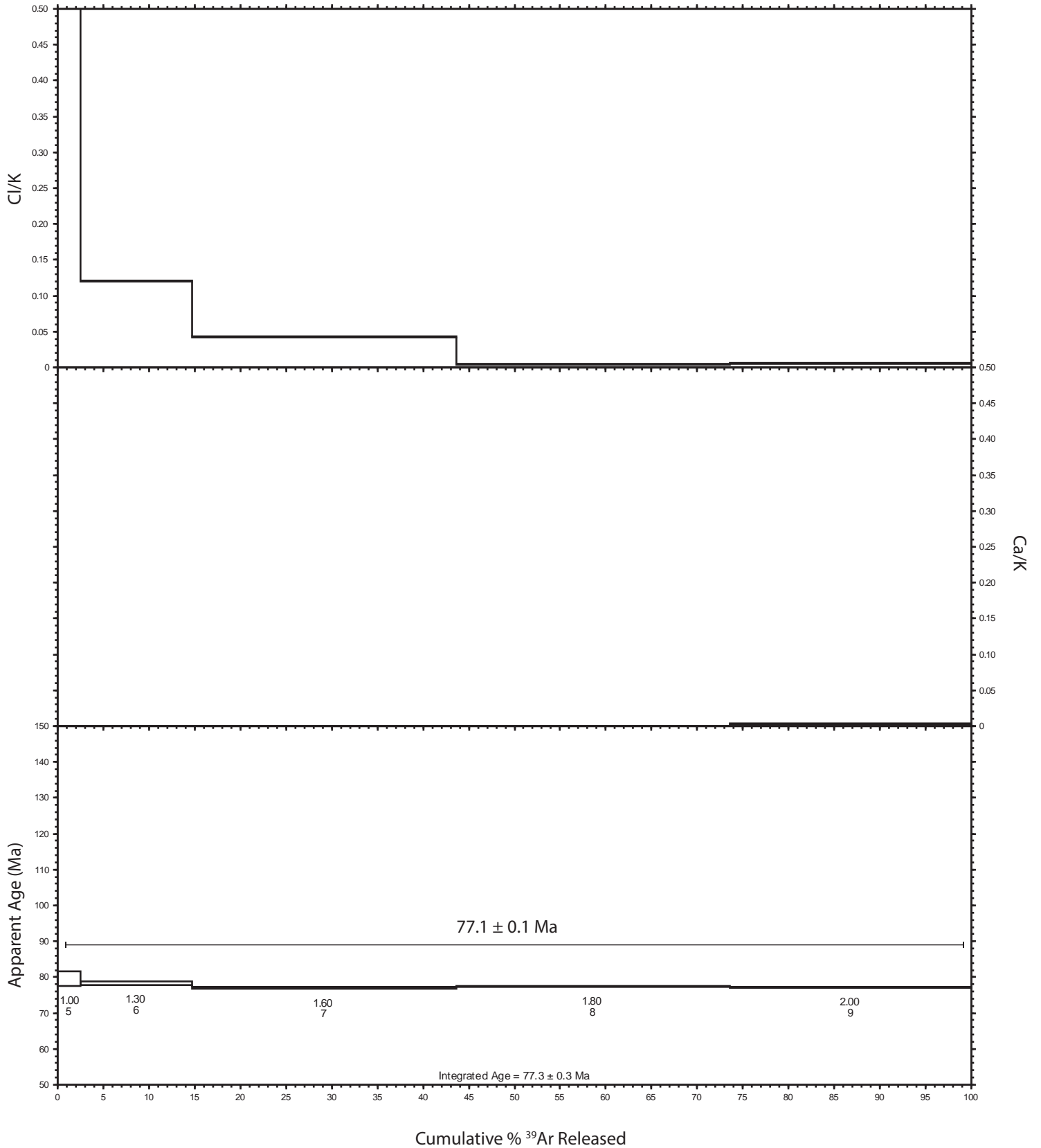


CASSIAR - quartz-sericite vein, Main Mine  
 04MM-36\_100.1m (sericite) - ALIQUOT 1





CASSIAR - biotite pyroxene lamprophyre, Bain mine  
 MA16-CS04 (biotite)

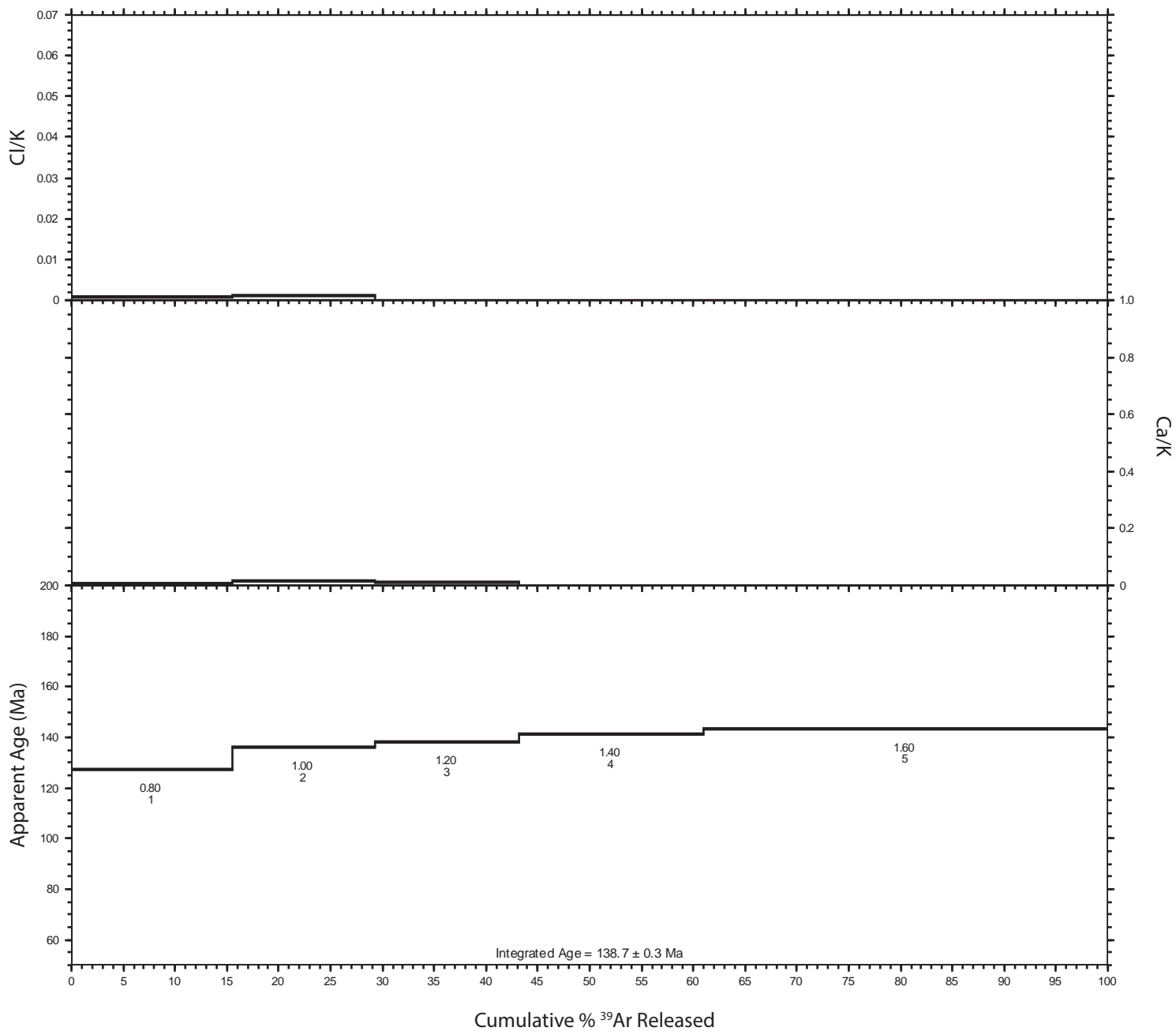


# CASSIAR - quartz-carbonate-sericite vein, Taurus T-95-35\_129.5m (sericite)

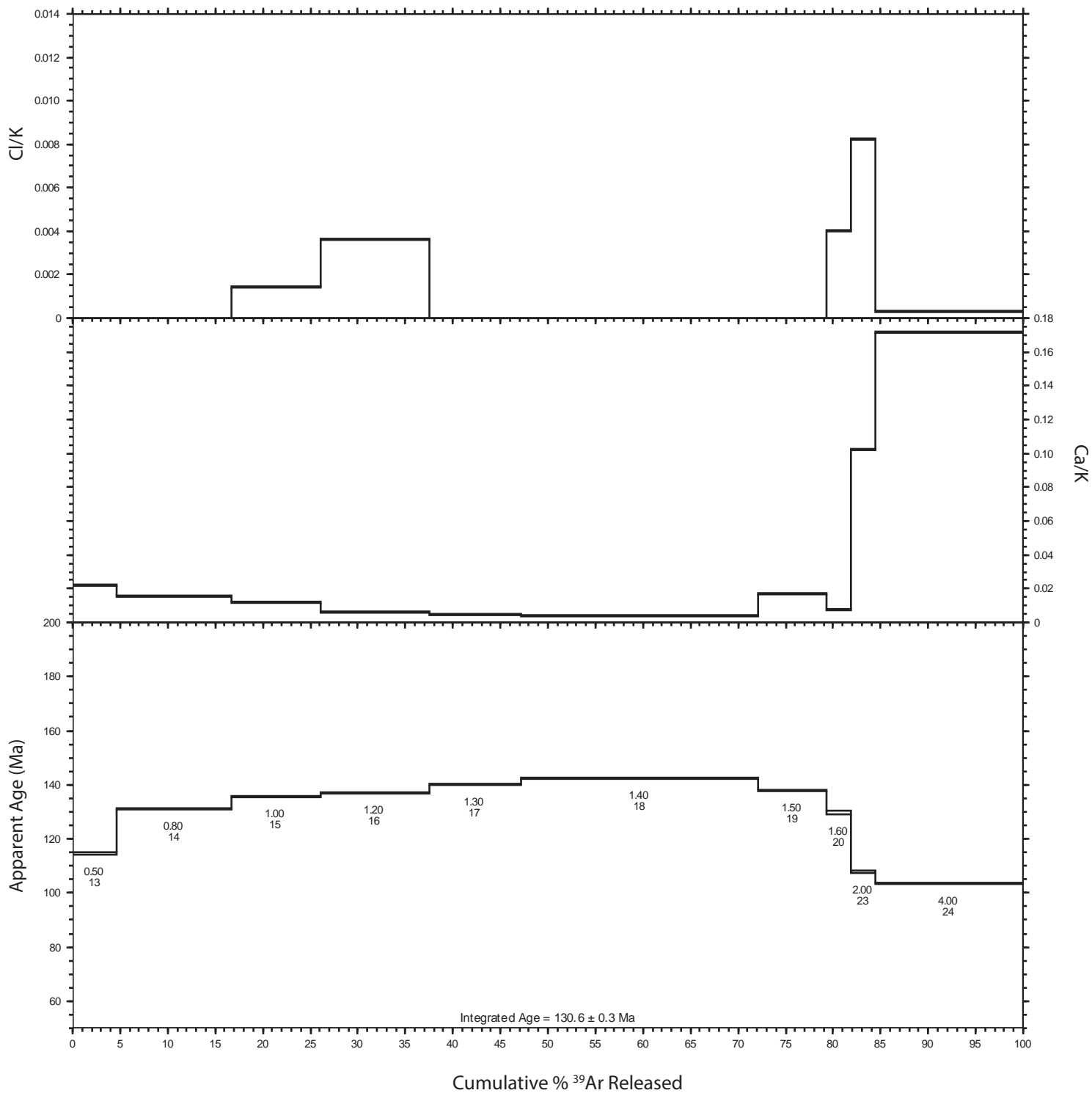
Sample	Mineral	J	± (1σ)	Relative Isotopic abundances (fAmps)*																			
T-95-35_129.5m	sericite	0.0018782	1.83E-06	Ar40	± (1σ)	Ar39	± (1σ)	Ar38	± (1σ)	Ar37	± (1σ)	Ar36	± (1σ)	Ca/K	± (1σ)	Cl/K	± (1σ)	<sup>40</sup> Ar+ <sup>39</sup> Ar <sub>(K)</sub>	± (1σ)	<sup>40</sup> Ar*	Age (Ma)	± (1σ)	
quartz-carbonate-sericite vein, Taurus																							
<b>ALIQUOT 1</b>																							
Power (%)																							
0.80	2422.4720	0.1991	60.7357	0.0720	0.7933	0.0309	0.0422	0.0268	0.1954	0.0023	0.008	0.005	0.001	0.002	38.909	0.057	97.62	127.2	0.2				
1.00	2260.6840	0.2129	53.6430	0.0692	0.6909	0.0336	0.0710	0.0281	0.0780	0.0016	0.015	0.006	0.001	0.002	41.687	0.063	98.98	136.0	0.2				
1.20	2332.3270	0.2291	54.5967	0.0671	0.6048	0.0292	0.0454	0.0277	0.0589	0.0017	0.009	0.006	-0.004	0.002	42.373	0.062	99.25	138.2	0.2				
1.40	3018.4540	0.2154	69.2322	0.0711	0.8377	0.0298	-0.0214	0.0281	0.0569	0.0016	-0.004	0.005	-0.001	0.001	43.327	0.055	99.44	141.1	0.2				
1.60	6714.8090	0.3375	152.0193	0.0843	1.8099	0.0313	-0.0116	0.0269	0.0815	0.0017	-0.001	0.002	-0.001	0.001	43.983	0.040	99.64	143.2	0.1				
1.80	343.5621	0.0971	7.9644	0.0665	0.0534	0.0305	-0.0441	0.0269	-0.0023	0.0009	-0.066	0.040	-0.016	0.011	43.192	0.373	100.20	140.7	1.2				
2.00	111.7067	0.0828	2.5290	0.0627	-0.0539	0.0323	-0.0560	0.0263	0.0010	0.0009	-0.262	0.124	-0.097	0.038	44.006	1.125	99.71	143.3	3.5				
2.20	67.2760	0.1661	1.3800	0.0577	-0.0109	0.0311	-0.0783	0.0299	0.0148	0.0012	-0.670	0.259	-0.064	0.066	45.517	1.976	93.45	148.0	6.2				
2.40	27.7910	0.0646	0.6327	0.0613	-0.0006	0.0312	-0.0413	0.0257	0.0014	0.0009	-0.771	0.489	-0.039	0.146	43.218	4.313	98.49	140.8	13.5				
2.60	37.8932	0.0669	0.8432	0.0635	-0.0045	0.0304	-0.0112	0.0262	-0.0025	0.0008	-0.157	0.371	-0.049	0.106	45.783	3.548	101.94	148.8	11.1				
3.00	22.1092	0.0622	0.5416	0.0598	0.0175	0.0295	-0.0958	0.0265	-0.0006	0.0008	-2.091	0.629	0.059	0.161	41.016	4.668	100.61	133.9	14.7				
4.00	50.6050	0.0701	1.0502	0.0639	0.0248	0.0281	0.0653	0.0303	0.0003	0.0008	0.736	0.347	0.033	0.079	48.119	3.012	99.90	156.1	9.4				
<b>ALIQUOT 2</b>																							
0.50	822.4930	0.1391	21.3395	0.0645	0.2780	0.0321	0.0409	0.0285	0.2656	0.0026	0.022	0.016	-0.004	0.004	34.844	0.118	90.46	114.4	0.4				
0.80	2245.9130	0.2373	55.4174	0.0733	0.6702	0.0301	0.0754	0.0291	0.0786	0.0016	0.016	0.006	-0.001	0.002	40.082	0.061	98.97	130.9	0.2				
1.00	1776.6280	0.1631	42.5540	0.0712	0.5481	0.0299	0.0431	0.0263	0.0380	0.0015	0.012	0.007	0.001	0.002	41.459	0.077	99.37	135.3	0.2				
1.20	2210.0590	0.1874	52.3354	0.0653	0.7135	0.0292	0.0301	0.0280	0.0469	0.0016	0.006	0.006	0.004	0.002	41.937	0.061	99.37	136.8	0.2				
1.30	1909.7030	0.1988	44.1433	0.0654	-0.4479	0.0319	-0.0188	0.0252	0.0378	0.0013	0.005	0.007	-0.006	0.002	42.980	0.072	99.41	140.1	0.2				
1.40	5021.7390	0.3120	114.1496	0.0718	1.3893	0.0316	0.0406	0.0264	0.0897	0.0018	0.004	0.003	-0.001	0.001	43.732	0.040	99.47	142.4	0.1				
1.50	1395.0980	0.1543	32.5707	0.0617	0.3258	0.0296	0.0469	0.0292	0.0613	0.0016	0.017	0.011	-0.007	0.003	42.249	0.088	98.70	137.8	0.3				
1.60	491.6942	0.1020	11.8991	0.0616	0.1749	0.0293	0.0082	0.0279	0.0695	0.0015	0.008	0.028	0.004	0.007	39.569	0.216	95.82	129.3	0.7				
1.70	344.9511	0.0908	8.8423	0.0616	0.1184	0.0296	0.0172	0.0276	0.0892	0.0016	0.023	0.038	-0.002	0.010	36.007	0.266	92.36	118.1	0.8				
1.80	327.2842	0.0936	8.6889	0.0610	0.1581	0.0274	0.0516	0.0265	0.0930	0.0017	0.071	0.037	0.012	0.009	34.484	0.258	91.61	113.2	0.8				
2.00	419.3416	0.1119	11.5329	0.0613	0.1998	0.0295	0.0993	0.0282	0.1405	0.0021	0.103	0.030	0.008	0.008	32.745	0.190	90.11	107.7	0.6				
4.00	2401.6010	0.1852	70.8935	0.0693	0.9827	0.0311	1.0172	0.0273	0.5835	0.0041	0.171	0.005	0.000	0.001	31.432	0.044	92.84	103.5	0.1				
* Corrected for blank, mass discrimination, and radioactive decay																							
Sensitivity 6.312E-17 ± 1.047E-18 (mol/fAmp)																							



CASSIAR - quartz-carbonate-sericite vein, Taurus  
 T-95-35\_129.5m (sericite) - ALIQUOT 1

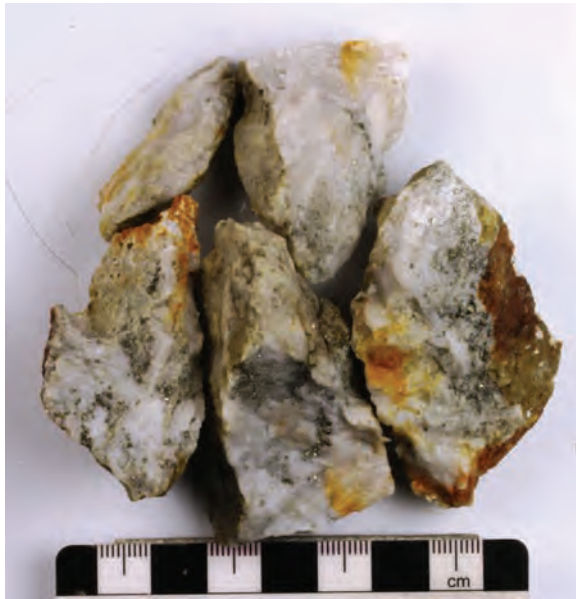


CASSIAR - quartz-carbonate-sericite vein, Taurus  
 T-95-35\_129.5m (sericite) - ALIQUOT 2



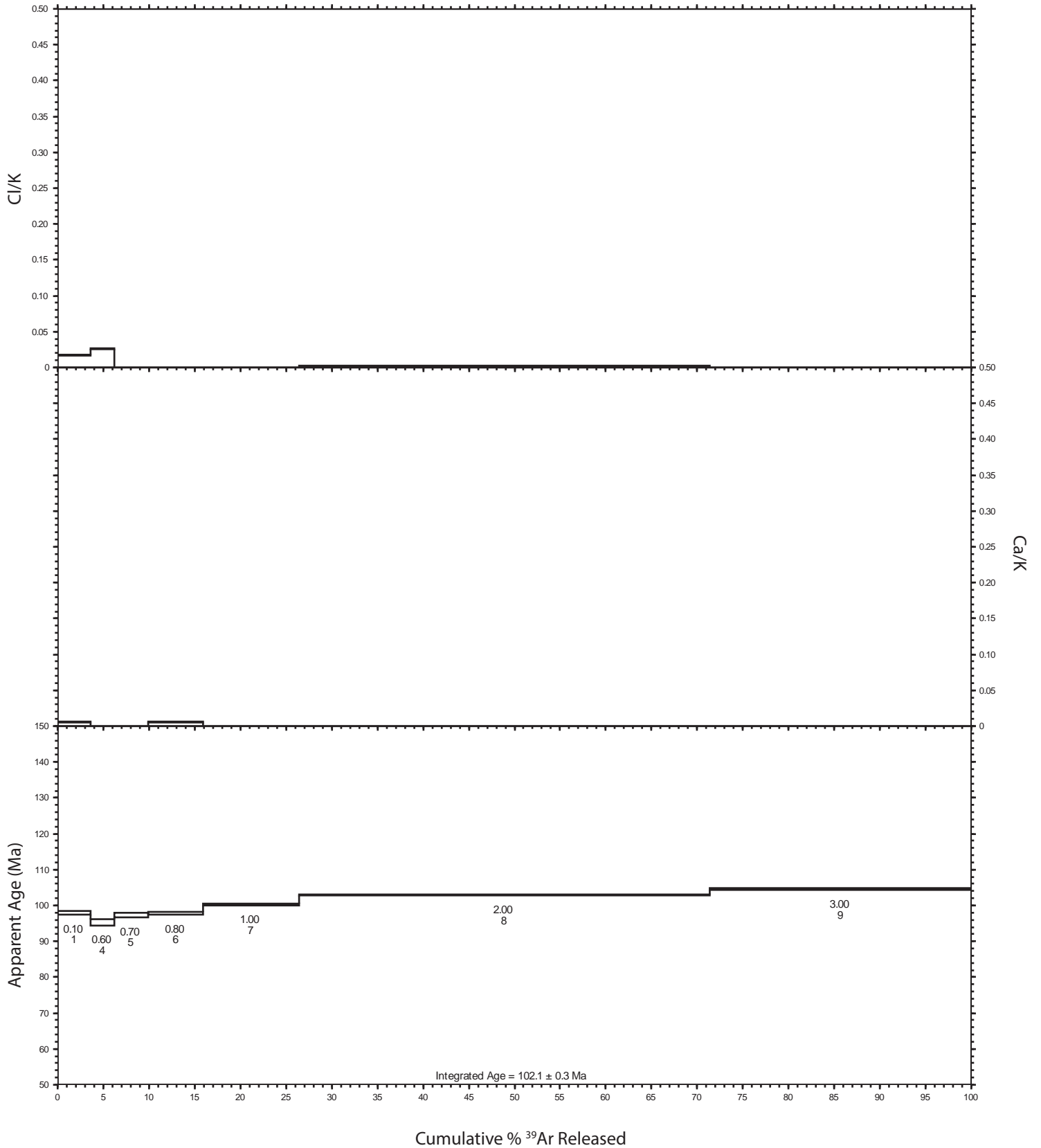
SHEEP CREEK - quartz-pyrite vein  
MA16-SH03 (sericite)

Sample	Mineral	J	$\pm (1\sigma)$	Relative Isotopic abundances (fAmps)*																
MA16-SH03	sericite	0.0018629	9.20E-07	auriferous quartz-pyrite vein with sericite seams, Nugget mine																
ALIQUOT 1				Relative Isotopic abundances (fAmps)*																
Power (%)	Ar40	$\pm (1\sigma)$	Ar39	$\pm (1\sigma)$	Ar38	$\pm (1\sigma)$	Ar37	$\pm (1\sigma)$	Ar36	$\pm (1\sigma)$	Ca/K	$\pm (1\sigma)$	Cl/K	$\pm (1\sigma)$	$^{40}\text{Ar}^*/^{39}\text{Ar}_{(K)}$	$\pm (1\sigma)$	$^{40}\text{Ar}^*$ (%)	Age (Ma)	$\pm (1\sigma)$	
0.10	315.7514	0.0988	10.4250	0.0616	0.1490	0.0311	0.0250	0.0266	0.0126	0.0009	0.018	0.019	0.005	0.009	29.916	0.188	98.82	97.8	0.6	
0.20	-0.1430	0.0641	-0.0265	0.0644	0.0504	0.0309	0.0166	0.0270	-0.0008	0.0007	-4.724	14.157	-5.566	14.378	-4.179	13.399	-77.52	-14.1	45.4	
0.40	33.3895	0.0693	1.2425	0.0652	0.0154	0.0294	0.0228	0.0271	-0.0031	0.0008	0.138	0.166	0.002	0.070	27.612	1.510	102.80	90.5	4.8	
0.60	220.0386	0.0805	7.5264	0.0651	0.0548	0.0300	0.0263	0.0288	0.0033	0.0008	0.026	0.029	-0.015	0.012	29.091	0.264	99.56	95.2	0.8	
0.70	316.3277	0.0921	10.6154	0.0623	0.1187	0.0296	-0.0242	0.0287	0.0026	0.0007	-0.018	0.021	-0.003	0.008	29.710	0.185	99.75	97.2	0.6	
0.80	513.0819	0.1078	17.1497	0.0681	0.2413	0.0297	-0.0518	0.0269	0.0009	0.0007	-0.023	0.012	0.005	0.005	29.886	0.128	99.95	97.7	0.4	
1.00	928.1574	0.1242	30.2272	0.0599	0.3294	0.0323	-0.0689	0.0278	0.0054	0.0009	-0.018	0.007	-0.004	0.003	30.637	0.073	99.83	100.1	0.2	
2.00	4049.6030	0.3275	128.4865	0.0897	1.5514	0.0293	0.0468	0.0278	0.0212	0.0013	0.002	0.002	0.000	0.001	31.453	0.044	99.85	102.7	0.1	
3.00	2917.5930	0.2829	81.9139	0.0716	1.1701	0.0324	-0.0515	0.0274	1.0034	0.0052	-0.005	0.003	-0.001	0.001	31.982	0.065	89.84	104.4	0.2	
ALIQUOT 2				Relative Isotopic abundances (fAmps)*																
0.60	1046.9500	0.1354	37.1572	0.0680	0.4437	0.0286	-0.0008	0.0255	0.0596	0.0015	-0.001	0.005	-0.002	0.002	27.688	0.061	98.32	90.7	0.2	
0.80	1483.7960	0.1718	50.7656	0.0703	0.6113	0.0316	-0.1218	0.0269	0.0160	0.0012	-0.019	0.004	-0.001	0.002	29.120	0.052	99.68	95.3	0.2	
1.00	2424.5750	0.1972	80.9830	0.0708	0.9377	0.0308	-0.0445	0.0284	0.0189	0.0012	-0.005	0.003	-0.002	0.001	29.855	0.041	99.77	97.6	0.1	
1.20	2955.8720	0.2273	97.4599	0.0765	1.1183	0.0328	0.0622	0.0278	0.0132	0.0012	0.004	0.002	-0.002	0.001	30.274	0.039	99.87	99.0	0.1	
1.40	2671.5450	0.2063	84.9485	0.0799	0.9791	0.0310	-0.0188	0.0285	0.0504	0.0016	-0.002	0.003	-0.002	0.001	31.258	0.045	99.44	102.1	0.1	
1.60	2463.5630	0.2068	77.9878	0.0740	0.9900	0.0299	0.0421	0.0277	0.1161	0.0018	0.004	0.003	0.001	0.001	31.134	0.045	98.61	101.7	0.1	
1.80	2873.9290	0.2138	88.5349	0.0687	1.0395	0.0332	-0.0270	0.0268	0.3169	0.0027	-0.003	0.002	-0.003	0.001	31.387	0.045	96.74	102.5	0.1	
2.00	4670.5300	0.2970	140.7549	0.0755	1.6940	0.0299	0.0429	0.0235	0.3734	0.0032	0.002	0.001	-0.002	0.001	32.382	0.040	97.64	105.7	0.1	
2.20	1078.5520	0.1407	29.5475	0.0680	0.3885	0.0338	0.0355	0.0265	0.2460	0.0025	0.009	0.007	-0.002	0.003	34.025	0.095	93.26	110.9	0.3	
2.50	547.3934	0.1204	14.6884	0.0609	0.1512	0.0315	0.1056	0.0265	0.1236	0.0020	0.054	0.014	-0.010	0.006	34.766	0.161	93.33	113.2	0.5	
3.00	414.3435	0.1007	11.2540	0.0618	0.1664	0.0295	0.0628	0.0281	0.0660	0.0015	0.042	0.019	0.004	0.008	35.069	0.207	95.30	114.2	0.7	
4.00	1483.6090	0.1428	41.6101	0.0655	0.4794	0.0316	0.0616	0.0269	0.0404	0.0012	0.011	0.005	-0.003	0.002	35.350	0.069	99.20	115.1	0.2	
* Corrected for blank, mass discrimination, and radioactive decay																				
Sensitivity				6.312E-17 $\pm$ 1.047E-18 (mol/fAmp)																

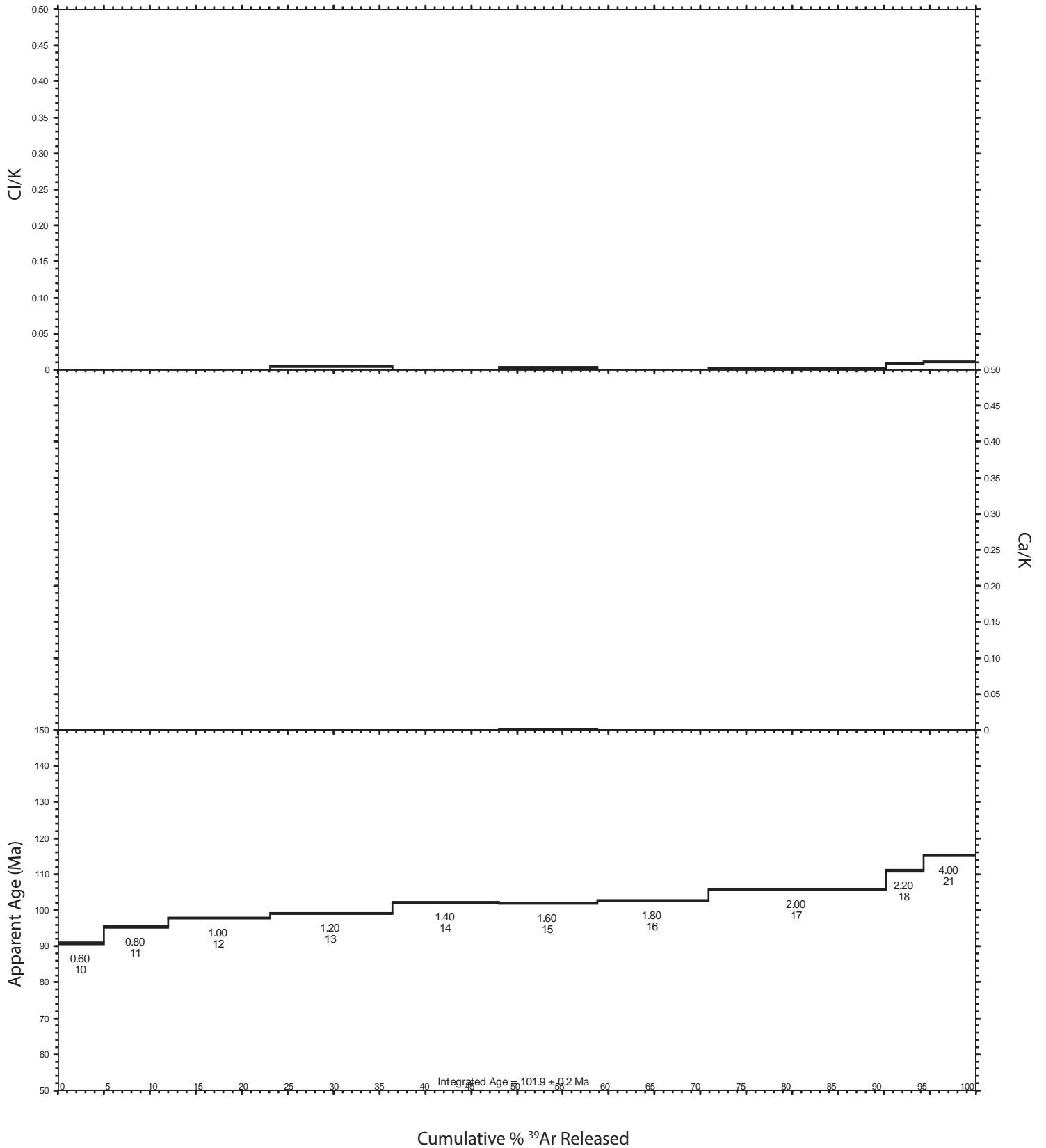




SHEEP CREEK - quartz-pyrite vein  
 MA16-SH03 (sericite) - ALIQUOT 1



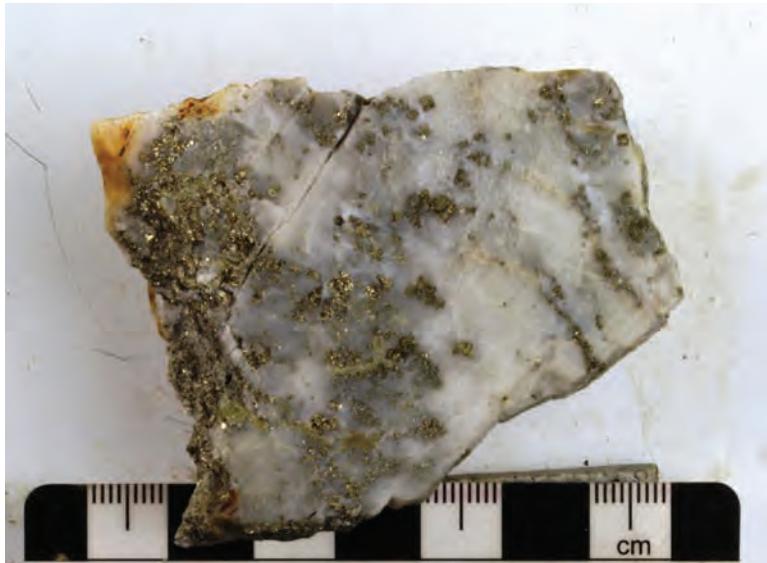
SHEEP CREEK - quartz-pyrite vein  
 MA16-SH03 (sericite) - ALIQUOT 2



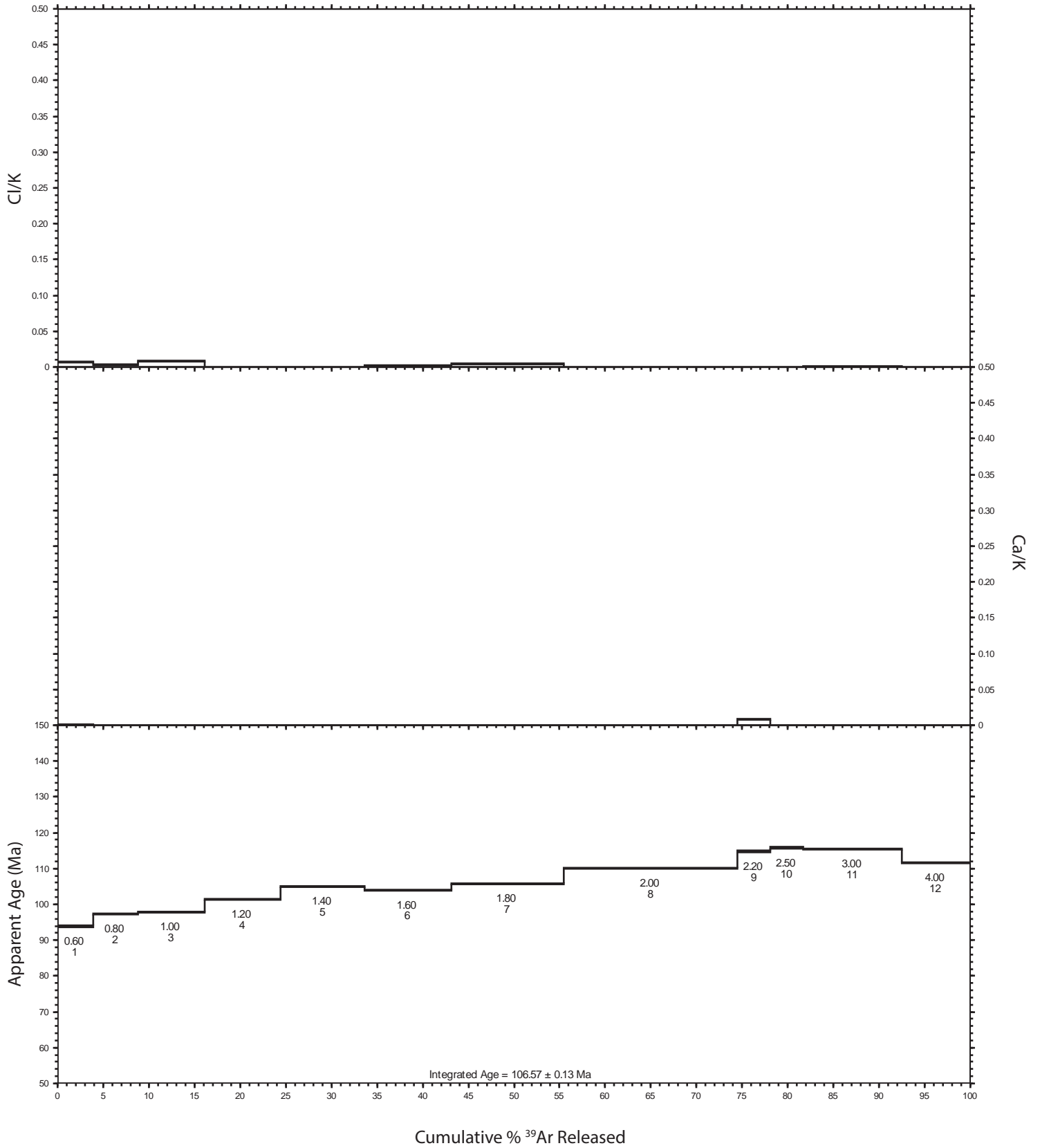
SHEEP CREEK - quartz-pyrite vein  
 MA16-SH05 (sericite)

Sample	Mineral	J	$\pm (1\sigma)$	Relative Isotopic abundances (fAmps)*																
MA16-SH05	sericite	0.0018453	9.80E-07	auriferous quartz-pyrite vein with sericite seams, Nugget mine																
ALIQUOT 1	Power (%)	Ar40	$\pm (1\sigma)$	Ar39	$\pm (1\sigma)$	Ar38	$\pm (1\sigma)$	Ar37	$\pm (1\sigma)$	Ar36	$\pm (1\sigma)$	Ca/K	$\pm (1\sigma)$	Cl/K	$\pm (1\sigma)$	$^{40}\text{Ar}^*/^{39}\text{Ar}_{(K)}$	$\pm (1\sigma)$	$^{40}\text{Ar}^*$ (%)	Age (Ma)	$\pm (1\sigma)$
	0.60	933.4342	0.1371	31.4527	0.0667	0.4025	0.0299	0.0311	0.0256	0.0805	0.0016	0.007	0.006	0.000	0.003	28.906	0.065	97.45	93.7	0.2
	0.80	1175.5280	0.1481	39.1511	0.0686	0.4705	0.0303	0.0179	0.0290	0.0049	0.0009	0.003	0.006	-0.001	0.002	29.973	0.055	99.88	97.1	0.2
	1.00	1767.0500	0.1563	58.5762	0.0758	0.6762	0.0288	0.0652	0.0292	0.0062	0.0010	0.008	0.004	-0.002	0.001	30.120	0.041	99.90	97.6	0.1
	1.20	2061.4500	0.6332	65.6806	0.0747	0.7548	0.0283	0.0003	0.0260	0.0131	0.0010	0.000	0.003	-0.002	0.001	31.311	0.038	99.81	101.3	0.1
	1.40	2385.9700	0.2045	73.4054	0.0737	0.8658	0.0318	-0.0031	0.0284	0.0171	0.0014	-0.001	0.003	-0.001	0.001	32.418	0.034	99.79	104.8	0.1
	1.60	2445.8860	0.1898	75.9083	0.0679	0.8872	0.0290	0.0246	0.0280	0.0180	0.0012	0.002	0.003	-0.002	0.001	32.135	0.030	99.78	103.9	0.1
	1.80	3206.3260	0.2301	97.9236	0.0704	1.1634	0.0279	0.0635	0.0270	0.0186	0.0011	0.005	0.002	-0.001	0.001	32.671	0.025	99.83	105.6	0.1
	2.00	5174.8340	0.2972	151.5511	0.0716	1.7700	0.0331	-0.0101	0.0280	0.0172	0.0012	-0.001	0.001	-0.002	0.001	34.095	0.017	99.90	110.1	0.1
	2.20	1024.8020	0.1326	28.7742	0.0628	0.4403	0.0286	-0.0697	0.0259	0.0037	0.0008	-0.019	0.007	0.009	0.003	35.559	0.081	99.89	114.7	0.3
	2.50	1043.6730	0.1467	28.9849	0.0643	0.2723	0.0330	-0.0207	0.0266	0.0104	0.0011	-0.006	0.007	-0.008	0.003	35.882	0.083	99.70	115.7	0.3
	3.00	3091.9480	0.1963	86.2474	0.0702	1.0384	0.0298	0.0165	0.0257	0.0255	0.0012	0.001	0.002	-0.001	0.001	35.744	0.030	99.76	115.2	0.1
	4.00	2052.3240	0.1855	59.0228	0.0636	0.6829	0.0307	-0.0187	0.0256	0.0441	0.0012	-0.003	0.003	-0.002	0.002	34.533	0.039	99.37	111.4	0.1

\* Corrected for blank, mass discrimination, and radioactive decay  
 Sensitivity 6.312E-17  $\pm$  1.047E-18 (mol/fAmp)



SHEEP CREEK - quartz-pyrite vein  
 MA16-SH05 (sericite)



# SHEEP CREEK - muscovite phyllite MA16-SH10 (muscovite)

Sample	Mineral	J	± (1σ)																
MA16-SH10	muscovite (pressed pellet)	0.001872	1.27E-06																
muscovite phyllite seam in quartzite and quartz gritstone, Three Sisters Fm.																			
ALIQUOT 1																			
Power (%)	Relative Isotopic abundances (fAmps)*										Ca/K	±	Cl/K	±	<sup>40</sup> Ar*/ <sup>39</sup> Ar <sub>(K)</sub>	±	<sup>40</sup> Ar* (%)	Age (Ma)	±
	Ar40	±	Ar39	±	Ar38	±	Ar37	±	Ar36	±									
0.50	840.8123	0.1084	28.4653	0.0626	0.4707	0.0303	0.0623	0.0261	0.3425	0.0030	0.015	0.006	0.006	0.003	25.971	0.070	87.97	85.6	0.2
0.70	946.7419	0.1395	32.0217	0.0638	0.4430	0.0316	0.0894	0.0247	0.2260	0.0027	0.019	0.005	0.001	0.003	27.468	0.065	92.95	90.5	0.2
0.90	2480.6460	0.1964	79.0535	0.0750	0.9592	0.0294	0.0862	0.0288	0.1775	0.0025	0.007	0.003	-0.001	0.001	30.701	0.036	97.89	100.8	0.1
1.00	2821.6360	0.2567	90.0509	0.0737	1.1023	0.0294	0.0801	0.0271	0.1084	0.0019	0.006	0.002	-0.001	0.001	30.963	0.032	98.87	101.7	0.1
1.10	2701.1680	0.2371	86.5577	0.0702	1.0246	0.0291	0.0895	0.0263	0.0887	0.0018	0.007	0.002	-0.002	0.001	30.889	0.032	99.03	101.4	0.1
1.20	2834.0510	0.2234	90.3197	0.0747	1.0777	0.0308	0.0789	0.0288	0.0667	0.0017	0.006	0.002	-0.001	0.001	31.145	0.032	99.30	102.2	0.1
1.30	2625.1690	0.1831	82.7824	0.0729	0.9701	0.0293	0.0472	0.0273	0.0781	0.0016	0.004	0.002	-0.002	0.001	31.418	0.034	99.12	103.1	0.1
1.40	2728.4050	0.2210	84.7164	0.0686	1.0199	0.0310	0.0749	0.0269	0.0762	0.0017	0.006	0.002	-0.001	0.001	31.926	0.033	99.18	104.7	0.1
1.50	2373.3120	0.2019	72.8226	0.0764	0.9249	0.0308	0.1976	0.0265	0.0783	0.0016	0.019	0.003	0.001	0.001	32.258	0.040	99.03	105.8	0.1
1.60	2079.9930	0.1829	63.0040	0.0647	0.7002	0.0282	0.1564	0.0283	0.0909	0.0017	0.017	0.003	-0.004	0.001	32.573	0.040	98.71	106.8	0.1
1.80	2382.6530	0.2076	70.6045	0.0679	0.8893	0.0279	0.1653	0.0284	0.1062	0.0018	0.016	0.003	0.000	0.001	33.287	0.039	98.68	109.1	0.1
2.00	1738.2120	0.1711	49.0981	0.0687	0.5799	0.0310	0.0949	0.0251	0.1098	0.0020	0.013	0.004	-0.002	0.002	34.726	0.055	98.13	113.6	0.2
2.50	926.3682	0.1326	24.2306	0.0616	0.2288	0.0274	0.1026	0.0304	0.0372	0.0013	0.030	0.009	-0.009	0.003	37.761	0.102	98.82	123.2	0.3
3.00	246.9612	0.0809	6.1034	0.0637	0.1184	0.0308	0.1087	0.0256	0.0036	0.0009	0.126	0.030	0.021	0.015	40.274	0.435	99.58	131.1	1.4
4.00	147.3821	0.0783	3.5959	0.0648	0.0209	0.0295	0.2276	0.0255	0.0066	0.0009	0.448	0.051	-0.020	0.024	40.450	0.754	98.72	131.7	2.4

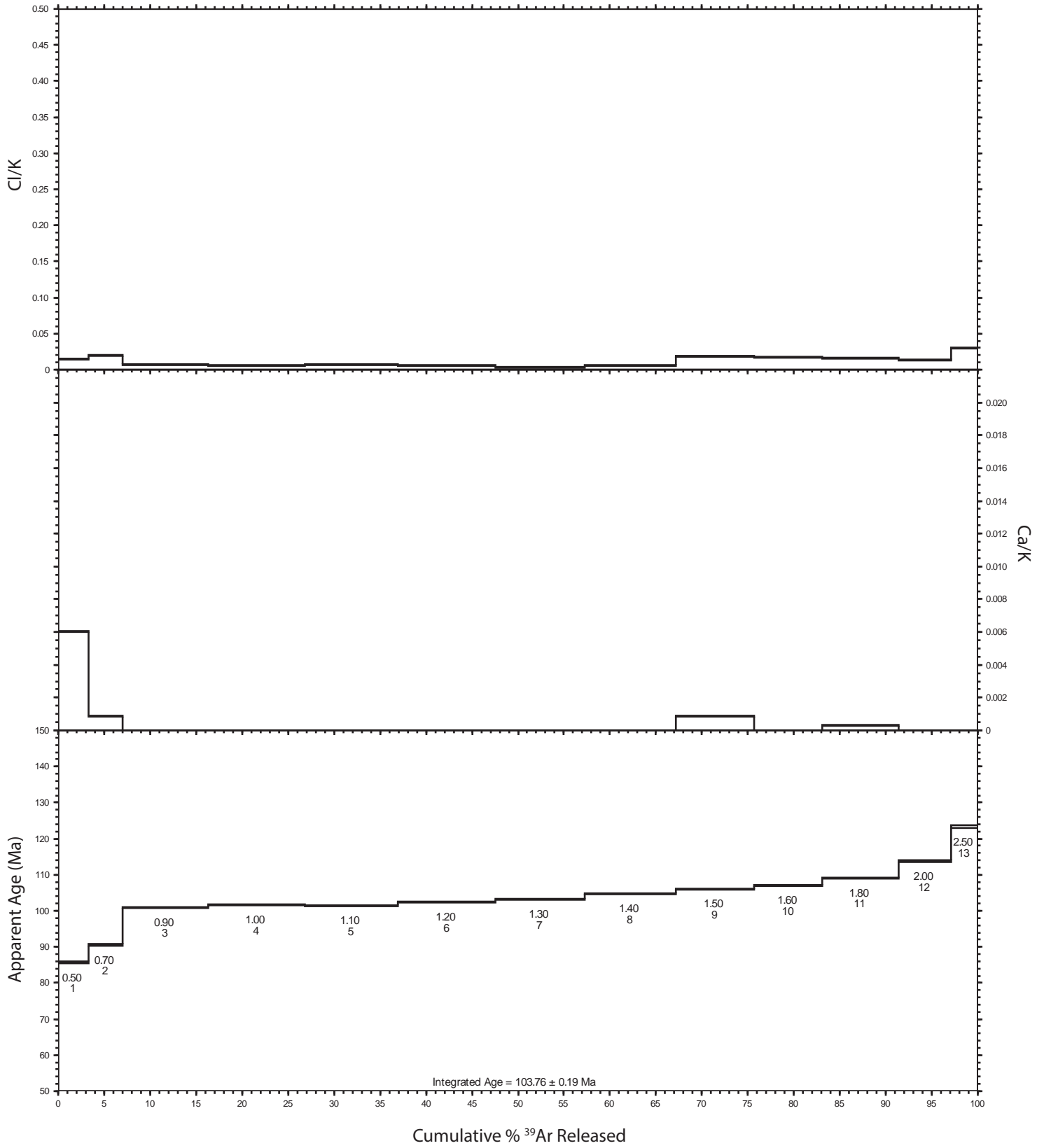
\* Corrected for blank, mass discrimination, and radioactive decay  
Sensitivity 6.312E-17 ± 1.047E-18 (mol/fAmp)

Sample	Mineral	J	± (1σ)																
MA16-SH10	muscovite	0.0018678	1.20E-06																
muscovite phyllite seam in quartzite and quartz gritstone, Three Sisters Fm.																			
ALIQUOT 1																			
Power (%)	Relative Isotopic abundances (fAmps)*										Ca/K	±	Cl/K	±	<sup>40</sup> Ar*/ <sup>39</sup> Ar <sub>(K)</sub>	±	<sup>40</sup> Ar* (%)	Age (Ma)	±
	Ar40	±	Ar39	±	Ar38	±	Ar37	±	Ar36	±									
0.50	229.3686	0.0909	9.7811	0.0657	0.1597	0.0300	0.0518	0.0288	0.0380	0.0011	0.036	0.020	0.010	0.009	22.293	0.161	95.11	73.6	0.5
0.70	460.3469	0.1067	17.1646	0.0662	0.2493	0.0301	0.0576	0.0285	0.0410	0.0012	0.022	0.011	0.005	0.005	26.102	0.110	97.37	85.9	0.4
0.90	1460.9240	0.1857	48.1943	0.0669	0.5632	0.0315	0.0583	0.0264	0.0058	0.0013	0.008	0.004	-0.002	0.002	30.264	0.054	99.88	99.2	0.2
1.00	1602.2520	0.1841	51.9424	0.0696	0.6433	0.0284	0.0495	0.0274	0.0137	0.0011	0.006	0.004	0.000	0.002	30.755	0.054	99.75	100.8	0.2
1.10	1627.3580	0.1795	52.8110	0.0718	0.6089	0.0299	0.0449	0.0256	0.0119	0.0011	0.005	0.003	-0.002	0.002	30.734	0.054	99.79	100.7	0.2
1.20	1894.9210	0.1951	60.4929	0.0647	0.7034	0.0297	0.0670	0.0269	0.0167	0.0013	0.007	0.003	-0.002	0.001	31.229	0.048	99.74	102.3	0.2
1.30	2402.0550	0.2113	75.6110	0.0760	0.8992	0.0316	0.0507	0.0282	0.0081	0.0010	0.004	0.003	-0.001	0.001	31.722	0.046	99.90	103.8	0.1
1.40	2582.1820	0.2079	80.9212	0.0677	0.9146	0.0325	0.1190	0.0264	0.0053	0.0011	0.010	0.002	-0.003	0.001	31.876	0.043	99.94	104.3	0.1
1.50	2554.3630	0.2292	79.8350	0.0671	0.9344	0.0313	0.0384	0.0289	0.0026	0.0011	0.003	0.003	-0.001	0.001	31.971	0.043	99.97	104.6	0.1
1.60	2847.2900	0.2230	89.0754	0.0655	0.9958	0.0300	0.0195	0.0262	0.0127	0.0011	0.001	0.002	-0.003	0.001	31.908	0.041	99.87	104.4	0.1
1.80	3225.6970	0.2301	100.5876	0.0728	1.1712	0.0283	0.0912	0.0270	0.0060	0.0011	0.006	0.002	-0.002	0.001	32.036	0.041	99.95	104.8	0.1
2.00	3076.0580	0.2164	95.0262	0.0687	1.0995	0.0327	-0.0735	0.0281	0.0026	0.0012	-0.006	0.002	-0.002	0.001	32.347	0.041	99.97	105.8	0.1
2.50	3069.7140	0.2079	91.8916	0.0669	1.0606	0.0293	0.2436	0.0277	0.0054	0.0010	0.018	0.002	-0.002	0.001	33.374	0.042	99.95	109.1	0.1
3.00	914.7061	0.1358	26.3146	0.0656	0.3080	0.0281	0.2123	0.0272	0.0034	0.0009	0.055	0.007	-0.002	0.003	34.709	0.097	99.90	113.3	0.3
4.00	298.3539	0.1017	8.5959	0.0649	0.0446	0.0304	0.3307	0.0291	0.0086	0.0009	0.264	0.024	-0.021	0.010	34.411	0.273	99.18	112.4	0.9
ALIQUOT 2																			
0.50	149.3069	0.0835	6.0638	0.0609	0.0854	0.0323	-0.0249	0.0268	0.0185	0.0010	-0.029	0.031	0.004	0.016	23.707	0.252	96.33	78.2	0.8
0.70	318.1191	0.0904	12.0920	0.0671	0.1617	0.0303	0.0163	0.0278	0.0193	0.0011	0.009	0.016	0.003	0.007	25.826	0.153	98.21	85.0	0.5
0.90	1006.7310	0.1300	33.1005	0.0680	0.4135	0.0313	0.0008	0.0267	-0.0006	0.0011	0.000	0.006	0.001	0.003	30.405	0.073	100.02	99.7	0.2
1.00	1096.3420	0.1299	35.5032	0.0707	0.4300	0.0280	0.0585	0.0298	0.0159	0.0010	0.011	0.005	-0.001	0.002	30.734	0.072	99.57	100.7	0.2
1.10	1214.7390	0.1516	39.0701	0.0659	0.5011	0.0300	0.0561	0.0252	0.0087	0.0010	0.010	0.006	0.002	0.002	31.011	0.064	99.79	101.6	0.2
1.20	1224.5990	0.1614	39.5170	0.0634	0.4045	0.0293	0.0698	0.0257	0.0086	0.0010	0.012	0.005	-0.006	0.002	30.910	0.061	99.79	101.3	0.2
1.30	1236.0590	0.1620	39.9298	0.0672	0.4972	0.0325	0.0861	0.0266	0.0083	0.0010	0.015	0.005	0.001	0.002	30.881	0.063	99.80	101.2	0.2
1.40	1701.6970	0.1843	53.3410	0.0705	0.6125	0.0315	0.0284	0.0256	0.0038	0.0010	0.003	0.003	-0.002	0.002	31.866	0.055	99.93	104.3	0.2
1.50	2088.0320	0.1934	63.9310	0.0741	0.7474	0.0297	0.0735	0.0279	0.0073	0.0010	0.008	0.003	-0.002	0.001	32.612	0.052	99.90	106.7	0.2
1.60	2219.7590	0.1955	68.4185	0.0692	0.8348	0.0297	0.0964	0.0266	0.0190	0.0011	0.009	0.003	0.000	0.001	32.347	0.048	99.75	105.8	0.2
1.80	2908.3070	0.2198	89.8238	0.0761	1.0139	0.0322	0.1089	0.0277	0.0126	0.0011	0.008	0.002	-0.003	0.001	32.322	0.044	99.87	105.7	0.1
2.00	3332.6130	0.2132	103.0754	0.0730	1.2201	0.0276	0.1549	0.0274	0.0080	0.0011	0.010	0.002	-0.001	0.001	32.294	0.041	99.93	105.7	0.1
2.50	5154.5750	0.3210	157.1143	0.0752	1.9607	0.0275	0.3952	0.0272	0.0146	0.0011	0.017	0.001	0.001	0.001	32.766	0.038	99.92	107.2	0.1
3.00	1994.6700	0.1925	56.5574	0.0684	0.6255	0.0303	0.1665	0.0262	0.0019	0.0010	0.020	0.003	-0.003	0.002	35.243	0.058	99.97	115.0	0.2
4.00	853.6039	0.1251	16.6281	0.0627	0.3988	0.0300	0.3087	0.0280	0.9421	0.0047	0.129	0.012	0.003	0.005	34.582	0.191	67.39	112.9	0.6

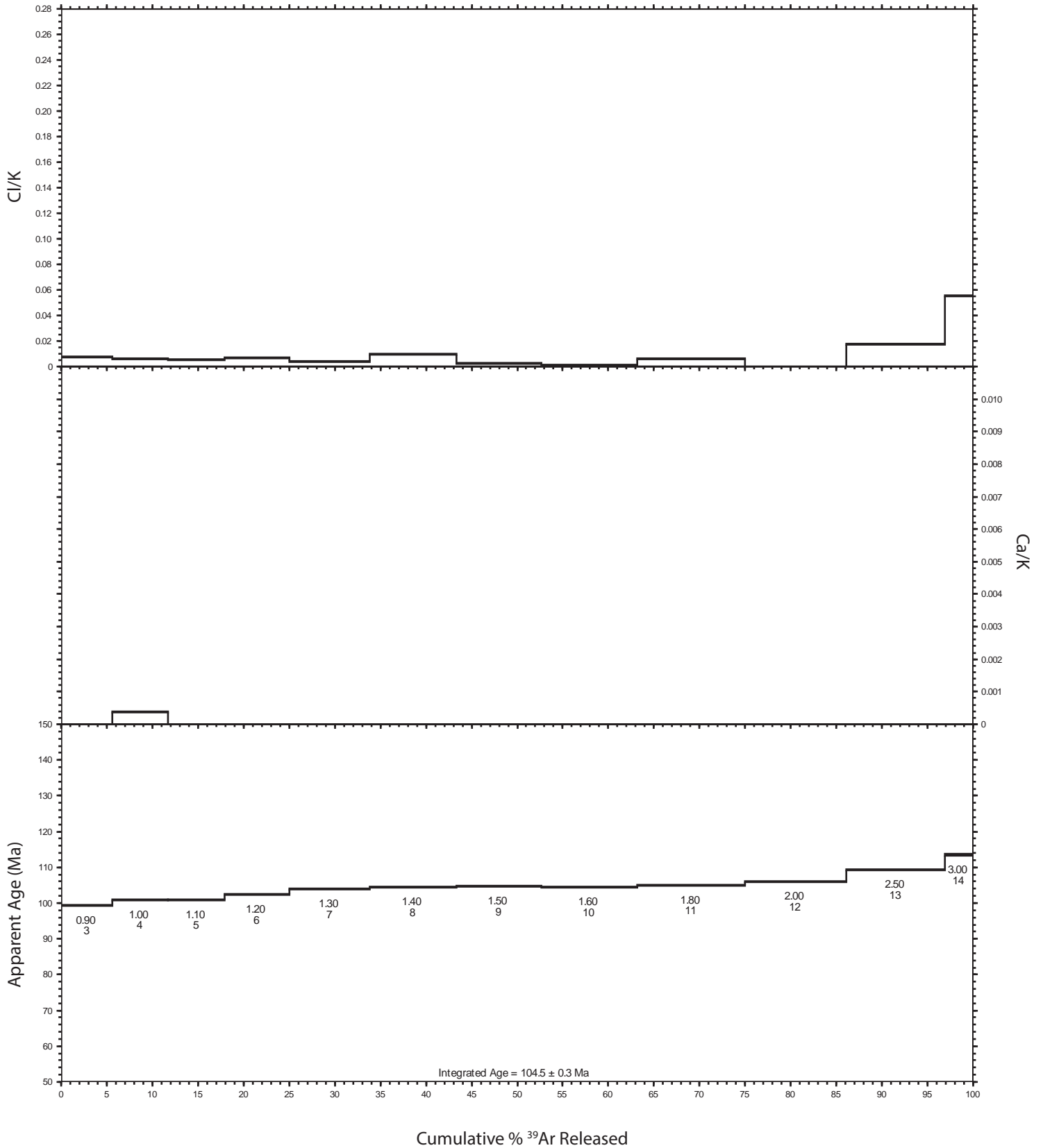
\* Corrected for blank, mass discrimination, and radioactive decay  
Sensitivity 6.312E-17 ± 1.047E-18 (mol/fAmp)



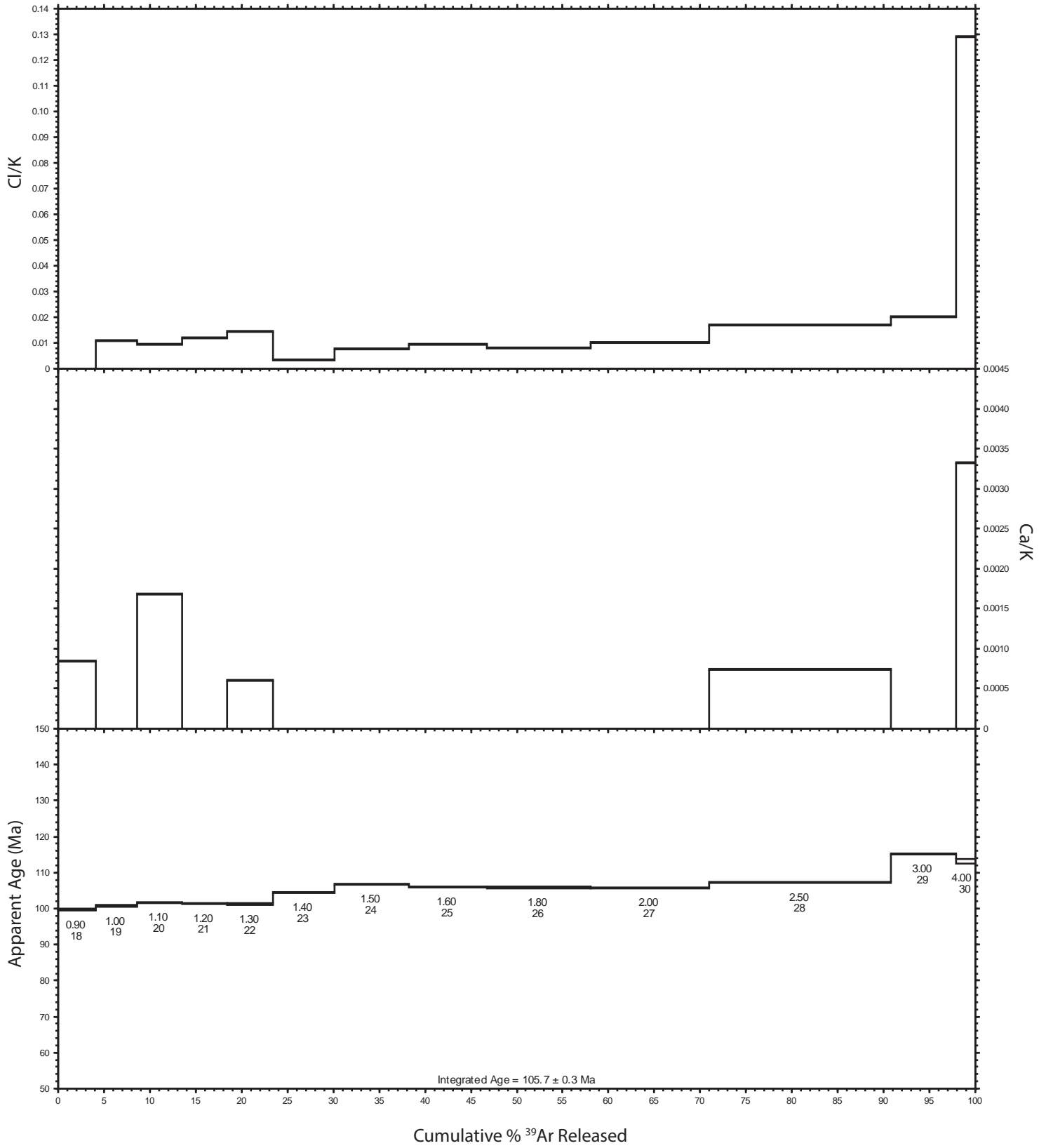
SHEEP CREEK - muscovite phyllite  
 MA16-SH10 (muscovite) - PRESSED PELLET



SHEEP CREEK - muscovite phyllite  
 MA16-SH10 (muscovite) - ALIQUOT 1



SHEEP CREEK - muscovite phyllite  
 MA16-SH10 (muscovite) -ALIQUOT 2



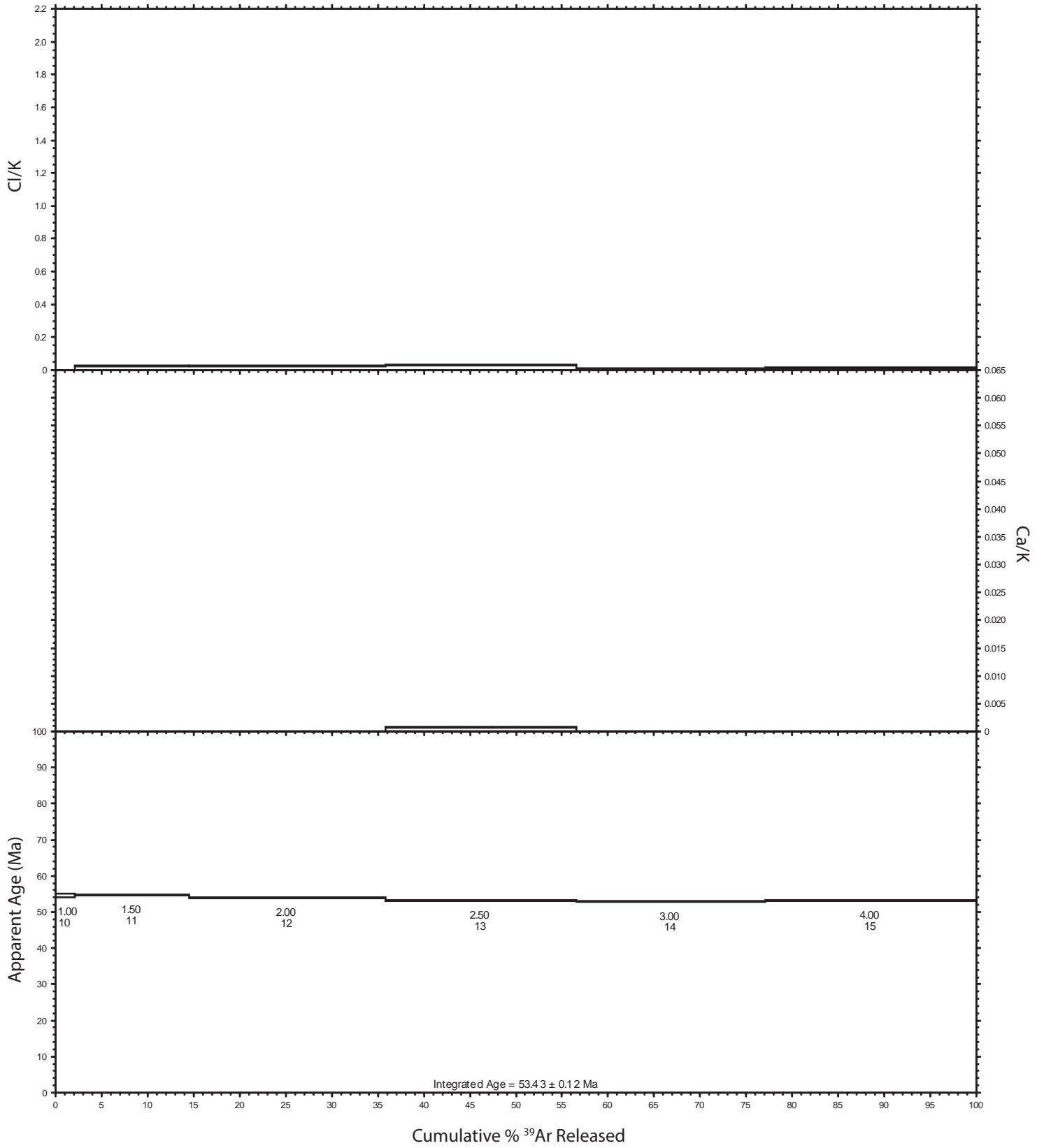
SHEEP CREEK - lamprophyre dike  
 MA16-SH13 (biotite)

Sample	Mineral	J	± (1σ)	Relative Isotopic abundances (fAmps)*															
MA16-SH13	biotite	0.001875	1.20E-06																
biotite-olivine lamprophyre dike cutting Sheep Creek stock																			
GRAIN 1	Relative Isotopic abundances (fAmps)*										Ca/K	±	Cl/K	±	<sup>40</sup> Ar* / <sup>39</sup> Ar(K)	±	<sup>40</sup> Ar*	Age	±
Power (%)	Ar40	± (1σ)	Ar39	± (1σ)	Ar38	± (1σ)	Ar37	± (1σ)	Ar36	± (1σ)	± (1σ)	± (1σ)	± (1σ)						
0.10	88.0039	0.0736	2.1548	0.0612	0.0181	0.0315	0.2227	0.0282	0.2019	0.0021	0.753	0.099	-0.062	0.043	13.181	0.493	32.28	44.0	1.6
0.40	4.4584	0.0645	0.3292	0.0645	-0.0236	0.0288	0.0938	0.0267	0.0071	0.0009	2.082	0.732	-0.255	0.264	7.295	1.675	53.85	24.5	5.6
0.50	14.2237	0.0610	0.8311	0.0655	0.0081	0.0312	0.2223	0.0272	0.0237	0.0012	1.957	0.289	-0.023	0.111	8.779	0.830	51.28	29.5	2.8
0.70	64.9006	0.0773	1.3115	0.0635	0.0024	0.0287	0.2307	0.0277	0.1685	0.0022	1.288	0.169	-0.100	0.065	11.565	0.765	23.37	38.7	2.5
0.80	362.6791	0.0957	2.1576	0.0590	0.2817	0.0296	0.1009	0.0269	1.1474	0.0053	0.342	0.093	0.054	0.041	10.960	0.893	6.52	36.7	3.0
0.90	130.8259	0.0687	4.0757	0.0647	0.0714	0.0310	0.0865	0.0279	0.2366	0.0024	0.155	0.051	-0.016	0.023	14.943	0.305	46.57	49.9	1.0
1.00	235.4245	0.0799	9.5187	0.0644	0.1189	0.0281	-0.0123	0.0286	0.2698	0.0027	-0.010	0.022	-0.015	0.009	16.347	0.147	66.13	54.5	0.5
1.50	1046.6390	0.1576	55.5641	0.0668	0.6975	0.0292	0.1896	0.0270	0.4532	0.0033	0.025	0.004	-0.003	0.002	16.419	0.032	87.21	54.7	0.1
2.00	1605.9150	0.1563	94.8735	0.0698	1.1932	0.0321	0.3638	0.0277	0.2528	0.0026	0.028	0.002	0.000	0.001	16.132	0.020	95.35	53.8	0.1
2.50	1497.6750	0.1688	92.4411	0.0766	1.1702	0.0272	0.3751	0.0265	0.0901	0.0019	0.029	0.002	0.001	0.001	15.906	0.019	98.23	53.0	0.1
3.00	1470.4830	0.1856	91.4427	0.0649	1.0784	0.0300	0.0919	0.0270	0.0532	0.0015	0.007	0.002	-0.002	0.001	15.901	0.017	98.93	53.0	0.1
4.00	1643.1000	0.1678	102.1438	0.0699	1.2270	0.0322	0.2253	0.0280	0.0540	0.0014	0.016	0.002	-0.001	0.001	15.922	0.017	99.03	53.1	0.1

\* Corrected for blank, mass discrimination, and radioactive decay  
 Sensitivity 6.312E-17 ± 1.047E-18 (mol/fAmp)



SHEEP CREEK - lamprophyre dike  
MA16-SH13 (biotite)



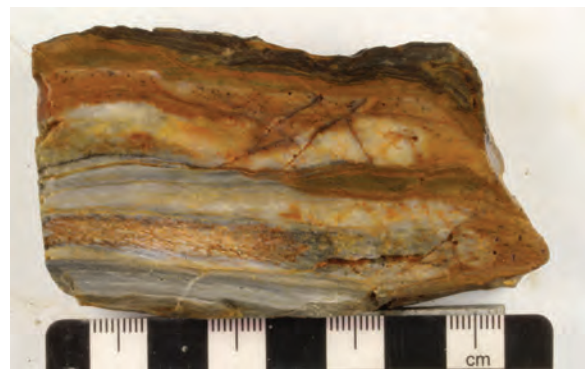
SHEEP CREEK - phyllite near Nugget/Fawn mines  
 MA16-SH14 (muscovite) - pressed pellet

Sample	Mineral	J	± (1σ)																
MA16-SH14	muscovite (pressed pellet)	0.0018518	8.91E-07																
muscovite phyllite cut by fibrous quartz veinlets																			
GRAIN 1																			
Relative Isotopic abundances (fAmps)*																			
Power (%)	Ar40	± (1σ)	Ar39	± (1σ)	Ar38	± (1σ)	Ar37	± (1σ)	Ar36	± (1σ)	Ca/K	± (1σ)	Cl/K	± (1σ)	<sup>40</sup> Ar*/ <sup>39</sup> Ar(K)	± (1σ)	<sup>40</sup> Ar* (%)	Age (Ma)	± (1σ)
0.50	722.7050	0.1275	22.1550	0.0662	0.2863	0.0319	0.2273	0.0269	0.2310	0.0024	0.066	0.008	-0.004	0.004	29.529	0.103	90.56	96.0	0.3
0.80	2306.9570	0.1813	71.1470	0.0738	0.9698	0.0286	1.1985	0.0283	0.3378	0.0030	0.108	0.003	0.002	0.001	31.014	0.047	95.69	100.7	0.1
1.00	2947.3310	0.2413	92.6434	0.0707	1.1526	0.0292	1.3702	0.0259	0.2154	0.0025	0.095	0.002	-0.001	0.001	31.117	0.039	97.85	101.1	0.1
1.20	3254.7520	0.2727	102.9615	0.0773	1.3393	0.0304	0.9509	0.0283	0.1526	0.0025	0.059	0.002	0.002	0.001	31.162	0.038	98.62	101.2	0.1
1.40	3098.4500	0.2036	98.4310	0.1103	1.2326	0.0350	0.8528	0.0297	0.1437	0.0029	0.056	0.002	0.000	0.001	31.036	0.046	98.64	100.8	0.1
1.60	2263.6180	0.1696	70.9773	0.0994	0.9382	0.0338	0.2738	0.0289	0.1071	0.0028	0.025	0.003	0.002	0.001	31.433	0.055	98.60	102.1	0.2
1.80	1012.1600	0.1381	29.9715	0.0619	0.3777	0.0308	0.1161	0.0263	0.0508	0.0016	0.025	0.006	0.000	0.003	33.256	0.079	98.52	107.8	0.2
2.00	724.5780	0.1341	20.2980	0.0656	0.1916	0.0310	0.0522	0.0263	0.0121	0.0017	0.017	0.009	-0.008	0.005	35.505	0.125	99.51	114.9	0.4
2.50	324.5461	0.0929	7.5859	0.0655	0.0573	0.0314	-0.0375	0.0281	0.0047	0.0011	-0.033	0.025	-0.014	0.012	42.579	0.384	99.57	136.9	1.2
2.75	69.7289	0.0741	1.7322	0.0630	0.0337	0.0292	0.0027	0.0277	0.0041	0.0009	0.010	0.107	0.020	0.050	39.539	1.495	98.27	127.5	4.7
3.00	36.2898	0.0672	0.9250	0.0640	0.0424	0.0312	-0.0125	0.0272	0.0029	0.0009	-0.090	0.198	0.096	0.100	38.281	2.752	97.62	123.6	8.6

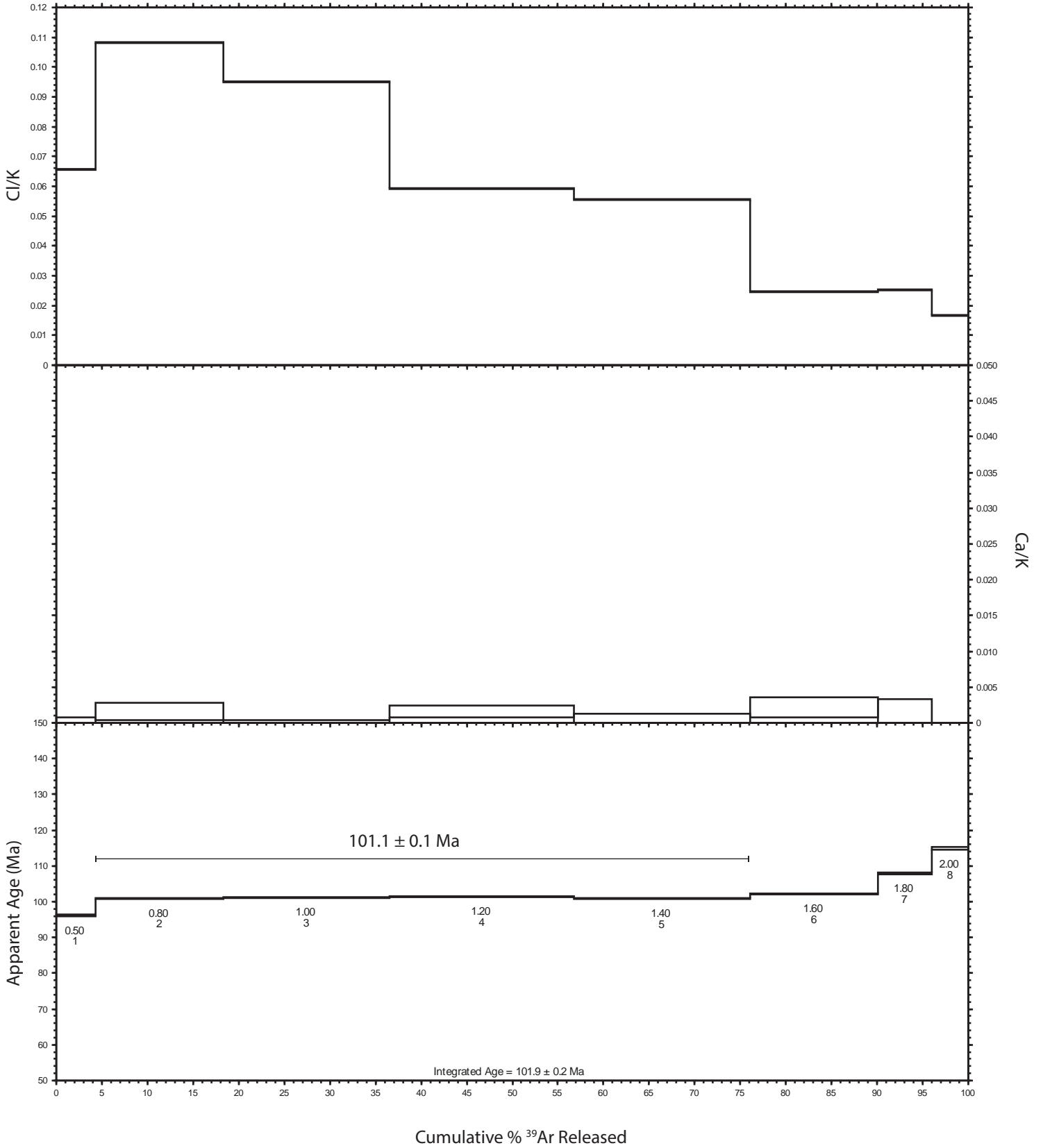
\* Corrected for blank, mass discrimination, and radioactive decay  
 Sensitivity 6.312E-17 ± 1.047E-18 (mol/fAmp)

Sample	Mineral	J	± (1σ)																
MA16-SH14	muscovite	0.0018708	1.10E-06																
muscovite phyllite cut by fibrous quartz veinlets																			
ALIQUOT 1																			
Relative Isotopic abundances (fAmps)*																			
Power (%)	Ar40	± (1σ)	Ar39	± (1σ)	Ar38	± (1σ)	Ar37	± (1σ)	Ar36	± (1σ)	Ca/K	± (1σ)	Cl/K	± (1σ)	<sup>40</sup> Ar*/ <sup>39</sup> Ar(K)	± (1σ)	<sup>40</sup> Ar* (%)	Age (Ma)	± (1σ)
0.50	567.7758	0.1075	22.5717	0.0625	0.3399	0.0304	0.0451	0.0290	0.0314	0.0011	0.014	0.009	0.008	0.004	24.732	0.075	98.37	81.6	0.2
0.70	932.8688	0.1314	30.7525	0.0597	0.3368	0.0286	-0.0056	0.0277	0.0164	0.0009	-0.002	0.006	-0.004	0.003	30.162	0.065	99.48	99.0	0.2
0.90	1817.7990	0.1686	59.2595	0.0733	0.6743	0.0320	-0.0491	0.0257	0.0135	0.0010	-0.006	0.003	-0.003	0.002	30.593	0.046	99.78	100.4	0.1
1.00	1870.9820	0.1927	60.2879	0.0670	0.7869	0.0320	0.0297	0.0287	0.0167	0.0011	0.003	0.003	0.002	0.002	30.937	0.043	99.74	101.5	0.1
1.10	1989.0350	0.1880	64.1854	0.0750	0.7199	0.0299	0.0602	0.0266	0.0115	0.0011	0.006	0.003	-0.003	0.001	30.921	0.044	99.83	101.5	0.1
1.20	2046.7540	0.2045	66.0297	0.0704	0.8384	0.0328	0.0000	0.0283	0.0099	0.0012	0.000	0.003	0.001	0.001	30.938	0.042	99.86	101.5	0.1
1.30	2144.4160	0.2097	69.1560	0.0690	0.8214	0.0308	0.0496	0.0265	-0.0036	0.0012	0.005	0.003	-0.001	0.001	31.009	0.040	100.05	101.7	0.1
1.40	2264.1840	0.1837	72.6609	0.0793	0.8642	0.0335	0.0732	0.0253	0.0262	0.0012	0.007	0.003	-0.001	0.001	31.040	0.043	99.66	101.8	0.1
1.50	2370.5100	0.2378	76.4476	0.0663	0.8921	0.0304	0.0402	0.0279	0.0077	0.0011	0.003	0.003	-0.002	0.001	30.964	0.037	99.90	101.6	0.1
1.60	2476.3750	0.1969	79.4529	0.0701	0.9496	0.0301	-0.0573	0.0275	0.0128	0.0011	-0.006	0.002	-0.001	0.001	31.105	0.037	99.85	102.0	0.1
1.80	3253.4830	0.2722	103.9711	0.0735	1.2462	0.0316	0.0712	0.0254	0.0098	0.0012	0.004	0.002	-0.001	0.001	31.249	0.033	99.91	102.5	0.1
2.00	4383.3270	0.2520	137.5905	0.0725	1.6955	0.0301	-0.0975	0.0286	0.0203	0.0012	-0.006	0.002	0.000	0.001	31.798	0.030	99.86	104.2	0.1
2.50	5118.6970	0.2702	150.0732	0.0717	1.7738	0.0304	0.0038	0.0285	0.0355	0.0014	0.000	0.001	-0.001	0.001	34.021	0.031	99.79	111.3	0.1
3.00	904.2433	0.1194	26.6393	0.0642	0.3669	0.0284	-0.0835	0.0271	0.0099	0.0010	-0.023	0.007	0.004	0.003	33.817	0.089	99.68	110.7	0.3
4.00	530.1878	0.1046	15.9490	0.0610	0.2010	0.0308	-0.0871	0.0279	0.0106	0.0009	-0.040	0.013	0.001	0.006	33.028	0.134	99.40	108.2	0.4

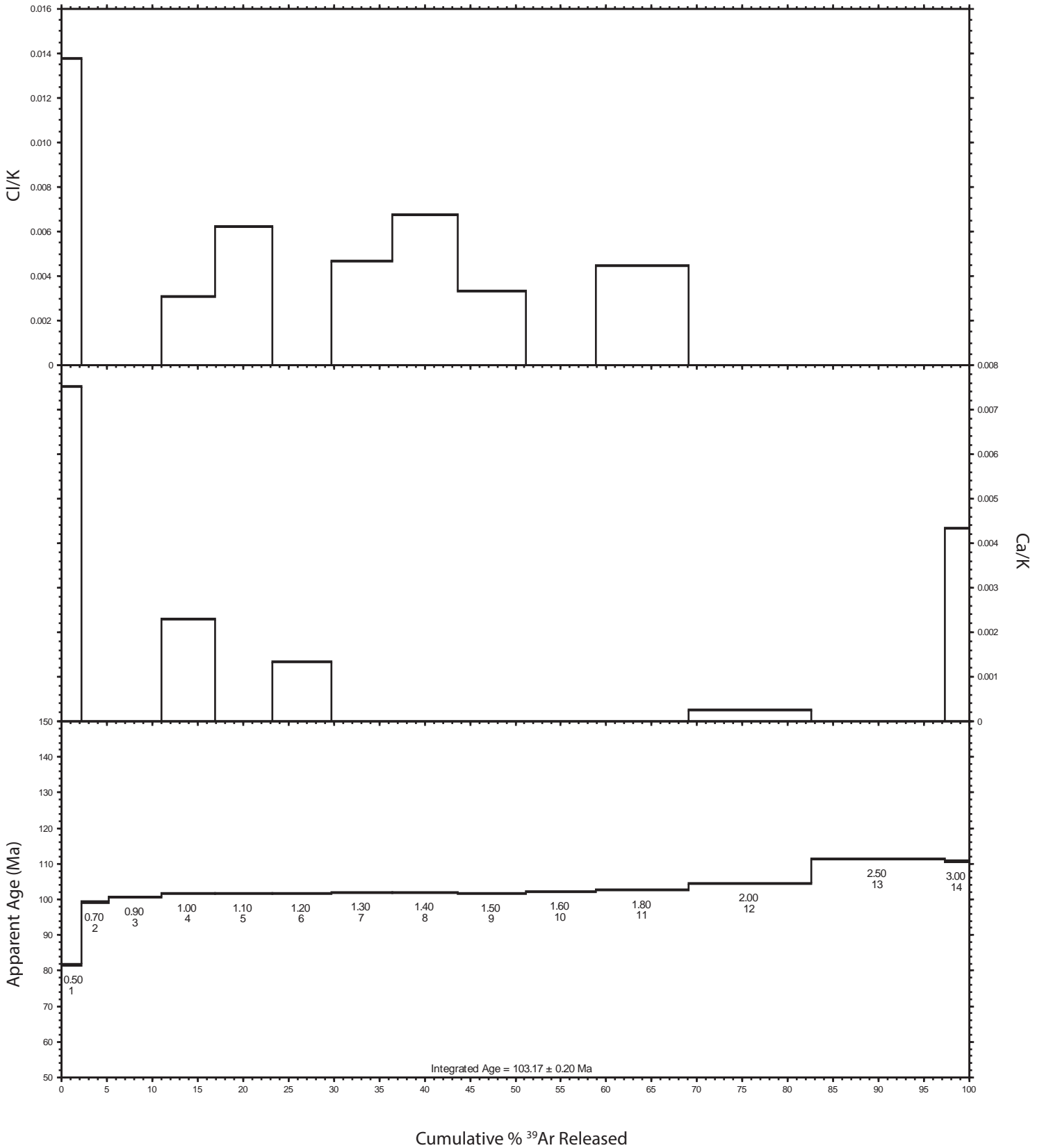
\* Corrected for blank, mass discrimination, and radioactive decay  
 Sensitivity 6.312E-17 ± 1.047E-18 (mol/fAmp)



SHEEP CREEK - phyllite near Nugget/Fawn mines  
 MA16-SH14 (muscovite) - pressed pellet



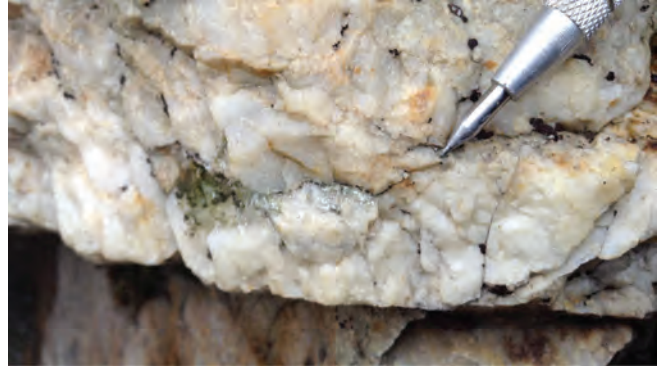
SHEEP CREEK - phyllite near Nugget/Fawn mines  
 MA16-SH14 (muscovite)



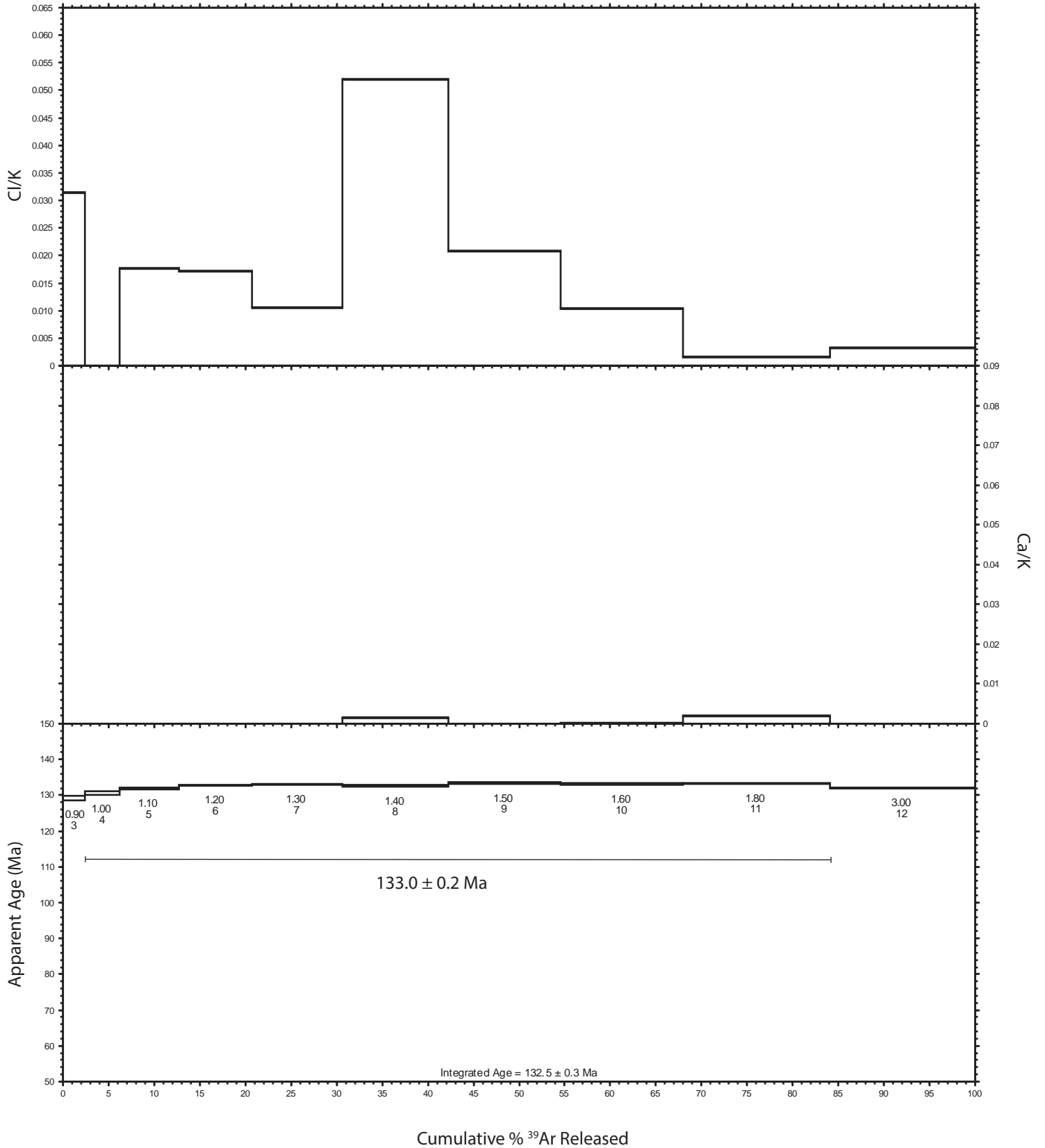
SHEEP CREEK - quartz-muscovite vein in Hamill Gp. quartzite  
 MA16-SH24 (muscovite)

Sample	Mineral	J	± (1σ)	Relative Isotopic abundances (fAmps)*																
GRAIN 1		Ar40	± (1σ)	Ar39	± (1σ)	Ar38	± (1σ)	Ar37	± (1σ)	Ar36	± (1σ)	Ca/K	± (1σ)	Cl/K	± (1σ)	<sup>40</sup> Ar*/ <sup>39</sup> Ar <sub>(K)</sub>	± (1σ)	<sup>40</sup> Ar*	Age	± (1σ)
Power (%)																		(%)	(Ma)	
MA16-SH24	muscovite (pressed pellet)	0.0018665	1.10E-06	quartz-muscovite vein cutting quartzite, Hammill Gp.																
0.50		7.0317	0.0685	0.2039	0.0595	-0.0258	0.0297	-0.0111	0.0259	-0.0001	0.0010	-0.365	0.865	-0.402	0.448	34.526	10.487	100.19	112.7	33.2
0.70		64.6053	0.0681	1.8745	0.0601	0.0669	0.0295	-0.0304	0.0256	-0.0036	0.0009	-0.109	0.093	0.069	0.047	35.011	1.166	101.63	114.2	3.7
0.90		508.7651	0.1033	12.6099	0.0670	0.1147	0.0281	0.0599	0.0304	0.0250	0.0012	0.031	0.016	-0.010	0.007	39.744	0.222	98.55	129.1	0.7
1.00		797.5451	0.1284	19.7393	0.0667	0.1903	0.0296	-0.0087	0.0275	0.0126	0.0010	-0.003	0.009	-0.008	0.004	40.196	0.145	99.53	130.5	0.5
1.10		1354.9880	0.1428	33.1698	0.0666	0.4049	0.0284	0.0893	0.0278	0.0235	0.0013	0.018	0.006	0.000	0.003	40.623	0.091	99.49	131.9	0.3
1.20		1696.2420	0.1925	41.3082	0.0707	0.4726	0.0292	0.1077	0.0292	0.0231	0.0011	0.017	0.005	-0.003	0.002	40.880	0.080	99.60	132.7	0.2
1.30		2103.9280	0.1884	51.1979	0.0648	0.5846	0.0315	0.0830	0.0266	0.0217	0.0012	0.010	0.004	-0.003	0.002	40.950	0.063	99.70	132.9	0.2
1.40		2449.5790	0.1986	59.6071	0.0700	0.7687	0.0308	0.4626	0.0258	0.0482	0.0013	0.052	0.003	0.002	0.002	40.840	0.060	99.42	132.5	0.2
1.50		2618.1930	0.2297	63.5611	0.0688	0.7263	0.0310	0.1992	0.0286	0.0197	0.0012	0.021	0.003	-0.002	0.001	41.082	0.056	99.78	133.3	0.2
1.60		2804.3970	0.2177	68.7643	0.0752	0.8309	0.0333	0.1102	0.0270	-0.0555	0.0019	0.010	0.003	0.000	0.001	41.003	0.056	100.59	133.0	0.2
1.80		3423.7150	0.2535	83.2274	0.0681	1.0758	0.0291	0.0249	0.0273	0.0212	0.0014	0.002	0.002	0.002	0.001	41.043	0.048	99.82	133.2	0.1
3.00		3324.8880	0.2187	81.3873	0.0638	0.9810	0.0313	0.0449	0.0285	0.0625	0.0015	0.003	0.002	-0.001	0.001	40.607	0.046	99.44	131.8	0.1

\* Corrected for blank, mass discrimination, and radioactive decay  
 Sensitivity 6.312E-17 ± 1.047E-18 (mol/fAmp)



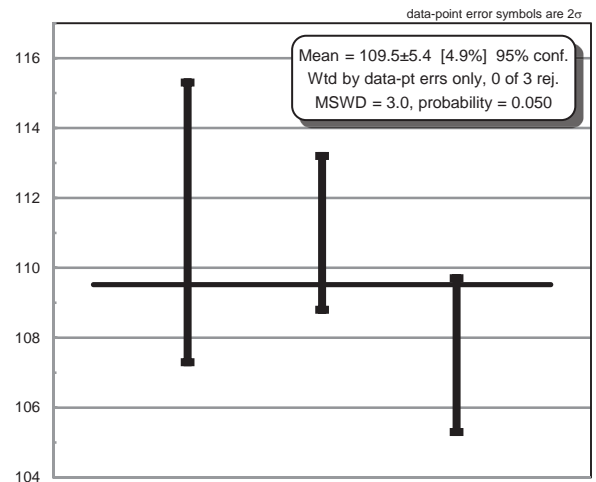
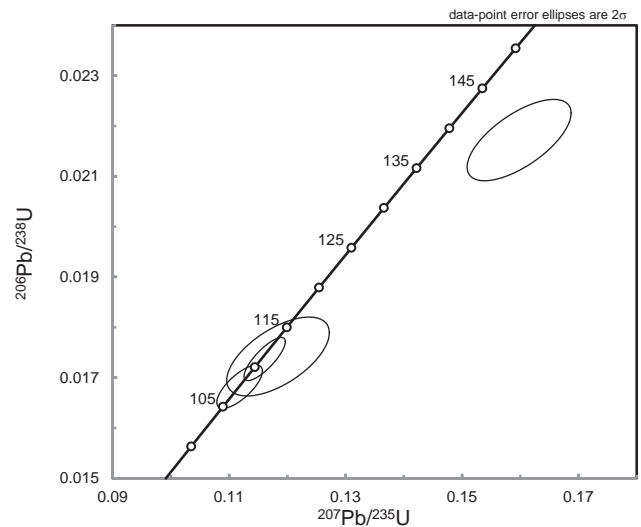
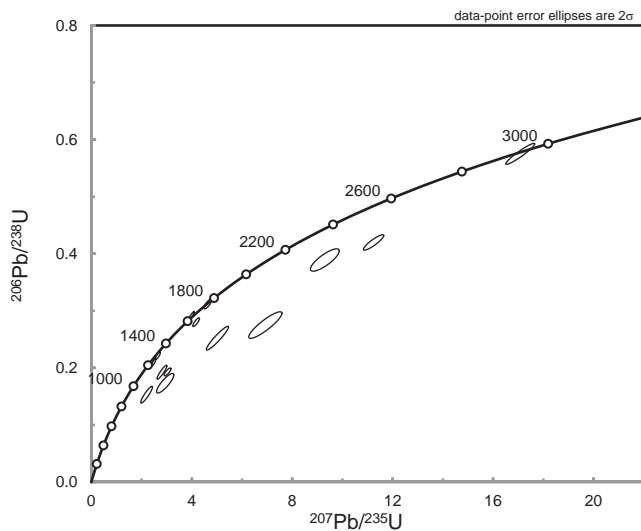
SHEEP CREEK - quartz-muscovite vein in Hamill Gp. quartzite  
 MA16-SH24 (muscovite)



# APPENDIX 3 - U-Pb Results

## CASSIAR - biotite pyroxene lamprophyre, Bain mine MA16-CS04

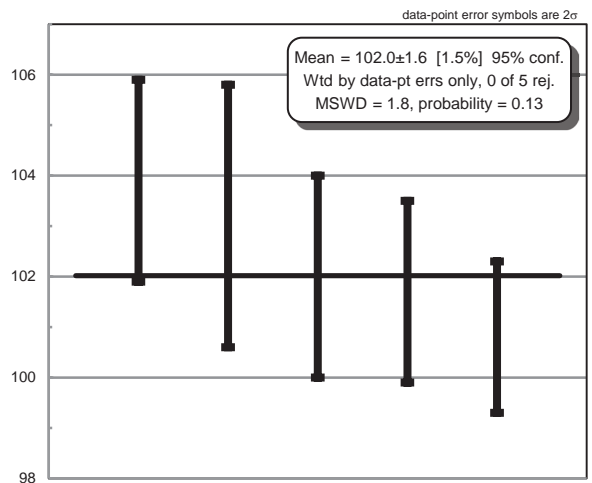
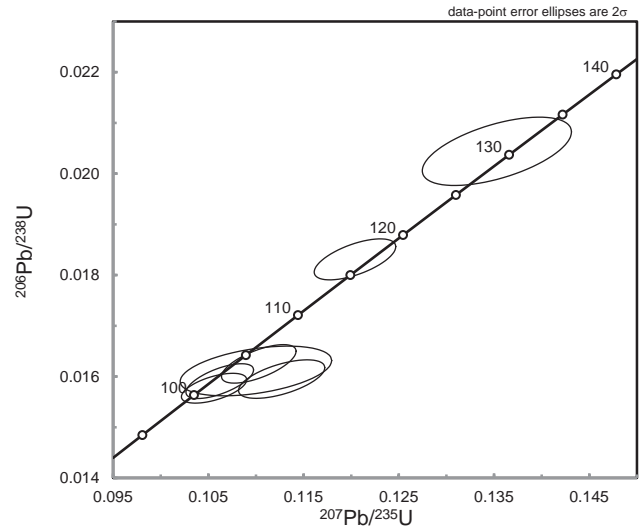
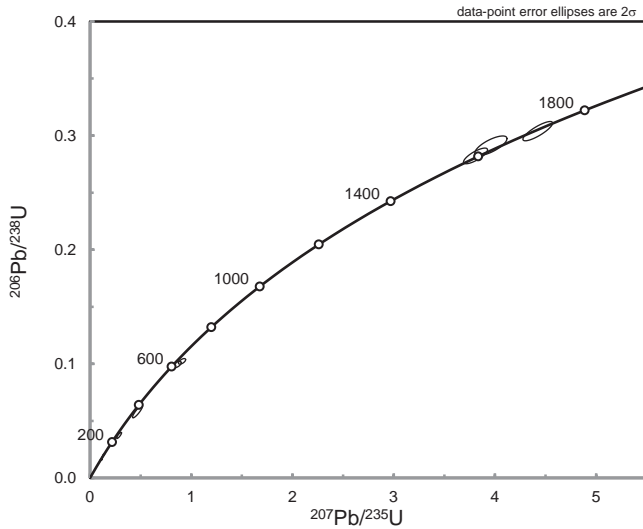
Fraction	Notes	Isotopic Ratios						Isotopic Ages						Background-corrected mean counts/s at specified mass								
		$^{207}\text{Pb}/^{235}\text{U}$	% 2s	$^{206}\text{Pb}/^{238}\text{U}$	% 2s	rho	$^{207}\text{Pb}/^{206}\text{Pb}$	% 2s	$^{207}\text{Pb}/^{235}\text{U}$	2s	$^{206}\text{Pb}/^{238}\text{U}$	2s	$^{207}\text{Pb}/^{206}\text{Pb}$	2s	202	204	206	207	208	232	235	238
CASSIAR																						
Sample: MA16-CS04 (lamprophyre, Bain Mine)																						
1		4.17200	0.11000	0.28000	0.00620	0.840	0.10770	0.00150	1665.0	21.0	1589.0	31.0	1752.0	25.0	58	7	103100	11150	12440	24280	1443	181100
2		2.65000	0.07900	0.22160	0.00530	0.802	0.08680	0.00220	1309.0	22.0	1289.0	28.0	1327.0	49.0	29	5	56300	4870	22010	53500	971	123800
3		0.11610	0.00290	0.01737	0.00035	0.807	0.04876	0.00072	111.4	2.6	111.0	2.2	132.0	31.0	37	1	175900	8520	697	13000	40300	4960000
4		0.15980	0.00730	0.02172	0.00066	0.665	0.05420	0.00200	149.9	6.3	138.5	4.2	354.0	80.0	40	-17	25800	1375	1232	5380	4850	603000
5		17.08000	0.47000	0.57500	0.01500	0.948	0.21940	0.00390	2932.0	26.0	2918.0	61.0	2972.0	29.0	45	-6	27620	5990	7060	7380	187	23930
6		4.638	0.13	0.312	0.0071	0.812	0.1103	0.002	1748	23	1750	35	1789	33	-27	-6	43200	4726	7510	13940	570	68900
7		0.1118	0.0032	0.01682	0.00035	0.727	0.0492	0.001	107.4	2.9	107.5	2.2	152	41	450	120	67200	3310	139	2270	15800	1940000
8		3.94	0.13	0.288	0.009	0.947	0.1013	0.0025	1616	27	1628	45	1641	49	-24	3	89100	8960	9740	19540	1229	154000
9		11.24	0.33	0.4198	0.011	0.892	0.1969	0.0026	2530	27	2249	50	2793	22	-11	19	88000	17250	9900	14410	839	105200
10		2.482	0.074	0.2095	0.0054	0.865	0.0872	0.0017	1259	22	1223	29	1339	38	-11	5	45900	3980	5430	12680	912	111200
11		3.035	0.11	0.1929	0.0057	0.815	0.1137	0.0024	1398	27	1136	31	1833	37	-5	0	31500	3570	4000	9490	680	85800
12		6.93	0.54	0.275	0.019	0.887	0.1658	0.0044	1874	86	1517	94	2457	49	58	1	79500	13280	8570	15090	1850	228000
13		0.1184	0.0072	0.01742	0.00064	0.604	0.0494	0.003	113.1	6.5	111.3	4	170	120	-17	-2	94000	464	48	358	2174	268200
14		2.2	0.19	0.153	0.012	0.908	0.0966	0.0028	1056	70	899	70	1510	60	-10	-15	41500	4250	9900	19800	1399	174000
15		2.81	0.16	0.1923	0.01	0.913	0.1026	0.0017	1281	50	1117	56	1654	30	111	17	58200	5970	8220	118000	1630	199000
16		2.94	0.28	0.173	0.014	0.85	0.1058	0.0039	1178	80	992	78	1623	75	72	-12	21300	2250	2030	12400	1002	121000
17		5.02	0.36	0.252	0.017	0.941	0.14	0.0048	1701	76	1415	89	2151	95	46	-7	50400	7160	10300	140000	841	104000
18		0.2161	0.0087	0.03165	0.00079	0.62	0.0491	0.0018	197.5	7.3	200.8	4.9	147	70	39	3	20140	992	2080	35200	2600	316000
19		9.3	0.47	0.389	0.016	0.814	0.1678	0.004	2294	55	2093	74	2505	40	24	-5	30700	5080	4670	7070	361	44200



Analysis by Murray Allan  
Pacific Centre for Isotopic and Geochemical Research,  
Dept Earth and Ocean Sciences,  
The University of British Columbia,  
Vancouver, BC., Canada

# SHEEP CREEK - quartz-feldspar granite porphyry MA16-SH11

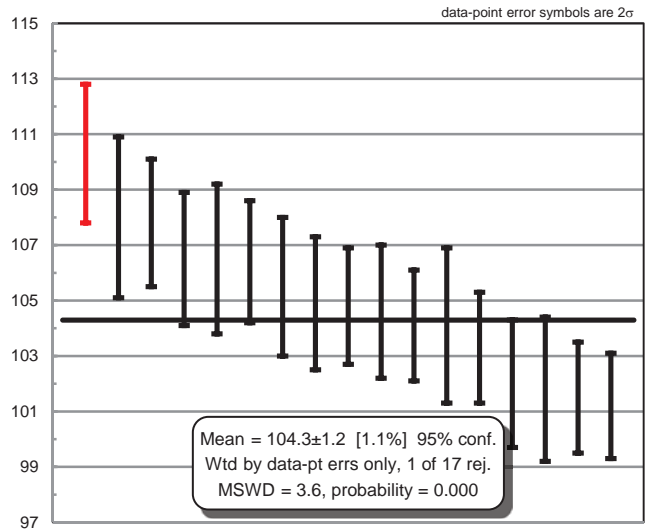
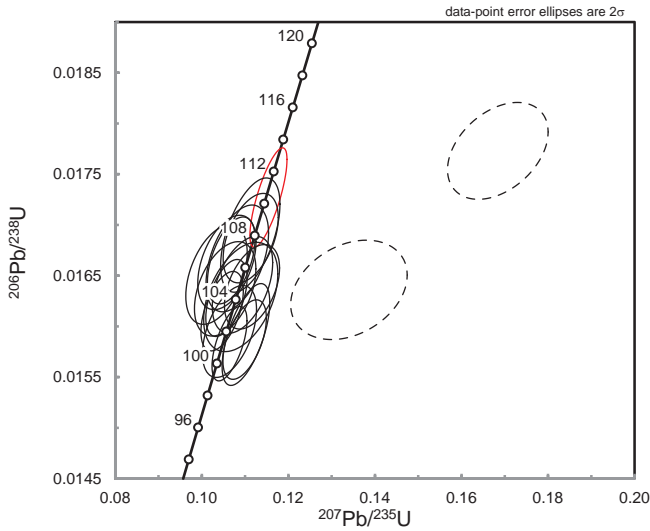
Fraction	Notes	Isotopic Ratios						Isotopic Ages						Background-corrected mean counts/s at specified mass								
		$^{207}\text{Pb}/^{235}\text{U}$	% 2s	$^{206}\text{Pb}/^{238}\text{U}$	% 2s	rho	$^{207}\text{Pb}/^{206}\text{Pb}$	% 2s	$^{207}\text{Pb}/^{235}\text{U}$	2s	$^{206}\text{Pb}/^{238}\text{U}$	2s	$^{207}\text{Pb}/^{206}\text{Pb}$	2s	202	204	206	207	208	232	235	238
SHEEP CREEK																						
Sample: MA16-SH11 (quartz-feldspar granite porphyry, Sheep Creek stock)																						
1		0.1127	0.0037	0.01595	0.00031	0.592	0.05	0.0015	108.2	3.3	102	2	185	58	12	14	24810	1241	1019	35160	6630	820000
2		0.861	0.033	0.0994	0.0023	0.604	0.0621	0.0023	627	18	612	13	605	80	37	27	13810	849	2019	11500	581	73000
3		0.287	0.02	0.0373	0.0022	0.846	0.0535	0.0016	250	15	235	13	320	62	50	35	22880	1205	1170	9300	3270	406000
4		0.1103	0.0032	0.01625	0.00031	0.658	0.0482	0.0012	106.1	2.9	103.9	2	117	51	-27	-18	64000	3080	9670	337000	16700	2070000
5		0.1062	0.0029	0.01591	0.00028	0.644	0.0481	0.0012	102.3	2.7	101.7	1.8	112	50	-7	-3	32630	1567	9960	361000	8730	1088000
6		0.1056	0.0028	0.01577	0.00024	0.574	0.04862	0.0012	101.7	2.6	100.8	1.5	131	48	34	4	40650	1980	12780	463500	10960	1381000
7		0.1204	0.0035	0.01831	0.00033	0.62	0.048	0.0013	115.4	3.2	116.9	2.1	99	52	28	7	30960	1476	749	24400	7240	905000
8		3.808	0.097	0.2822	0.0056	0.779	0.099	0.0022	1588	21	1599	28	1590	42	-22	-6	53800	5370	9290	21520	816	103100
9		0.11	0.0065	0.01611	0.0004	0.42	0.0505	0.0031	104.8	5.9	103.2	2.6	170	110	-27	-1	3870	197	992	36330	1047	129600
10		0.1353	0.0064	0.02044	0.00055	0.569	0.0491	0.0023	128.1	5.7	130.4	3.5	145	88	-16	-3	14160	692	740	23400	2960	374000
11		3.96	0.13	0.2911	0.007	0.733	0.1007	0.0033	1615	28	1643	35	1598	63	69	13	17850	1771	2730	6130	278	33390
12		4.423	0.12	0.3039	0.0069	0.837	0.1078	0.0022	1710	23	1705	34	1748	37	32	-5	87800	9430	8420	17500	1251	158400
13		0.469	0.04	0.0581	0.0044	0.888	0.0565	0.0015	365	27	359	27	431	56	9	-1	34900	2010	4790	35700	3520	433000
14		0.909	0.029	0.1022	0.002	0.613	0.0654	0.0019	651	15	627	12	749	65	25	13	33910	2203	7440	67400	1422	178500



Analysis by Murray Allan  
Pacific Centre for Isotopic and Geochemical Research,  
Dept Earth and Ocean Sciences,  
The University of British Columbia,  
Vancouver, BC., Canada

SHEEP CREEK - biotite granite (Sheep Creek stock)  
 MA16-SH12

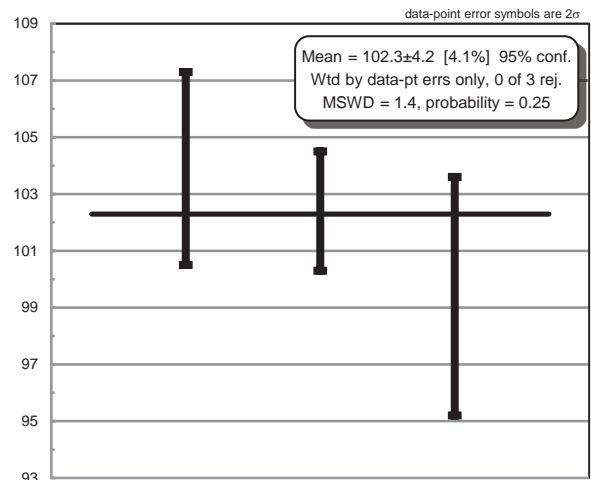
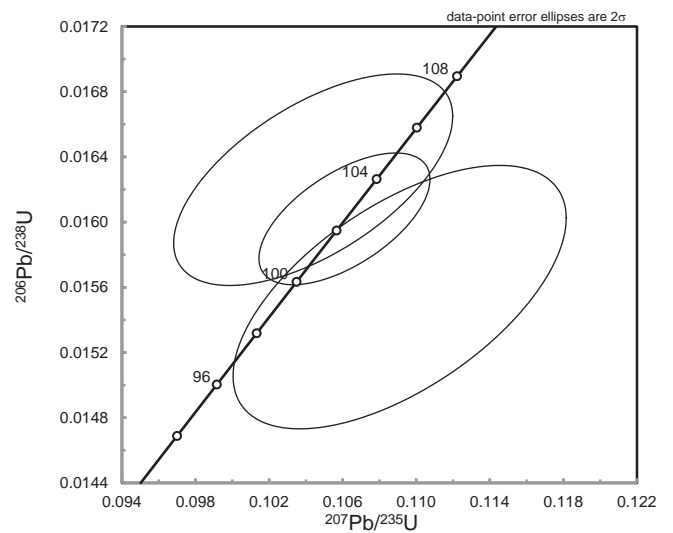
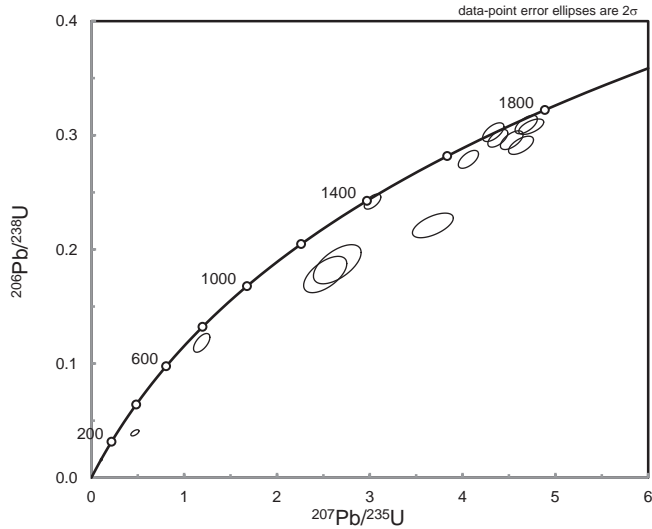
Fraction	Notes	Isotopic Ratios						Isotopic Ages						Background-corrected mean counts/s at specified mass								
		$^{207}\text{Pb}/^{235}\text{U}$	% 2s	$^{206}\text{Pb}/^{238}\text{U}$	% 2s	rho	$^{207}\text{Pb}/^{206}\text{Pb}$	% 2s	$^{207}\text{Pb}/^{235}\text{U}$	2s	$^{206}\text{Pb}/^{238}\text{U}$	2s	$^{207}\text{Pb}/^{206}\text{Pb}$	2s	202	204	206	207	208	232	235	238
SHEEP CREEK																						
Sample: MA16-SH12 (biotite granite, Sheep Creek stock)																						
1		0.1116	0.0052	0.01639	0.00034	0.445	0.0502	0.0023	106.8	4.7	104.8	2.1	167	85	22	-13	8290	419	2730	98500	2197	272000
2		0.1047	0.004	0.01615	0.00032	0.519	0.0478	0.0018	100.7	3.7	103.3	2	93	69	59	13	14030	675	2120	74200	3750	465000
3		0.1057	0.0039	0.01628	0.00031	0.516	0.0484	0.0018	101.9	3.6	104.1	2	125	70	66	6	11890	586	2630	93200	3220	396000
4		0.1054	0.0058	0.01637	0.00038	0.422	0.0488	0.0029	100.8	5.3	104.6	2.4	104	100	30	1	4610	222	1048	37100	1242	152700
5		0.109	0.007	0.01629	0.00044	0.421	0.0503	0.0033	104.3	6.4	104.1	2.8	130	110	18	0	4070	203	1161	40890	1093	137300
6		0.1068	0.0045	0.01665	0.00035	0.499	0.0475	0.002	102.8	4.2	106.4	2.2	84	78	42	16	9180	439	3076	109400	2454	300900
7		0.1112	0.0056	0.0169	0.00046	0.54	0.0491	0.0025	106.4	5.1	108	2.9	115	90	27	14	8350	408	1248	43000	2200	268500
8		0.1034	0.0058	0.01651	0.0004	0.432	0.0464	0.0027	99	5.3	105.5	2.5	29	98	10	-2	5910	272	1166	44200	1522	191000
9		0.1113	0.0052	0.01687	0.00036	0.457	0.0487	0.0023	106.4	4.7	107.8	2.3	110	83	27	6	7310	354	2320	78100	1893	234800
10		0.1058	0.0055	0.01663	0.00038	0.44	0.0479	0.0027	101.7	5.1	106.5	2.4	61	96	-7	37	5310	252	1869	70300	1365	172600
11		0.1154	0.0035	0.01727	0.0004	0.764	0.0481	0.0013	110.7	3.2	110.3	2.5	112	56	-6	5	79800	3850	11990	408000	20200	2474000
12		0.134	0.011	0.01636	0.0004	0.298	0.0593	0.0045	125	9.1	104.6	2.5	410	130	24	22	5020	276	1479	48700	1300	163900
13		0.1064	0.0051	0.01595	0.00037	0.484	0.0485	0.0024	101.9	4.7	102	2.3	99	87	-21	-13	6630	323	1470	53600	1737	223000
14		0.1064	0.0033	0.01583	0.0003	0.611	0.0484	0.0012	102.4	3	101.2	1.9	118	50	-9	-7	32670	1589	3710	133200	8840	1109000
15		0.1099	0.0041	0.01587	0.00032	0.54	0.0503	0.0019	105.4	3.8	101.5	2	187	72	20	18	13600	682	7200	311000	3620	468000
16		0.1684	0.0095	0.01773	0.00039	0.39	0.066	0.003	157.6	8.3	113.3	2.5	723	96	-49	65	37700	2690	8620	238000	9010	1097000
17		0.1082	0.0059	0.01667	0.00043	0.473	0.0474	0.0024	103.8	5.3	106.5	2.7	63	91	-25	11	11520	542	1680	57500	2990	369000
18		1.84	0.12	0.1649	0.0086	0.8	0.0787	0.0033	996	47	972	48	1043	92	13	1	8450	657	827	3810	303	37600
19		0.1102	0.0045	0.01592	0.00041	0.631	0.0501	0.002	105.8	4.1	101.8	2.6	178	78	52	-5	25200	1260	431	13800	6870	860000
20		0.1094	0.0057	0.01641	0.00039	0.456	0.0486	0.0026	104.6	5.2	104.9	2.4	100	94	42	2	6160	292	1123	36620	1614	200800



Analysis by Murray Allan  
 Pacific Centre for Isotopic and Geochemical Research,  
 Dept Earth and Ocean Sciences,  
 The University of British Columbia,  
 Vancouver, BC., Canada

# SHEEP CREEK - quartz porphyry (Nugget-Fawn Mine area) MA16-SH16

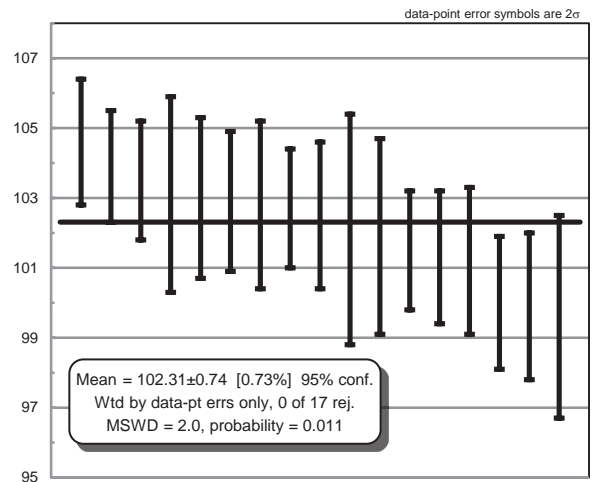
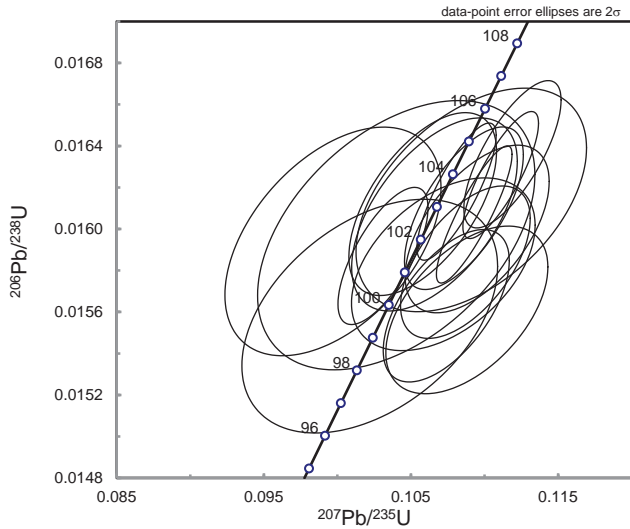
Fraction	Notes	Isotopic Ratios						Isotopic Ages						Background-corrected mean counts/s at specified mass								
		$^{207}\text{Pb}/^{235}\text{U}$	% 2s	$^{206}\text{Pb}/^{238}\text{U}$	% 2s	rho	$^{207}\text{Pb}/^{206}\text{Pb}$	% 2s	$^{207}\text{Pb}/^{235}\text{U}$	2s	$^{206}\text{Pb}/^{238}\text{U}$	2s	$^{207}\text{Pb}/^{206}\text{Pb}$	2s	202	204	206	207	208	232	235	238
SHEEP CREEK																						
Sample: MA16-SH16 (quartz porphyry, Nugget-Fawn Mine area, Sheep Creek)																						
1		0.1061	0.0038	0.01602	0.00033	0.575	0.0483	0.0019	102.2	3.4	102.4	2.1	113	73	-22	-5	11630	561	1057	36300	3030	379000
2		3.03	0.073	0.2419	0.0054	0.927	0.0905	0.0021	1409	19	1394	28	1423	45	-11	-20	68100	6170	7810	18960	1161	146000
3		4.63	0.11	0.2912	0.0065	0.94	0.1146	0.0021	1743	19	1643	32	1864	34	-27	9	221000	25420	17100	55500	3220	399000
4		4.063	0.089	0.2789	0.0064	1.048	0.1055	0.0022	1643	18	1583	32	1716	37	-15	-7	103800	10880	10830	22040	1550	193800
5		1.189	0.072	0.1181	0.0067	0.937	0.0705	0.0017	752	37	712	39	930	48	46	12	67000	4770	5890	34900	3120	383000
6		0.1044	0.0062	0.01626	0.00053	0.549	0.0472	0.0029	100.6	5.7	103.9	3.4	60	110	-81	-21	26300	1234	2880	99100	6710	843000
7		3.68	0.18	0.221	0.0088	0.814	0.1158	0.0029	1503	46	1274	48	1866	43	-3	30	80100	9260	11100	33800	1712	202600
8		4.74	0.11	0.3075	0.0055	0.771	0.1109	0.0025	1769	19	1726	27	1806	44	37	19	47600	5320	3240	6460	643	80400
9		4.686	0.098	0.3094	0.0066	1.02	0.1092	0.0023	1759	18	1735	32	1775	38	3	-32	131600	14330	9500	17700	1806	217500
10		4.331	0.094	0.3027	0.0067	1.02	0.104	0.0023	1693	18	1700	33	1677	40	4	9	55100	5690	7110	14030	753	93700
11		4.53	0.1	0.2957	0.0067	1.026	0.1113	0.0026	1728	19	1665	33	1802	42	34	31	48200	5320	11300	25000	690	85300
12		2.52	0.19	0.178	0.013	0.969	0.0937	0.003	1127	68	1025	70	1427	73	22	0	51300	5200	6250	24000	1531	189000
13		4.38	0.088	0.2973	0.0063	1.055	0.107	0.0023	1701	17	1674	31	1728	40	50	5	68000	7190	5680	10760	952	118000
14		0.469	0.036	0.0393	0.0022	0.729	0.0771	0.0032	367	25	247	14	976	93	24	236	131000	13300	17300	142000	11100	1360000
15		2.65	0.21	0.187	0.014	0.945	0.0905	0.0035	1151	77	1076	77	1330	88	37	-10	42100	4060	10010	40000	1770	222000
16		0.1091	0.0074	0.01554	0.00066	0.626	0.0511	0.0035	104.7	6.8	99.4	4.2	210	130	40	19	13510	671	1520	46200	3590	454000



Analysis by Murray Allan  
Pacific Centre for Isotopic and Geochemical Research,  
Dept Earth and Ocean Sciences,  
The University of British Columbia,  
Vancouver, BC., Canada

SHEEP CREEK - feldspar-quartz porphyry (Sheep Creek stock)  
 MA16-SH17

Fraction	Notes	Isotopic Ratios						Isotopic Ages						Background-corrected mean counts/s at specified mass								
		<sup>207</sup> Pb/ <sup>235</sup> U	% 2s	<sup>206</sup> Pb/ <sup>238</sup> U	% 2s	rho	<sup>207</sup> Pb/ <sup>206</sup> Pb	% 2s	<sup>207</sup> Pb/ <sup>235</sup> U	2s	<sup>206</sup> Pb/ <sup>238</sup> U	2s	<sup>207</sup> Pb/ <sup>206</sup> Pb	2s	202	204	206	207	208	232	235	238
SHEEP CREEK																						
Sample: MA16-SH17 (feldspar-quartz qtz porphyry, Sheep Creek stock)																						
1		0.1111	0.0021	0.01626	0.00025	0.813	0.0498	0.0011	106.9	1.9	103.9	1.6	180	47	21	15	49000	2443	1978	63700	12490	1557000
2		0.104	0.0077	0.01597	0.00053	0.448	0.0485	0.0038	99.9	7.1	102.1	3.3	60	130	-6	11	2542	122.6	393	13450	652	82700
3		0.1119	0.0027	0.01636	0.00029	0.735	0.05	0.0014	107.5	2.4	104.6	1.8	181	56	21	6	34800	1748	13520	463000	8780	1100000
4		0.1031	0.0025	0.01587	0.00027	0.702	0.0472	0.0012	99.5	2.3	101.5	1.7	80	51	79	22	33120	1573	4560	165000	8690	1077000
5		0.1095	0.004	0.016	0.00033	0.565	0.0507	0.0022	105.3	3.7	102.5	2.1	189	80	7	11	8810	434	1441	48820	2263	281800
6		0.1086	0.0033	0.0161	0.00032	0.654	0.0495	0.0016	104.3	3	102.9	2	151	62	-9	13	16530	809	539	19300	4210	537000
7		0.1091	0.0064	0.01614	0.00044	0.465	0.0503	0.0032	103.9	5.8	103.1	2.8	130	110	16	-2	4160	205	485	16620	1069	134100
8		0.0997	0.006	0.01594	0.00045	0.469	0.0475	0.0032	95.9	5.6	101.9	2.8	30	110	19	10	3319	152.5	388	13290	892	108700
9		0.1022	0.0071	0.01558	0.00046	0.425	0.0489	0.0036	97.8	6.5	99.6	2.9	80	120	35	20	2689	127.6	596	20630	738	89800
10		0.1088	0.0045	0.01561	0.00033	0.511	0.0504	0.0022	104.2	4.1	99.9	2.1	178	82	59	-9	11210	558	2020	68800	2970	366000
11		0.1074	0.0035	0.01563	0.0003	0.589	0.05	0.0018	103.2	3.2	100	1.9	177	69	60	4	16500	813	1040	37500	4410	556000
12		0.1058	0.0041	0.01612	0.00036	0.576	0.0482	0.002	102.1	3.8	103	2.3	111	78	22	10	27500	1330	3230	110000	7030	870000
13		0.1087	0.0036	0.01584	0.0003	0.572	0.0494	0.0019	104.4	3.3	101.3	1.9	159	71	16	-1	22700	1110	2420	83000	5940	740000
14		0.1093	0.0021	0.01607	0.00027	0.874	0.0488	0.0011	105.2	1.9	102.7	1.7	147	46	-7	6	60600	2940	2348	78900	15750	1951000
15		0.1072	0.0051	0.01583	0.00034	0.451	0.0494	0.0025	102.6	4.6	101.2	2.1	118	89	34	18	6780	330	1973	72400	1786	222400
16		0.1066	0.0046	0.01607	0.00038	0.548	0.048	0.0021	103.1	4.2	102.8	2.4	102	79	14	5	9810	464	1628	54400	2487	310900
17		0.1081	0.0022	0.01618	0.00027	0.82	0.04795	0.0011	104.1	2	103.5	1.7	107	47	24	-4	52700	2537	2880	97500	13320	1666000
18		1.983	0.068	0.183	0.00046	0.733	0.079	0.0032	1094	23	1080	25	1090	84	-41	-7	9570	739	1200	3620	220	27500



Analysis by Murray Allan  
 Pacific Centre for Isotopic and Geochemical Research,  
 Dept Earth and Ocean Sciences,  
 The University of British Columbia,  
 Vancouver, BC., Canada